Technical Report

TR-10-43

Experimental study on Ra^{2+} uptake by barite ($BaSO_4$)

Kinetics of solid solution formation via $BaSO_4$ dissolution and $Ra_xBa_{1-x}SO_4$ (re) precipitation

Dirk Bosbach, Melanie Böttle, Volker Metz
Karlsruher Institut für Technologie,
Institut für Nukleare Entsorgung (INE)

March 2010

Svensk Kärnbränslehantering AB
Swedish Nuclear Fuel
and Waste Management Co

Box 250, SE-101 24 Stockholm
Phone +46 8 459 84 00

Experimental study on Ra^{2+} uptake by barite ($BaSO_4$)

Kinetics of solid solution formation via $BaSO_4$ dissolution and $Ra_xBa_{1-x}SO_4$ (re) precipitation

Dirk Bosbach, Melanie Böttle, Volker Metz
Karlsruher Institut für Technologie,
Institut für Nukleare Entsorgung (INE)

March 2010

Abstract

$^{226}Ra^{2+}$ and $^{133}Ba^{2+}$ uptake by barite in aqueous solution is studied on the basis of batch type experiments with two different barite powders with different specific surface area (0.5 m^2/g and 3.2 m^2/g, respectively). The uptake of $^{226}Ra^{2+}$ and $^{133}Ba^{2+}$ is not only limited to adsorption reactions but proceeds significantly into the bulk of the barite crystals. $^{133}Ba^{2+}$ uptake kinetics is affected by various parameters, such as amount of sample, specific surface area, sample type and solution composition.

In the case of $^{133}Ba^{2+}$, complete isotopic equilibration of the $^{133}Ba^{2+}$ spiked solution with the barite powder occurs within 50 to 600 days. This information is derived by monitoring the aqueous $^{133}Ba^{2+}$ concentration combined with simple mass balance calculations.

In the case of $^{226}Ra^{2+}$ a $Ra_xBa_{1-x}SO_4$ solid solution forms and the uptake rate drops significantly within 400 days. The observed $^{226}Ra^{2+}$ concentration in solution is controlled by the solubility of a $Ra_xBa_{1-x}SO_4$ solid solution and several orders of magnitude below the Ra^{2+} solubility with respect to a pure $RaSO_4$(s) endmember. It cannot be demonstrated unambiguously that a zero exchange rate and therefore thermodynamic equilibrium has been established within the observation period. The observed concentrations may be interpreted either as (1) a partial equilibration of 20 to 50% of the barite crystals with $^{226}Ra^{2+}$ or (2) as complete equilibration of a $Ra_{0.000128}Ba_{0.999872}SO_4$ solid solution with $^{226}Ra^{2+}$ with no pure barite left. In both cases it is concluded that equilibration between aqueous Ra^{2+} and barite involves the replacement of a substantial fraction of the initial barite and proceeds significantly beyond pure surface adsorption processes.

Contents

1 Introduction

During corrosion of spent nuclear fuel, barium isotopes (mainly ^{134}Ba, ^{135}Ba and ^{138}Ba) may be released as decay products of cesium fission products from the waste matrix. Together with sulfate in the ground water these stable isotopes may form barite ($BaSO_4(s)$). ^{226}Ra forms within the decay chain of ^{238}U, which may be released from the waste matrix at a later stage. In contrast to the knowledge on barium, the current thermodynamic database for solid radium phases is very small /e.g. Hummel et al. 2002/. Thus, in various performance assessment studies performed for ^{226}Ra it is assumed that its solubility is limited by precipitation of pure $RaSO_4(s)$, however, only at rather high ^{226}Ra concentrations.

Solubility of $RaSO_4(s)$ had been determined experimentally by /Lind et al. 1918/ in water and sulfuric acid up to an ionic strength of $I = 6$ mol (kg $H_2O)^{-1}$ at 25°C and by /Nikitin and Tolmatscheff 1933/ in water and Na_2SO_4 solutions up to $I = 0.015$ mol (kg $H_2O)^{-1}$ at 20°C. Based on the experimental data of /Nikitin and Tolmatscheff 1933, Langmuir and Riese 1985/ estimated the solubility product of $RaSO_4(s)$ ($K_{sp,\,RaSO4}$) and derived a value of $K_{sp,\,RaSO4} = 10.38\pm0.02$ at 20°C. Alternatively /Langmuir and Riese 1985/ derived the enthalpy of formation for $RaSO_4(s)$ by linear regression of the respective values of barite and celestite with the effective 8-fold ionic radii of Ba^{2+} and Sr^{2+}. Using this approach they estimated a solubility constant of $\log K^0_{sp,\,RaSO4} = 10.26\pm0.02$ at 25°C. /Paige et al. 1998/ have used the data of /Nikitin and Tolmatscheff 1933/ in pure water and a selected data set of /Lind et al. 1918/ in sulfuric acid in order to calculate values for $\log K^0_{sp,\,RaSO4}$ in the range of 10.41±0.03 and 10.21±0.06 at 25°C.

Abundant information from radiochemical experimental studies and studies on natural as well as anthropogenic systems indicate that Ra^{2+} is retained when in contact with barite /Grandia et al. 2008 and references therein/. Considering the fate of ^{226}Ra released from corroding spent nuclear fuel, the released Ra^{2+} may either adsorb onto barite surfaces or equilibrate with the earlier precipitated barite to form a $Ra_xBa_{1-x}SO_4$ solid solution. Following this latter scenario, the solubility of Ra^{2+} would be controlled by the solubility product of the $Ra_xBa_{1-x}SO_4$ solid solution, which would be significantly lower compared to the Ra^{2+} solubility controlled by the solubility product of pure $RaSO_4$.

Formation of $Ra_xBa_{1-x}SO_4$ solid solution during co-precipitation of Ra^{2+} and Ba^{2+} into barite is a known phenomenon which has been investigated extensively already in the 1920s and 1950s /Doerner and Hoskins 1925, Germann 1921, Gordon and Rowley 1957/. Considering the 12-fold coordination of divalent cations in the barite structure /e.g. Lee et al. 2005/ and the similar effective ionic radii of 12-fold coordinated Ba^{2+} and Ra^{2+}, 1.61 Å and 1.70 Å respectively /Shannon 1976/, a simple substitution is expected, where Ra^{2+} occupies Ba^{2+} lattice sites. /Grandia et al. 2008/ present a review of the extensive literature concerning the mechanisms and processes which control the solid solution formation behavior of the $Ra_xBa_{1-x}SO_4$ system.

Incorporation of Ra^{2+} into the mixed solid phase, $Ra_xBa_{1-x}SO_4$ can be described as a solid solution reaction /e.g. Langmuir and Riese 1985, Zhu 2004/:

$$BaSO_{4,S} + Ra^{2+}_{(aq)} \leftrightarrow RaSO_{4,S} + Ba^{2+}_{(aq)} \tag{1-1}$$

For equilibrium between the aqueous- and the solid solution the Ra^{2+}, Ba^{2+} and SO_4^{2-} concentrations are defined by the equations /Glynn 2000/:

$$m_{Ba^{2+}} \cdot m_{SO_4^{2-}} \cdot \gamma_{Ba^{2+}} \cdot \gamma_{SO_4^{2-}} = K^0_{sp,barite} \cdot X_{barite} \cdot f_{barite} \tag{1-2}$$

and

$$m_{Ra^{2+}} \cdot m_{SO_4^{2-}} \cdot \gamma_{Ra^{2+}} \cdot \gamma_{SO_4^{2-}} = K^0_{sp,RaSO_4} \cdot X_{RaSO_4} \cdot f_{RaSO_4} \tag{1-3}$$

where K^0_{sp} is the thermodynamic solubility product of the pure phase end members, m_j and γ_j are the molality and activity coefficient of aqueous ions j, and X_i and f_j are the mole fraction and rational activity coefficient of component i in the solid phase, respectively.

Equations (1-2) and (1-3) can be used to calculate the equilibrium constant, K_{eq}, for the reaction in Equation (1-1) /e.g. Langmuir and Riese 1985/:

$$K_{eq} = \frac{K_{sp,barite}}{K_{sp,RaSO_4,S}} = \left(\frac{X_{RaSO_4} f_{RaSO_4}}{X_{BaSO_4} f_{BaSO_4}}\right) \Big/ \left(\frac{m_{Ra^{2+}}}{m_{Ba^{2+}}} \cdot \frac{\gamma_{Ra^{2+}}}{\gamma_{Ba^{2+}}}\right) \tag{1-4}$$

The Ra^{2+}–Ba^{2+}-exchange may be established either via solid state diffusion or via a ($BaSO_4$) dissolution/($Ra_xBa_{1-x}SO_4$ solid solution) re-precipitation reaction. There seems to be a consensus that solid state diffusion can be excluded as a possible reaction mechanism at temperatures <100°C. Therefore it seems reasonable to consider exclusively a re-crystallization process (i.e. dissolution and consecutive re-precipitation) and/or surface adsorption processes. However, the equilibration reaction via dissolution/re-precipitation may be limited to the barite surface in contact with the Ra^{2+} containing aqueous solution. In such a case a $Ra_xBa_{1-x}SO_4$ solid solution would only form at the mineral/aqueous solution interface forming layers enriched in radium to some extent that would prevent the further equilibration reaction. One could also think of an intermediate state in between (a) complete re-equilibration of the bulk barite crystals or (b) a surface adsorption reaction: a re-equilibrated surface coating with a limited thickness. In such a case, however, metastable compositional heterogeneities would be established.

In their classical publication, /Doerner and Hoskins 1925/ defined the partition coefficient for radium coprecipitation with barite as the proportionality factor between the ratio of the amounts of radium atoms to barium atoms on the surface on one side of the equation and the ratio of the concentrations of radium ions to barium ions in solution on the other side of the equation. For the relative low ionic strength of the present study total concentrations of radium and barium in solutions are about the same as concentrations of Ra^{2+} and Ba^{2+}. According to /Rosenberg et al. 2010/ the $\gamma_{Ra2+}/\gamma_{Ba2+}$ ratio deviates from unity less than 1% at low ionic strength, i.e. $I \leq 0.1$ mol (kg H_2O)$^{-1}$ (as will be shown later, $\gamma_{Ra2+}/\gamma_{Ba2+} = 1.009$ under the conditions of the present study). If we assume that the co-precipitation occurs near equilibrium, then the *apparent* partition coefficient ($K_{D,app}$) may be defined as:

$$K_{D,app} = \left(\frac{X_{Ra}}{X_{Ba}}\right)_{surface} \Big/ \left(\frac{m_{Ra}}{m_{Ba}}\right)_{solution} = \left(\frac{X_{RaSO_4}}{X_{barite}}\right)_{surface} \Big/ \left(\frac{m_{Ra^{2+}}}{m_{Ba^{2+}}} \cdot \frac{\gamma_{Ra^{2+}}}{\gamma_{Ba^{2+}}}\right)_{solution} \tag{1-5}$$

As point out by /Curti 1999/, the qualification surface implies that the aqueous Ra^{2+} and Ba^{2+} are "not in equilibrium with the bulk solid, but only with the uppermost monolayer of the mineral structure exposed to the solution". It is emphasized that $K_{D,app}$ is an apparent (phenomenological) rather than a thermodynamic quantity. If Equations 1-2 and 1-3 are introduced into Equation 1-5 the following expression is obtained for the equilibrium value of the partition coefficient, K_D:

$$K_D = \left(\frac{K_{sp}^{barite}}{K_{sp}^{RaSO_4,S}}\right) \cdot \left(\frac{\gamma_{Ra^{2+}}}{\gamma_{Ba^{2+}}}\right) \cdot \frac{f_{barite}}{f_{RaSO_4}} \tag{1-6}$$

The rational activity coefficients, f_i, are not constant. They are a function of the solid solution composition. For the simple case of a regular solid solution as it can be used to describe the $Ra_xBa_{1-x}SO_4$ system /Zhu 2004/ the dependence on the solid solution composition can be described by one Guggenheim Parameter, α, /Glynn 2000, Guggenheim 1937/:

$$\ln f_{barite} = \alpha X_{RaSO_4}^2 \tag{1-7}$$

$$\ln f_{RaSO_4} = \alpha X_{barite}^2 \tag{1-8}$$

The non-dimensional Guggenheim interaction parameter, α, is equivalent to the Margules parameter for binary solid solutions, w_H. The conversion of α into w_H is based on the assumption of zero excess entropy of mixing, i.e. the Gibbs energy ΔG_m of mixing equals the enthalpy of mixing ΔH_m /Bruno et al. 2007/:

$$\Delta G_m = \Delta H_m = R \cdot T \cdot \alpha \cdot X_{RaSO_4} \cdot X_{BaSO_4} = w_H \cdot X_{RaSO_4} \cdot X_{BaSO_4} \tag{1-9}$$

$$\alpha = w_H \cdot (R \cdot T)^{-1} \tag{1-10}$$

Using Equations 1-6 to 1-8 we obtain the following expression for the partition coefficient, K_D:

$$K_D = \left(\frac{K_{sp}^{barite}}{K_{sp}^{RaSO_4,S}}\right) \cdot \left(\frac{\gamma_{Ra^{2+}}}{\gamma_{Ba^{2+}}}\right) \cdot \exp(\alpha \cdot (X_{RaSO_4}^2 - X_{barite}^2)) \tag{1-11}$$

Equations 1-2, 1-3, 1-5 to 1-8 and 1-11 provide all the relations needed to describe the aqueous solution – solid solution equilibrium system.

There is a long discussion in the literature how the apparent partition coefficient is affected both by the thermodynamics of the solution and the precipitation kinetics of the host-mineral /Berner and Curti 2002, Curti 1997, Curti 1999, Langmuir and Melchior 1985, McIntire 1963, Rimstidt et al. 1998, Tesoriero and Pankow 1996, Wang and Xu 2001/.

It is well known from natural systems that in some cases non-equilibrium configurations in minerals (e.g. compositional gradients, heterogeneities, oscillatory zoning) remain metastable over extended periods of time. In many other cases, however, compositional variations within a mineral equilibrate rather quickly via dissolution and re-precipitation processes.

With respect to the scenario of Ra^{2+} interactions with barite as outlined above, it is not clear whether a Ra^{2+} containing aqueous solution would completely re-equilibrate with a $Ra_xBa_{1-x}SO_4$ solid solution.

In this study, batch type sorption/ion exchange experiments with two different barite powders in aqueous solution were performed at room temperature. $^{133}Ba^{2+}$ was used as an indicator for the re-crystallization process in one series of experiments. In parallel, experiments with $^{226}Ra^{2+}$ were conducted in order to demonstrate to what extent the equilibration of the $Ra_xBa_{1-x}SO_4$ solid solution proceeds. Both experimental series focused on (1) establishing the equilibrium conditions of the solid solution and (2) identifying the effect of solution composition and barite surface area to solution volume ratio on the exchange kinetics.

This report provides a detailed description of batch type exchange experiments, which were performed at the Institut für Nukleare Entsorgung (INE), Forschungszentrum Karlsruhe/Karlsruher Institut für Technologie during February 2008–January 2010.

2 Materials and methods

Static batch type experiments were performed in closed 20 mL polyethylene flasks ("Zinsser flasks" from Zinsser Analytical) with 10 or 100 mg of two different barite powders at room temperature (20°C) in order to quantify the $^{133}Ba^{2+}$ and $^{226}Ra^{2+}$ exchange reactions. The $^{133}Ba^{2+}$ and $^{226}Ra^{2+}$ activities in solution were monitored frequently over 100 days, while the solution was in contact with a defined amount of barite powder. In selected experiments, $^{226}Ra^{2+}$ and $^{133}Ba^{2+}$ activities in solution were analyzed again after more than one year. To interpret the experimental results thermodynamic calculations were conducted using the PHREEQC geochemical software /Parkhurst and Appelo 1999/ and the Nagra/PSI thermodynamic database /Hummel et al. 2002, release NAPSI_290502(260802).DAT/.

In the following sub-sections, the preparation of the aqueous solutions, the characterization of the different barite powders, the analytical methods as well as the $^{133}Ba^{2+}$ and $^{226}Ra^{2+}$ exchange experiments are described.

2.1 Preparation of aqueous solutions

In principle, three groups of initial chemical compositions for the aqueous solutions were selected:

1. **0.1 mol/L NaCl solution, free of Ba^{2+} and SO_4^{2-}**
2. **0.1 mol/L NaCl solution, saturated with respect to barite, $[Ba^{2+}]/[SO_4^{2-}] = 1$**
3. **0.1 mol/L NaCl solution, saturated with respect to barite, $[Ba^{2+}]/[SO_4^{2-}] = 10^{-5}$**

$^{133}Ba^{2+}$ – barite exchange experiments were conducted in solutions of type (1) to (3), whereas $^{226}Ra^{2+}$ batch experiments were conducted only in solution of type (1). Initial Ba^{2+} und SO_4^{2-} concentrations of solution type (2) and type (3) were chosen based on thermodynamic calculations, to represent equilibrium with barite powder (see Table 2-1 and Table 2-2). The aqueous solutions were prepared by adding NaCl to deionized water (solution type (1)), and adding NaCl, Na_2SO_4 and $BaCl_2{:}2H_2O$ to deionized water (solution type (2) and (3)). The used salts were of "pro analysis" quality (Merck, Darmstadt, Germany) and deionized water was generated by a Milli-Q Plus/Elix10 system (Millipore, Bedford, USA).

In order to ensure equilibrium conditions in solutions of type (1) to (3), barite powder was added to solutions. After an equilibration time of up to four weeks the solutions were used in the experiments. Solution compositions were analytically confirmed by ICP-MS for Ba^{2+} and by ion chromatography for SO_4^{2-}. The pH was measured to be approximately 6. Since sulfate concentration and pH were not varied systematically, they were not monitored during the $^{226}Ra^{2+}$ and $^{133}Ba^{2+}$ exchange experiments.

0.1 mol/L NaCl was chosen as background electrolyte. Although it is well known that ionic strength may affect reaction kinetics of mineral dissolution and precipitation it is not expected to affect considerably the equilibrium thermodynamics at this low ionic strength. Furthermore, 0.1 mol/L NaCl solution was chosen to approximate to some extent a typical ground water ionic strength in crystalline rocks such as granitic groundwater /e.g. formation water of Äspö borehole KAS02; Ekberg 1999/.

For experiments on barite re-crystallization monitored by the uptake of $^{133}Ba^{2+}$ a carrier-free $^{133}BaCl_2$ solution with an activity concentration of 10^7 Bq/mL was purchased from Eckert & Ziegler in January 2008. A stock solution was prepared by diluting 100 µL of that solution (10^6 Bq) to 10 mL (10^5 Bq/mL).

For experiments on $^{226}Ra^{2+}$ uptake by barite a 1 mol/L HNO_3 ^{226}Ra stock solution was used, which was available at INE. The stock solution had been originally purchased in 1992. 20 mL of that stock solution was partially neutralized with 2 mL of a 10 M NaOH solution resulting in a total volume of 22 mL and a pH of approximately 5. Using α-spectrometry, the ^{226}Ra activity in the stock solution was determined to be 5,148 Bq/mL, corresponding to a concentration of $6.2 \cdot 10^{-7}$ mol/L.

2.2 Barite powders

2.2.1 Characterization of barite samples

Two commercially available barite powders were used in this study: SIGMA barite, which was purchased from SIGMA ALDRICH, and SACHTLEBEN barite, which was obtained from SACHTLEBEN Chemie GmbH. Figures 2-1 and 2-2 show SEM images of both barite powders.

Most particles of the SIGMA sample look rounded and form aggregates (Figure 2-1). A large fraction of the barite particles seems to have a diameter of less than 1 µm. Most particles do not have a typical barite morphology, which is dominated by (001) and (210) crystal faces. Specific surface area of SIGMA barite is S_{BET} = 3.2 +/–0.1 m^2/g, as determined by the N_2-BET method (Figure 2-3). SEM images of SACHTLEBEN barite show that most barite particles are almost euhedral with typical barite morphologies, such as significant contributions by (001) and (210) crystal faces (Figure 2-2). Unlike the SIGMA barite, a significant fraction of SACHTLEBEN barite particles has a diameter much larger than 1 µm, and the SACHTLEBEN barite has a relatively small specific surface area, i.e. S_{BET} = 0.5 +/–0.1 m^2/g. A smaller S_{BET} value or SACHTLEBEN barite had been determined by Dr. Enzo Curti (S_{BET} = 0.31 m^2/g, pers. comm.).

2.2.2 Pre-equilibration of barite samples

The $^{226}Ra^{2+}$(aq)-barite equilibration process is expected to occur via barite dissolution and subsequent re-precipitation of a homogeneous $Ra_xBa_{1-x}SO_4$ solid solution. It is well known that heterogeneous reactions – such as dissolution and precipitation – are controlled to a large extent by the physico-chemical properties of the aqueous solution/mineral interface. This includes various aspects such as nanotopography, particle size, surface defects and morphology which will not be considered here.

Dissolution and precipitation kinetics depend on the available surface area or to be more precise on reactive surface sites. Therefore, two different commercially available barite powders with different specific surface areas were used in this study. Furthermore, $^{133}Ba^{2+}$ exchange experiments were performed with different amounts of sample material to vary the ratio between surface area and solution volume (see Table 2-1).

It is well known that the nanotopography of a mineral surface has a significant impact on dissolution as well as crystal growth processes. Here, nanotopography primarily refers to the density of molecular steps on a mineral surface, which are considered to be the most reactive parts of a dissolving or growing mineral surface. In that sense, nanotopography is related to the sample history (e.g. preparation and/or formation of the sample). If the production of the sample material includes precipitation from aqueous solution, nanotopography is related to the degree of supersaturation. Furthermore, if the material has been mechanically treated (e.g. by grinding) surface defects may have been introduced and dissolution or crystal growth processes are linked to the density of surface defects (some of the surface defects may also be intrinsic – independent of the sample treatment). In order to minimize interferences from such issues, the barite powders used for the exchange experiments were pre-equilibrated with a saturated solution. Re-crystallization of the barite powders already started during the four weeks pre-equilibration period. There is hardly any information on this initial stage of the experiments, because the composition of the barite suspensions was analyzed only at the end of this period. It is also well established that crystal morphology affects mineral dissolution and precipitation, because mineral surface reactivity depends on the crystallographic orientation. Nevertheless, in this study a systematic evaluation of kinetic effects due to crystal morphology was not performed.

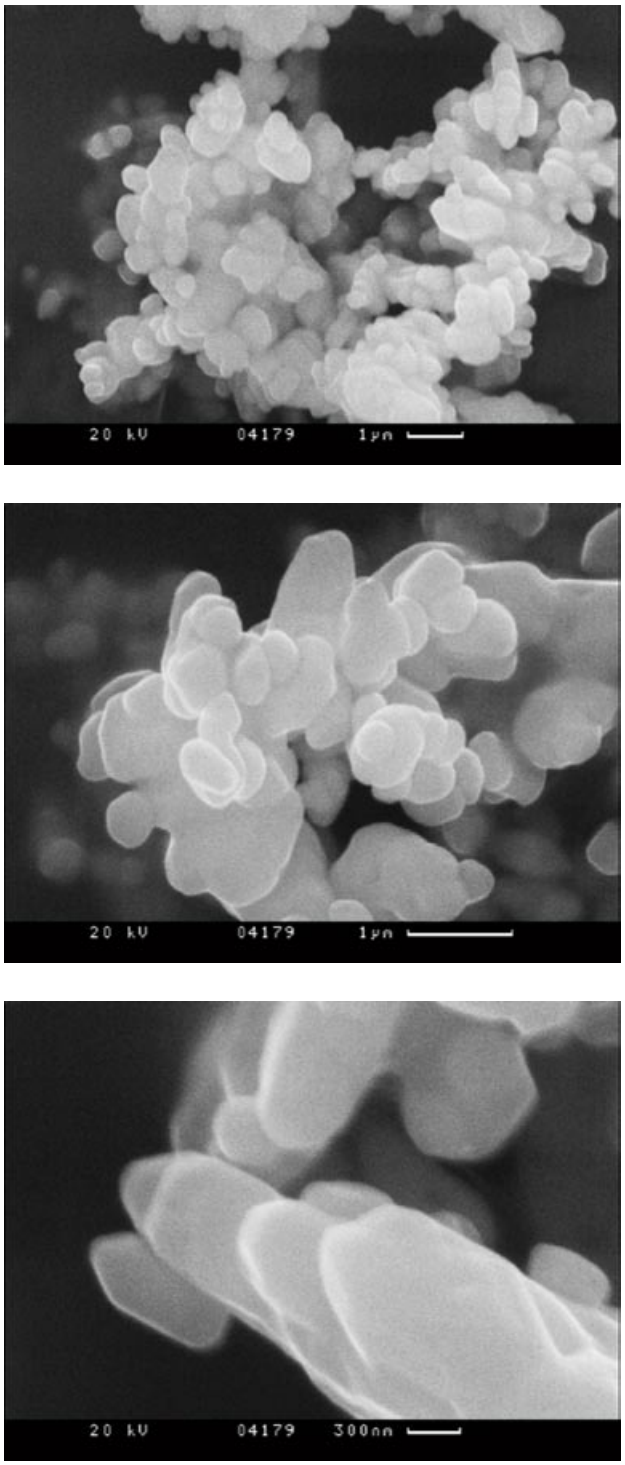

Figure 2-1. *SEM images of SIGMA barite.*

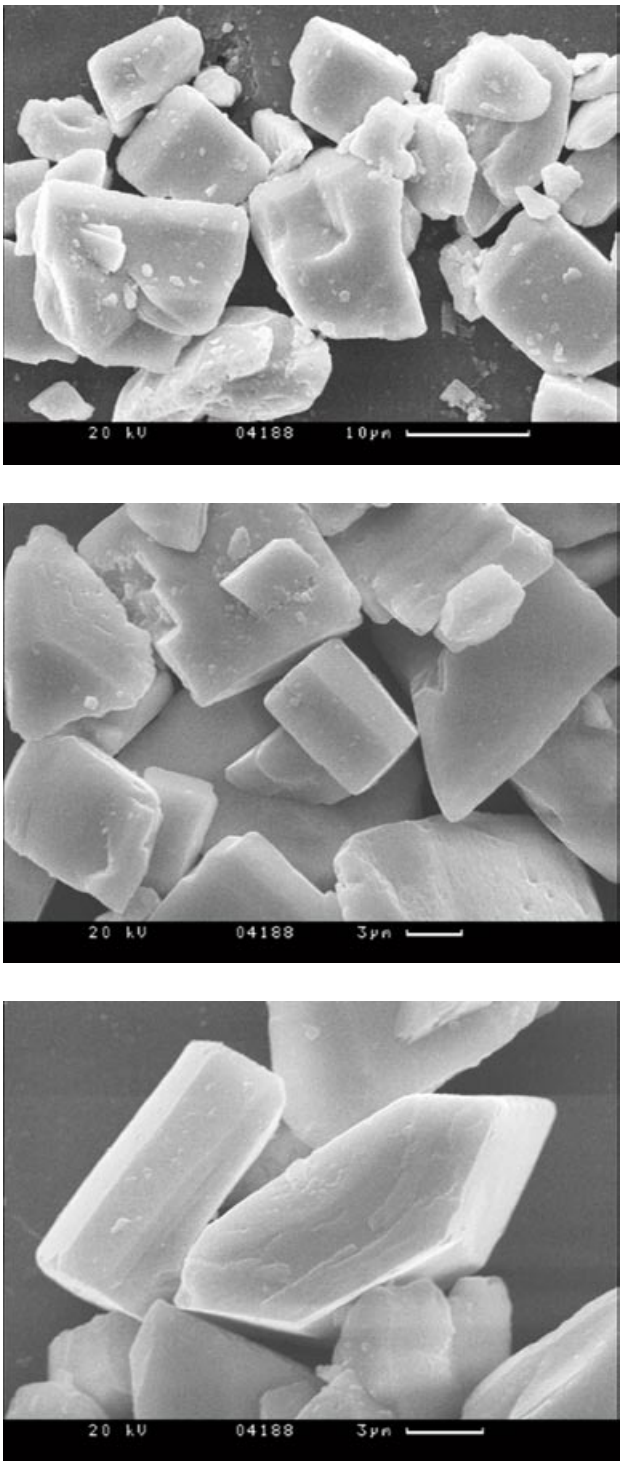

Figure 2-2. *SEM images of SACHTLEBEN barite.*

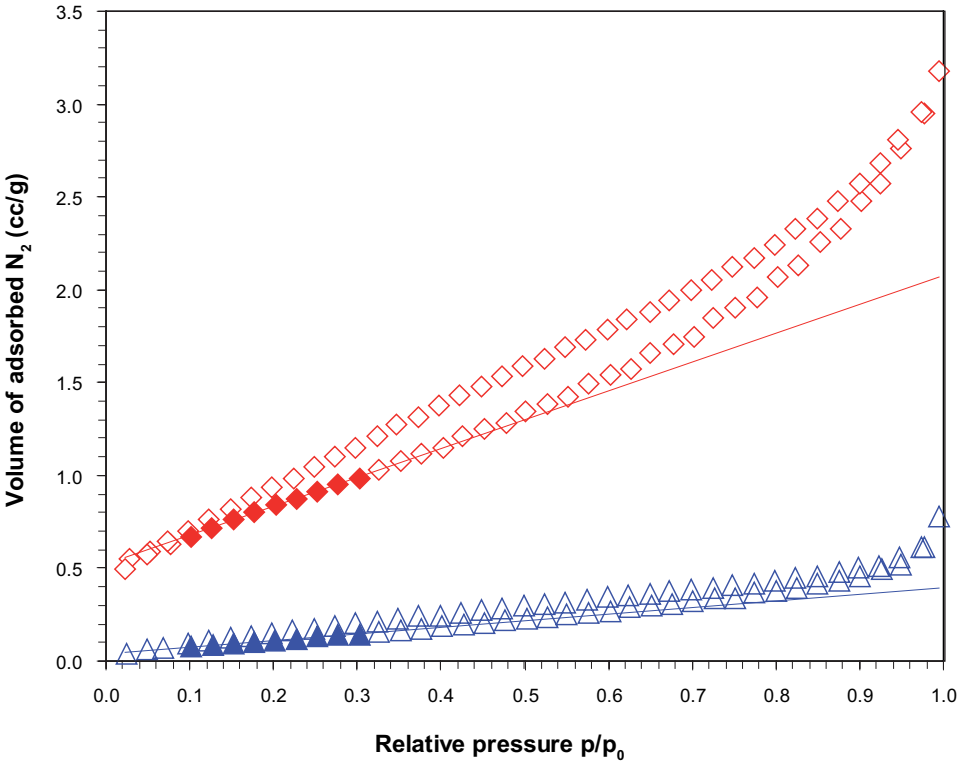

Figure 2-3. *Exemplary N_2 adsorption and desorption isotherms of SIGMA and SACHTLEBEN samples. Data of SIGMA barite are denoted as diamonds and data of SACHTLEBEN as triangles. Filled symbols and regression lines indicate data used for 9-point BET analyses.*

2.3 Analytical methods

Ba^{2+} and SO_4^{2-} concentrations were measured in solutions type (2) and (3) (see section *Preparation of aqueous solutions*) before they had been contacted with barite powder. Barite suspensions of the $^{133}Ba^{2+}$ and $^{226}Ra^{2+}$ batch experiments had not been analyzed for Ba^{2+} and SO_4^{2-}. Sulfate was measured by ion chromatography using a DX300 Dionex, and barium was measured with mass spectrometry using a ICP-MS Perkin Elmer ELAN 6100. Detection limit of the sulfate analysis was at $1 \cdot 10^{-8}$ mol/L with a precision of ± 5%, the detection limit of the barium analysis was $<10^{-10}$ mol/L with a precision of ± 5%. The precision of sulfate measurements was around 30–40% for concentrations close to the detection limit. The pH of the inactive solutions was measured using a ROSS semi-micro combination electrode coupled to a 691pH METROHM pH meter. The estimated precision of these measurements was ±0.3 pH units.

The ^{133}Ba activity in solution was monitored by γ-spectrometry, using a Canberra GX3018-7500SL Germanium detector with an efficiency of >30% at 1.3 MeV. For this purpose the peak area of the 0.356 MeV γ-line emitted from an excited nuclear state of ^{133}Cs after electron capture decay of ^{133}Ba ($^{133}Ba \xrightarrow{\varepsilon\,(10.5a)} {}^{133}Cs$) was analyzed. Solutions with ^{133}Ba activities above ~200 Bq/mL were measured for 10 minutes, whereas solutions with lower activities were analyzed for up to 20 hours in order to lower the detection limit of 0.0075 Bq/mL (corresponding to $1 \cdot 10^{-14}$ mol/L). The analytical uncertainty of the ^{133}Ba measurement is about 5% for most samples of the present study, which have activities significantly higher than the detection limit. The uncertainty is 12% for the lowest ^{133}Ba activity measured in this study (0.03 Bq/mL).

^{226}Ra activity in solution was analyzed by liquid scintillation counting (LSC) and α-spectrometry. Monitoring the ^{226}Ra activity in the experiments was performed by LSC, measuring solution aliquots of 0.1 mL mixed with 10 mL of a LSC-cocktail (Ultima Gold XR, Packard, Meriden) by means of a Tri-Carb 2500 TR/AB LSC device (Canberra, Packard, Meriden). Intensities of the α-peak were used to calculate ^{226}Ra activities. The detection limit for ^{226}Ra of ~1 Bq/mL corresponds to $\sim 10^{-9}$ mol/L. Selected solution aliquots were analyzed by α-spectrometry using a Canberra 74/01 analysis cham-

ber with a PIPS detector and a S100 multi channel analysator. Solution aliquots were evaporated on small stainless steel dishes and then heated to redness prior to measurement in order to avoid thick sample layers showing self-absorption of α-radiation. Detection limit of the α-spectrometry was at 10^{-2} Bq/mL and the precision ± 10% for activities at ~10^2 Bq/mL.

Morphology and particle size of both barite samples were analyzed qualitatively using a scanning electron microscope (CamScan FE44 SEM). The specific surface area of the barite samples was estimated by the Brunauer-Emmett-Teller (BET) method /Brunauer et al. 1938/, using 9 points of the N_2 adsorption isotherms. Nitrogen adsorption and desorption isotherms were measured employing a Quantachrome Autosorb 1 surface area analyzer. At least 0.3 g of sample powder were flushed with He and afterwards outgassed at 85°C in vacuum for at least 24 hours before measurement of the isotherms. The precision of the BET surface area analysis is 10% for samples with $S_{BET} > 1$ m²/g. For samples with 0.1 m²/g ≤ S_{BET} ≤ 1 m²/g the precision is about 20%.

2.4 $^{133}Ba^{2+}$ batch experiments

In order to be able to monitor the exchange reaction, the $^{133}Ba^{2+}$ activity in solution was measured. Therefore it is crucial to select experimental conditions with $^{133}Ba^{2+}$ activity concentrations that allow straight forward application of γ-spectrometry. The exchange kinetics as well the re-equilibrated $^{133}Ba^{2+}$ uptake by barite is affected by the amount of barite powder, the solution volume, the specific surface area/particle size, $^{133}Ba^{2+}$ activity, total Ba^{2+} concentration in solution (defined by solubility product of barite) and the Ba^{2+} to SO_4^{2-} ratio in solution. To accommodate all these aspects, a series of experimental conditions were selected, which are summarized in Table 2-1.

After pre-equilibration of the barite samples in the solution of type (1) to (3), 100 µL of the $^{133}BaCl_2$ stock solution (corresponding to 10^4 Bq = $8.08 \cdot 10^{-12}$ mol ^{133}Ba) were added to the 20 mL barite suspension. Addition of the $^{133}Ba^{2+}$ spike did not significantly change the Ba^{2+} concentration of the aqueous solutions which had been pre-equilibrated with barite powder leading to a barium concentration in the range of 10^{-5} to 10^{-7} mol/L.

Table 2-1. Initial Ba^{2+} (inactive) and SO_4^{2-} concentrations, barite mass, initial saturation indices SI_{BaSO4} and S/V ratios in batch experiments with barite powders and in blank experiments doped with $^{133}Ba^{2+}$. 0.1 mol/L NaCl as background electrolyte and 20 mL total volume were used in all experiments.

Label	Barite	Mass [mg]	Ba^{2+}(i) [mol/L]	SO_4^{2-}(i) [mol/L]	SI_{BaSO4}(i)	S/V [m²/mL]
C001	w/o barite	0	1.5E-07	1.0E-02		blank
C002	SIGMA	10	1.5E-07	1.0E-02	–0.08	0.001
C003	SIGMA	100	1.5E-07	1.0E-02	–0.08	0.01
C004	w/o barite	0	3.0E-05	3.0E-05		blank
C005	SIGMA	10	3.0E-05	3.0E-05	0	0.001
C006	SIGMA	100	3.0E-05	3.0E-05	0	0.01
C007	w/o barite	0	0	0		blank
C008	SIGMA	10	0	0	undersat.	0.001
C009	SIGMA	100	0	0	undersat.	0.01
D001	w/o barite	0	1.5E-07	1.0E-02		blank
D002	Sachtleben	10	1.5E-07	1.0E-02	–0.08	1.6E-04
D003	Sachtleben	100	1.5E-07	1.0E-02	–0.08	1.6E-03
D004	w/o barite	0	3.0E-05	3.0E-05		blank
D005	Sachtleben	10	3.0E-05	3.0E-05	0	1.6E-04
D006	Sachtleben	100	3.0E-05	3.0E-05	0	1.6E-03
D007	w/o barite	0	0	0		blank
D008	Sachtleben	10	0	0	undersat.	1.6E-04
D009	Sachtleben	100	0	0	undersat.	1.6E-03

In experiments C008, C009, D008 and D009 initial solutions were strongly undersaturated with respect to barite or any other solid phase in the Na^+-Ba^{2+}-Cl^--SO_4^{2-}-OH^--H_2O system. Na_2SO_4 and $BaCl_2$:$2H_2O$ were added to experiments C002, C003, C005, C006, D002, D003, D005 and D006. Initial solutions of these experiments were saturated or slightly undersaturated with respect to barite, according to PHREEQC calculations using $K^0_{sp,barite} = 10^{-9.97}$ /Nordstrom et al. 1990, Table 1/. After adding barite powder, the suspensions of the 12 experiments equilibrated within few days. In case the initial solution would have been supersaturated, the observed reduction in $^{133}Ba^{2+}$ activity in the solution would be simply a consequence of crystal growth and not of ion exchange. Taking into account the uncertainties in the barite solubility product, it cannot be completely ruled out, that solutions with high SO_4^{2-} concentration (C002, C003, D002, D003) were slightly supersaturated (see discussion in section Results of batch experiments).

In general sampled solution aliquots of the batch experiments were unfiltered. After more than 580 days two solution aliquots of experiments C003, D003, C008 and D009 were taken: one set of aliquots was filtered with 10 kDalton ultrafilters, and the other set was unfiltered. In the unfiltered aliquots of C003 and D003 $^{133}Ba^{2+}$ concentrations of 0.03 to 0.23 Bq/mL were measured, whereas $^{133}Ba^{2+}$ concentrations in the filtered aliquots were below detection limit of 0.0075 Bq/mL (corresponding to $1 \cdot 10^{-14}$ mol/L). In contrast, experiments C008 and D009 with relatively high $^{133}Ba^{2+}$ concentrations (0.3 to 2.9 Bq/mL) did not show a reduction in $^{133}Ba^{2+}$ concentrations due to filtration with 10 kDalton ultrafilters. It cannot be ruled out that $^{133}Ba^{2+}$ concentrations were reduced by sorption onto the material of the 10 kDalton filters in case of experiments C003 and D003.

It should be mentioned that suspensions of the batch experiments were not stirred. Therefore, the observed exchange kinetics may be affected by transport/diffusion in solution and may not reflect surface reaction controlled dissolution/re-precipitation kinetics. Nevertheless, these rather static conditions may mimic the situation in a waste repository system quite well.

Control (blank) experiments C001, C004, C007, D001, D004 and D007 were conducted without barite powder but with the appropriate initial Ba^{2+} and SO_4^{2-} concentrations (Table 2-1). As in the batch experiments with barite suspension, aliquots of the $^{133}BaCl_2$ stock solution were added to the control experiments to achieve an initial $^{133}Ba^{2+}$ concentration of 500 Bq/ml. Solution aliquots of 0.5 mL were sampled after different time intervals (see Figure 3-1). $^{133}Ba^{2+}$ concentration in aliquots of C001 and D001 filtered with 10 kDalton ultrafilters differed by less than 1% from unfiltered aliquots.

2.5 $^{226}Ra^{2+}$ batch experiments

Two batch type $^{226}Ra^{2+}$ exchange experiments for selected conditions were performed over 436 days. Based on results of the $^{133}Ba^{2+}$ batch experiments, radium batch experiments were started with 0.1 mol/L NaCl solutions without adding Na_2SO_4 and $BaCl_2$:$2H_2O$ (solution type (1) in section *Preparation of aqueous solutions*). In contrast to the $^{133}Ba^{2+}$ – barite exchange experiments, which are compared to parallel running $^{133}Ba^{2+}$ blank experiments, two $^{226}Ra^{2+}$ – barite exchange experiments without blank experiments were conducted. Experimental conditions of the $^{226}Ra^{2+}$ exchange experiments are summarized in Table 2-2.

10 mg of each barite powder were pre-equilibrated for one week in 10 mL NaCl solution. Pre-equilibration of the barite powders before the $^{226}Ra^{2+}$ exchange experiments were shorter than pre-equilibration before the $^{133}Ba^{2+}$ batch experiments. Besides equilibration of the barite topography the aim of the pre-treatment in solution of type (1) was approaching to an equilibrium between the solid and the solution from undersaturation, whereas pre-equilibration in solutions of type (2) and (3) was approaching to an equilibrium between the solid and a solution containing concentrations of Ba^{2+} and SO_4^{2-} close to saturation.

After the pre-equilibration 9 mL of the $^{226}Ra(NO_3)_2$ stock solution were added to each suspension resulting in a pH of 5. Consequently, the initial $^{226}Ra^{2+}$ concentration was $2.95 \cdot 10^{-7}$ mol/L. The drop in pH is neither relevant to saturation with respect of barite nor does it significantly affect kinetics of the $Ba^{2+/226}Ra^{2+}$ exchange.

The batch experiments were subsequently sampled by taking 100 µL solution. $^{226}Ra^{2+}$ concentrations in the solution aliquots were determined by liquid scintillation counting, LSC, during the first 50 days. Few samples taken between 92 and 436 days were analyzed by α-spectrometry.

Table 2-2. Initial barite mass and S/V ratios in $^{226}Ra^{2+}$ equilibration experiments with barite suspensions. 0.1 M NaCl as background electrolyte and 19 mL total volume were used in both experiments.

label	Barite	mass [mg]	S/V [m^2/mL]
R1	SIGMA	10	1.1E-03
R2	Sachtleben	10	1.6E-04

3 Results of batch experiments

3.1 $^{133}Ba^{2+}$ concentrations in control (blank) experiments

In general, the $^{133}Ba^{2+}$ activity in control experiments C001, C004, C007, D001, D004 and D007 scatter between 250 and 220 Bq/0.5 mL and is slightly less (<12%) than the expected 250 Bq/0.5 mL (Figure 3-1). $^{133}Ba^{2+}$ activities of 222 and 224 Bq/0.5 mL were measured in experiments C001 and D001 after 646 and 657 days, respectively.

In the case of runs C001 and D001 one may conclude that there is a slight decrease in the observed $^{133}Ba^{2+}$ activity. A decrease of the activity concentration by <10% is slightly higher than the analytical uncertainty of the γ-spectrometric measurements (about 5%). In these experiments the initial SO_4^{2-} and Ba^{2+} concentrations were $1.0 \cdot 10^{-2}$ and $1.5 \cdot 10^{-7}$ mol/L, respectively. Addition of the $^{133}Ba^{2+}$ spike with a concentration of $4.04 \cdot 10^{-10}$ mol/L and/or inaccurate weighing of the sulfate salts may have generated slightly supersaturated solution. One may argue that the observed slight decrease in $^{133}Ba^{2+}$ concentration may be the consequence of $BaSO_4$(s) precipitation. However, since the blank experiments did not contain any barite, precipitation of barite in these solutions had to be via nucleation. From crystal growth theory it is well known that nucleation required significant supersaturation level – in particular for relatively insoluble compounds such as barite. Moreover, no visible $BaSO_4$(s) precipitates could be identified.

In conclusion, the control (blank) experiments indicate that no separate Ba-phase forms under the experimental conditions used in this study. Furthermore, the results indicate that no significant Ba^{2+} sorption onto the walls of the 20 mL Zinsser flasks takes place.

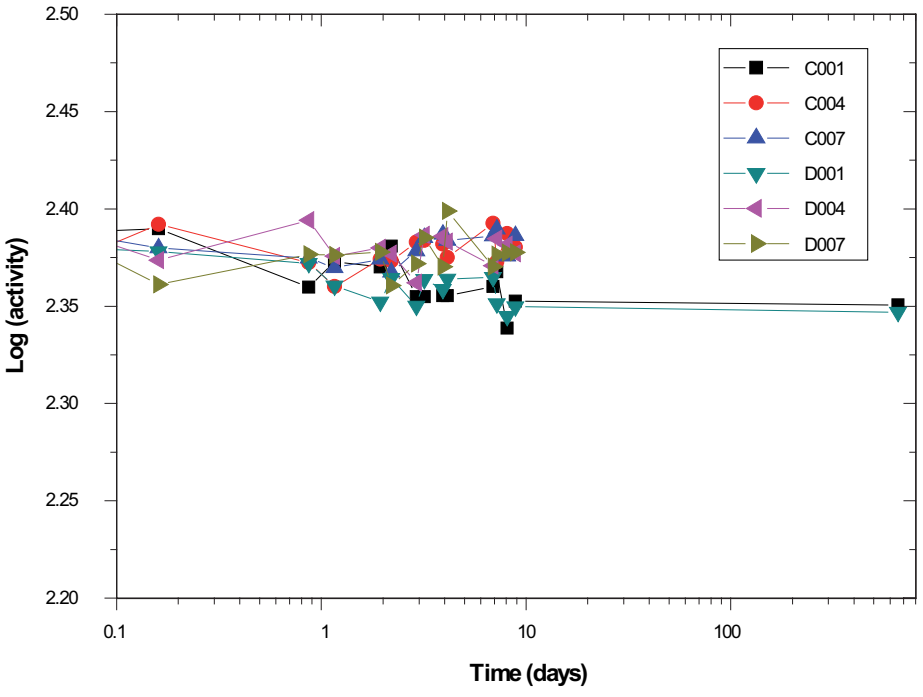

Figure 3-1. *$log_{10}(^{133}Ba^{2+})$ activity versus time in solution of the control experiments without barite powder. Activity is given in units of Bq per 0.5 mL.*

3.2 Variation of $^{133}Ba^{2+}$ concentration in $^{133}Ba^{2+}$ – barite exchange experiments

Figures 3-2 and 3-3 summarize the $^{133}Ba^{2+}$–barite exchange experiments with SIGMA and SACHTLEBEN samples. All batch experiments show a rapid decrease in ^{133}Ba activity within the first ten days. During the first 200 hours, the apparent $^{133}Ba^{2+}$ uptake kinetics varies by two orders of magnitude between experiments which had been saturated with respect to barite from the beginning and initially undersaturated experiments. The fastest decrease in ^{133}Ba activity is observed in experiments with an initial SO_4^{2-} concentration of 10^{-2} mol/L (C002, C003, D002 and D003) corresponding to a relatively low ratio of $Ba^{2+}/SO_4^{2-} = 10^{-5}$ (Figures 3-2 and 3-3). In the initial stage of the batch experiments the change of ^{133}Ba activity with time, $dA(^{133}Ba)/dt$, correlates roughly with the SO_4^{2-} concentration at the beginning of the experiments. Thus, differences in the apparent $^{133}Ba^{2+}$ uptake kinetics are related to mass balance effects on $^{133}BaSO_4$ precipitation rather than to different $^{133}Ba^{2+}$– barite exchange rates.

^{133}Ba activity was monitored relatively frequently in experiments with solution type (1), i.e. initially undersaturated experiments C008, D008, C009 and D009 in order to compare $dA(^{133}Ba)/dt$ with results $^{226}Ra^{2+}$ uptake experiments, which were done in 0.1 mol/L NaCl solution without adding $BaCl_2$ and Na_2SO_4.

Figure 3-4 shows the effect of surface area to solution volume ratio, S/V, on the activity of dissolved $^{133}Ba^{2+}$ in experiments with initially saturated $BaSO_4$ solution (C005, C006, D005, D006). For both types of barite powder, a significantly faster decrease in $^{133}Ba^{2+}$ activity with higher total surface area is observed. However, the decrease rate in experiment C002 (SIGMA barite, $S/V = 1 \cdot 10^{-3}$ m²/mL) is about the same as in experiment D002 (SACHTLEBEN barite, $S/V = 1.6 \cdot 10^{-4}$ m²/mL), indicating that $^{133}Ba^{2+}$ activity is reduced faster in contact with SACHTLEBEN barite than in contact with SIGMA barite. Therefore, it seems that $^{133}Ba^{2+}$ exchange kinetics do not simply scale with specific surface area. At present we do not have a clear explanation for intrinsic effects on the kinetics of $^{133}Ba^{2+}$ exchange with the solid. In order to unravel these details, further systematic experiments would be required. The use of reactive surface area or the number of reactive sites as a measure would probably more suitable. Yet, it is much more difficult to quantify and goes beyond the scope of this study.

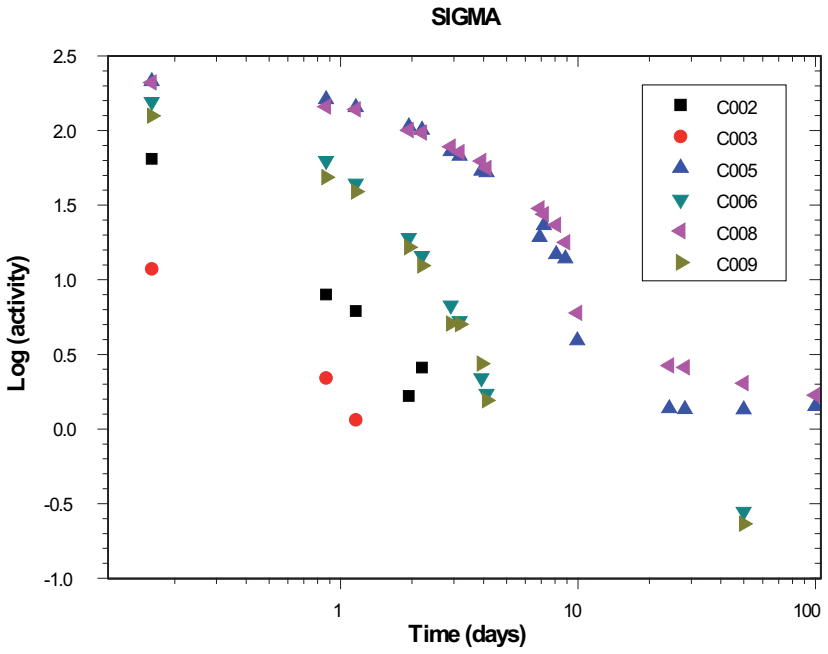

Figure 3-2. *$log_{10}(^{133}Ba^{2+}$ activity) in solution versus time in experiments with SIGMA barite. Activity is given in units of Bq per 0.5 mL.*

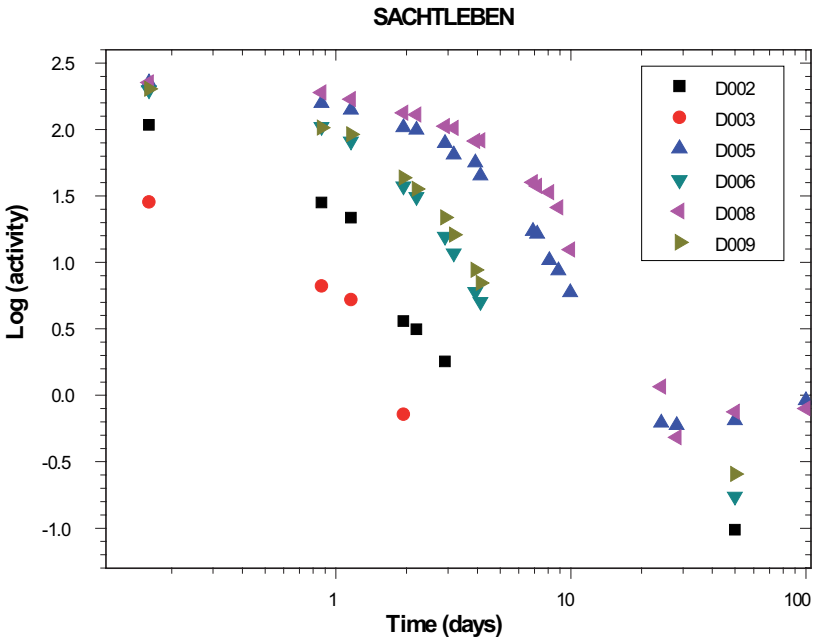

Figure 3-3. *$log_{10}(^{133}Ba^{2+}$ activity) in solution versus time in experiments with SACHTLEBEN barite. Activity is given in units of Bq per 0.5 mL.*

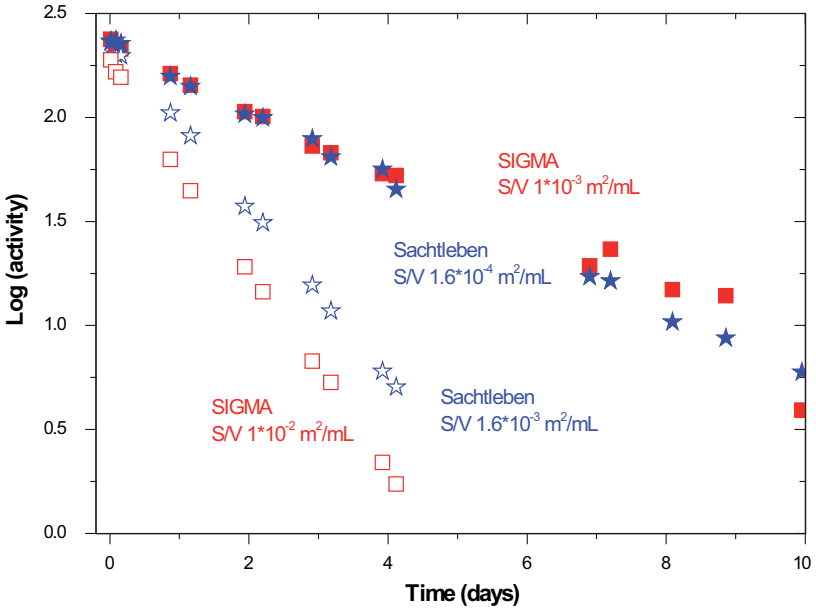

Figure 3-4. *$log_{10}(^{133}Ba^{2+}$ activity) in solution as function of surface area to solution volume ratio during the first 10 days of the experiments. Data of experiments with initially saturated $BaSO_4$ solution are shown. Activity is given in units of Bq per 0.5 mL.*

As described above the first two weeks of the $^{133}Ba^{2+}$ – barite exchange experiments are characterized by a relatively fast decrease of the $^{133}Ba^{2+}$ activity. Experiments C005, C008, D005 and D008 were sampled frequently until 100 days. Since the temporal change of $^{133}Ba^{2+}$ activity, $dA(^{133}Ba^{2+})/dt$, approached close to zero in these experiments, it is assumed that the suspensions equilibrated within the observation period. As shown in Figure 3-5, final measurements show relatively low $^{133}Ba^{2+}$ activities ranging between detection limit and 0.3 Bq/mL in experiments with 100 mg of SIGMA and SACHTLEBEN barite (C003, D003, C006, D006, C009 and D009). $^{133}Ba^{2+}$ activities in experiments C005, D005, C008 and D008 with 100 mg of SIGMA and SACHTLEBEN barite are in the range of 2 to 4 Bq/mL after 100 days (Figure 3-5).

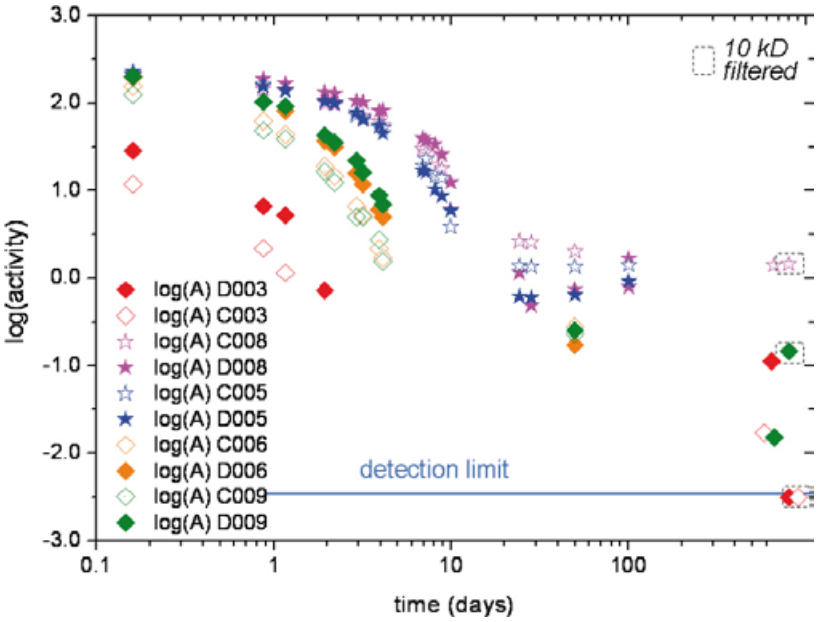

Figure 3-5. *$log_{10}(^{133}Ba^{2+}$ activity) in experiments C003, D003, C005, D005, C006, D006, C008 and D008 as function of time. Activity is given in units of Bq per 0.5 mL. Experiments with SIGMA barite are denoted by open symbols, experiments with SACHTLEBEN barite by closed symbols. The line indicates the detection limit.*

3.3 Variation of $^{226}Ra^{2+}$ concentrations in $^{226}Ra^{2+}$ uptake experiments

From a radioanalytical perspective, experiments with $^{226}Ra^{2+}$ are much more challenging than the $^{133}Ba^{2+}$ experiments due to intrinsic difficulties in measuring the α-decay of $^{226}Ra^{2+}$ and some of the daughters as well as the rather complex decay chain (Table 3-1).

Activities of ^{226}Ra and its daughter nuclides were analyzed using α-spectrometry. The net activities were derived by subtracting the background radiation after each sample measurement (Figure 3-6). Due to their short half-lives the daughters ^{222}Rn (3.8 days), ^{218}Po (3.1 min), ^{214}Po (164.3 µs) should reach a secular equilibrium with ^{226}Ra (1,600 a) within a few weeks. As a consequence, four peaks with identical activities are expected in α-spectra. The energy positions of the observed peaks correspond to the α-decay of ^{226}Ra (4.784 MeV), ^{222}Rn (5.490 MeV), ^{218}Po (6.002 MeV) and ^{214}Po (7.687 MeV) (Figure 3-6). The measured net peak areas correspond to the following activities:

^{226}Ra: 5,148 Bq/mL (= $6.23 \cdot 10^{-7}$ mol/L)

^{222}Rn: 4,504 Bq/mL

^{218}Po: 3,920 Bq/mL

^{214}Po: 3,773 Bq/mL

In the $^{226}Ra(NO_3)_2$ standard solution, activities of ^{226}Ra, ^{222}Rn, ^{218}Po and ^{214}Po are very similar, but not identical. In order to interpret the activity distribution of mainly α-emitting daughter nuclides, the decay of 1 gram ^{226}Ra was calculated using the NUCLIDES-2000 code /Magill 1999, Table 4/.

The observed lower activities of the daughter nuclides, as compared to the ^{226}Ra activity (Figure 3-6), are related to a partial loss of radon during sample preparation and measurements in the evacuated α-spectroscopy chamber. ^{210}Po activity cannot be expected to be in secular equilibrium with parent nuclides. The reason is that the half life of the precursor ^{210}Pb (22.3 a) is too long to reach equilibrium. Only a small α-peak of ^{210}Po can be observed in the spectrum at 5.3 MeV being visible as a shoulder at the low energy side of the ^{222}Rn α-peak (Figure 3-6). The $^{226}Ra(NO_3)_2$ stock solution was originally purchased in 1992. During 16 years (1992–2008) ^{210}Po build-up should amount to 38% of the ^{226}Ra activity (Table 3-2) which is obviously not the case. We can roughly estimate that only about 10% of the ^{210}Po equilibrium activity concentration is present indicating that ^{210}Pb has been separated from our ^{226}Ra stock solution about 3.5 years ago.

Table 3-1. Nuclear properties of ^{226}Ra and its decay products /after Nebelung and Baraniak 2007/.

Nuclide	Half-life	Main energies α (MeV), β (keV (%))
Ra-226 (α)	***1,600 a***	***4.601 (5.5), 4.784 (94)***
Rn-222 (α)	***3.842 d***	***5.490 (100)***
Po-218 (α,β$^-$)	***3.10 m***	***6.002 (99.9)***
Pb-214 (β$^-$)	26.8 m	185.0 (2.8), 672.2 (48.9) , 728.8 (42.2), 1,024 (6.3)
Bi-214 (β-,α)	19.9 m	824.3 (2.8), 1,067 (5.7), 1,135 (4.2), 1,254 (2.2), 1,424 (8.2), 1,507 (17), 1,542 (17.8), 1,728 (3.0), 1,894 (7.4), 3,272 (18.2)
Po-214 (α)	***164.3 µs***	***7.687 (99.99)***
Pb-210 (β$^-$,α)	22.3 a	17.0 (84), 63.5 (16)
Bi-210 (β-,α)	5.031 d	1,162 (100)
Po-210 (α)	***138.4 d***	***5.304 (100)***
Pb-206		

Table 3-2. Calculated decay of 1 gram ^{226}Ra and corresponding activity distribution of daughter nuclides, $A_{\alpha\text{-RN}}$, after 16 years. Only activities of daughter nuclides are given, that mainly have an α-decay mode.

Ra-226, daughters	$A_{\alpha\text{-RN}}$ (Bq)	$A_{\alpha\text{-RN}}/A_{\text{Ra-226}}$
Ra-226 (α)	3.63E+10	
Rn-222 (α)	3.63E+10	100%
Po-218 (α)	3.63E+10	100%
At-218 (α)	7.26E+06	0.02%
Po-214 (α)	3.63E+10	100%
Po-210 (α)	1.39E+10	38%

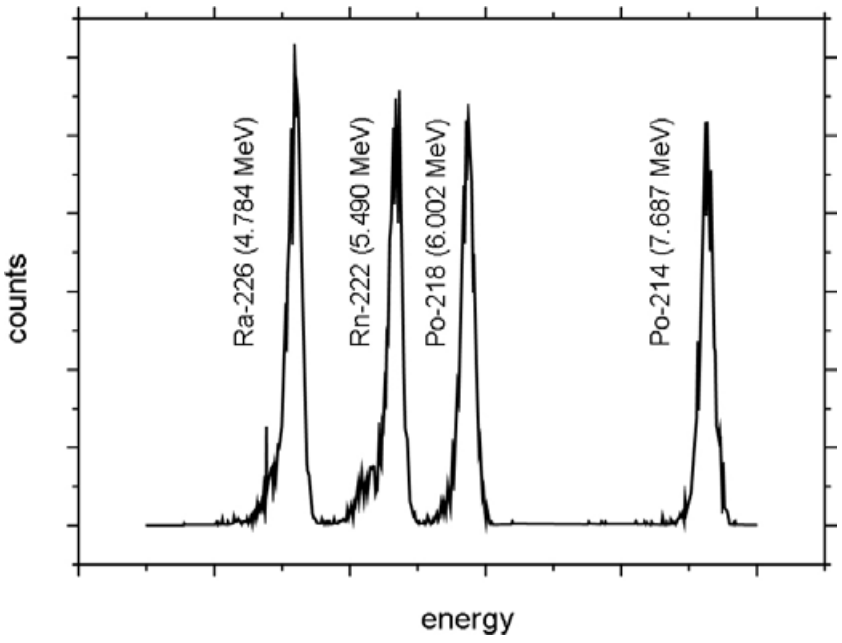

Figure 3-6. *α-spectrum of the $^{226}Ra(NO_3)_2$ standard solution used for the $^{226}Ra^{2+}$ exchange experiments. The $^{226}Ra^{2+}$ activity is 5,148 Bq/mL, which corresponds to a concentration of 0.6 µmol/L.*

Another drawback of such α-spectrometry measurements is that it takes about 24 hours per sample plus background measurements. Therefore, it was only used for reference measurements, whereas routine analysis was done by liquid scintillation counting. A typical LSC spectrum is shown in Figure 3-7. β- and α-decays can be easily distinguished. However, since there are several α-emitters in the decay chain, the broad peak between channels 130 and 630 includes the emissions of ^{226}Ra, ^{222}Rn and ^{218}Po (and ^{210}Po). The specific contributions of these nuclides cannot be resolved with the used analytical method, because they show up as one peak. The ^{214}Po peak at a higher α-energy can be identified separately.

A secular equilibrium will be established between ^{226}Ra, ^{222}Rn, ^{218}Po, ^{214}Po within about four weeks. In such a case, the measured total α-activity in the selected energy interval with LSC should represent four times the ^{226}Ra activity. However, in case of an aqueous solution with ^{226}Ra, ^{222}Rn may partly emanate from the solution and the equilibrium will be disturbed. A secular equilibrium between ^{222}Rn, ^{218}Po and ^{214}Po is established within 3 hours. In that case, the ^{214}Po activity (peak #2 in Figure 3-7) equals the ^{222}Rn and the ^{218}Po activity. Thus, by subtracting the ^{222}Rn and ^{218}Po activity from the ^{226}Ra, ^{222}Rn, ^{218}Po peak (peak #1 in Figure 3-7) gives the ^{226}Ra activity, if secular equilibrium has been established between ^{222}Rn, ^{218}Po and ^{214}Po. We noted that this was not the case for all samples. Appendix B gives a detailed overview of the α-activities measured by LSC during the first 50 days.

The temporal evolution of the apparent $^{226}Ra^{2+}$ activity in solution while in contact with barite is presented in Figure 3-8. The $^{226}Ra^{2+}$ uptake was monitored by LSC during the first 50 days. Although the LSC data presented in Figure 3-8 show a considerable scattering, especially after ten days when the total activity has been reduced, there is a clear trend in the temporal evolution of the aqueous $^{226}Ra^{2+}$ activity. A significant decrease in α-activity in solution by at least one order of magnitude within the first 50 days can be observed. The apparent ^{226}Ra was derived by assuming a secular equilibrium of ^{222}Rn with ^{218}Po and ^{214}Po as outlined above. ^{210}Po activity can be neglected as long as it amounts to only 10% or less of the ^{226}Ra activity. This is certainly the case in the stock solution. However, as will be shown below, ^{210}Po activity cannot be ignored any more when significant $^{226}Ra^{2+}$ uptake by barite has occurred. Therefore, this potential complication has been resolved by α-spectrometric analyses for solutions sampled between 92 to 436 days.

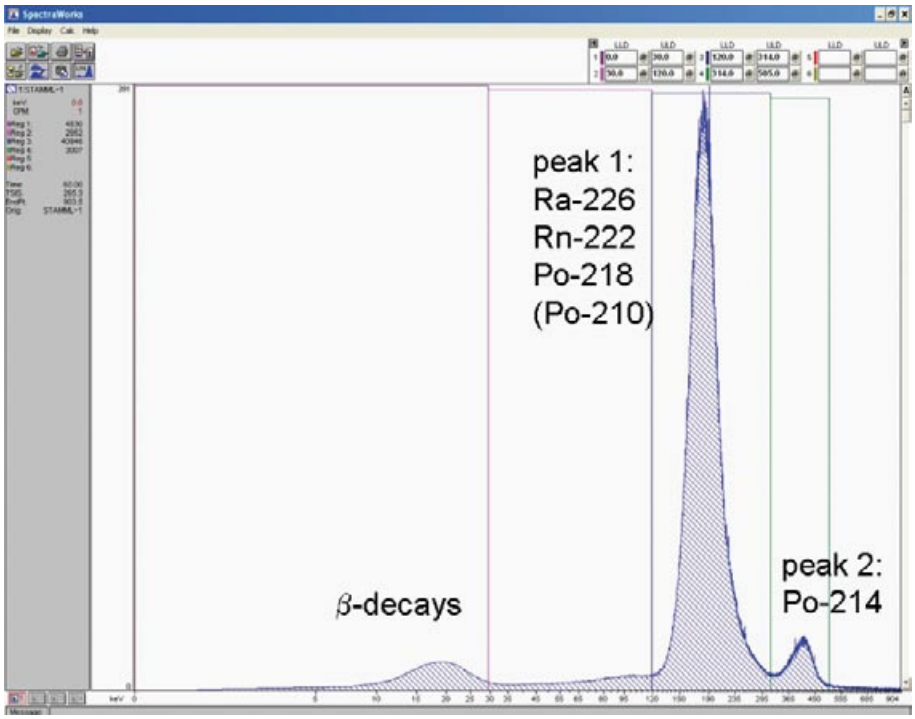

Figure 3-7. *LSC measurement of the $^{226}Ra(NO_3)_2$ standard solution. The β^--decays can be easily distinguished from the α-decays. However ^{226}Ra, ^{222}Rn, ^{218}Po and the relatively small contribution of ^{210}Po cannot be resolved. The contribution of ^{214}Po is observed in the high energy interval.*

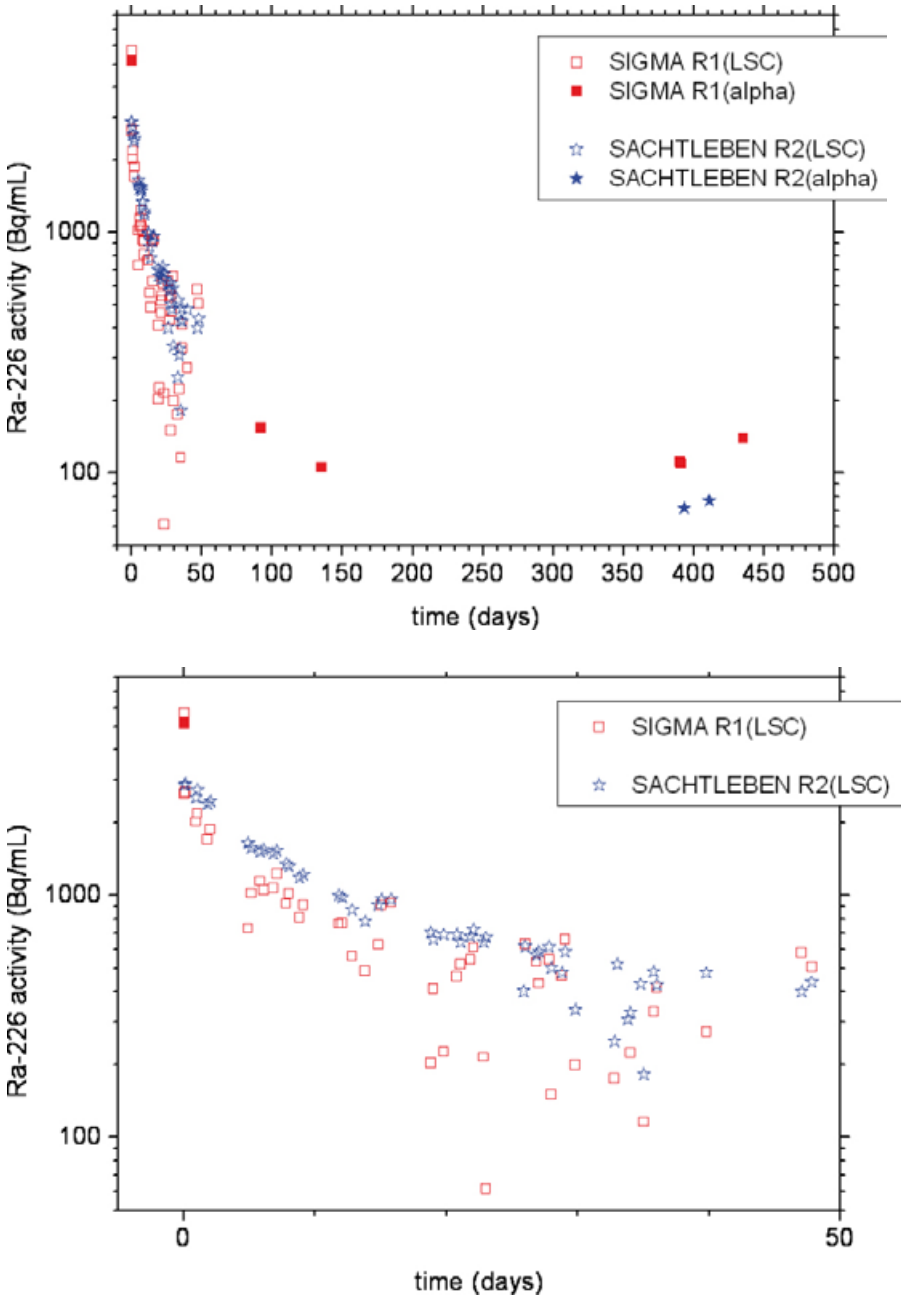

Figure 3-8. *$^{226}Ra^{2+}$ activity in solution versus time in experiments with SIGMA and SACHTLEBEN barite. Open symbols denote activities measured by LSC, closed symbols denote activities measured by α-spectrometry. The upper diagram shows $^{226}Ra^{2+}$ activity over the complete observation period of 435 days, the lower diagram resolves the first 50 days interval which was monitored by LSC.*

Since the LSC data are apparently not reliable for a quantitative interpretation due to a lack of a secular equilibrium and a significant contribution of ^{210}Po, α-spectrometry was used to determine the long-term $^{226}Ra^{2+}$ uptake resulting in low concentrations of dissolved $^{226}Ra^{2+}$. ^{226}Ra activities measured by α-spectrometry between 92 and 436 days are presented in Figure 3-8 and Table 3-3. Unfortunately, α-spectra of experiment R2 sampled after 96 and 139 days showed relatively broad peaks, so that the peaks of ^{226}Ra, ^{210}Po and ^{222}Rn could not be resolved. Apparently, sample preparation for this sample had not been adequate, which led to a relatively thick sample layer and consequently self absorption effects which are responsible for the peak broadening.

Figures 3-9 and 3-10 show two exemplary α-spectra of experiment R1 with SIGMA barite (after 92 and 391 days) and an exemplary α-spectrum of experiment R2 with SACHTLEBEN barite (after 393 days). In these α-spectra five peaks are identified, which correspond to ^{226}Ra, ^{222}Rn, ^{214}Po, ^{218}Po

Table 3-3. ^{226}Ra activities measured by α-spectrometry.

Time (days)	R1 A_{Ra-226} (Bq/mL)	Time (days)	R2 A_{Ra-226} (Bq/mL)
92	155	96	not resolved
135	106	139	not resolved
390	112	393	72
391	110	411	77
435	139		

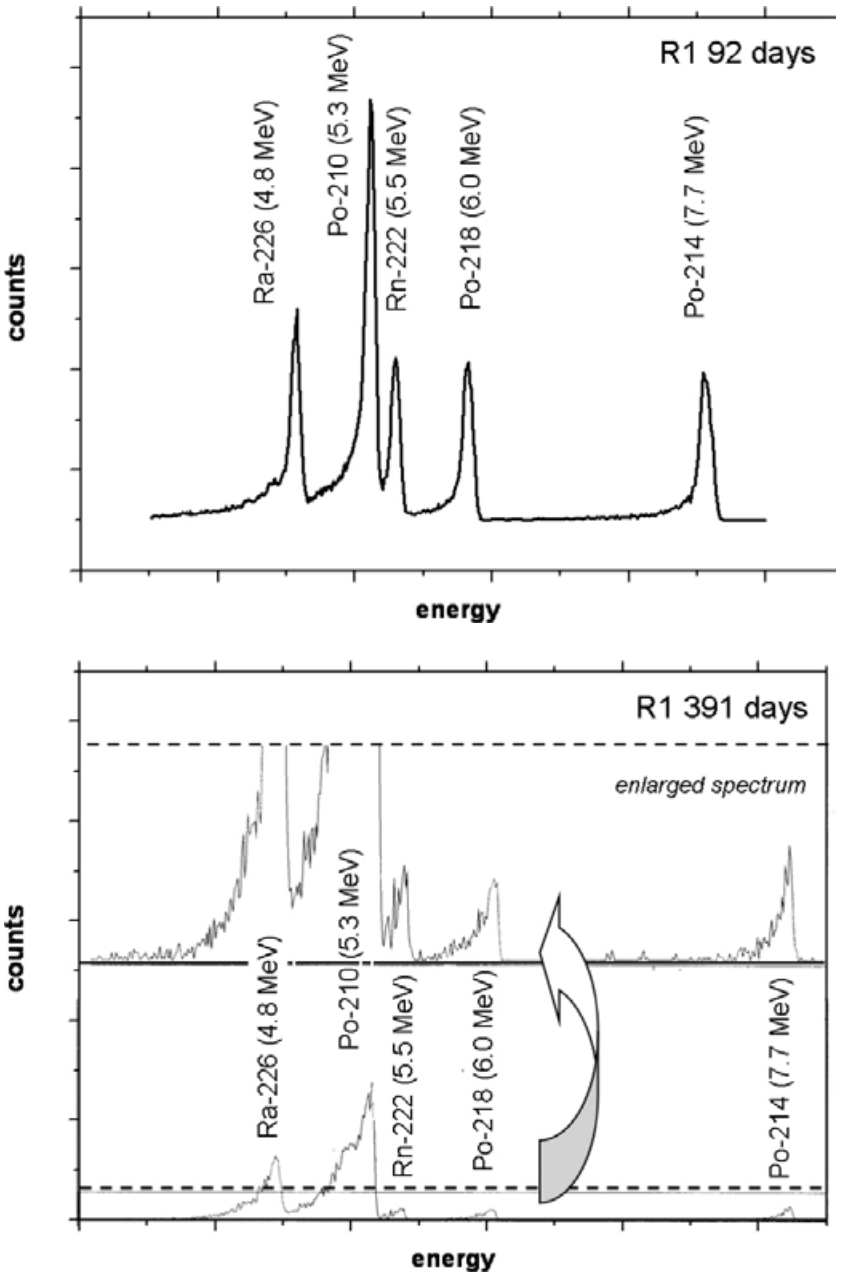

Figure 3-9. *α-spectrometry data of the aqueous solution in experiment R1 with SIGMA barite after 92 and 391 days.*

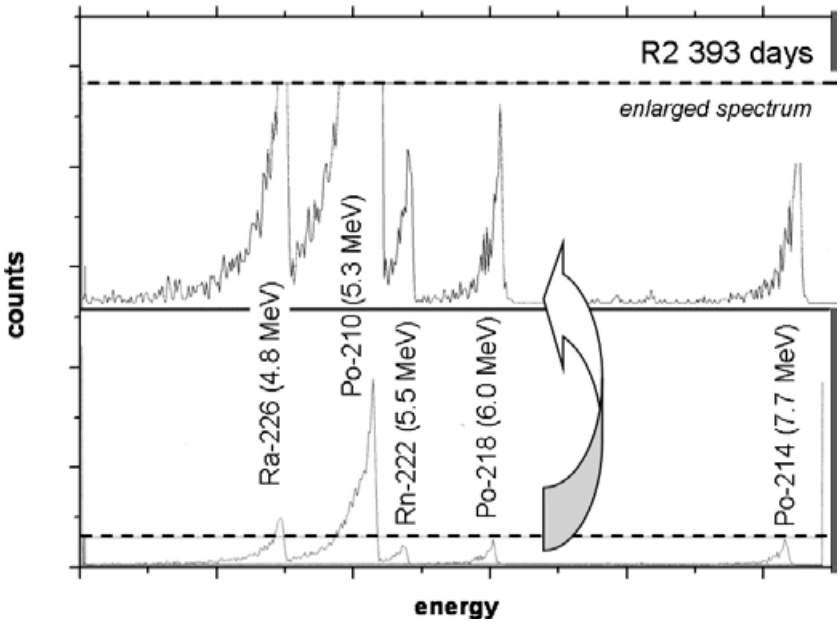

Figure 3-10. *α-spectrometry data of the aqueous solution in experiment R2 with SACHTLEBEN barite after 393 days.*

and ^{210}Po. As in the $^{226}Ra(NO_3)_2$ stock solution, the ^{226}Ra activity is slightly higher than the ^{222}Rn, ^{214}Po and ^{218}Po activities, which indicates a partial loss of ^{222}Rn. Quite interesting is the large peak at 5.3 MeV which represents ^{210}Po. This observation proves that the LSC data for samples with relatively low ^{226}Ra concentrations are obscured by the presence of ^{210}Po.

According to the α-spectrometry data the ^{226}Ra activity in solution decreases in the experiment with SIGMA barite (R1) from 155 Bq/mL after 92 days to 120 ±10 Bq/mL after 390 to 435 days; in the experiment with SACHTLEBEN barite (R2), ^{226}Ra activity in solution (75 Bq/mL) is slightly below the measured activity in experiment R1 (Table 3-3 and Figure 3-8). Since only few long term measurements have been done, both experiments are continued to determine accurately wether a constant $^{226}Ra^{2+}$ concentration, $dC(^{226}Ra^{2+})/dt = 0$, has been attained and at which concentration level they have been fully equilibrated.

The presence of ^{210}Po in the α-spectra (Figure 3-9 and Figure 3-10) shows that while $^{226}Ra^{2+}$ sorbs or forms a solid solution, polonium remains preferentially in the aqueous phase. After 92 to 135 days, the measured ^{210}Po activity in experiment R1 is about a factor of two higher than the ^{226}Ra activity, and this ^{210}Po activity (269–299 Bq/mL) corresponds roughly to the estimated activity in the initially added ^{226}Ra-solution (^{210}Po activity equals about 10% of 2,411 Bq/mL ^{226}Ra). In solutions sampled from experiments R1 and R2 after 390 to 436 days, the ^{210}Po activity is by a factor of 2–3 higher than the ^{226}Ra-activity.

4 Discussion

4.1 Isotopic equilibration of $^{133}Ba^{2+}$ spiked solution with barite

With respect to the question of re-equilibration of a spiked solution with barite, the $^{133}Ba^{2+}$ uptake after an extended period of time is of primary interest. There are various ways to estimate whether equilibrium conditions have been established.

One way is related to the change of $^{133}Ba^{2+}$ activity in solution as a function of time. Figure 3-2, 3-3 and 3-5 show that the rate of $^{133}Ba^{2+}$ removal from solution, which is represented by the slope in the log(activity) versus time plots, $dA(^{133}Ba^{2+})/dt$, is fast during the first 20 days (depending on various parameters as discussed earlier) and slows down significantly afterwards. After about three weeks, $dA(^{133}Ba^{2+})/dt$ is close to zero, as observed in experiments C005, D005, C008 and D008 (Figure 3-5). The $^{133}Ba^{2+}$-barite system apparently approached equilibrium. However, due to the analytical uncertainty it cannot be demonstrated in an absolute sense (in senso stricto) that equilibrium, $\Delta G_r = 0$, has been achieved. Furthermore, it is not clear if equilibrium involves the entire bulk of the barite crystals or is limited to a more or less thin surface coating.

A second way of estimating whether equilibrium has been established is to perform a simple mass balance calculation. As for Ra^{2+} (cf. Equation 1-4), partitioning of the trace component $^{133}Ba^{2+}$ between solution and barite can be described by an equilibrium constant

$$K_{eq} = \frac{K_{sp,barite}}{K_{sp,^{133}BaSO_4}} = \left(\frac{X_{^{133}BaSO_4} f_{^{133}BaSO_4}}{X_{BaSO_4} f_{BaSO_4}} \right) \Bigg/ \left(\frac{[m_{^{133}Ba^{2+}}]}{[m_{Ba^{2+}}]} \cdot \frac{\gamma_{^{133}Ba^{2+}}}{\gamma_{Ba^{2+}}} \right) \quad (4\text{-}1)$$

In the experiments with $^{133}Ba^{2+}$ presented here, one does not expect differences in the γ_{Ba2+} and f_{Ba2+} activity coefficients of different Ba isotopes neither for the solid nor the aqueous phase. Also, the solubility product of the $^{133}BaSO_4$ compound is about the same the solubility product of barite, built up by the stable nuclides ^{138}Ba, ^{137}Ba, ^{136}Ba, ^{135}Ba and ^{134}Ba. Therefore, an equilibrium constant of $K_{eq} = 1$ can be expected.

A simple mass balance calculation considering the measured $^{133}Ba^{2+}$ activity in solution assuming complete re-equilibration is very straight forward since all relevant parameters are known: The amount of initially added barite (10 mg = $4.2753 \cdot 10^{-5}$ mol and 100 mg = $4.2753 \cdot 10^{-4}$ mol), the solution volume (20 mL) and the solution composition (incl. $^{133}Ba^{2+}$ activity). The total barium inventory is defined by the mass of barite, initially added $BaCl_2$ and the $^{133}Ba^{2+}$ spike. According to thermodynamic calculations (using the solubility product $K^0_{sp,barite} = 10^{-9.97 \pm 0.01}$, /Blount 1977, Nordstrom et al. 1990/, barite saturated solutions – with a Ba^{2+} to SO_4^{2-} ratio close to unity contain $3 \cdot 10^{-5}$ mol/L Ba^{2+} and SO_4^{2-} corresponding to $6 \cdot 10^{-7}$ mol per 20 mL (Table 4-1). Since Ba^{2+} and SO_4^{2-} concentrations were not measured in the experiments, the mass balance calculations are based on the assumption of a thermodynamic equilibrium, i.e. solubility controlled Ba^{2+} and SO_4^{2-} concentrations. In the batch experiments there are basically two reservoirs which exchange Ba^{2+}: the solid phase, i.e. barite, and the aqueous solution. The Ba^{2+} inventory in solution is defined by the barite solubility, whereas the Ba^{2+} inventory in the solid equals the amount of barite reduced by the amount of Ba^{2+} released. In case of the initially undersaturated experiments (1) C008 and D008 with 10 mg barite and (2) C009 and D009 with 100 mg barite), the Ba^{2+} inventory in the solid is reduced to $4.2751 \cdot 10^{-5}$ mol (1) and $4.2751 \cdot 10^{-4}$ mol (2), respectively. According to this mass balance, in case of experiments C008 and D008 1.40% of the total Ba^{2+} is in the solution and 98.60% in the solid phase, and 0.14% in solution and 99.86% in the solid in case of experiments C009 and D009. Taking into account the total inventory $^{133}Ba^{2+}$ in suspension ($8 \cdot 10^{-12}$ mol ^{133}Ba per 20 mL) and the calculated distribution between solid and solution, the $^{133}Ba^{2+}$ concentration is calculated for complete re-equilibration. In experiments with 10 mg barite a $^{133}Ba^{2+}$ concentration of $5.7 \cdot 10^{-12}$ mol/L and in experiments with 100 mg barite $5.7 \cdot 10^{-13}$ mol/L are expected (indicated by stippled lines in Figure 4-1). These molarities correspond to $^{133}Ba^{2+}$ activities of $10^{0.5}$ and $10^{-0.5}$ Bq per 0.5 mL. Similar $^{133}Ba^{2+}$ concentrations are calculated for experiments C005, D005, C006 and D006, which had been started already with barite saturated solutions.

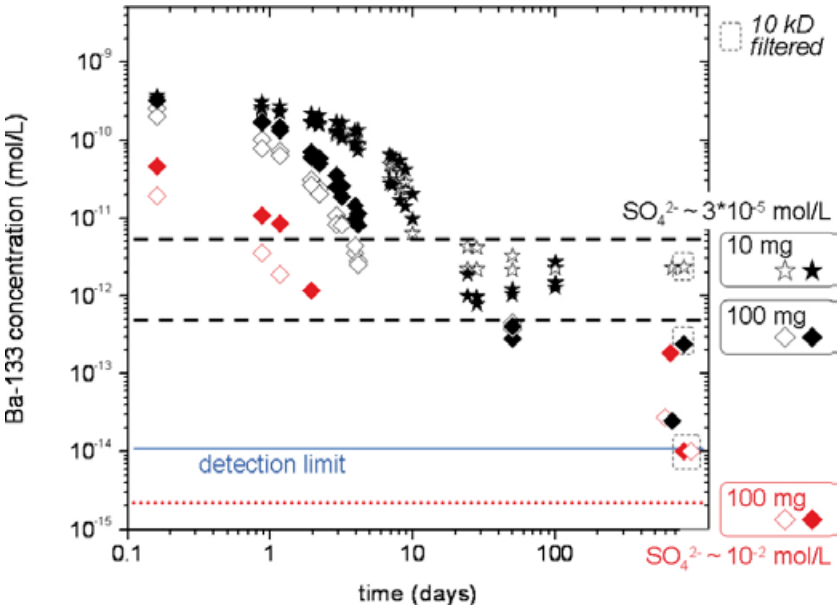

Figure 4-1. *Measured $^{133}Ba^{2+}$ concentrations as function of time compared to $^{133}Ba^{2+}$ concentrations calculated for complete isotopic exchange between barite and aqueous $^{133}Ba^{2+}$. The upper stippled (black) line denotes the expected $^{133}Ba^{2+}$ in solution assuming complete re-equilibration for 10 mg barite; the lower stippled (black) and doted (red) lines denote the expected $^{133}Ba^{2+}$ in solution assuming complete re-equilibration for 100 mg barite, respectively. Stars denote data of experiments with 10 mg barite, diamonds denote data of experiments with 100 mg barite; black symbols and lines denote conditions at $SO_4^{2-} \sim 3 \cdot 10^{-5}$ mol/L; red symbols and lines denote conditions at $SO_4^{2-} \sim 1 \cdot 10^{-2}$ mol/L. The full (blue) line denotes the detection limit.*

Table 4-1. Calculated molal concentrations of Ra^{2+}, $RaCl^+$, Ba^{2+}, $BaCl^+$ and SO_4^{2-}, corresponding log(SI), γ_{Ra2+} and γ_{Ba2+}: (1) 0.1 mol/L NaCl solution saturated with barite and $RaSO_4$(s), (2) initial solution composition of the $^{226}Ra^{2+}$ batch experiments (saturated with barite), (3) 0.1 mol/L NaCl solution with an initial Na_2SO_4 concentration of 0.01 mol/L after saturation with barite.

Condition	$Log(SI_{RaSO4})$	Ra^{2+}	SO_4^{2-}	$RaCl^+$	γ_{Ra2+}
1	0	$2 \cdot 10^{-5}$	$2 \cdot 10^{-5}$	$6 \cdot 10^{-7}$	0.378
2	–1.68	$3 \cdot 10^{-7}$	$3 \cdot 10^{-5}$	$9 \cdot 10^{-9}$	0.378
	$Log(SI_{barite})$	Ba^{2+}	SO_4^{2-}	$BaCl^+$	γ_{Ba2+}
1 and 2	0	$3 \cdot 10^{-5}$	$3 \cdot 10^{-5}$	$4 \cdot 10^{-7}$	0.375
3	0	$1 \cdot 10^{-7}$	$8 \cdot 10^{-3}$	$1 \cdot 10^{-9}$	0.348

Experiments C003 and D003 were conducted with 100 mg barite in 0.1 mol/L NaCl solution containing initially $1.5 \cdot 10^{-7}$ mol/L Ba^{2+} and $1.0 \cdot 10^{-2}$ mol/L SO_4^{2-}. Due to the relatively high SO_4^{2-} concentration, the Ba^{2+} concentration is limited to $1 \cdot 10^{-7}$ mol/L in equilibrium with barite (Table 4-1). According to the mass balance for these conditions only 0.0005% of the total Ba^{2+} is in the solution and 99.9995% in the solid phase. As a consequence, $2 \cdot 10^{-15}$ mol/L ($10^{-2.9}$ Bq per 0.5 mL) $^{133}Ba^{2+}$ is expected for complete re-equilibration.

Figure 4-1 shows a comparison of the $^{133}Ba^{2+}$ concentrations calculated for complete re-equilibration of the $^{133}Ba^{2+}$ – barite suspensions with experimentally determined $^{133}Ba^{2+}$ concentrations. Apparently, after 50 to 100 days the measured $^{133}Ba^{2+}$ is close to the calculated concentration for experiments C008 to D009 with Ba^{2+} and SO_4^{2-} concentrations of about $3 \cdot 10^{-5}$ mol/L. Although there is a significant scattering in the experimental data, it seems that the measured $^{133}Ba^{2+}$ concentrations are slightly below the expected values. Mass balance for experiments C003 and D003 with initially $SO_4^{2-} = 1.0 \cdot 10^{-2}$ mol/L predicts a $^{133}Ba^{2+}$ concentration of $2 \cdot 10^{-15}$ mol/L, which is about one order of magnitude below the detection limit. These experiments were sampled in the first hours and once

after 580 days. With respect to the long-term samples, $^{133}Ba^{2+}$ concentrations in the unfiltered aliquots were between $3 \cdot 10^{-14}$ and $2 \cdot 10^{-13}$ mol/L, whereas in the 10 kDalton filtered samples concentrations were below the detection, i.e. $1 \cdot 10^{-14}$ mol/L (Figure 4-1). It is not clear if the relatively low $^{133}Ba^{2+}$ concentration in ultrafiltered solution aliquots reflects a potential colloidal effect or a retention of $^{133}Ba^{2+}$ onto the material of the 10 kDalton filters. Still, concentrations in the unfiltered solutions of C003 and D003 are significantly lower than in the experiments with $SO_4^{2-} \sim 3 \cdot 10^{-5}$ mol/L and close to the detection limit as predicted by the mass balance (i.e. $^{133}Ba^{2+}$ $2 \cdot 10^{-15}$ mol/L).

The deviation between calculated $^{133}Ba^{2+}$ equilibrium concentrations and experimental results are related rather to experimental uncertainties than to uncertainties in the thermodynamic database. It is questionable if barite solubility is achieved completely within 50 to 100 days in the initially undersaturated experiments C008, C009, D008 and D009. In future it has to be demonstrated that the suspensions are saturated with respect to barite (by determining total Ba^{2+} and SO_4^{2-} concentrations) and that a isotopic equilibration has been achieved (by determining $^{133}Ba^{2+}$ concentrations for extended time interval until $dC(^{133}Ba^{2+})/dt$ equals zero within error. The calculated $^{133}Ba^{2+}$ equilibrium concentration in experiments C003 and D003 is below the detection limit, thus complete re-equilibration cannot be validated unambiguously in the experiments with $SO_4^{2-} \sim 3 \cdot 10^{-5}$ mol/L.

The measured $^{133}Ba^{2+}$ concentrations in solution after 100 days cannot be explained by a surface/surface layer limited exchange reaction, because these processes would cause equilibrium concentration significantly higher than the observed concentrations. With exception of the experiments with relatively high SO_4^{2-} concentration, the experimental data are close to or slightly below the $^{133}Ba^{2+}$ concentrations, which are predicted for complete re-equilibration. Therefore it is concluded that re-equilibration involves the entire mass of barite crystals.

4.2 Equilibration of $^{226}Ra^{2+}$ spiked solution with barite

In both batch experiments with SIGMA and SACHTLEBEN barite samples a decrease of $^{226}Ra^{2+}$ concentration in solution by about one to two orders of magnitude was measured within the observation time. Since the experiments were sampled only three times between 390 and 436 days, there are not sufficient $^{226}Ra^{2+}$ analyses to validate complete equilibration, when the reaction rate is expected to be zero, i.e. $dC(^{226}Ra^{2+})/dt = 0$. Two questions arise from the experimental results: (1) What is the $^{226}Ra^{2+}$ concentration in solution after complete equilibration? (2) To what extent is the $Ra_xBa_{1-x}SO_4$ solid solution equilibrated with the Ra^{2+} spiked solution and is formation of the solid solution limited to a Ra^{2+} containing surface coating or does it involve the entire bulk barite crystals?

Both questions are addressed on the basis of thermodynamic calculations with respect to formation of a $Ra_xBa_{1-x}SO_4$ solid solution. The mixing of $RaSO_4$ and $BaSO_4$ endmembers is assumed to be via a simple substitution where Ra^{2+} occupies a Ba^{2+} lattice site. Considering the similarity of the ionic radii of Ba^{2+} and Ra^{2+} extended mixing can be expected even at relatively low, ambient temperatures. Treating a $RaSO_4$–$BaSO_4$ binary solid solution as an ideal solid solution can be justified (but should be refined/validated at a later stage). The uptake of Ra^{2+} by barite is controlled by the solubility product of the end members – barite and $RaSO_4(s)$ – as well as the Guggenheim interaction parameter for the $Ra_xBa_{1-x}SO_4$ solid solution. A simple mass balance calculation as in the case of the $^{133}Ba^{2+}$ uptake experiments is of course not appropriate. Using PHREEQC and the Nagra/PSI thermodynamic database thermodynamic calculations were performed to interpret the experimental observations. The key parameters for the calculations are related to the **initial solution composition**, the **solid solution thermodynamics** and the **amount of barite** involved. Since neither specific surface area nor any other barite intrinsic parameter are used for the calculations, the results are applicable both to the experiment with SIGMA and SACHTLEBEN barite.

- ***Initial solution composition:*** The initial conditions of the $^{226}Ra^{2+}$ batch experiments R1 and R2 are defined mainly by the concentration of NaCl (0.1 mol/L) and Ra^{2+} ($2.95 \cdot 10^{-7}$ mol/L), a pH value of 5 and a temperature of 20°C. Concentrations of Ba^{2+} and SO_4^{2-} are defined by the solubility of barite. Concentrations of Ra^{2+}, $RaCl^+$, Ba^{2+}, $BaCl^+$ and SO_4^{2-}, corresponding saturation indices and activity coefficients γ_{Ra2+} and γ_{Ba2+} were calculated for the initial solution composition. Additionally theses parameters were calculated for 0.1 mol/L NaCl solutions (free of barite) saturated with $RaSO_4(s)$ (Table 4-1).

- ***Solid solution thermodynamics:*** The thermodynamic description of the $Ra_xBa_{1-x}SO_4$ solid solution follows a regular solid solution model for which the most important thermodynamic equilibrium relations have been given in the introduction (cp. Equations 1-2 to 1-11). For the $Ra_xBa_{1-x}SO_4$ solid solution /Zhu 2004/ estimated a Margules parameter, w_H "of about 210 cal/mol" (page 3330) His estimation is based on the partition coefficient for the Ra^{2+}/barite interaction in 0.005 mol/L HCl determined by /Doerner and Hoskins 1925/. A value of $w_H \approx 210$ cal/mol corresponds to a Guggenheim interaction parameter of $\alpha \approx 0.36$. Additionally, a calculation is conducted, which is based on the assumption of an ideal solid solution ($\alpha = 0$). As will be shown below, the calculation with $\alpha = 0$ yields a solubility of the $Ra_xBa_{1-x}SO_4$ solid solution slightly less than the solubility calculated with $\alpha \approx 0.36$.
- ***Amount of barite*** – The Ra^{2+} exchange experiments R1 and R2 were done with 19 mL aqueous solution and 10 mg of barite powder, corresponding to $2.263 \cdot 10^{-3}$ mol/L BaSO4(s).

The PHREEQC code uses the REACTION option in order to add certain amounts of barite to the initial aqueous solution and calculates the equilibrium condition considering the solubility of the most stable $Ra_xBa_{1-x}SO_4$ solid solution. Following PHREEQC input file was used to calculate $Ra_xBa_{1-x}SO_4$ solubilities, assuming equilibration with 100% and 20% of barite powder:

```
DATABASE NAPSI_290502(260802).DAT
TITLE Radium -Barium Sulfate solid solution
SOLUTION 1
      -units mol/kgw
      Temp 20.0
      pH 5.0
      Na 0.1
      Cl 0.1
      Ra 2.95E-7
SAVE solution 1
END
USE solution 1
SOLID_SOLUTIONS 1
      Ra(x)Ba(1-x)SO4
      -comp RaSO4(cr)  0
      -comp Barite     0
      -Gugg_nondim 0.36
REACTION 1
      Barite 1.0
      2.263E-3
END
```

Results of the calculations for 20% to 100% equilibration are summarized in Table 4-2 and Figure 4-2. Using $\alpha = 0.36$ for complete re-equilibration with the bulk of the barite crystals a solid solution composition $Ra_{0.000131}Ba_{0.999869}SO_4$ is predicted, which limits the Ra^{2+} concentration in solution at $3 \cdot 10^{-9}$ mol/L. About the same solid solution composition and aqueous Ra^{2+} concentration is predicted for the assumption of an ideal solid solution ($\alpha = 0$). When only 20% of the barite powder is equilibrated with the $^{226}Ra^{2+}$, a significantly higher $^{226}Ra^{2+}$ concentration in solution ($1.5 \cdot 10^{-8}$ mol/L) in contact with $Ra_{0.000662}Ba_{0.999338}SO_4$ is predicted.

The measured $^{226}Ra^{2+}$ concentration after 390 days in the exchange experiments R1 and R2 ($1–2 \cdot 10^{-8}$ mol/L and $9 \cdot 10^{-9}$ mol/L, respectively) were about a factor of 3 to 5 above the calculated solubility of the $Ra_xBa_{1-x}SO_4$ solid solution with $\alpha \approx 0.36$ (Figure 4-2). The discrepancy between the measured and calculated $^{226}Ra^{2+}$ concentration may be interpreted as partial equilibration of the barite crystals. Based on the calculated solubility of $Ra_{0.000131}Ba_{0.999869}SO_4$ only 20 to 50% of the barite crystal would have exchanged with $^{226}Ra^{2+}$ within the observation time period. The calculations of the solid solution solubility are based on a relatively small Guggenheim interaction parameter ($\alpha \approx 0.36$) which represents only a slight deviation from ideality. Probably, the regular solution interaction parameter for the $Ra_xBa_{1-x}SO_4$ solid solution is to some extent larger than the value approximated by /Zhu 2004/. Other isostructural solid solutions are described by significantly larger Guggenheim interaction parameters such as $\alpha = 2.34$ for $Sr_xBa_{1-x}SO_4$ or $\alpha = 3.43$ for $Ca_xBa_{1-x}SO_4$ solid solutions, respectively. A value of $\alpha = 1.5$ for the $Ra_xBa_{1-x}SO_4$ solid solution corresponds to an equilibrium $^{226}Ra^{2+}$ concentration of $9 \cdot 10^{-9}$ mol/L (Table 4-2), which is in agreement with the measured concentrations in experiment R2 after 390 days.

Table 4-2. Calculated Ra^{2+} concentration and log(SI_{RaSO4}) controlled by formation of a $Ra_xBa_{1-x}SO_4$ solid solution, assuming equilibration with 100%, 30% and 20% of barite powder. For equilibration with 100% barite, results are given for Guggenheim interaction parameters of α = 0, 0.36 and 1.5.

Equilibrated barite	α	Log(SI_{barite})	log(SI_{RaSO4})	Ra^{2+} (mol/L)	X(Ra)
100% (10 mg)	0.36	0	–3.73	3.0E-09	1.31E-04
100% (10 mg)	0	0	–3.70	2.1E-09	1.31E-04
100% (10 mg)	1.5	0	–3.23	0.9E-08	1.28E-04
30% (3 mg)	0.36	0	–3.20	1.0E-08	4.39E-04
20% (2 mg)	0.36	0	–3.02	1.5E-08	6.62E-04

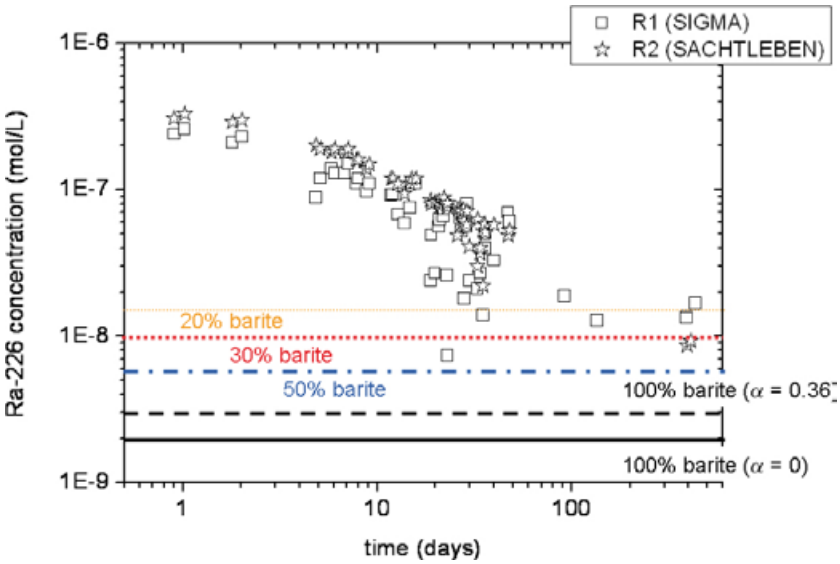

Figure 4-2. *Measured $^{226}Ra^{2+}$ concentrations as function of time compared to $^{226}Ra^{2+}$ concentrations calculated for partial to full equilibration between a $Ra_xBa_{1-x}SO_4$ solid solution and aqueous $^{226}Ra^{2+}$. The lines indicates the calculated $^{226}Ra^{2+}$ in solution assuming 20%, 30%, 50% and 100% equilibration calculated with Guggenheim interaction parameters α = 0.36 (20%, 30%, 50% and stippled line for 100% equilibration) and α = 0 (lower full line for 100% equilibration), respectively.*

5 Conclusions

The applicability of solid solution formation in aqueous systems under nuclear waste repository relevant conditions depends on the availability of (1) a molecular level understanding of the mixing mechanisms, (2) thermodynamic data for the end-members, e.g. the Gibbs free energy of mixing and (3) information on kinetic limitations.

In the first part of this study, equilibration of a $^{133}Ba^{2+}$ containing $BaSO_4$ solution saturated with barite was studied to determine the re-crystallization kinetics of barite under the studied conditions. In conclusion, one can state that during batch type $^{133}Ba^{2+}$ uptake experiments, the exchange of aqueous $^{133}Ba^{2+}$ with barite was neither limited to an interfacial process nor to a thin surface coating. Complete re-equilibration with the bulk of the barite crystals (100% of the total barite mass) was achieved within 100 to 600 days. In the case of $^{133}Ba^{2+}$/barite system the equilibration reaction is purely entropy driven.

In the case of the $^{226}Ra^{2+}$/barite system, the observed $^{226}Ra^{2+}$ concentration is several orders of magnitude below the Ra^{2+} solubility with respect to a pure $RaSO_4$(s) endmember – depending on the geochemical conditions. For the chemical conditions used in these experiments (0.1 mol/L NaCl solution with barite), the solubility of Ra^{2+} was $2 \cdot 10^{-5}$ mol/L if determined by $RaSO_4$(s). Since the aqueous Ra^{2+} was controlled by the solubility of a $Ra_xBa_{1-x}SO_4$ solid solution, an equilibrium concentration of $3 \cdot 10^{-9}$ mol/L was calculated based on a published approximation for the Guggenheim interaction parameter of the solid solution. Considering the calculated solubility of $3 \cdot 10^{-9}$ mol/L for $Ra_{0.000131}Ba_{0.999869}SO_4$, one may conclude that less than 50% of the barite crystals were equilibrated with $^{226}Ra^{2+}$ within the observation period. Alternatively, one may assume complete equilibration and consider the measured concentration of dissolved $^{226}Ra^{2+}$, i.e. $9 \cdot 10^{-9}$ mol/L, as solubility of a $Ra_{0.000128}Ba_{0.999872}SO_4$ solid solution, which corresponds to a 4.2 times higher Guggenheim interaction parameter. In both cases it is concluded that equilibration between aqueous Ra^{2+} and the solid over 435 days reaction time involves a substantial fraction of the barite crystals and proceeds significantly beyond pure surface adsorption processes.

6 Outlook

With respect to the formation of a $Ra_xBa_{1-x}SO_4$ solid solution during barite dissolution and $Ra_xBa_{1-x}SO_4$ re-precipitation it is proposed to extend the experimental run time to at least 2 years. Since only few long term measurements were done, both $^{226}Ra^{2+}$/barite experiments are continued at INE to determine accurately wether a constant $^{226}Ra^{2+}$ concentration, $dC(^{226}Ra^{2+})/dt = 0$, has been attained and at which concentration level the experiments have been fully equilibrated.

Furthermore, it is proposed to initiate similar static batch type exchange experiments with significantly higher Ra^{2+} concentrations and different ionic strengths.

Acknowledgements

The authors would like to thank our colleagues at INE, in particular to A Goertzen, A Bluss, M Fuss, T Kisely, K Scheubeck and E Soballa for carrying out the (radio)chemical analyses, BET and SEM analyses, as well as E Bohnert and C Bube for technical assistance and thermodynamic calculations during the study. We are grateful to H Geckeis and F Heberling, as well as J Ganor and Y Rosenberg, for fruitful discussions and valuable comments regarding the applied radioanalytical methods, solid solution theory and the aquatic geochemistry of radium. The thorough review of the report by E Curti is gratefully acknowledged. His comments considerably helped to improve the study.

7 References

Berner U, Curti E, 2002. Radium solubilities from SF/HLW wastes using solid solution and co-precipitation models. Paul Scherrer Institute, Villigen, Switzerland, Internal Report TM-44-02-04.

Blount C W, 1977. Barite solubilities and thermodynamic quantities up to 300°C and 1,400 bars. American Mineralogist, 62, 942–957.

Brunauer S, Emmett P H, Teller E, 1938. Adsorption of gases in multimolecular layers. Journal of the American Chemical Society 60, 309–319.

Bruno J, Bosbach D, Kulik D, Navrotsky A, 2007. Chemical thermodynamics of solid solutions of interest in nuclear waste management. OECD Nuclear Energy Agency, Elsevier Science Publ. North Holland.

Curti E, 1997. Coprecipitation of radionuclides: basic concepts, literature review and first applications. PSI-Report 97-10, Paul Scherrer Institut, Villigen, Switzerland. Also published as Nagra Technical Report NTB 97-08 by the National Cooperative for the Disposal of Radioactive Waste (Nagra), Wettingen, Switzerland.

Curti E, 1999. Coprecipitation of radionuclides with calcite: estimation of partition coefficients based on a review of laboratory investigations and geochemical data. Applied Geochemistry 14, 433–445.

Doerner H A, Hoskins W M, 1925. Co-Precipitation of Radium and Barium Sulfates. Journal of American Chemical Society 47, 662–675.

Ekberg C, 1999. Uncertainties in actinide solubility calculations illustrated using the Th-OH-PO4 system. Ph. D. thesis, Chalmers University of Technology, Göteborg, Sweden.

Germann F E E, 1921. Adsorption of radium by barium sulfate. Journal of the American Chemical Society 43, 1615–1621.

Glynn P D, 2000. Solid-solution solubilities and thermodynamics: Sulfates, carbonates, and halides. Sulfate Minerals: Crystallography, Geochemistry, and Environmental Significance. C N Alpers, J L Jambor and D K Nordstrom, Mineralogical Society of America 40, 480–511.

Gordon L, Rowley K, 1957. Coprecipitation of Radium with Barium Sulfate. Analytical Chemistry 29, 34–37.

Grandia F, Merino J, Bruno J, 2008. Assessment of the radium-barium co-precipitation and its potential influence on the solubility of Ra in the near-field. SKB TR-08-07, Svensk Kärnbränslehantering AB.

Guggenheim E A, 1937. Theoretical basis of Raoult's law. Transactions of the Faraday Society 33, 151–159.

Hummel W, Berner U R, Curti E, Pearson F J, Thoenen T, 2002. Nagra/PSI chemical thermodynamic data base 01/01. Universal Publishers, Parkland, USA.

Langmuir D, Melchior D, 1985. The geochemistry of Ca, Sr, Ba and Ra sulfates in some deep brines from the Palo Duro Basin, Texas. *Geochimica et Cosmochimica Acta,* 49, 2423–2432.

Langmuir D, Riese A C, 1985. The Thermodynamic Properties of Radium. Geochimica Et Cosmochimica Acta 49, 1593–1601.

Lee J S, Wang H R, Iizuka Y, Shucheng Y, 2005. Crystal structure and Raman spectral studies of $BaSO_4$-$PbSO_4$ solid solution. Zeitschrift für Kristallographie 220, 1–9.

Lind S C, Underwood J E, Whittemore C F, 1918. The solubility of pure readium sulfate. Journal of American Chemical Society 40, 465.

Magill J, 1999. NUCLIDES-2000. An electronic chart of the nuclides. European Commission Joint Research Centre Karlsruhe, Germany.

McIntire W L, 1963. Trace element partition coefficients – a review of theory and applications to geology. Geochimica et Cosmochimica Acta 27, 1209.

Nebelung C, Baraniak L, 2007. Simultaneous determination of Ra-226, U-233 and Np-237 by liquid scintillation spectrometry. Applied Radiation and Isotopes 65, 209–217.

Nikitin B, Tolmatscheff P, 1933. Ein Beitrag zur Gültigkeit des Massenwirkungsgesetzes. II. Quantitative Bestimmung der Löslichkeit des Radiumsulfats in Natriumsulfatlösungen und in Wasser. Zeitschrift fuer physikalische Chemie A167, 260–272.

Nordstrom D K, Plummer L N, Langmuir D, Busenberg E, May H M, Jones B F, Parkhurst D L, 1990. Revised chemical equilibrium data for major water–mineral reactions and their limitations. In: Melchior D C, Bassett R L, eds. Chemical modeling of aqueous systems II. Washington D C, American Chemical Society, ACS Symposium Series 416, 398–413.

Paige C R, Kornicker W A, Hileman O E, Snodgrass W J, 1998. Solution equilibria for uranium ore processing: The $BaSO_4$-H_2SO_4-H_2O system and the $RaSO_4$-H_2SO_4-H_2O system. Geochimica et Cosmochimica Acta 62, 15–23.

Parkhurst D L, Appelo C A J, 1999. PHREEQC 2.15 A computer program for speciation, batch-reaction, one-dimentional transport and inverse geochemical calculation. Water-Resources Investigation Report 99-4259. U.S. Geological Survey.

Rimstidt J D, Balog A, Webb J, 1998. Distribution of trace elements between carbonate minerals and aqueous solutions. Geochimica et Cosmochimica Acta 62, 1851–1863.

Rosenberg Y O, Metz V, Ganor J, 2010. Thermodynamic properties of the Na-Ra-Cl-SO_4-H_2O system: Estimating Pitzer parameters for $RaCl_2$. Submitted to Geochimica et Cosmochimica Acta.

Shannon R D, 1976. Revised effective ionic radius and systematic studies of interatomic distances in halides and chalcogenides. Acta Crystallographica A312, 751–767.

Tesoriero A J, Pankow J F, 1996. Solid solution partitioning of Sr^{2+}, Ba^{2+}, and Cd^{2+} to calcite. Geochimica et Cosmochimica Acta 60, 1053.

Wang Y, Xu H, 2001. Prediction of trace metal partitioning between minerals and aqueous solutions: a linear free energy correlation approach. Geochimica et Cosmochimica Acta 65, 1529.

Zhu C, 2004. Coprecipitation in the Barite isostructural family: 1. Binary mixing properties. Geochimica et Cosmochimica Acta 68, 3327–3337.

Appendix A

^{133}Ba recrystallisation experiments

1 mL of a carrier-free $^{133}BaCl_2$ solution with an activity of 10^7 Bq was purchased from Eckert & Ziegler in January 2008. A stock solution was prepared by diluting 100 µL of that solution (10^6 Bq) to 10 mL (10^5 Bq/mL). 100 µL (10^4 Bq = 8.08E-12 mol ^{133}Ba) of that stock solution was added to the 20 mL barite suspension. Aliquots of 0.5 mL were sampled after different time intervals. The ^{133}Ba activity ($^{133}Ba \xrightarrow{\varepsilon\,(10.5a)} {}^{133}Cs$) in solution was monitored with γ-spectrometry, using a Canberra GX3018-7500SL Germanium detector with an efficienty of >30% at 1.3 MeV instrument. The peak area of the 0.356 MeV gamma line of ^{133}Ba was analysed. In Appendix A, experimental conditions and ^{133}Ba activities during the first 100 days are presented.

C001		
Ba++	1.50E-07	M
SO4--	1.00E-02	M
NaCl	0.1	M
pH	6	
SIGMA barite	0	mg

Sample	Time [d]	Peak area	Activity [Bq/0.5 ml]
C001/01	0.017	3,476	235.34
C001/02	0.087	3,615	244.75
C001/03	0.16	3,624	245.36
C001/04	0.87	3,382	228.98
C001/05	1.16	3,485	235.95
C001/06	1.94	3,463	234.46
C001/07	2.2	3,550	240.35
C001/08	2.91	3,344	226.40
C001/09	3.18	3,343	226.34
C001/10	3.92	3,348	226.68
C001/11	4.12	3,348	226.68
C001/12	6.9	3,384	229.11
C001/13	7.2	3,444	233.18
C001/14	8.09	3,222	218.14
C001/15	8.86	3,326	225.19

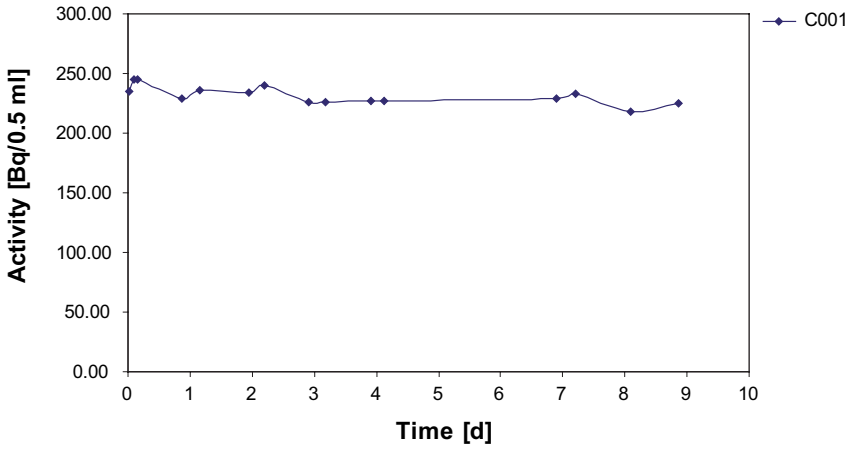

C002		
Ba++	1.50E-07	M
SO4--	1.00E-02	M
NaCl	0.1	M
pH	6	
SIGMA barite	10	mg

Sample	Time [d]	Peak area	Activity [Bq/0.5 ml]
C002/01	0.017	2,022	136.90
C002/02	0.087	1,224	82.87
C002/03	0.16	954.3	64.61
C002/04	0.87	117.7	7.97
C002/05	1.16	91.03	6.16
C002/06	1.94	24.53	1.66
C002/07	2.2	38.09	2.58
C002/08	2.91	63.69	4.31
C002/09	3.18	62.33	4.22
C002/10	3.92	62.33	4.22
C002/11	4.12	0	0.00
C002/12	6.9	0	0.00
C002/13	7.2	0	0.00
C002/14	8.09	65.33	4.42
C002/15	8.86	0	0.00
C002/16	49.88	742.7	0.44

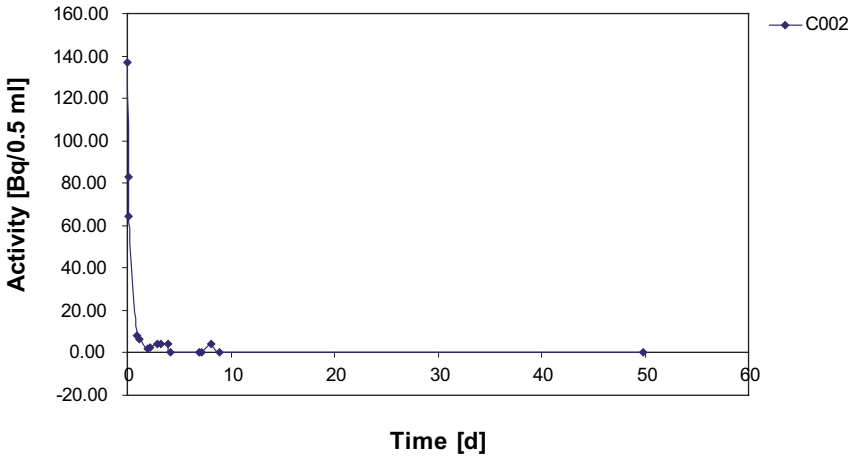

C003		
Ba++	1.50E-07	M
SO4--	1.00E-02	M
NaCl	0.1	M
pH	6	
SIGMA barite	100	mg

Sample	Time [d]	Peak area	Activity [Bq/0.5 ml]
C003/01	0.017	457.7	30.99
C003/02	0.087	273.3	18.50
C003/03	0.16	174.6	11.82
C003/04	0.87	32.42	2.19
C003/05	1.16	16.98	1.15
C003/06	1.94	0	0.00
C003/07	2.2	0	0.00
C003/08	2.91	0	0.00
C003/09	3.18	0	0.00
C003/10	3.92	0	0.00
C003/11	4.12	0	0.00
C003/12	6.9	0	0.00
C003/13	7.2	0	0.00
C003/14	8.09	0	0.00
C003/15	8.86	0	0.00
C003/16	49.88	0	0.00

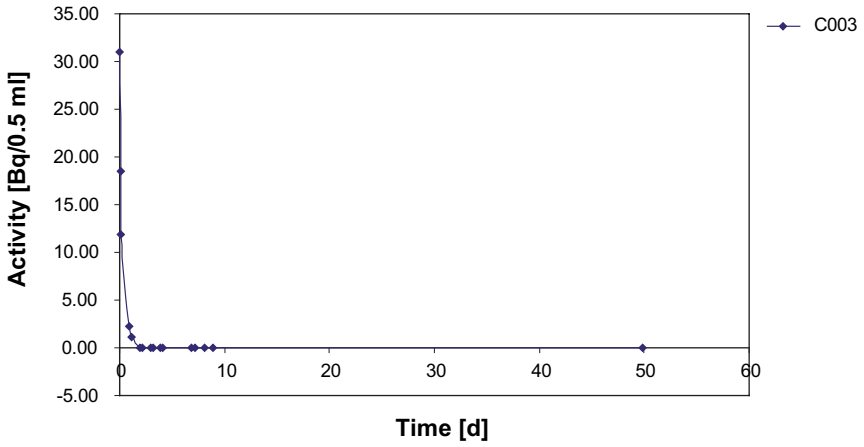

C004		
Ba++	3.00E-05	M
SO4--	3.00E-05	M
NaCl	0.1	M
pH	6	
SIGMA barite	0	mg

Sample	Time [d]	Peak area	Activity [Bq/0.5 ml]
C004/01	0.017	3,578	242.25
C004/02	0.087	3,545	240.01
C004/03	0.16	3,642	246.58
C004/04	0.87	3,482	235.75
C004/05	1.16	3,385	229.18
C004/06	1.94	3,495	236.63
C004/07	2.2	3,489	236.22
C004/08	2.91	3,567	241.50
C004/09	3.18	3,574	241.98
C004/10	3.92	3,559	240.96
C004/11	4.12	3,503	237.17
C004/12	6.9	3,647	246.92
C004/13	7.2	3,484	235.88
C004/14	8.09	3,603	243.94
C004/15	8.86	3,545	240.01

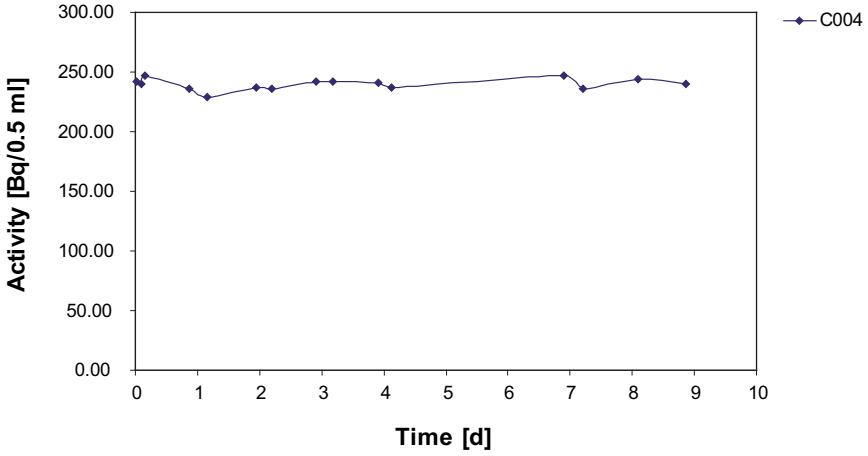

C005		
Ba++	3.00E-05	M
SO4--	3.00E-05	M
NaCl	0.1	M
pH	6	
SIGMA barite	10	mg

Sample	Time [d]	Peak area	Activity [Bq/0.5 ml]
C005/01	0.017	3,512	237.78
C005/02	0.087	3,233	218.89
C005/03	0.16	3,151	213.34
C005/04	0.87	2,394	162.09
C005/05	1.16	2,111	142.92
C005/06	1.94	1,573	106.50
C005/07	2.2	1,493	101.08
C005/08	2.91	1,075	72.78
C005/09	3.18	998.3	67.59
C005/10	3.92	791.8	53.61
C005/11	4.12	775.6	52.51
C005/12	6.9	284.8	19.28
C005/13	7.2	343.3	23.24
C005/14	8.09	219.2	14.84
C005/15	8.86	204.9	13.87
E005/03	9.95	5,994	3.91
E005/05	24.24	1,054	1.38
E005/06	28.19	1,039	1.36
C005/16	49.88	2,301	1.35
C005/17	100.08	2,371	1.42

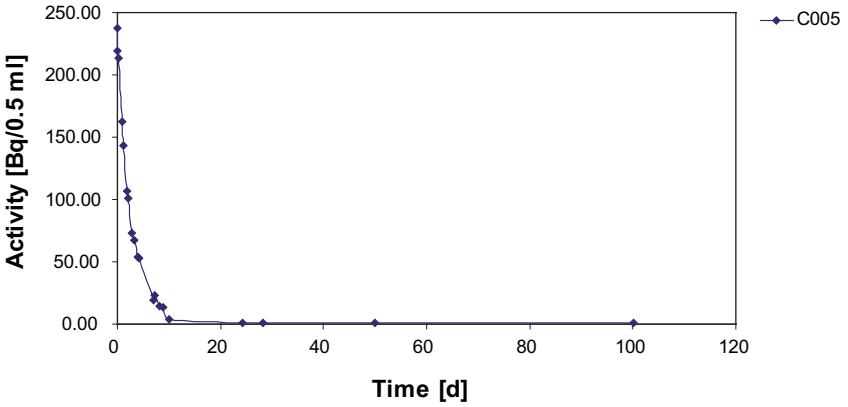

C006		
Ba++	3.00E-05	M
SO4--	3.00E-05	M
NaCl	0.1	M
pH	6	
SIGMA barite	100	mg

Sample	Time [d]	Peak area	Activity [Bq/0.5 ml]
C006/01	0.017	2,789	188.83
C006/02	0.087	2,450	165.88
C006/03	0.16	2,300	155.72
C006/04	0.87	928.5	62.86
C006/05	1.16	654.7	44.33
C006/06	1.94	282.4	19.12
C006/07	2.2	214.3	14.51
C006/08	2.91	99.44	6.73
C006/09	3.18	78.39	5.31
C006/10	3.92	32.35	2.19
C006/11	4.12	25.49	1.73
C006/12	6.9	0	0.00
C006/13	7.2	0	0.00
C006/14	8.09	0	0.00
C006/15	8.86	0	0.00
C006/16	49.88	477.1	0.28

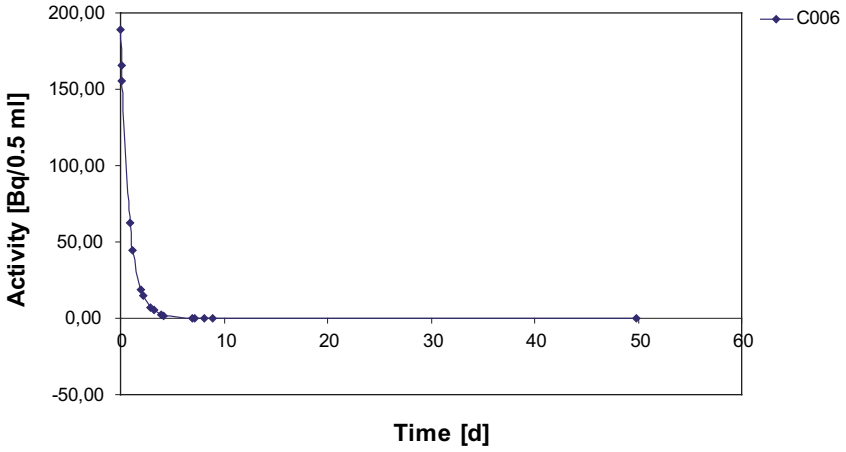

C007		
Ba++	0	M
SO4--	0	M
NaCl	0.1	M
pH	6	
SIGMA barite	0	mg

Sample	Time [d]	Peak area	Activity [Bq/0.5 ml]
C007/01	0.017	3,552	240.49
C007/02	0.087	3,581	242.45
C007/03	0.16	3,543	239.88
C007/04	0.87	3,500	236.97
C007/05	1.16	3,461	234.33
C007/06	1.94	3,495	236.63
C007/07	2.2	3,442	233.04
C007/08	2.91	3,530	239.00
C007/09	3.18	3,586	242.79
C007/10	3.92	3,600	243.74
C007/11	4.12	3,574	241.98
C007/12	6.9	3,593	243.26
C007/13	7.2	3,622	245.23
C007/14	8.09	3,508	237.51
C007/15	8.86	3,595	243.40

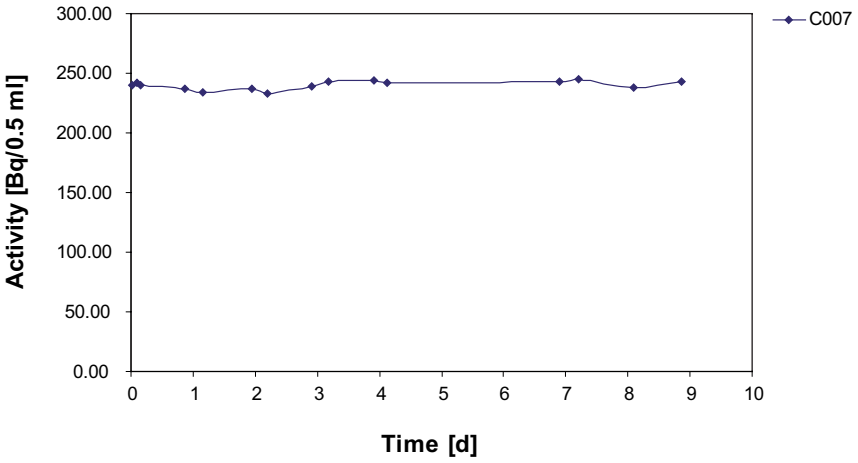

C008		
Ba++	0	M
SO4--	0	M
NaCl	0.1	M
pH	6	
SIGMA barite	10	mg

Sample	Time [d]	Peak area	Activity [Bq/0.5 ml]
C008/01	0.017	3,457	234.06
C008/02	0.087	3,232	218.82
C008/03	0.16	3,093	209.41
C008/04	0.87	2,133	144.41
C008/05	1.16	2,048	138.66
C008/06	1.94	1,482	100.34
C008/07	2.2	1,432	96.95
C008/08	2.91	1,149	77.79
C008/09	3.18	1,058	71.63
C008/10	3.92	920.5	62.32
C008/11	4.12	826.7	55.97
C008/12	6.9	444.3	30.08
C008/13	7.2	405.1	27.43
C008/14	8.09	343.8	23.28
C008/15	8.86	262.6	17.78
E008/03	9.95	4,591	6.00
E008/05	24.24	2,037	2.66
E008/06	28.19	1,979	2.58
C008/16	49.88	3,459	2.03
C008/17	100.08	2,817	1.69

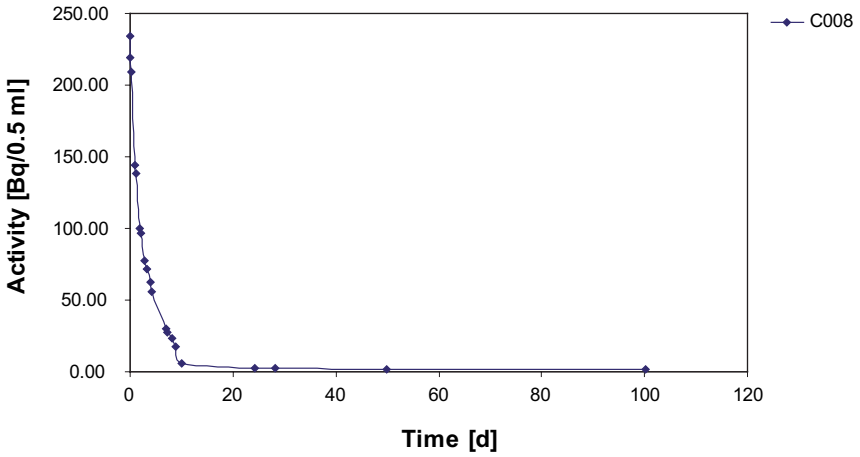

C009		
Ba++	0	M
SO4--	0	M
NaCl	0.1	M
pH	6	
SIGMA barite	100	mg

Sample	Time [d]	Peak area	Activity [Bq/0.5 ml]
C009/01	0.017	2,767	187.34
C009/02	0.087	2,196	148.68
C009/03	0.16	1,856	125.66
C009/04	0.87	720	48.75
C009/05	1.16	576.7	39.05
C009/06	1.94	243.7	16.50
C009/07	2.2	183.8	12.44
C009/08	2.91	74.88	5.07
C009/09	3.18	74.46	5.04
C009/10	3.92	40.53	2.74
C009/11	4.12	22.93	1.55
C009/12	6.9	0	0.00
C009/13	7.2	0	0.00
C009/14	8.09	0	0.00
C009/15	8.86	0	0.00
C009/16	49.88	394.1	0.23

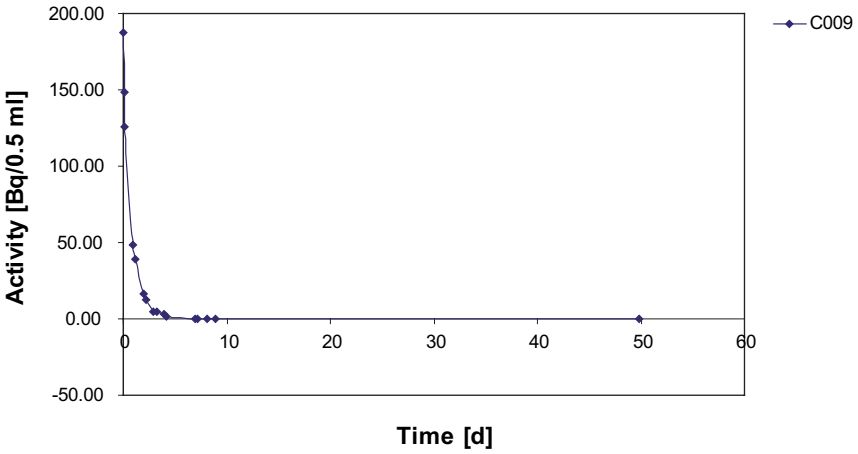

D001		
Ba++	1.50E-07	M
SO4--	1.00E-02	M
NaCl	0.1	M
pH	6	
SACHTLEBEN barite	0	mg

Sample	Time [d]	Peak area	Activity [Bq/0.5 ml]
D001/01	0.017	3,485	235.95
D001/02	0.087	3,538	239.54
D001/03	0.16	3,527	238.79
D001/04	0.87	3,478	235.48
D001/05	1.16	3,387	229.32
D001/06	1.94	3,324	225.05
D001/07	2.2	3,418	231.42
D001/08	2.91	3,307	223.90
D001/09	3.18	3,413	231.08
D001/10	3.92	3,373	228.37
D001/11	4.12	3,414	231.14
D001/12	6.9	3,421	231.62
D001/13	7.2	3,317	224.58
D001/14	8.09	3,267	221.19
D001/15	8.86	3,305	223.76

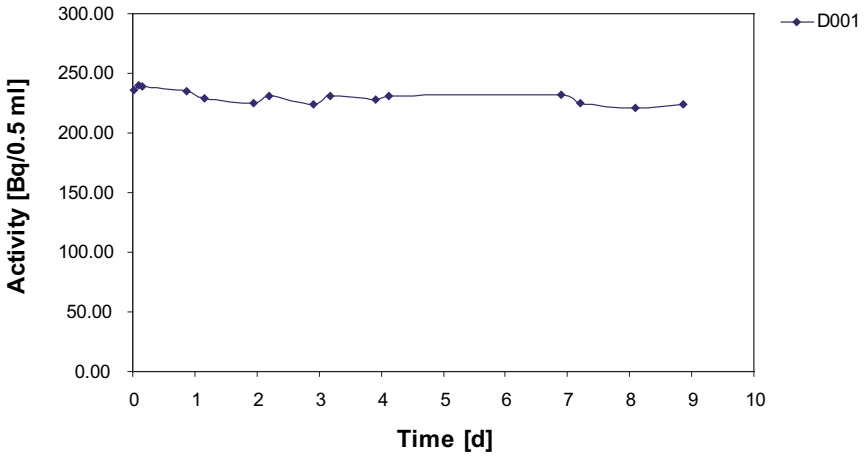

D002		
Ba++	1.50E-07	M
SO4--	1.00E-02	M
NaCl	0.1	M
pH	6	
SACHTLEBEN barite	10	mg

Sample	Time [d]	Peak area	Activity [Bq/0.5 ml]
D002/01	0.017	2,172	147.05
D002/02	0.087	1,715	116.11
D002/03	0.16	1,597	108.12
D002/04	0.87	416.8	28.22
D002/05	1.16	319.3	21.62
D002/06	1.94	53.45	3.62
D002/07	2.2	46.16	3.13
D002/08	2.91	26.45	1.79
D002/09	3.18	0	0.00
D002/10	3.92	0	0.00
D002/11	4.12	0	0.00
D002/12	6.9	0	0.00
D002/13	7.2	0	0.00
D002/14	8.09	0	0.00
D002/15	8.86	0	0.00
D002/16	49.88	165.2	0.10

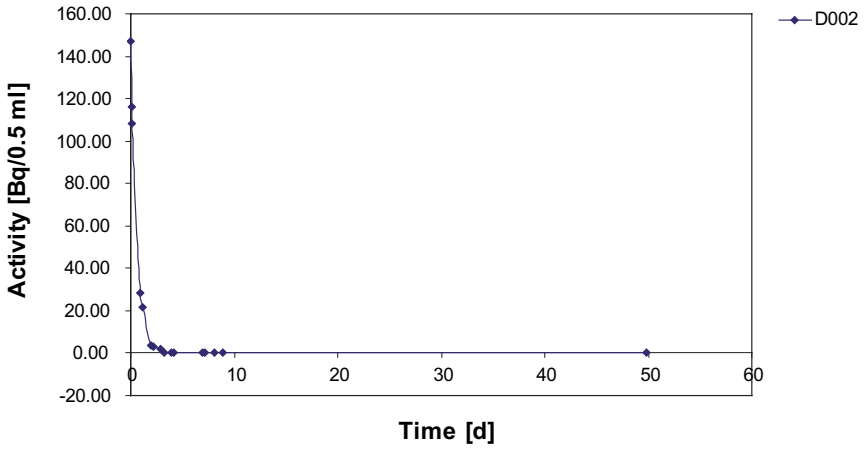

D003		
Ba++	1.50E-07	M
SO4--	1.00E-02	M
NaCl	0.1	M
pH	6	
SACHTLEBEN barite	100	mg

Sample	Time [d]	Peak area	Activity [Bq/0.5 ml]
D003/01	0.017	682.6	46.22
D003/02	0.087	508	34.39
D003/03	0.16	420.2	28.45
D003/04	0.87	98.25	6.65
D003/05	1.16	77.61	5.25
D003/06	1.94	10.61	0.72
D003/07	2.2	0	0.00
D003/08	2.91	0	0.00
D003/09	3.18	0	0.00
D003/10	3.92	0	0.00
D003/11	4.12	0	0.00
D003/12	6.9	0	0.00
D003/13	7.2	0	0.00
D003/14	8.09	0	0.00
D003/15	8.86	73.4	4.97
D003/16	49.88	0	0.00

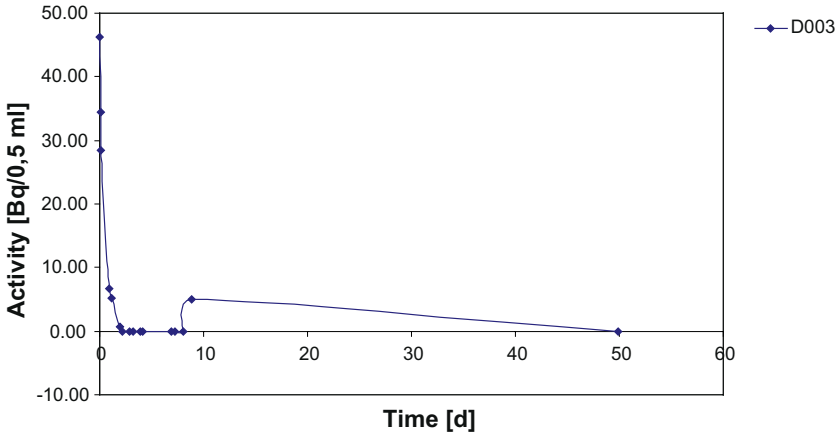

D004		
Ba++	3.00E-05	M
SO4--	3.00E-05	M
NaCl	0.1	M
pH	6	
SACHTLEBEN barite	0	mg

Sample	Time [d]	Peak area	Activity [Bq/0.5 ml]
D004/01	0.017	3,485	235.95
D004/02	0.087	3,568	241.57
D004/03	0.16	3,492	236.43
D004/04	0.87	3,660	247.80
D004/05	1.16	3,508	237.51
D004/06	1.94	3,542	239.81
D004/07	2.2	3,518	238.19
D004/08	2.91	3,399	230.13
D004/09	3.18	3,598	243.60
D004/10	3.92	3,591	243.13
D004/11	4.12	3,569	241.64
D004/12	6.9	3,469	234.87
D004/13	7.2	3,582	242.52
D004/14	8.09	3,556	240.76
D004/15	8.86	3,520	238.32

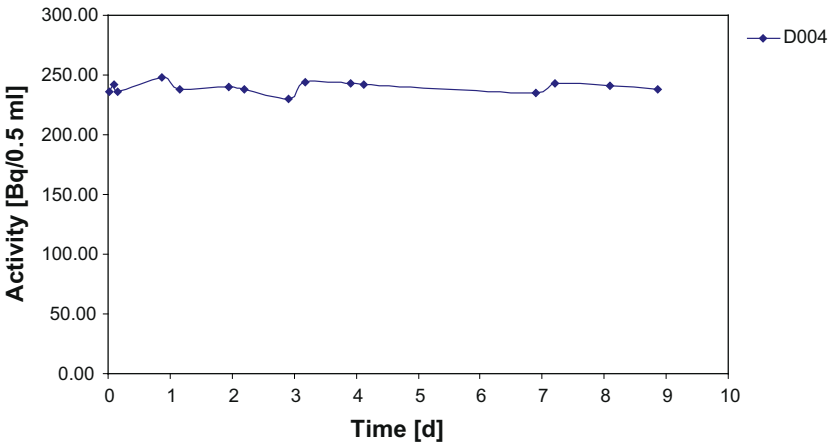

D005		
Ba++	3.00E-05	M
SO4--	3.00E-05	M
NaCl	0.1	M
pH	6	
SACHTLEBEN barite	10	mg

Sample	Time [d]	Peak area	Activity [Bq/0.5 ml]
D005/01	0.017	3,440	232.90
D005/02	0.087	3,474	235.21
D005/03	0.16	3,342	226.27
D005/04	0.87	2,329	157.68
D005/05	1.16	2,078	140.69
D005/06	1.94	1,530	103.59
D005/07	2.2	1,470	99.53
D005/08	2.91	1,167	79.01
D005/09	3.18	953	64.52
D005/10	3.92	833.9	56.46
D005/11	4.12	666	45.09
D005/12	6.9	253.3	17.15
D005/13	7.2	242	16.38
D005/14	8.09	153.6	10.40
D005/15	8.86	128.2	8.68
F005/03	9.95	4,563	5.96
F005/05	24.24	475.4	0.62
F005/06	28.19	455.7	0.60
D005/16	49.88	1,104	0.65
D005/17	100.08	1,531	0.92

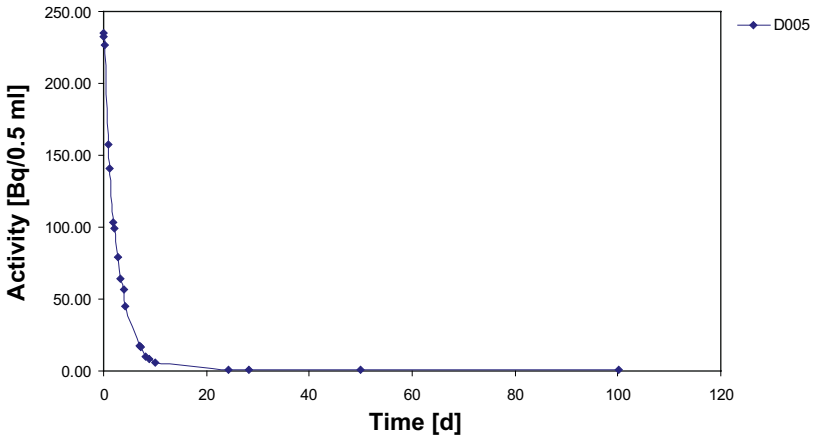

D006		
Ba++	3.00E-05	M
SO4--	3.00E-05	M
NaCl	0.1	M
pH	6	
SACHTLEBEN barite	100	mg

Sample	Time [d]	Peak area	Activity [Bq/0.5 ml]
D006/01	0.017	3,404	230.47
D006/02	0.087	2,975	201.42
D006/03	0.16	2,923	197.90
D006/04	0.87	1,551	105.01
D006/05	1.16	1,204	81.52
D006/06	1.94	552	37.37
D006/07	2.2	459.7	31.12
D006/08	2.91	230.6	15.61
D006/09	3.18	173.2	11.73
D006/10	3.92	88.89	6.02
D006/11	4.12	74.65	5.05
D006/12	6.9	0	0.00
D006/13	7.2	0	0.00
D006/14	8.09	0	0.00
D006/15	8.86	0	0.00
D006/16	49.88	295.7	0.17

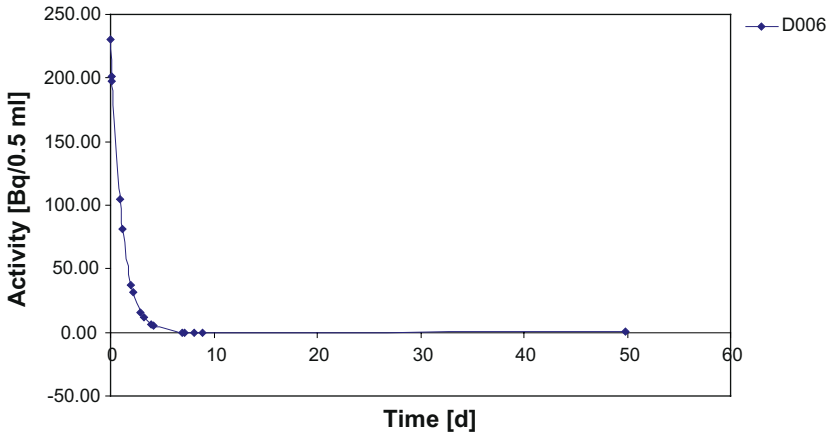

D007		
Ba++	0	M
SO4--	0	M
NaCl	0.1	M
pH	6	
SACHTLEBEN barite	0	mg

Sample	Time [d]	Peak area	Activity [Bq/0.5 ml]
D007/01	0.017	3,539	239.61
D007/02	0.087	3,506	237.37
D007/03	0.16	3,392	229.65
D007/04	0.87	3,516	238.05
D007/05	1.16	3,513	237.85
D007/06	1.94	3,526	238.73
D007/07	2.2	3,389	229.45
D007/08	2.91	3,477	235.41
D007/09	3.18	3,585	242.72
D007/10	3.92	3,464	234.53
D007/11	4.12	3,700	250.51
D007/12	6.9	3,464	234.53
D007/13	7.2	3,514	237.91
D007/14	8.09	3,523	238.52
D007/15	8.86	3,524	238.59

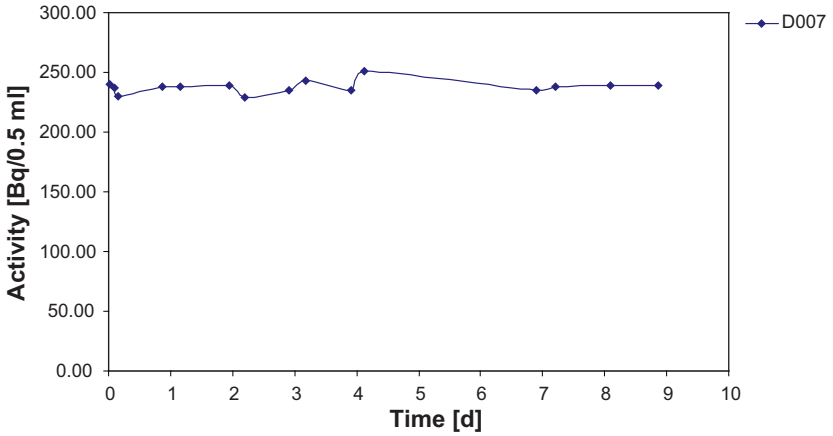

D008		
Ba++	0	M
SO4--	0	M
NaCl	0.1	M
pH	6	
SACHTLEBEN barite	10	mg

Sample	Time [d]	Peak area	Activity [Bq/0.5 ml]
D008/01	0.017	3,582	242.52
D008/02	0.087	3,491	236.36
D008/03	0.16	3,336	225.86
D008/04	0.87	2,798	189.44
D008/05	1.16	2,491	168.65
D008/06	1.94	1,974	133.65
D008/07	2.2	1,909	129.25
D008/08	2.91	1,566	106.03
D008/09	3.18	1,518	102.78
D008/10	3.92	1,207	81.72
D008/11	4.12	1,220	82.60
D008/12	6.9	591.1	40.02
D008/13	7.2	556.5	37.68
D008/14	8.09	498.1	33.72
D008/15	8.86	382.3	25.88
F008/03	9.95	9,558	12.48
F008/05	24.24	888.5	1.16
F008/06	28.19	370.3	0.48
D008/16	49.88	1,282	0.75
D008/17	100.08	1,324	0.79

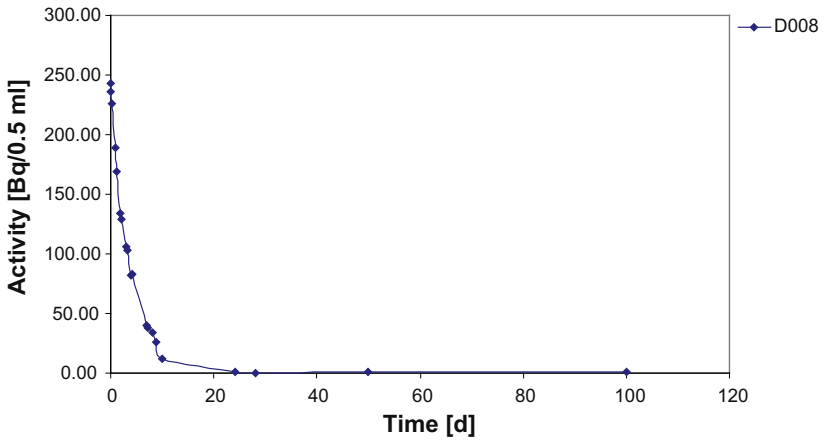

D009		
Ba++	0	M
SO4--	0	M
NaCl	0.1	M
pH	6	
SACHTLEBEN barite	100	mg

Sample	Time [d]	Peak area	Activity [Bq/0.5 ml]
D009/01	0.017	3,387	229.32
D009/02	0.087	3,054	206.77
D009/03	0.16	2,990	202.44
D009/04	0.87	1,524	103.18
D009/05	1.16	1,354	91.67
D009/06	1.94	641.3	43.42
D009/07	2.2	527.4	35.71
D009/08	2.91	321.8	21.79
D009/09	3.18	238.4	16.14
D009/10	3.92	129.7	8.78
D009/11	4.12	103.4	7.00
D009/12	6.9	0	0.00
D009/13	7.2	0	0.00
D009/14	8.09	0	0.00
D009/15	8.86	0	0.00
D009/16	49.88	436.2	0.26

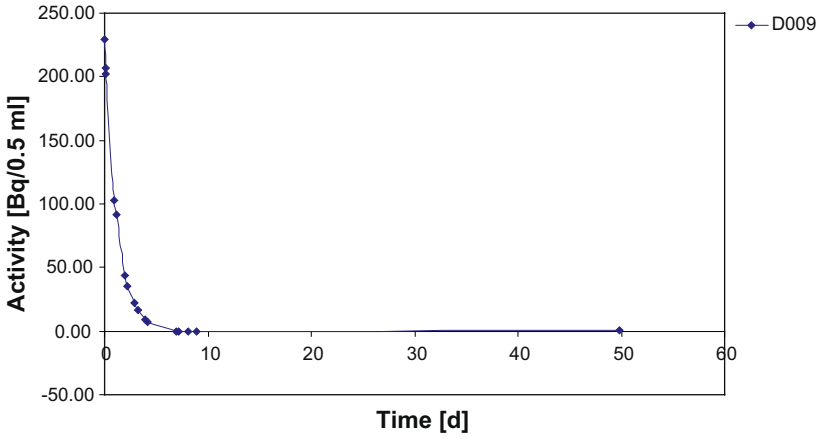

Appendix B

^{226}Ra recrystallisation experiments

The ^{226}Ra activity in solution was determined by using a TRICARB liquid scintillation counter (Canberra Packard 2500 TR). Since there are several α-emitters in the decay chain, the two peaks between channels 130 and 630 are related to these radionuclides – ^{226}Ra, ^{222}Rn and ^{218}Po (and ^{210}Po) cannot be resolved with the used equipment – they show up as one peak. The ^{214}Po peak at higher energy and the lower energy peak of β-emitters can accurately be discriminated.

Appendix B is intended to provide a detailed overview of the measured α-activities by LSC including peak intensities, peak shape, background etc.

Standard

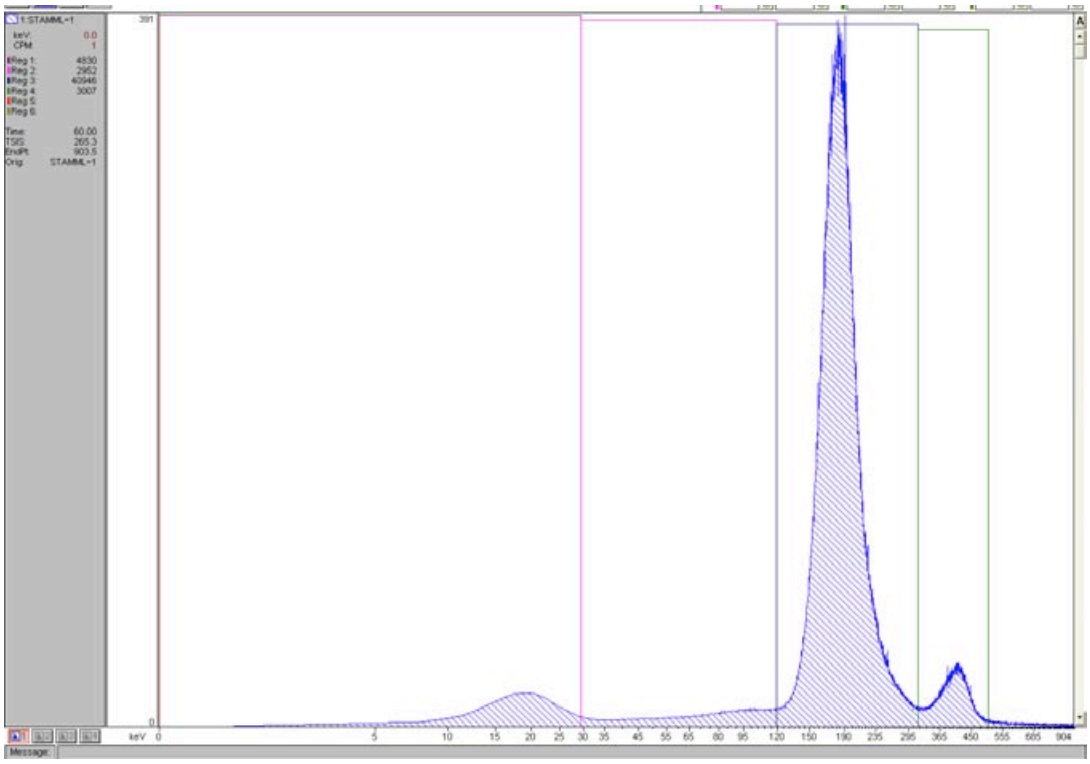

Peak 1: 38,909 [counts]
Peak 2: 2,338 [counts]

R1-01 (0.028 days)

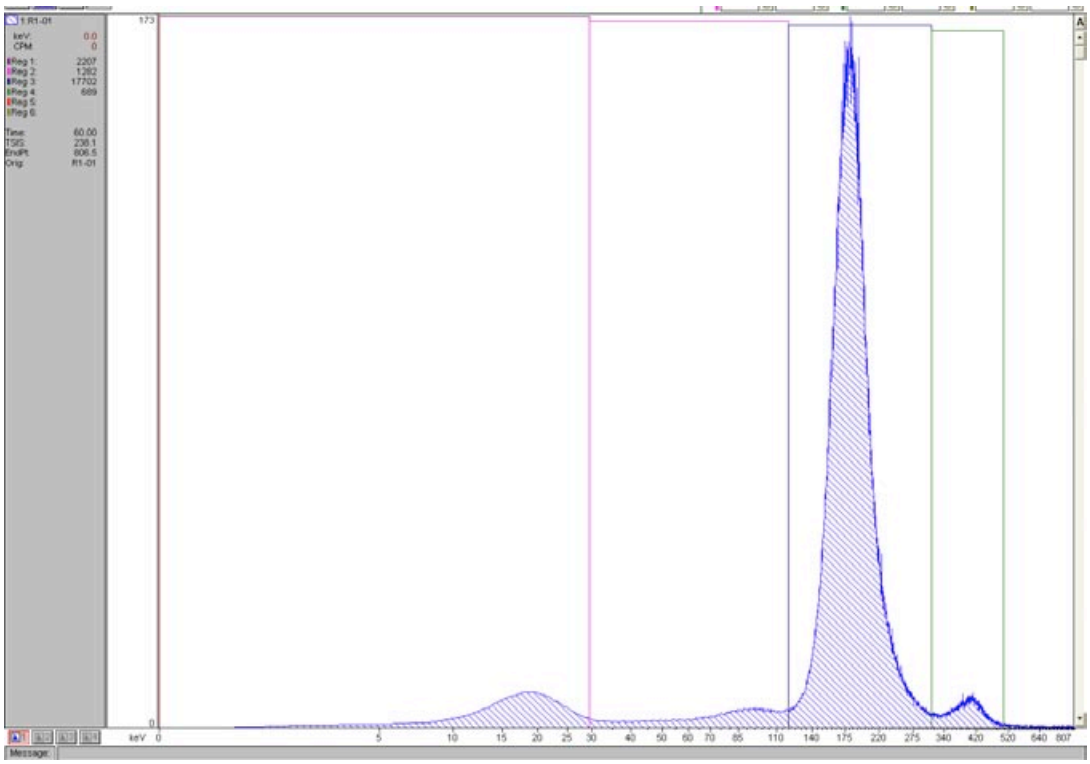

Peak 1: 16,829 [counts]
Peak 2: 498 [counts]

R1-02 (0.108 days)

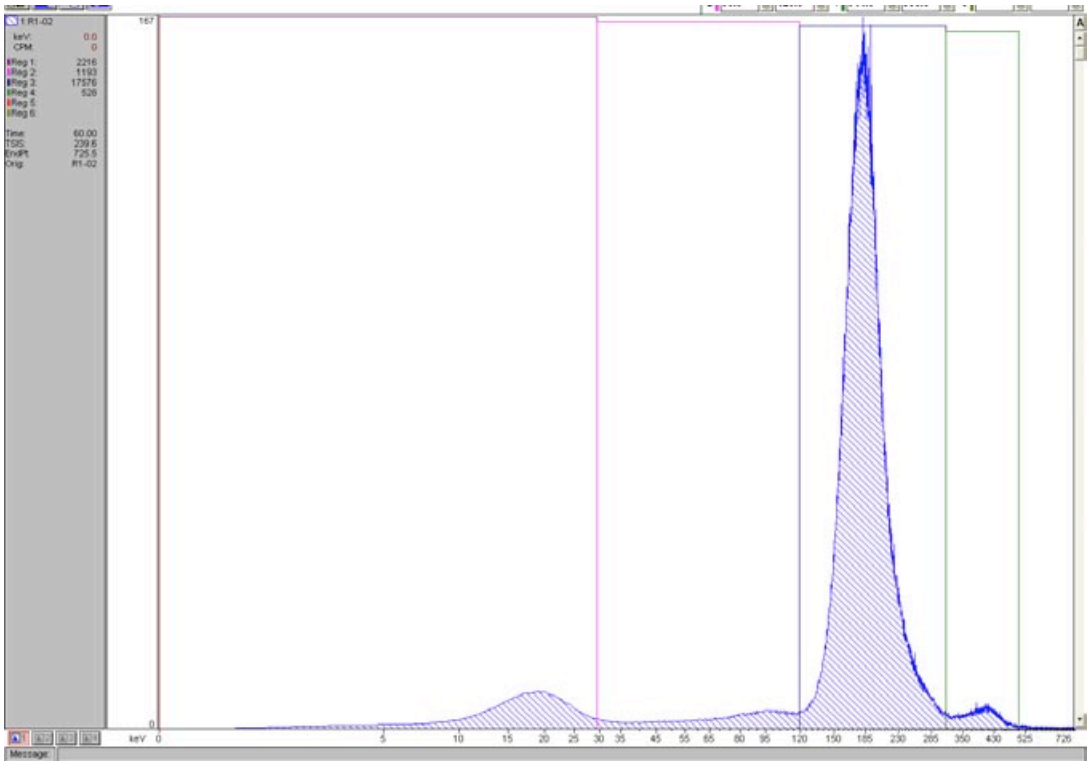

Peak 1: 16,800 [counts]
Peak 2: 337 [counts]

R1-03 (0.903 days)

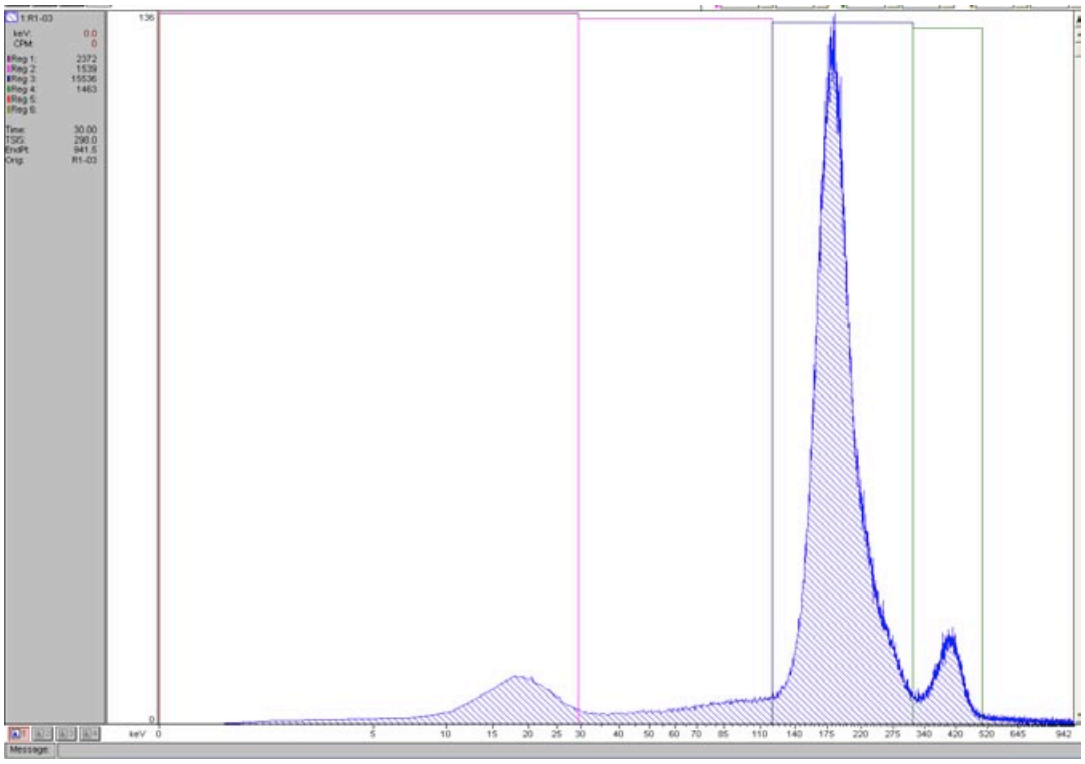

Peak 1: 14,469 [counts]
Peak 2: 1,176 [counts]

R1-04 (1.024 days)

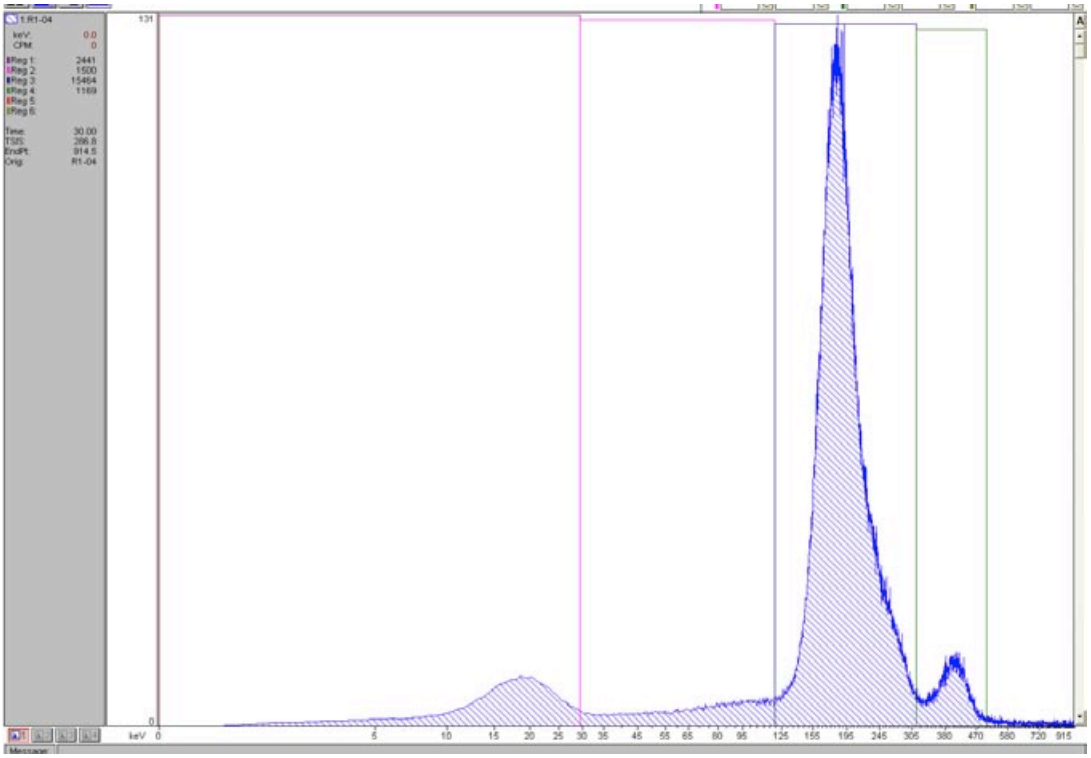

Peak 1: 14,494 [counts]
Peak 2: 691 [counts]

R1-05 (1.802 days)

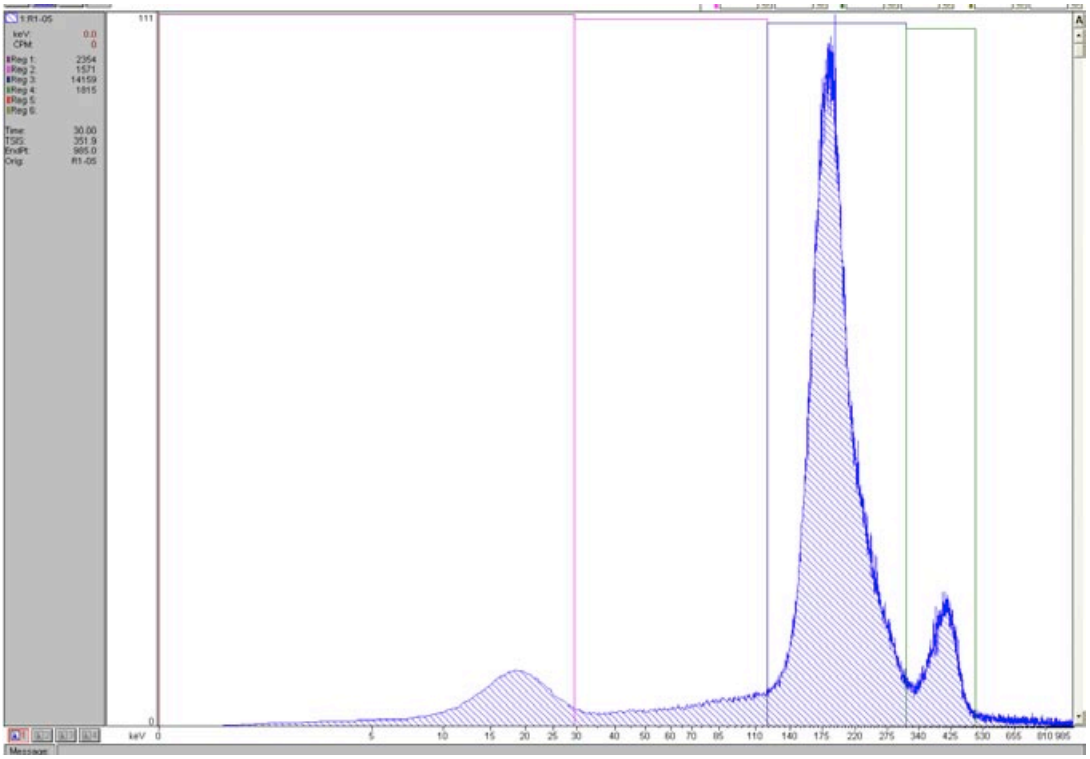

Peak 1: 12,898 [counts]
Peak 2: 1,337 [counts]

R1-06 (2.01 days)

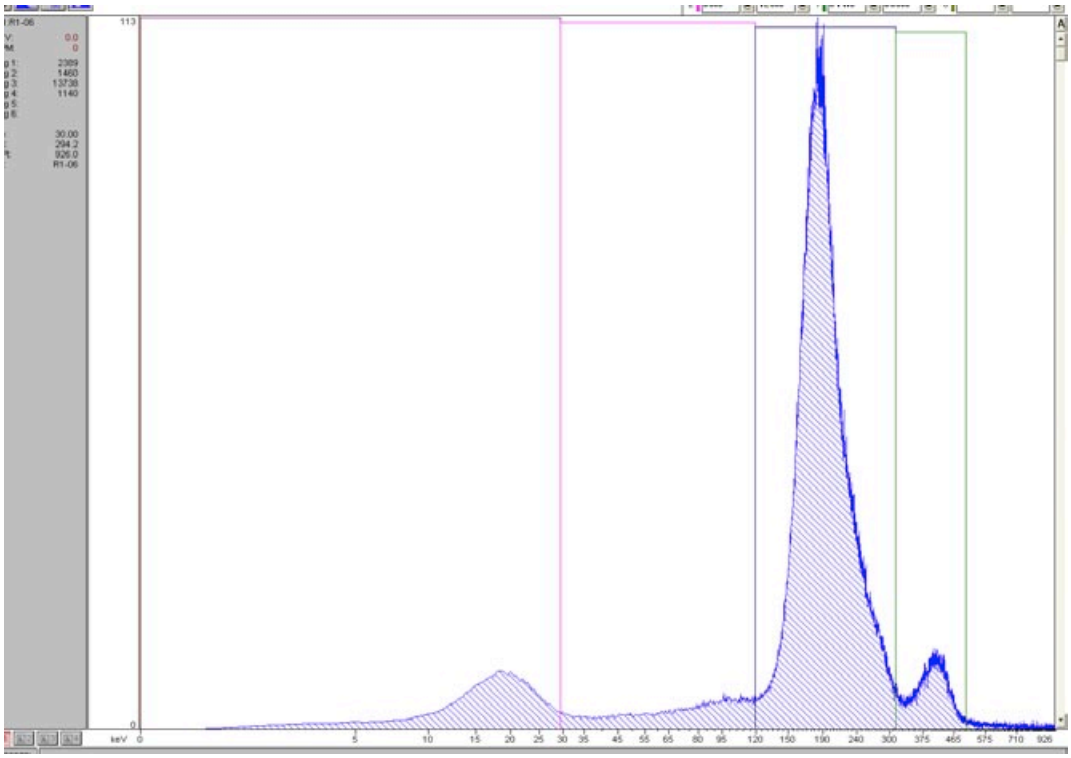

Peak 1: 12,768 [counts]
Peak 2: 758 [counts]

R1-07 (4.858 days)

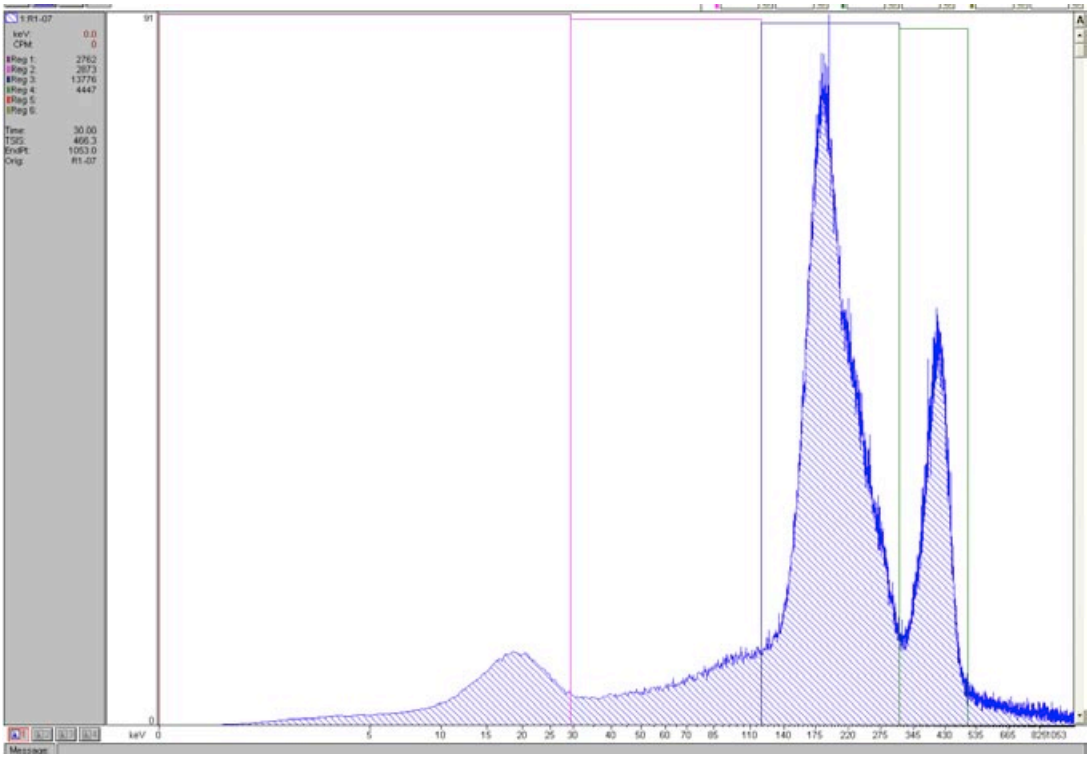

Peak 1: 11,739 [counts]
Peak 2: 3,683 [counts]

R1-08 (5.097 days)

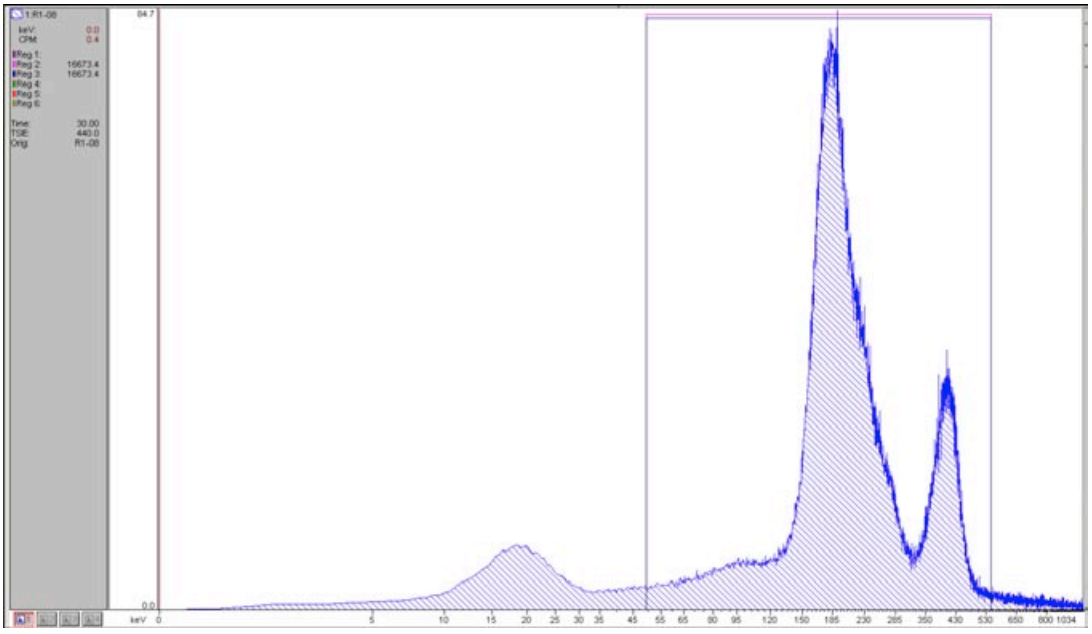

Peak 1: 10,589 [counts]
Peak 2: 2,229 [counts]

R1-09 (5.806 days)

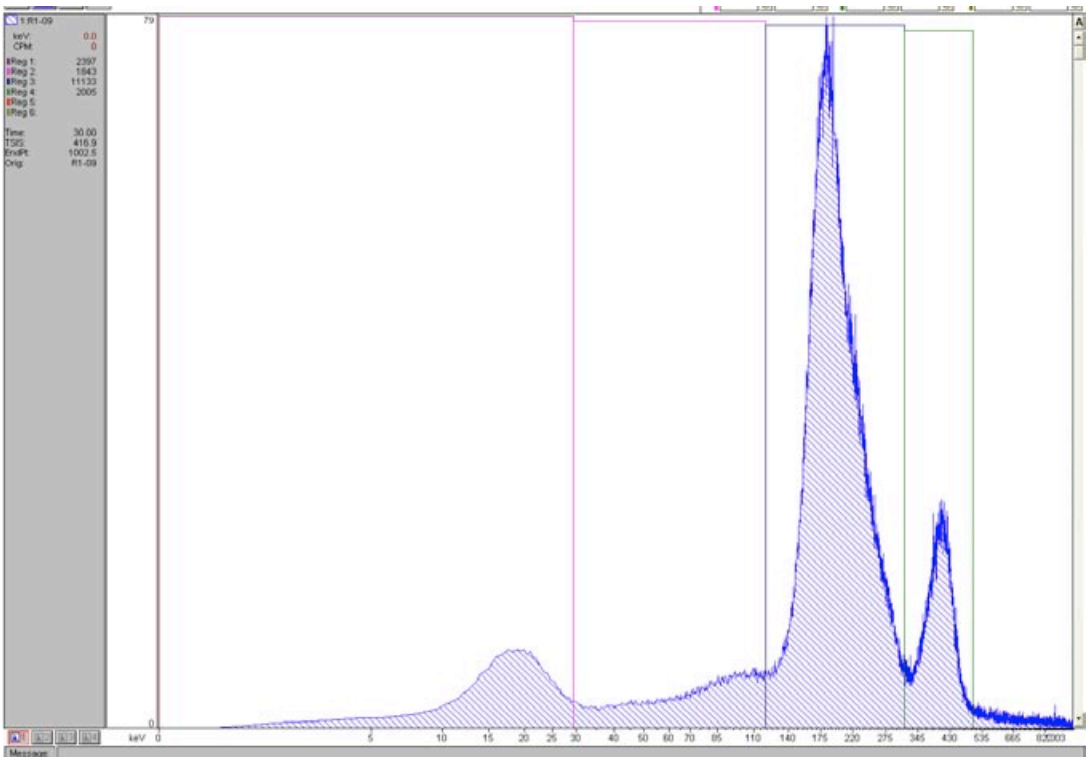

Peak 1: 9,775 [counts]
Peak 2: 1,432 [counts]

R1-10 6.049 days)

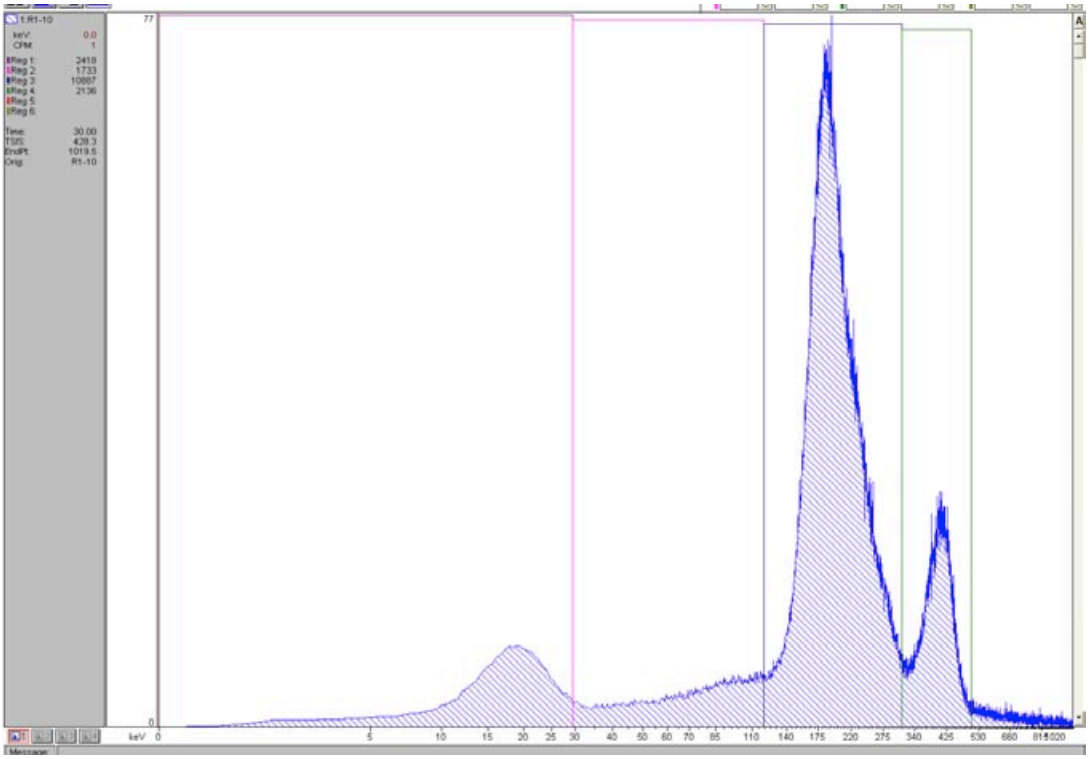

Peak 1: 9,626 [counts]
Peak 2: 1,658 [counts]

R1-11 (6.792 days)

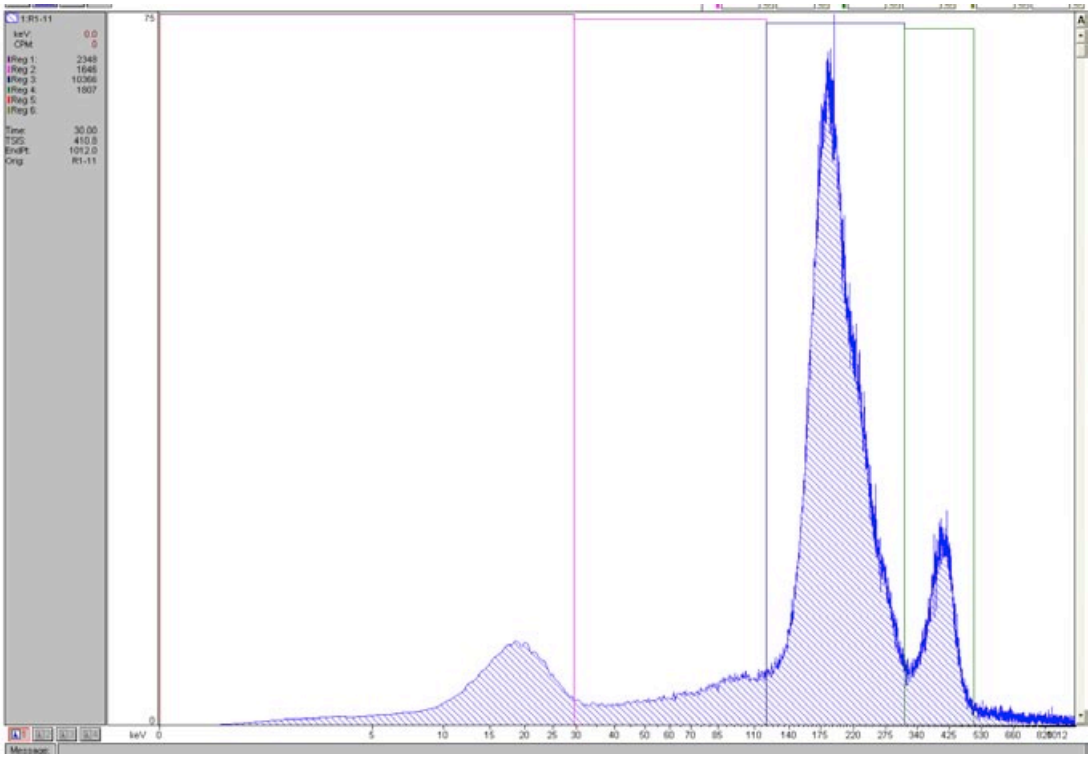

Peak 1: 9,105 [counts]
Peak 2: 1,329 [counts]

R1-12 (7.089 days)

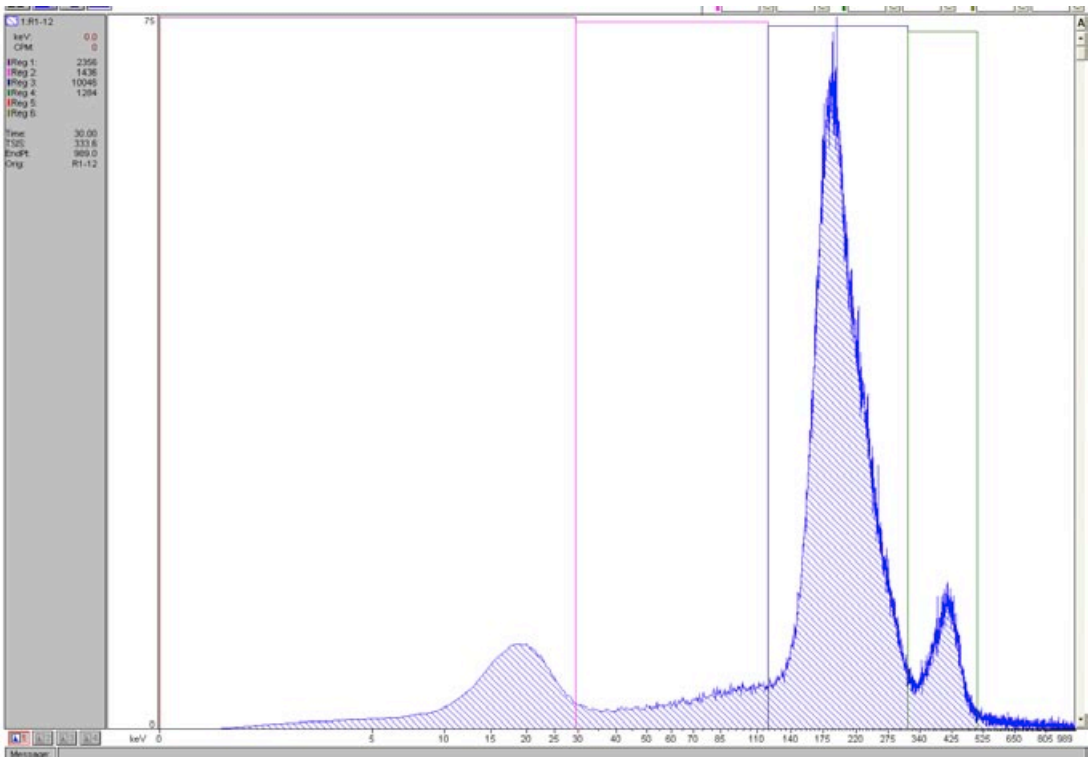

Peak 1: 8,979 [counts]
Peak 2: 806 [counts]

R1-13 (7.795 days)

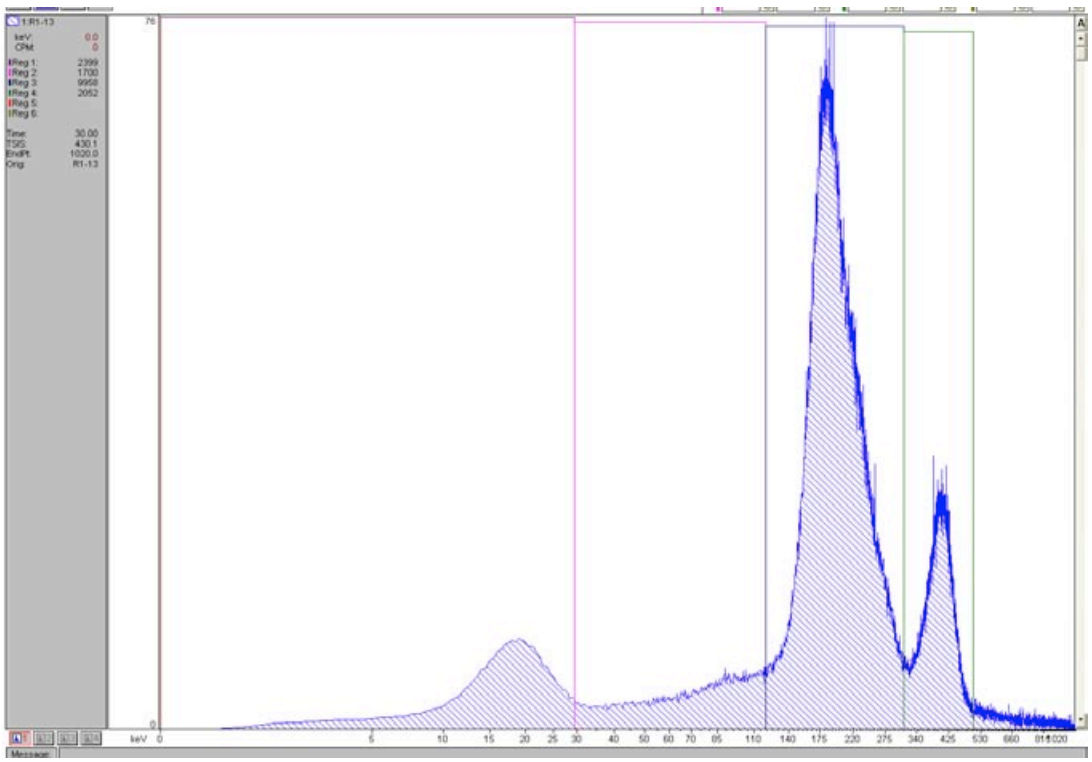

Peak 1: 8,697 [counts]
Peak 2: 1,574 [counts]

R1-14 (8.014 days)

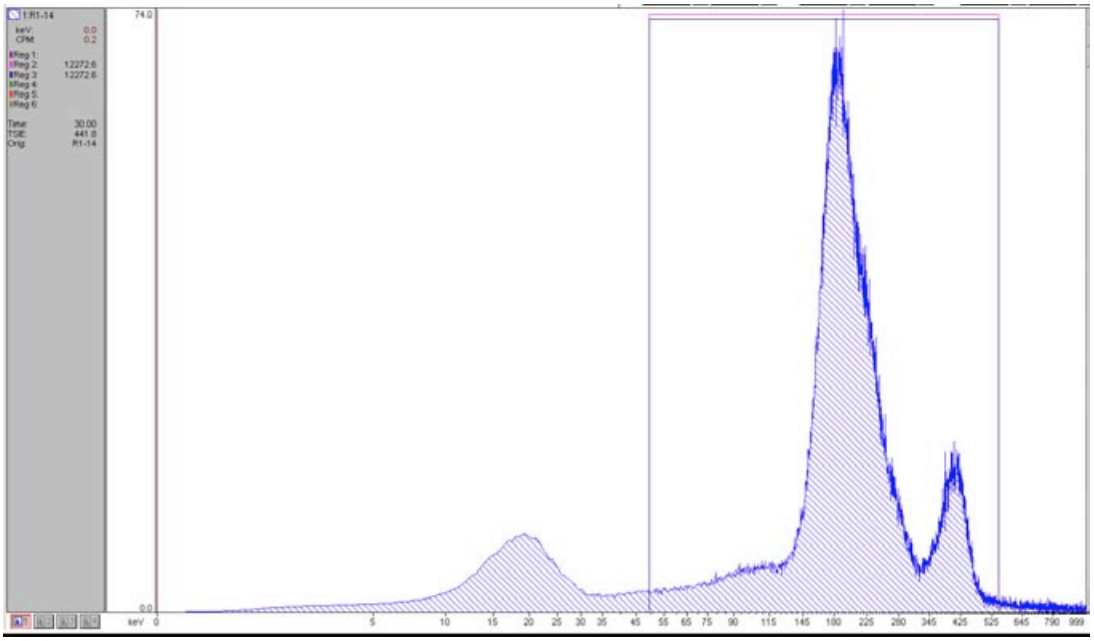

Peak 1: 8,446 [counts]
Peak 2: 1,169 [counts]

R1-15 (8.799 days)

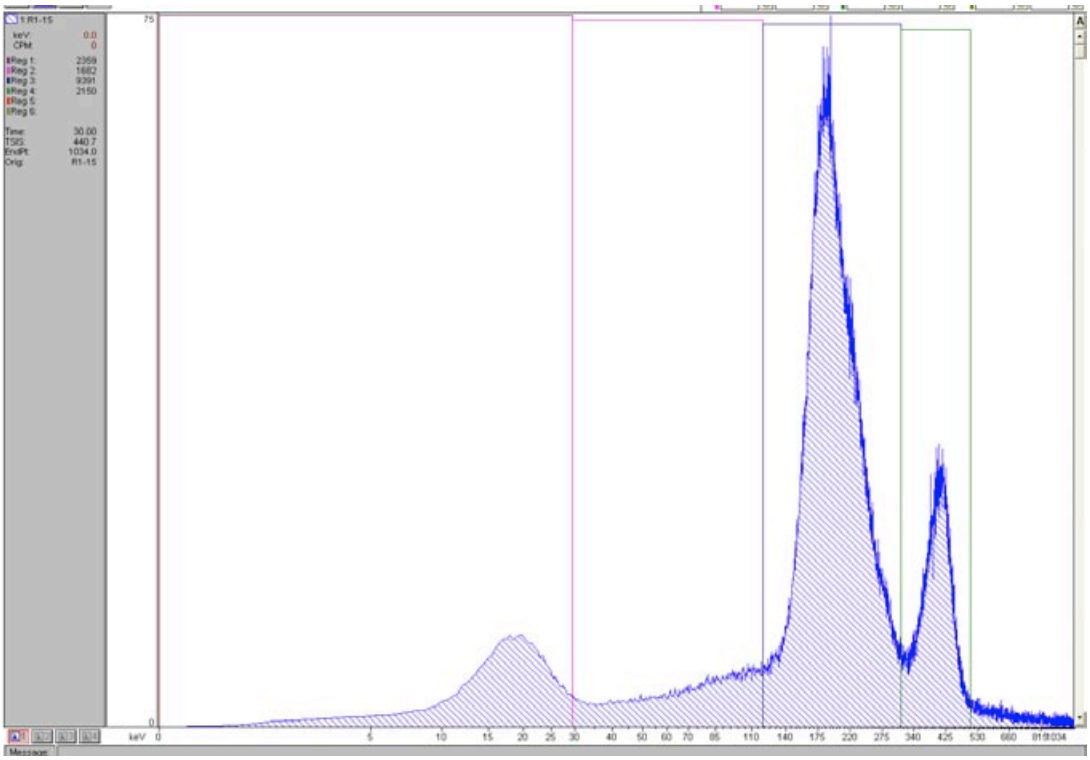

Peak 1: 8,227 [counts]
Peak 2: 1,672 [counts]

R1-16 (9.09 days)

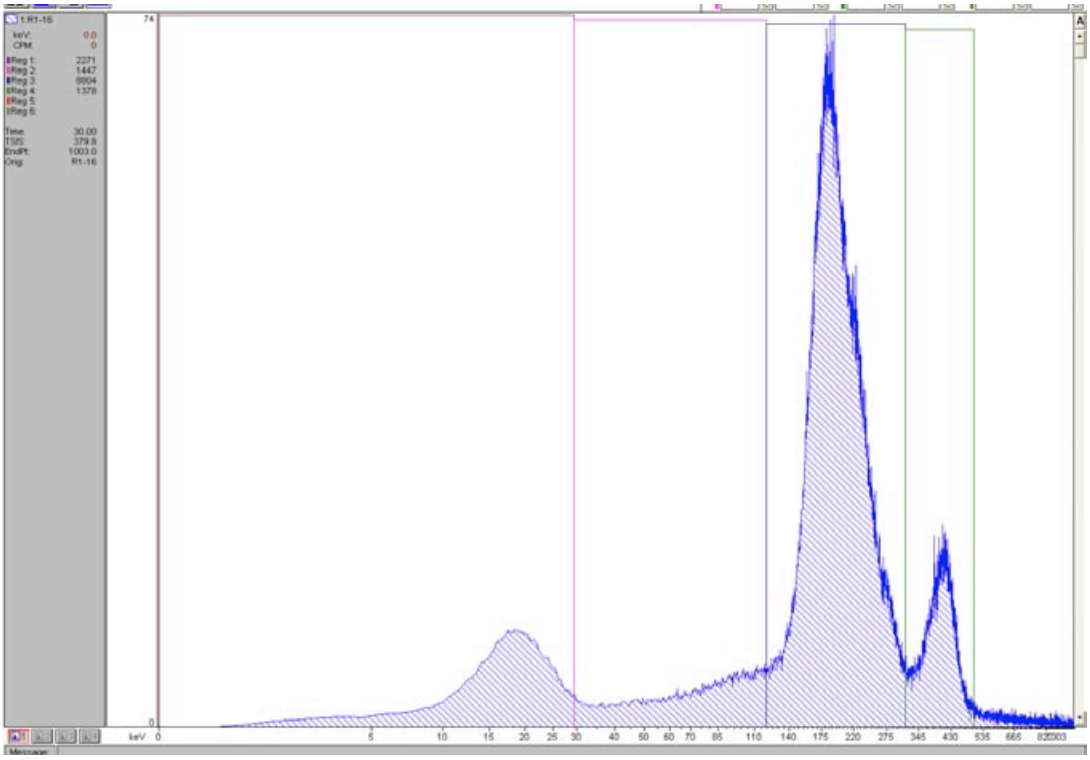

Peak 1: 7,640 [counts]
Peak 2: 1,091 [counts]

R1-17 (11.8 days)

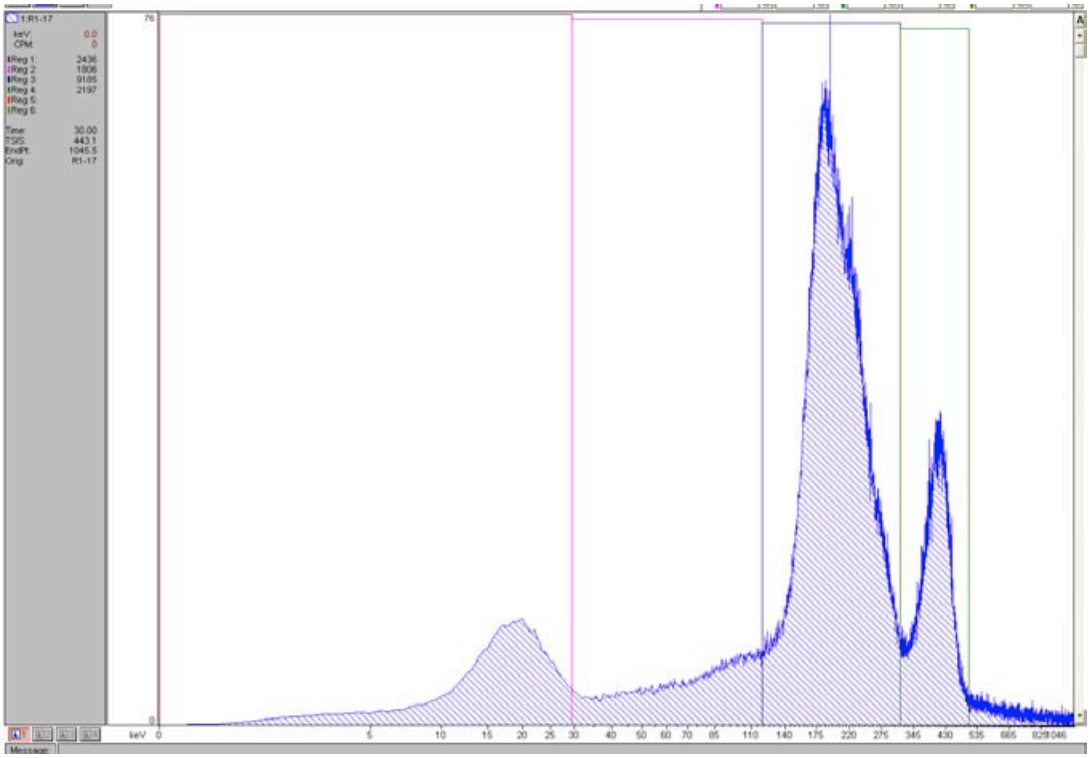

Peak 1: 7,827 [counts]
Peak 2: 1,624 [counts]

R1-18 (12.04 days)

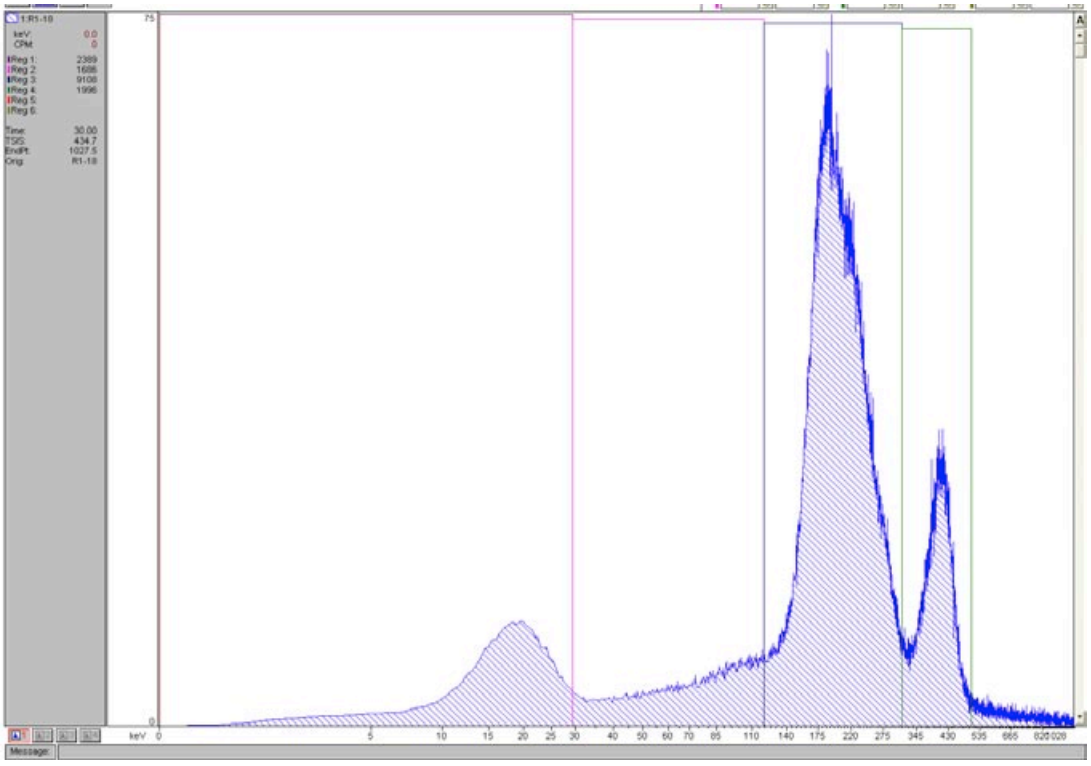

Peak 1: 7,847 [counts]
Peak 2: 1,614 [counts]

R1-19 (12.81 days)

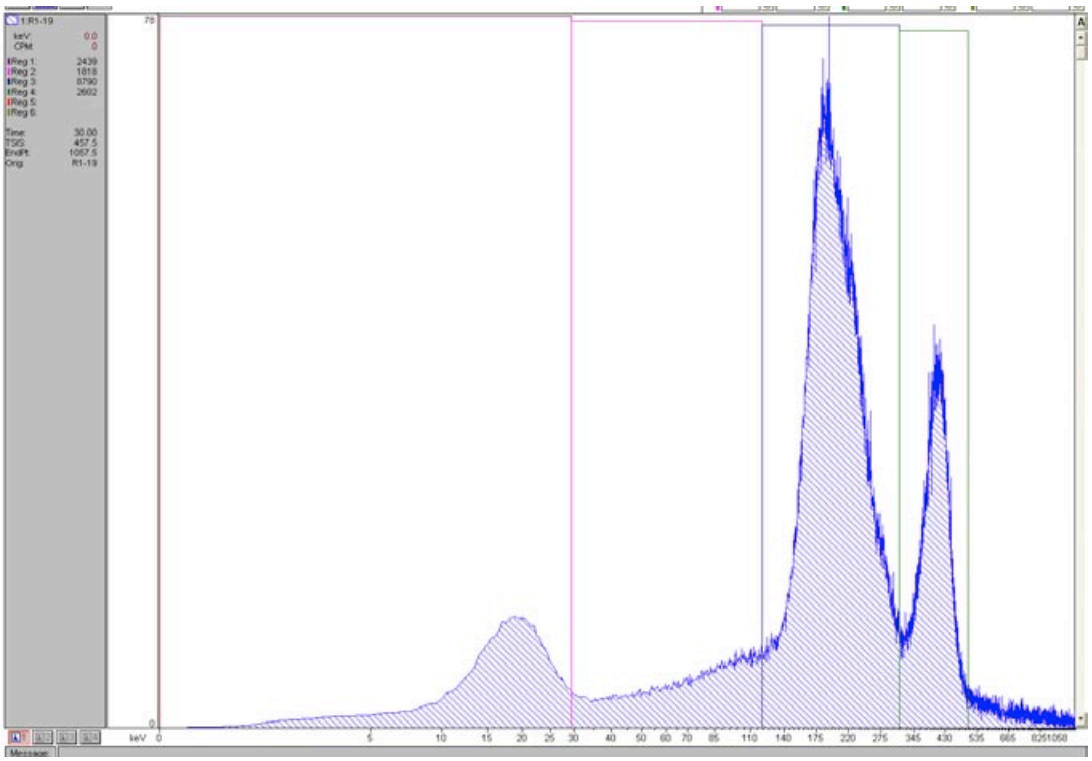

Peak 1: 7,432 [counts]
Peak 2: 2,029 [counts]

R1-20 (13.81 days)

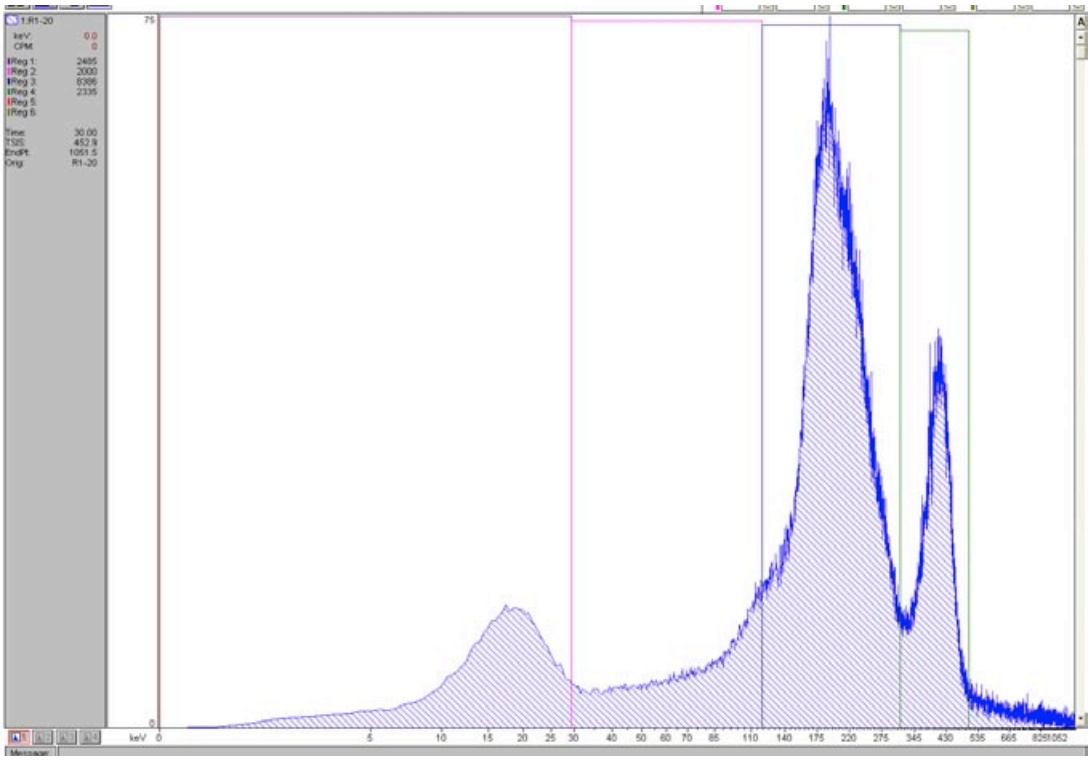

Peak 1: 6,446 [counts]
Peak 2: 1,762 [counts]

R1-21 (14.79 days)

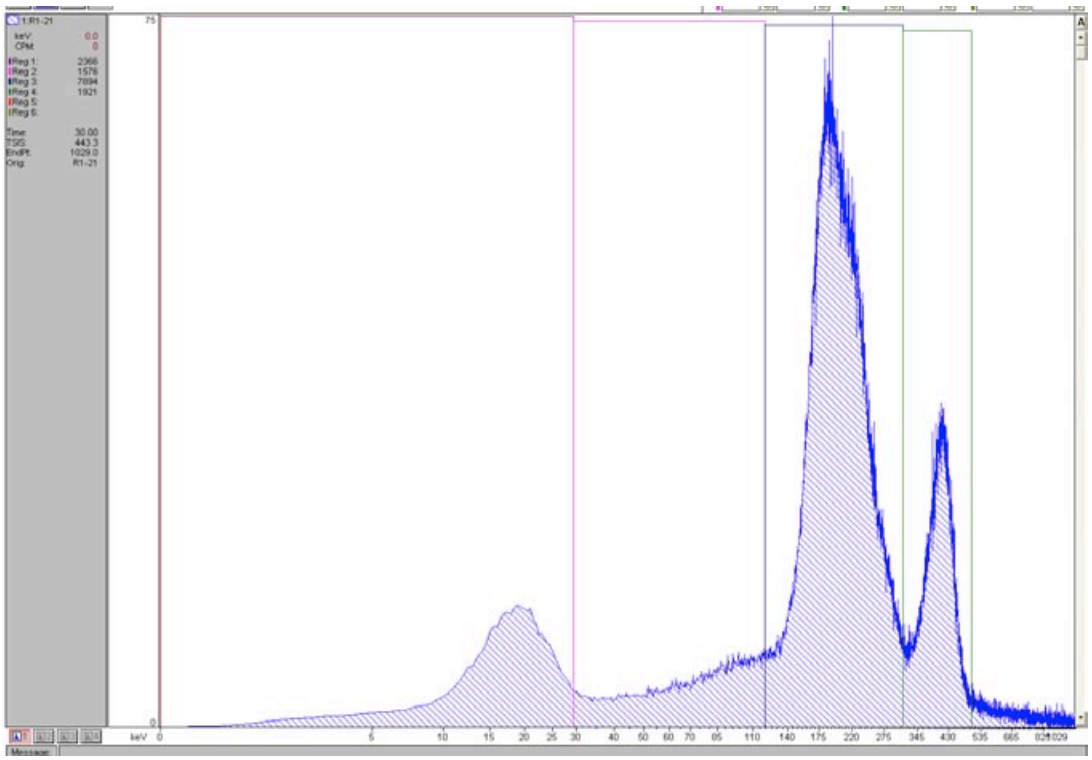

Peak 1: 6,827 [counts]
Peak 2: 1,539 [counts]

R1-22 (15.04 days)

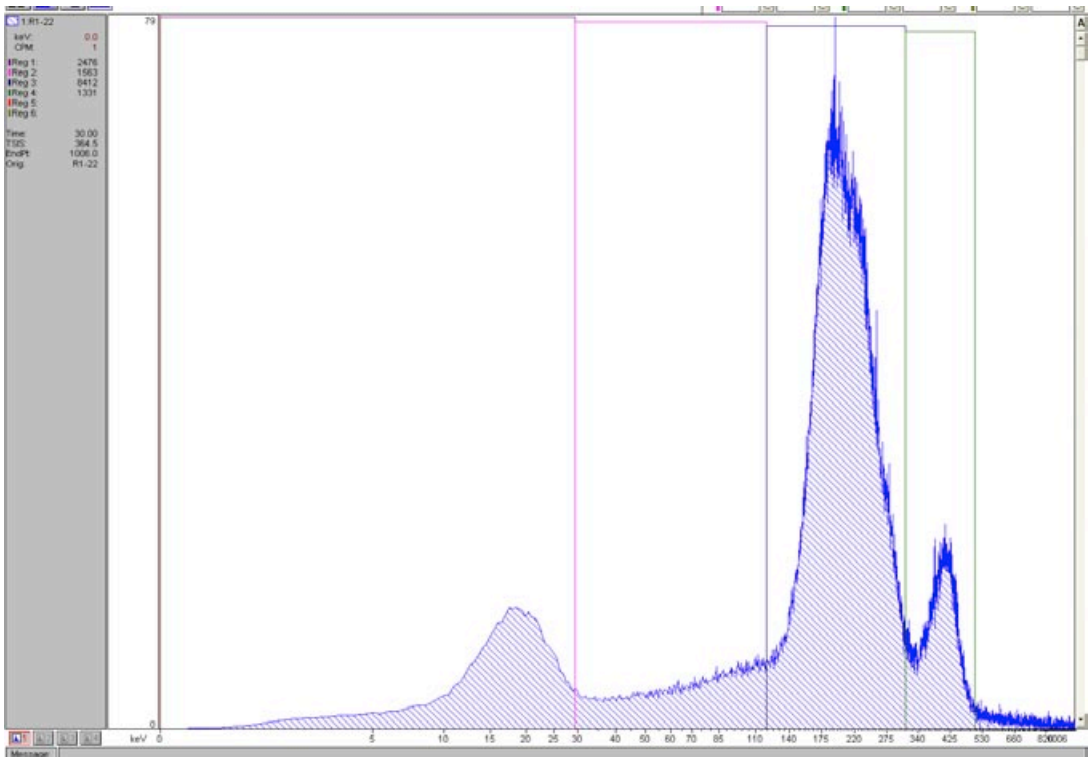

Peak 1: 7,361 [counts]
Peak 2: 949 [counts]

R1-23 (15.8 days)

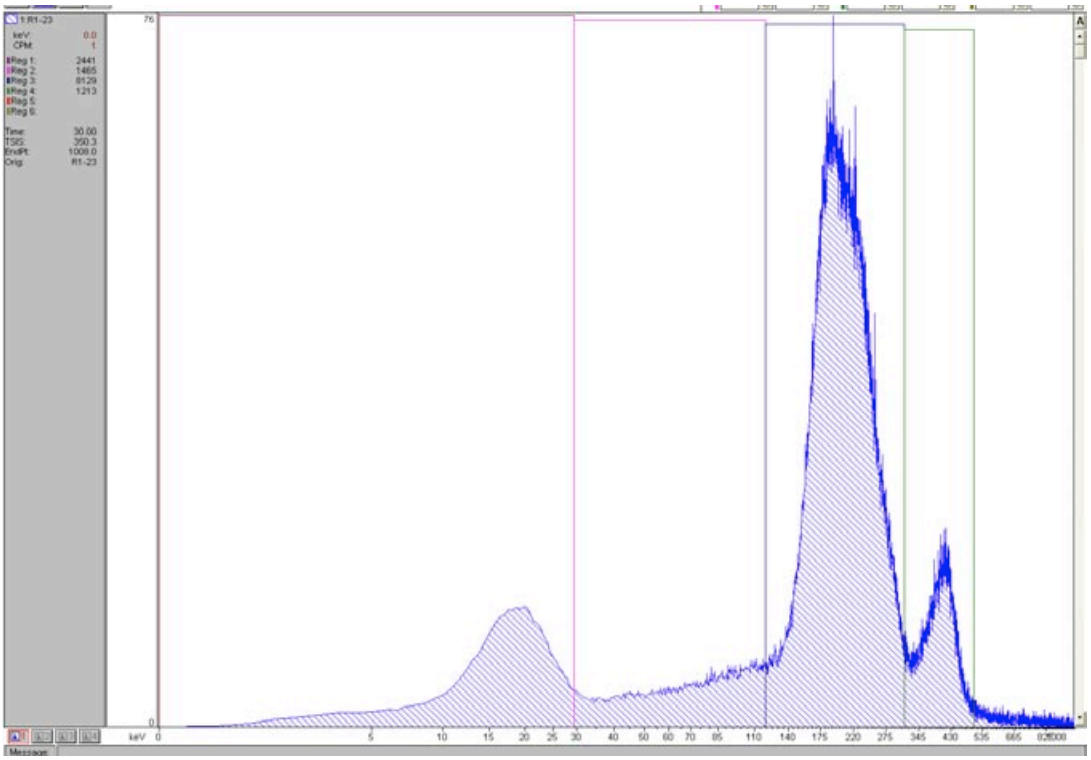

Peak 1: 7,062 [counts]
Peak 2: 735 [counts]

R1-24 (18.8 days)

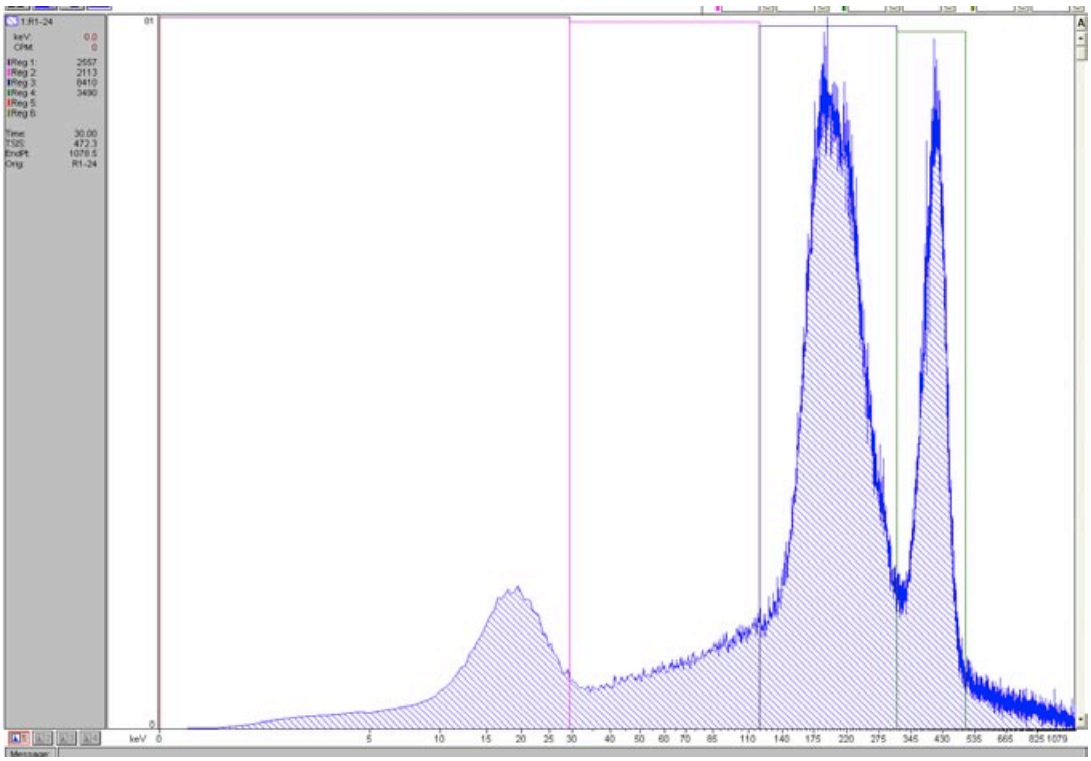

Peak 1: 6,858 [counts]
Peak 2: 2,821 [counts]

R1-25 (19 days)

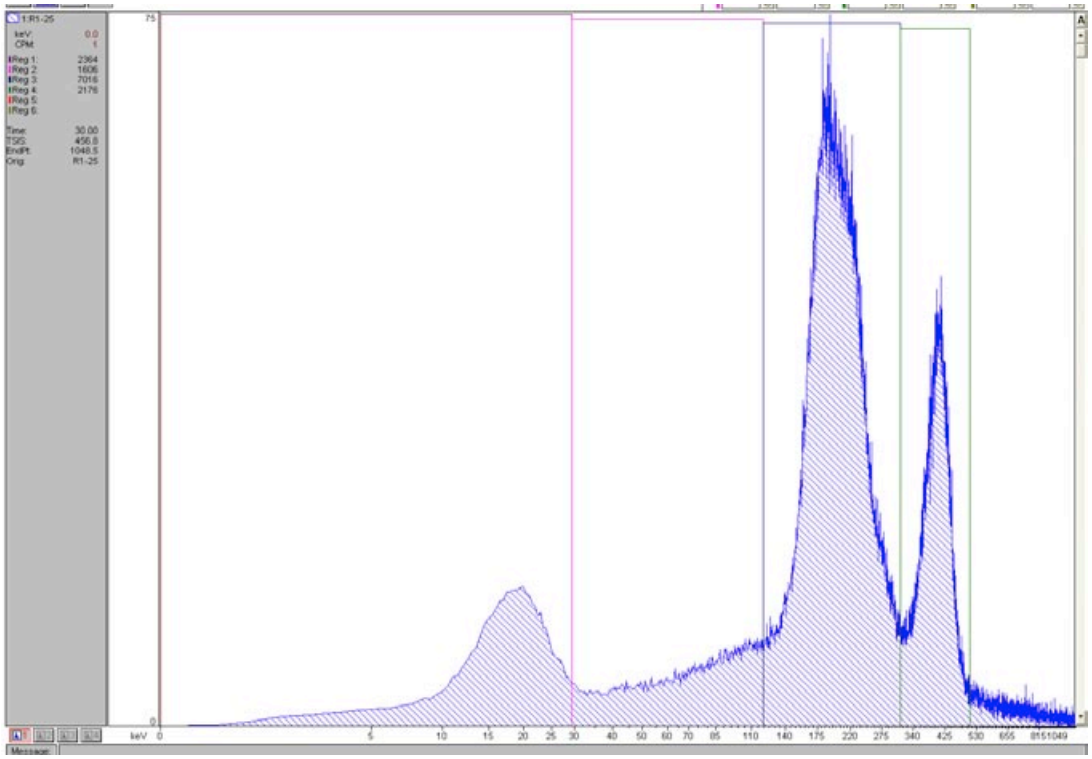

Peak 1: 5,852 [counts]
Peak 2: 1,698 [counts]

R1-26 (19.79 days)

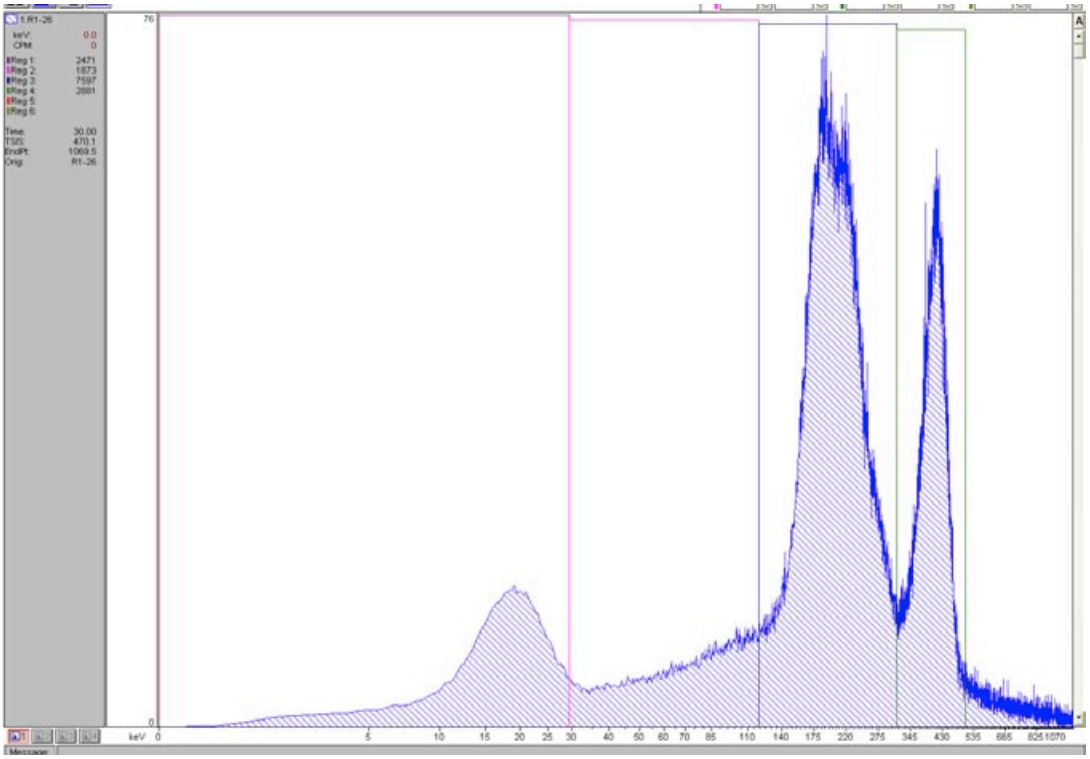

Peak 1: 6,164 [counts]
Peak 2: 2,403 [counts]

R1-27 (20.79 days)

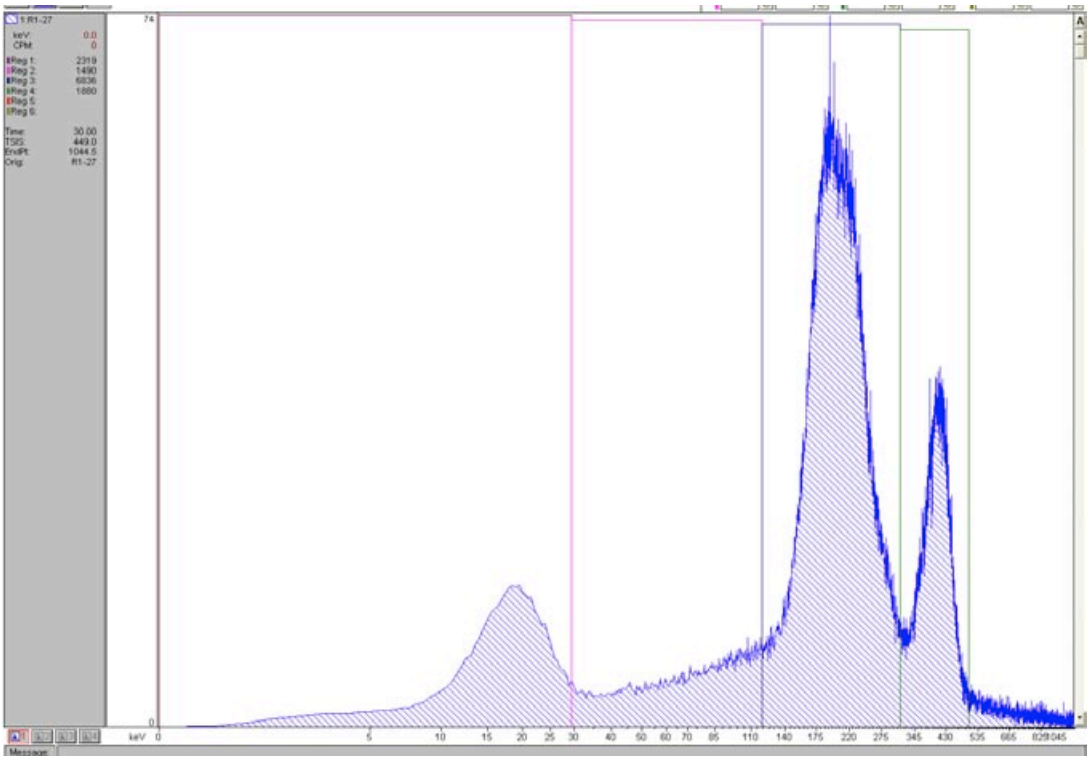

Peak 1: 5,769 [counts]
Peak 2: 1,498 [counts]

R1-28 (21.06 days)

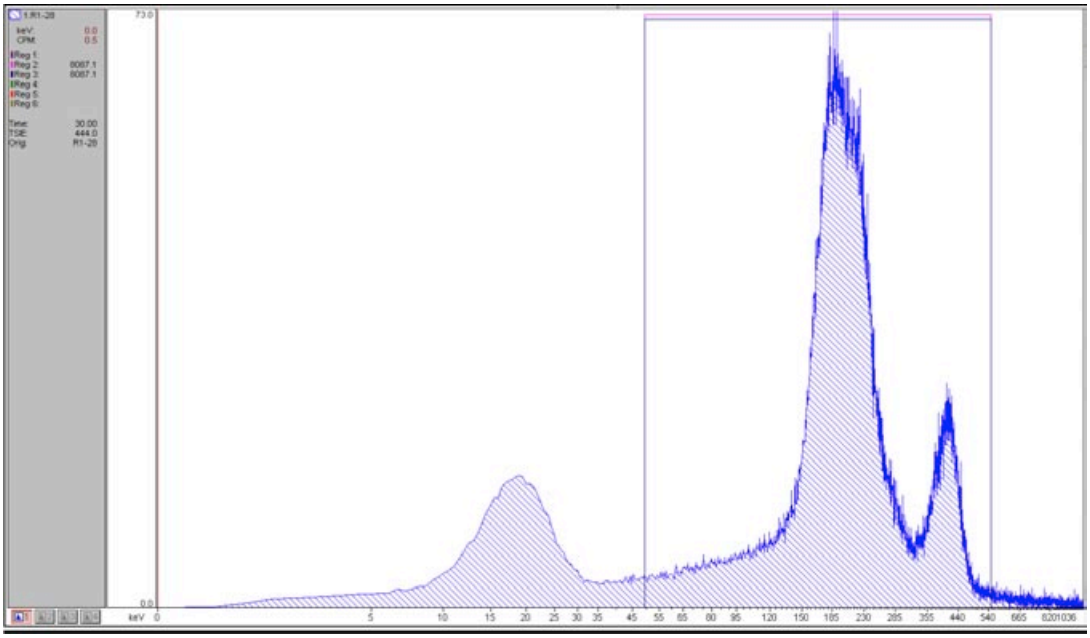

Peak 1: 5,041 [counts]
Peak 2: 957 [counts]

R1-29 (21.82 days)

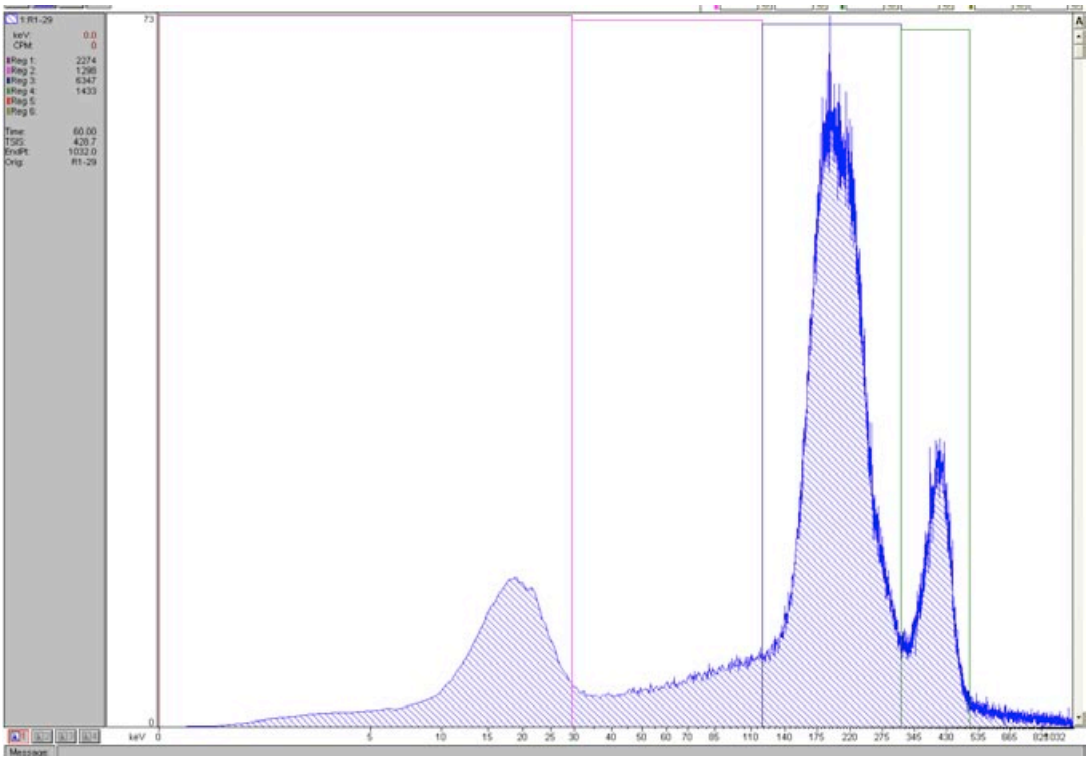

Peak 1: 5,377 [counts]
Peak 2: 1,051 [counts]

R1-30 (22.04 days)

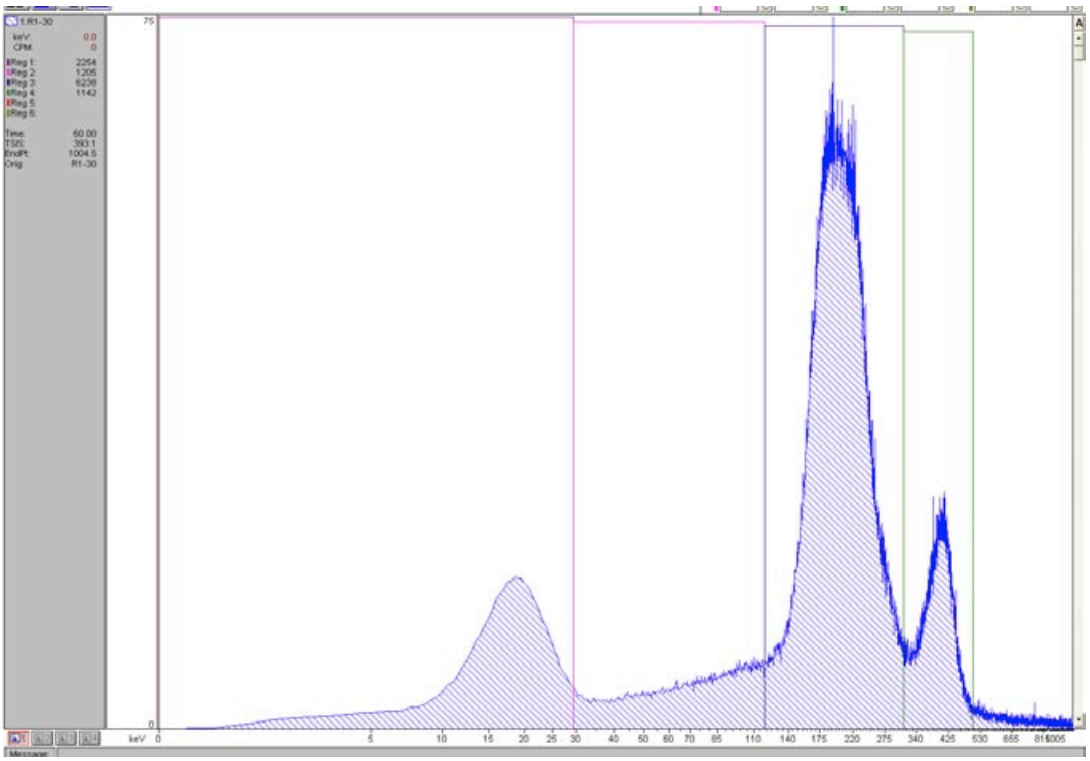

Peak 1: 5,365 [counts]
Peak 2: 855 [counts]

R1-31 (22.83 days)

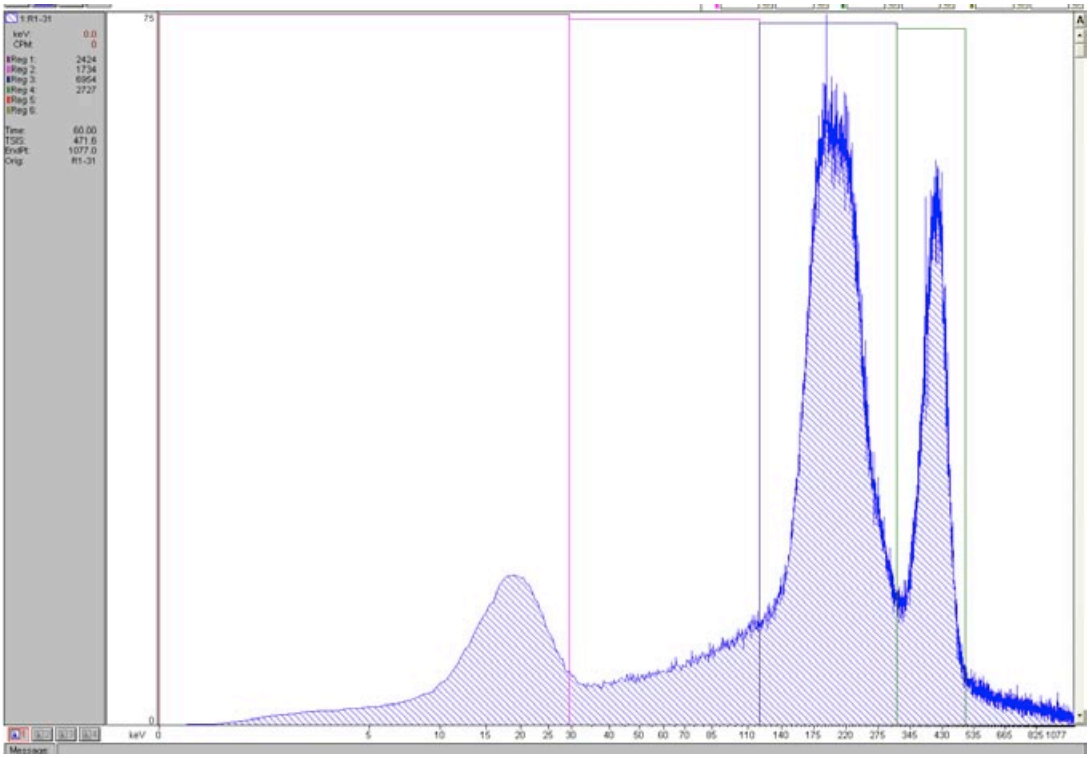

Peak 1: 5,790 [counts]
Peak 2: 2,249 [counts]

R1-32 (22.99 days)

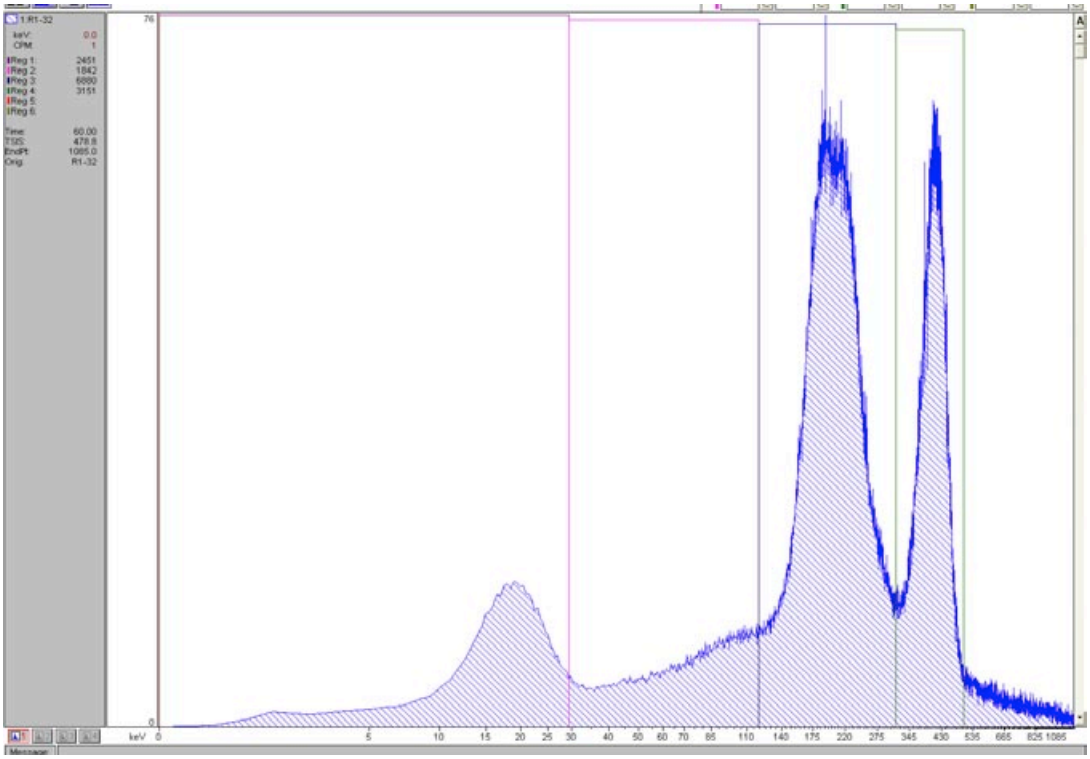

Peak 1: 5,522 [counts]
Peak 2: 2,578 [counts]

R1-33 (25.88 days)

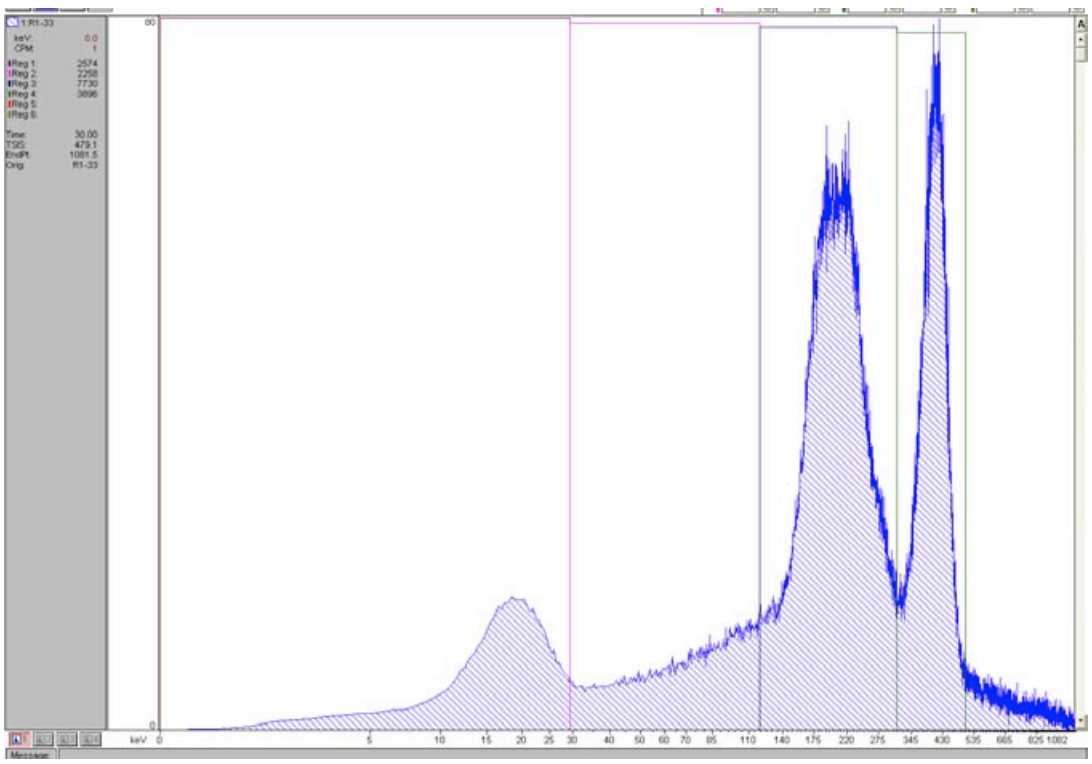

Peak 1: 6,081 [counts]
Peak 2: 3,227 [counts]

R1-34 (25.99 days)

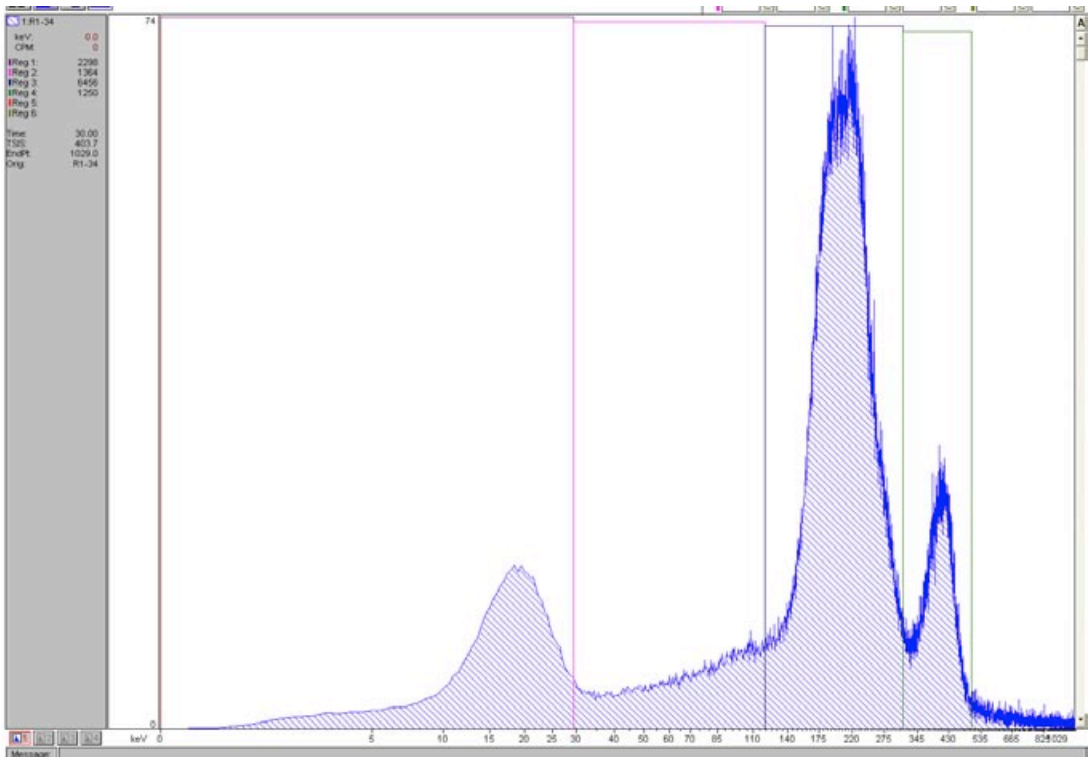

Peak 1: 5,501 [counts]
Peak 2: 868 [counts]

R1-35 (26.84 days)

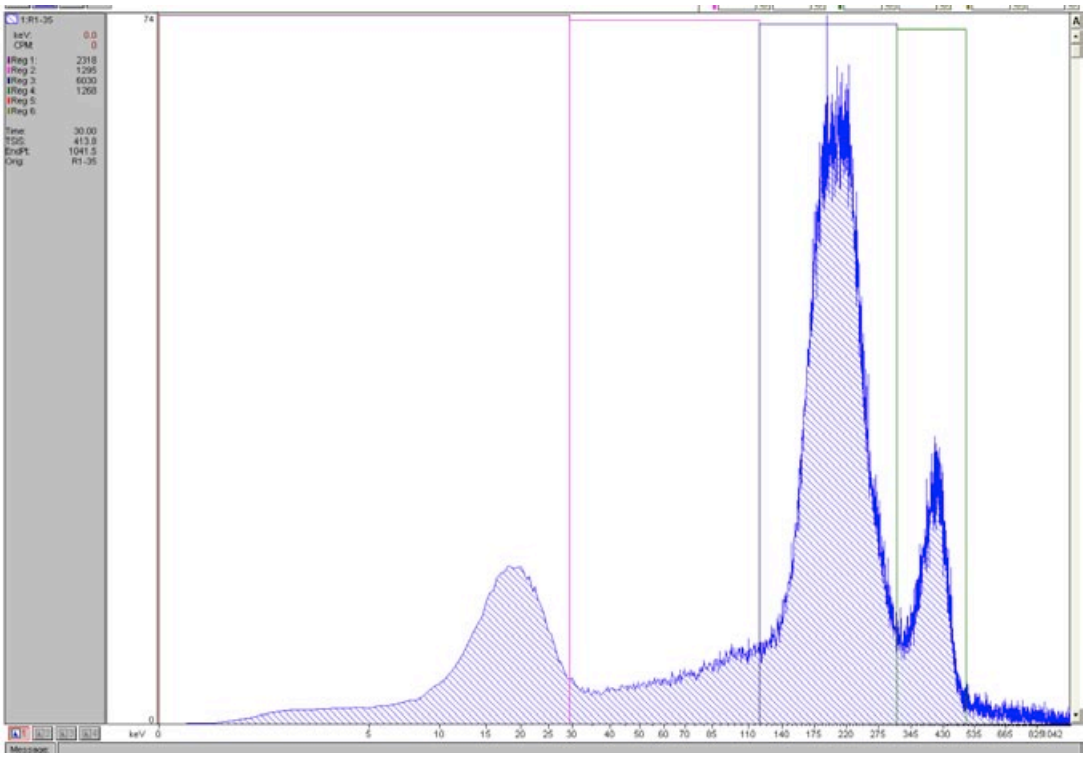

Peak 1: 5,157 [counts]
Peak 2: 981 [counts]

R1-36 (27.02 days)

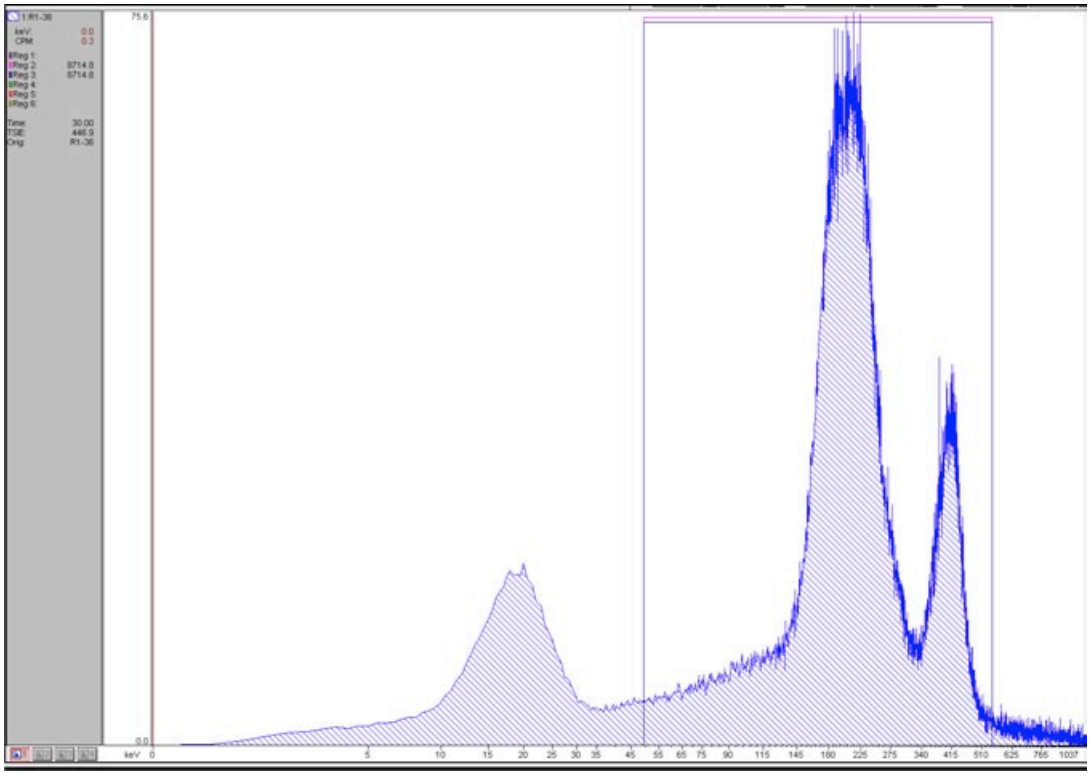

Peak 1: 5,121 [counts]
Peak 2: 1,267 [counts]

R1-37 (27.81 days)

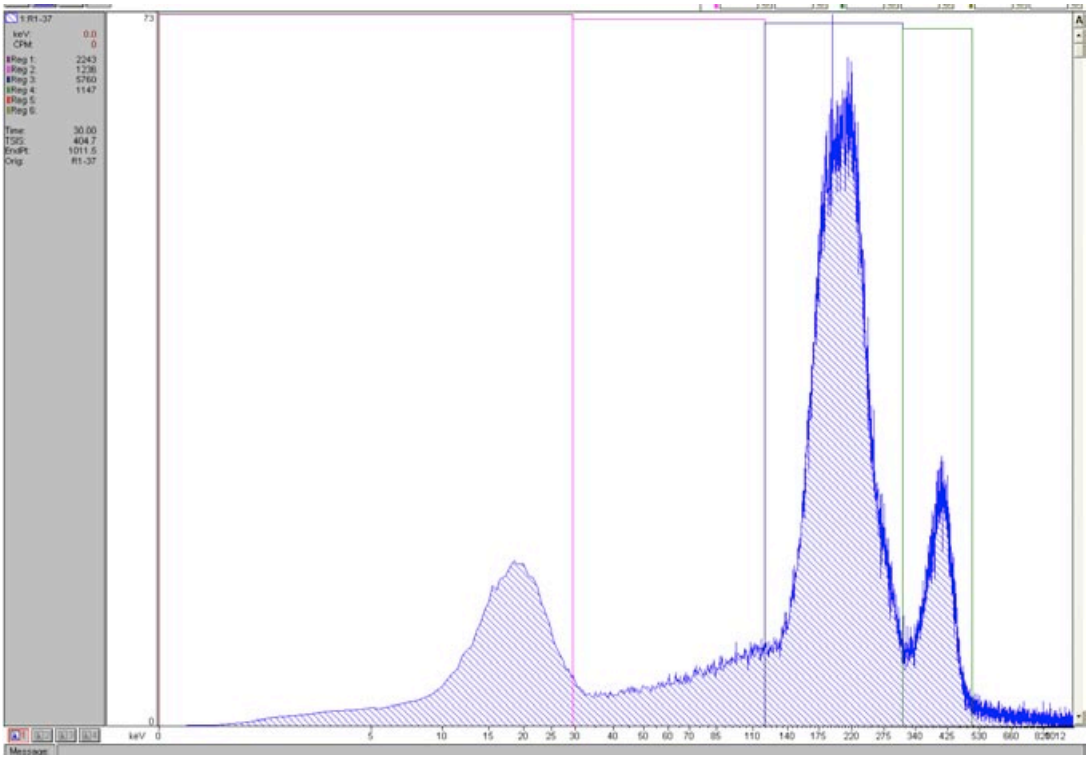

Peak 1: 4,790 [counts]
Peak 2: 765 [counts]

R1-38 (28 days)

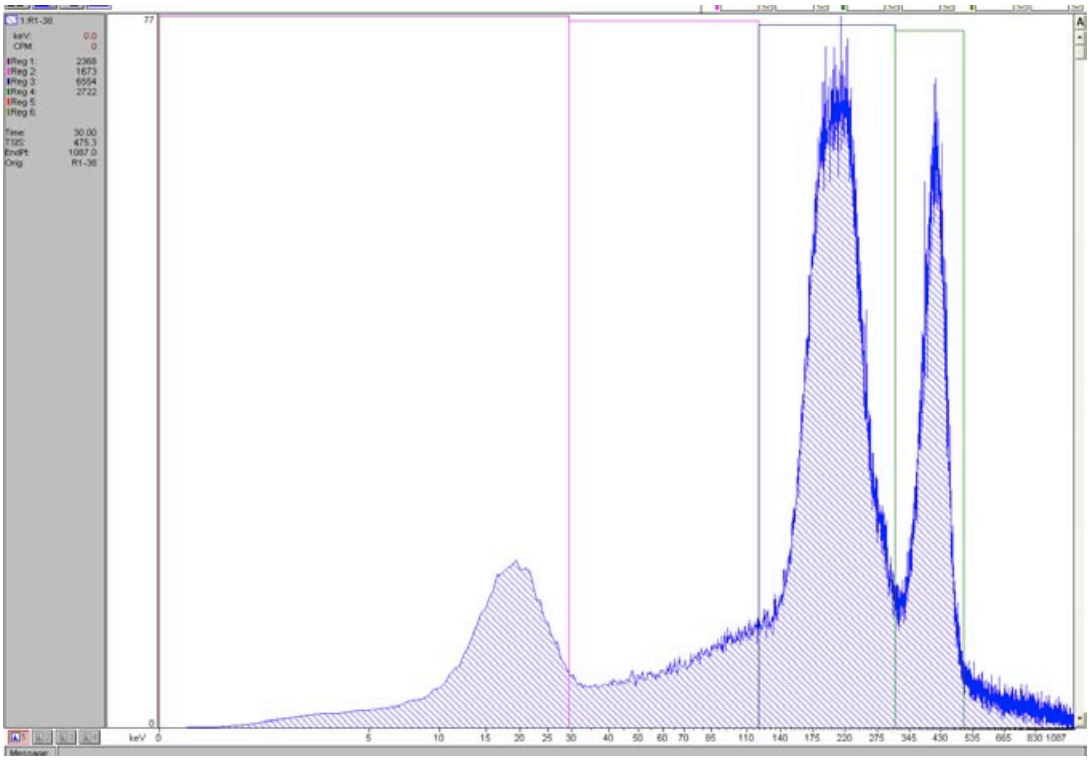

Peak 1: 5,196 [counts]
Peak 2: 2,149 [counts]

R1-39 (28.29 days)

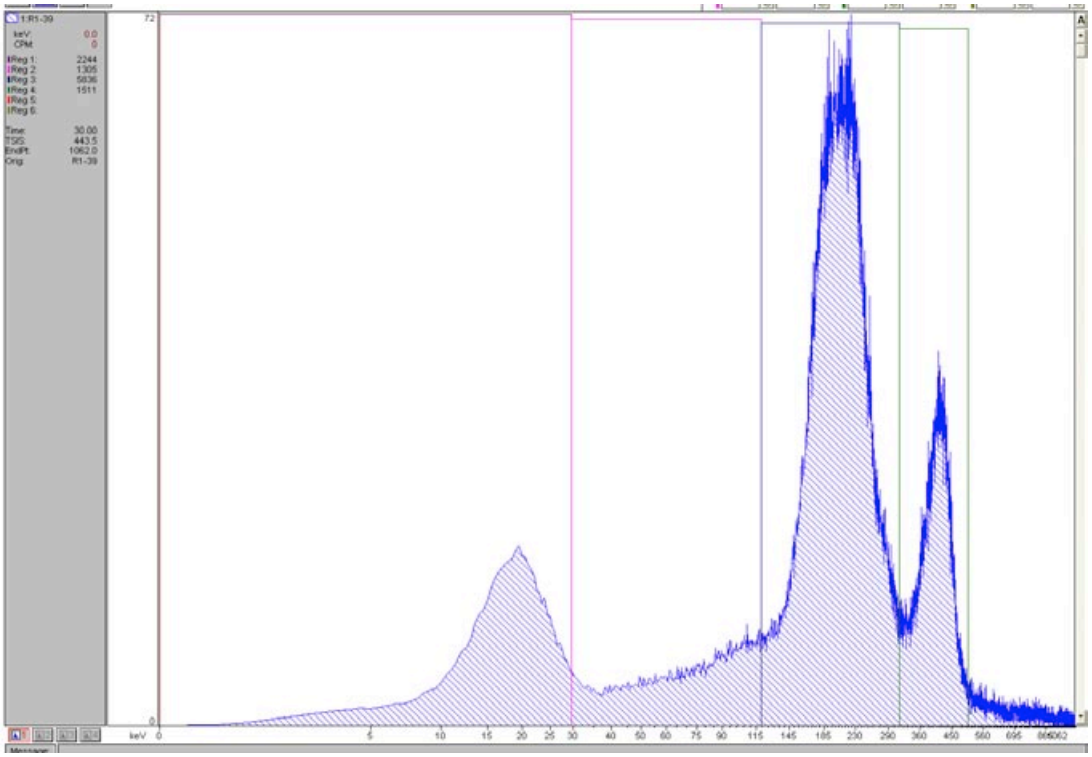

Peak 1: 4,869 [counts]
Peak 2: 1,033 [counts]

R1-40 (29.04 days)

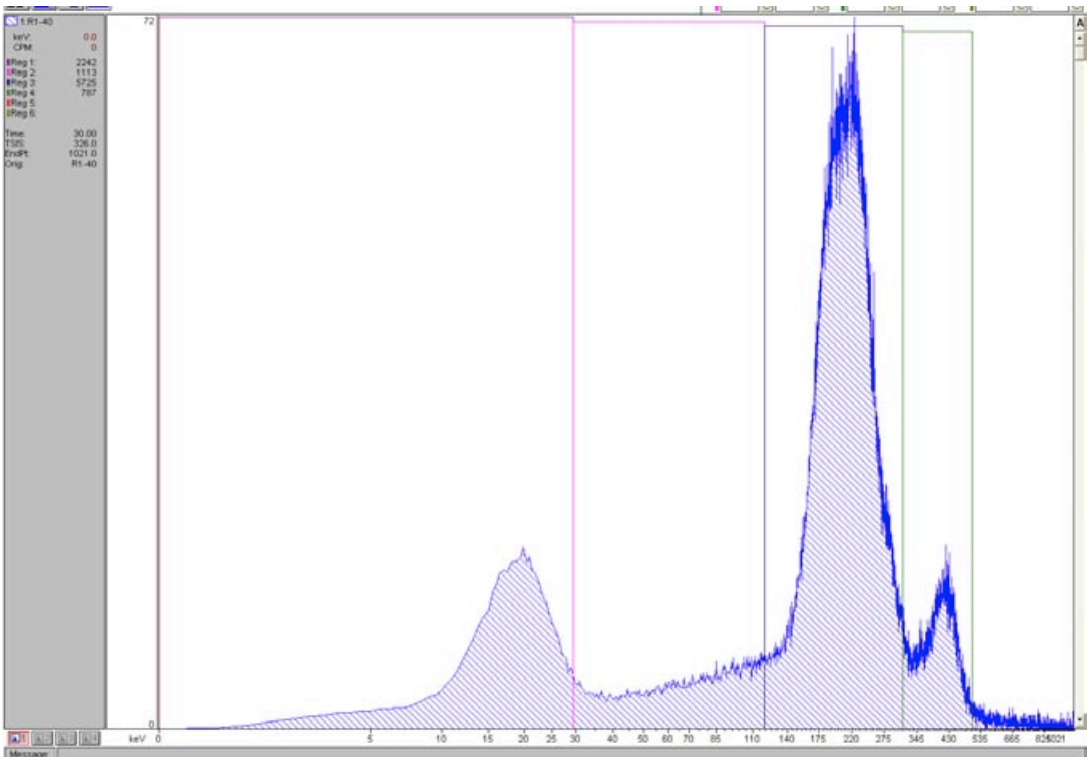

Peak 1: 4,949 [counts]
Peak 2: 500 [counts]

R1-41 (29.79 days)

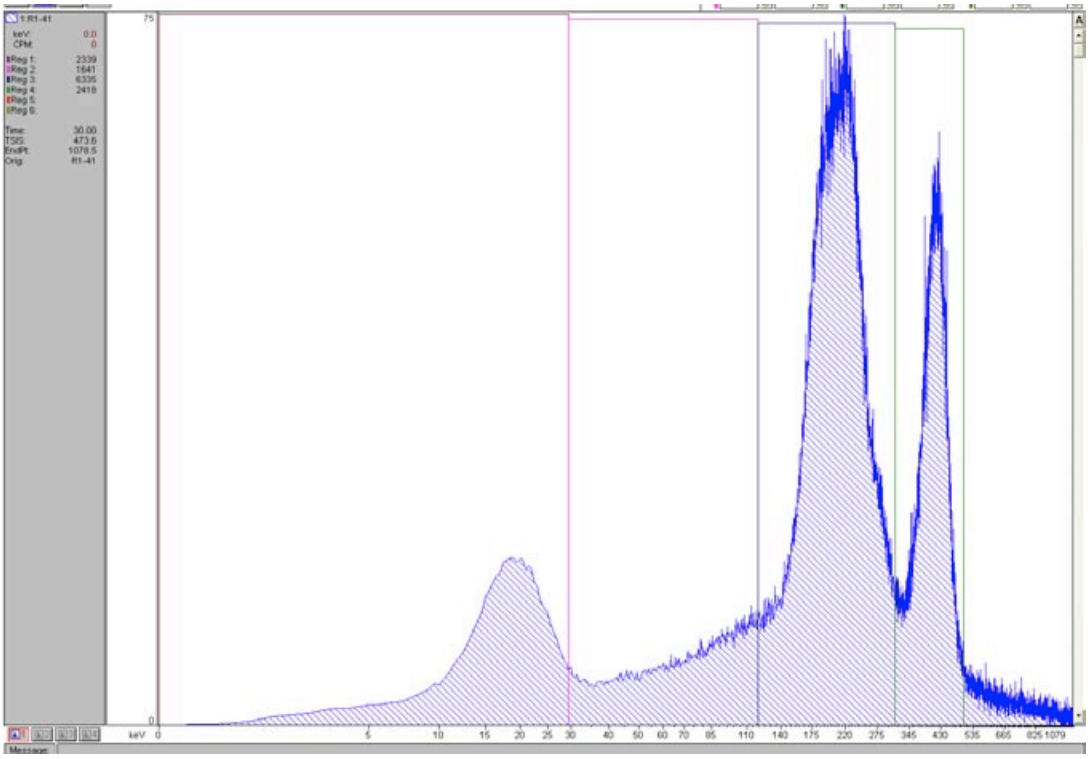

Peak 1: 5,074 [counts]
Peak 2: 1,940 [counts]

R1-42 (32.79 days)

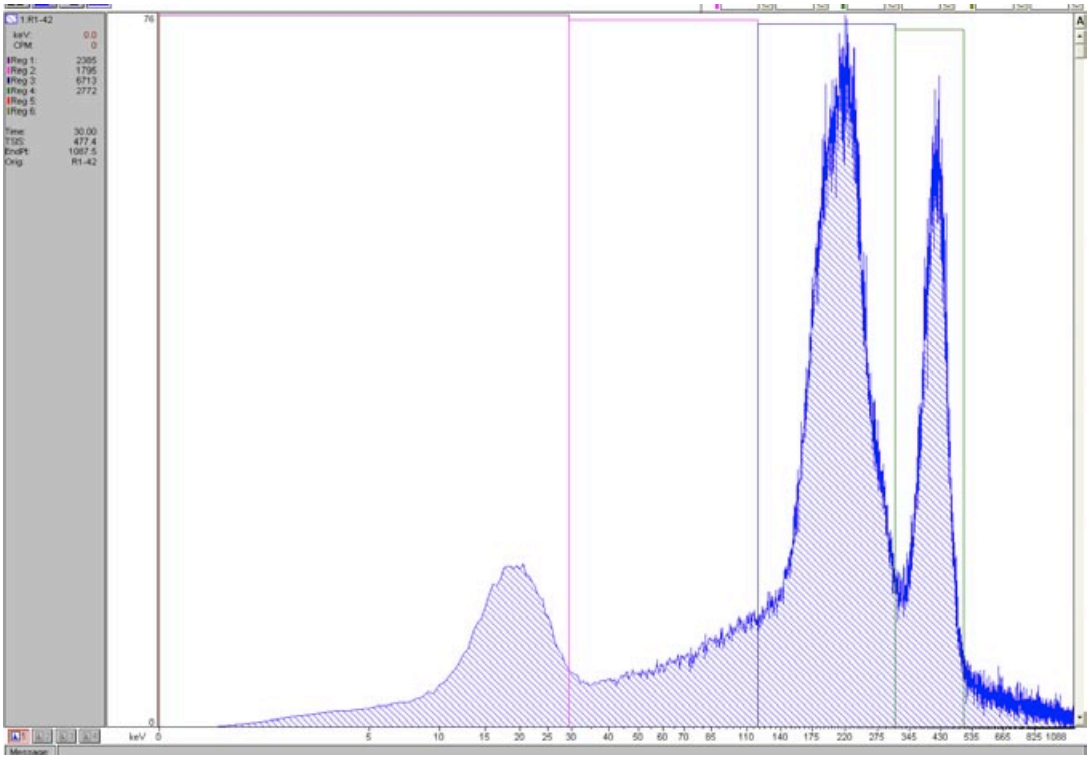

Peak 1: 5,452 [counts]
Peak 2: 2,199 [counts]

R1-43 (33.02 days)

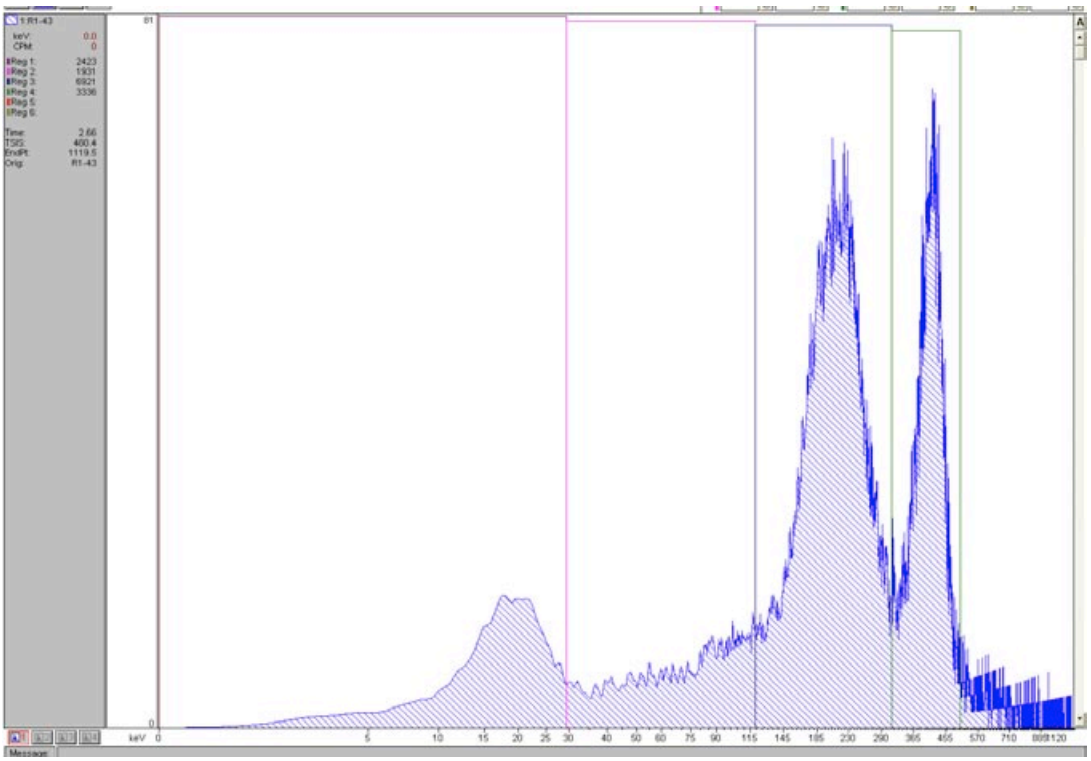

Peak 1: 5,369 [counts]
Peak 2: 2,667 [counts]

R1-44 (33.79 days)

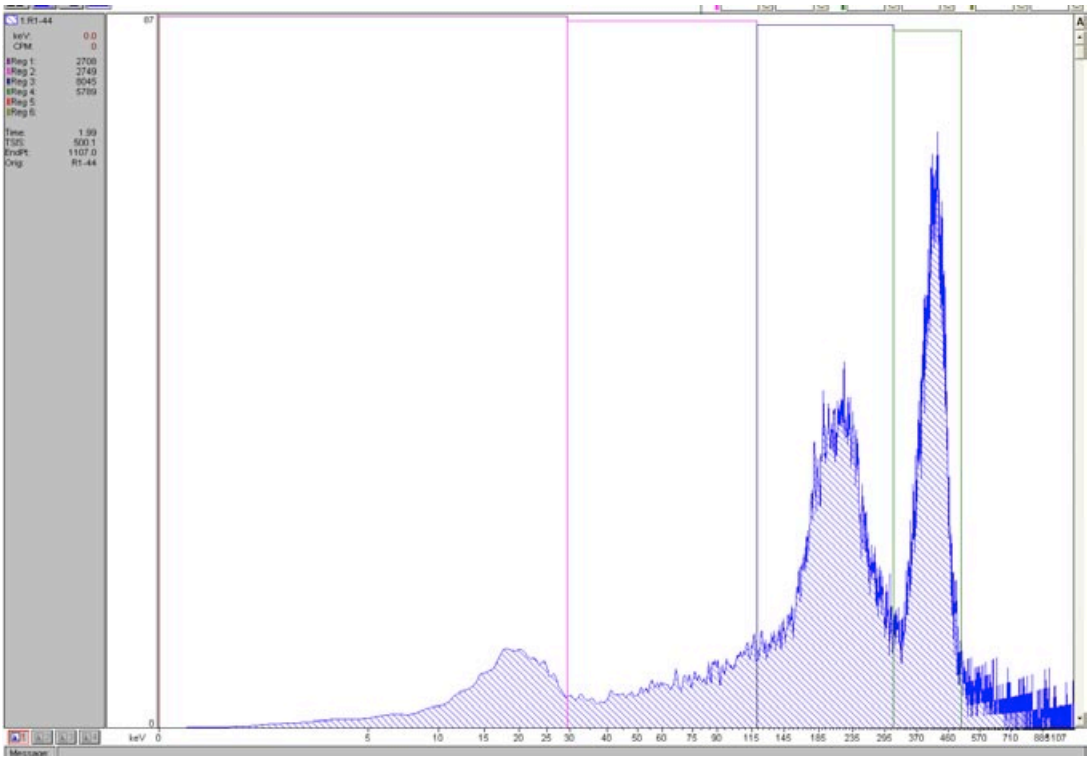

Peak 1: 5,911 [counts]
Peak 2: 4,738 [counts]

R1-45 (34.02 days)

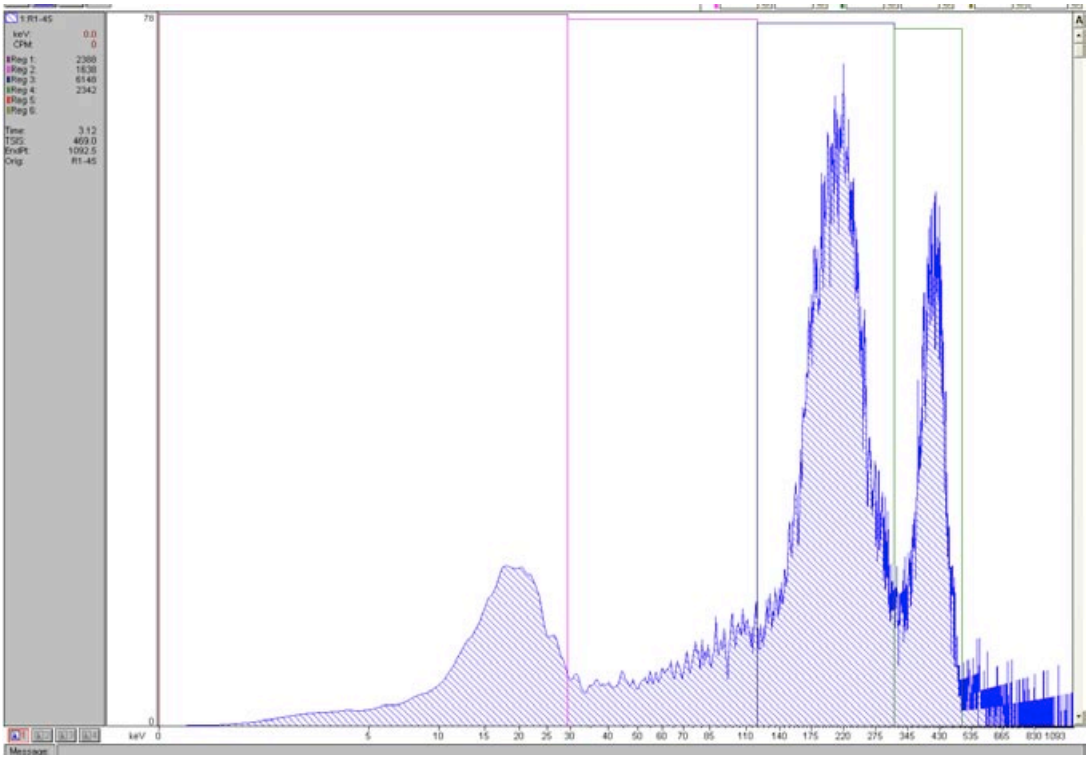

Peak 1: 4,499 [counts]
Peak 2: 1,579 [counts]

R1-46 (34.79 days)

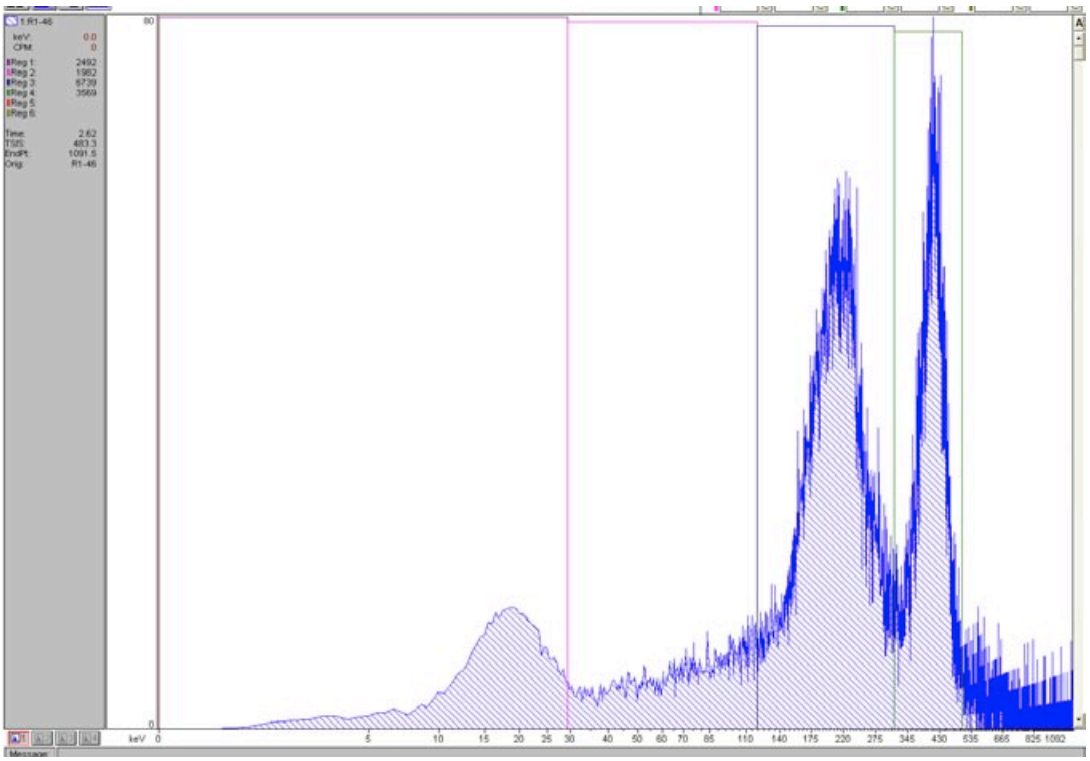

Peak 1: 5,211 [counts]
Peak 2: 2,805 [counts]

R1-47 (35.02 days)

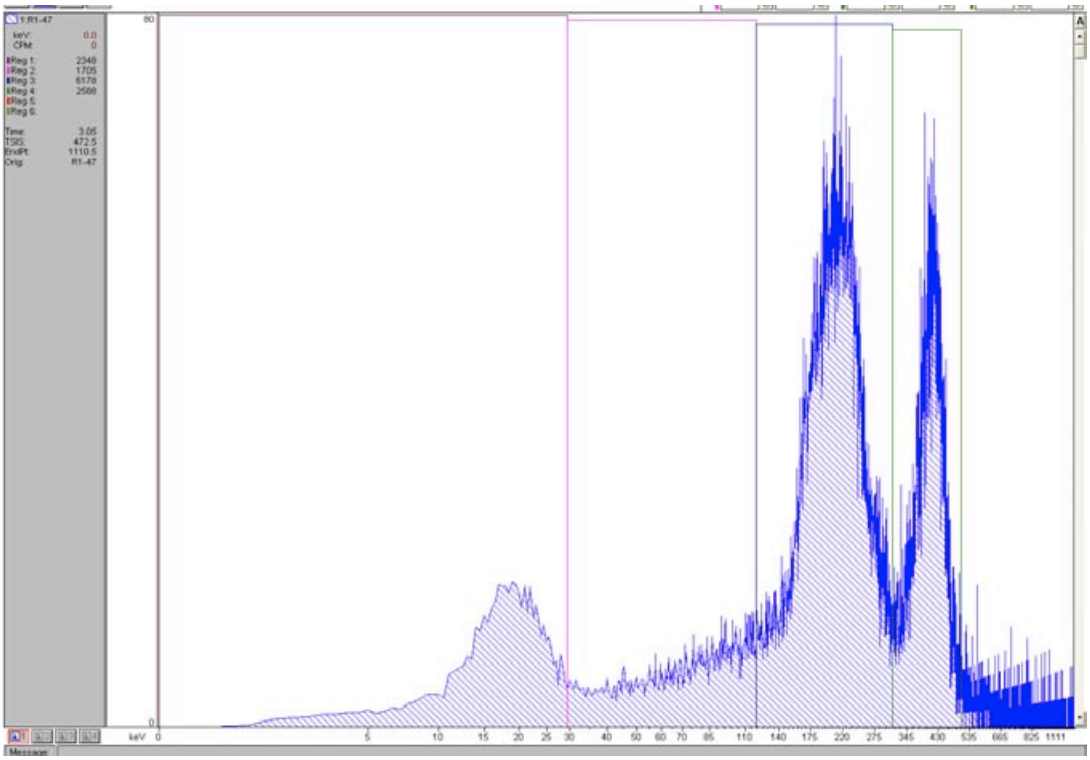

Peak 1: 4,917 [counts]
Peak 2: 2,110 [counts]

R1-48 (35.79 days)

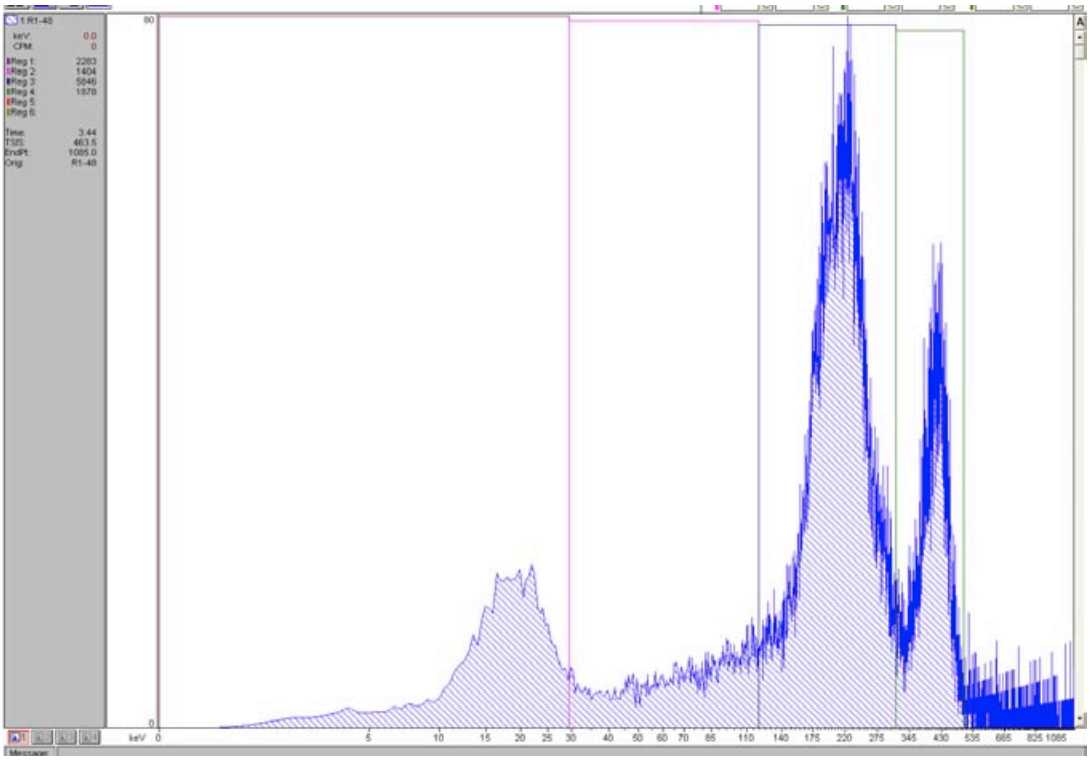

Peak 1: 5,167 [counts]
Peak 2: 1,591 [counts]

R1-49 (36.02 days)

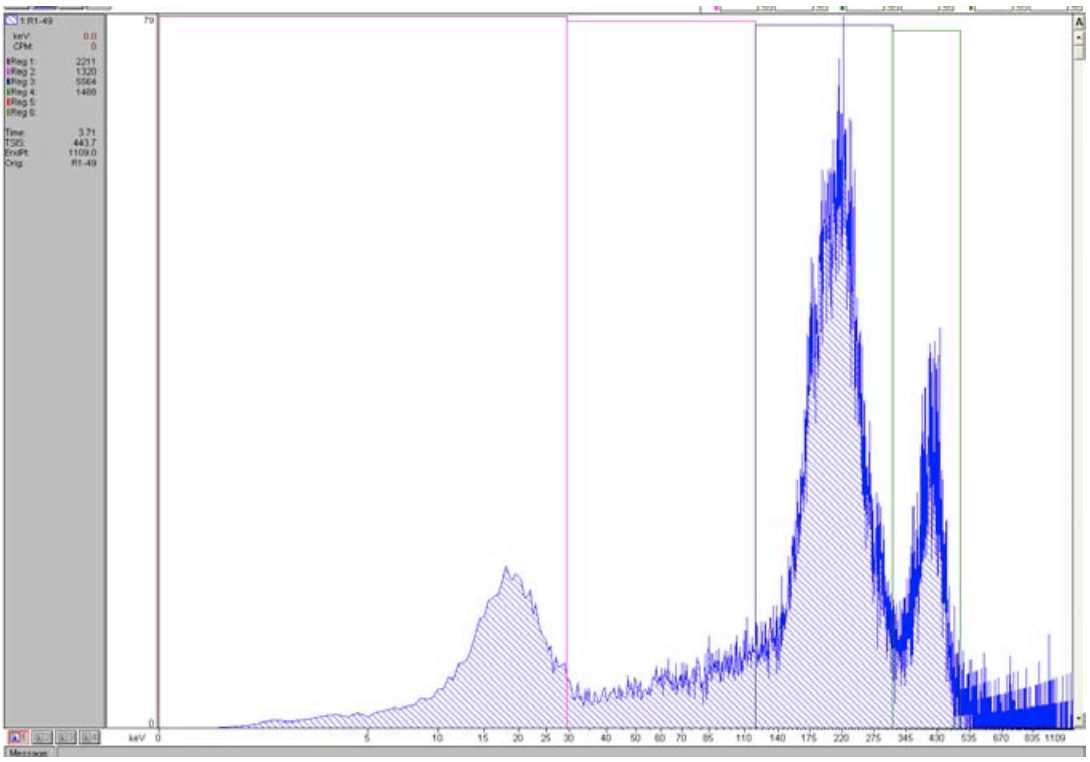

Peak 1: 4,885 [counts]
Peak 2: 1,201 [counts]

R1-50 (39.79 days)

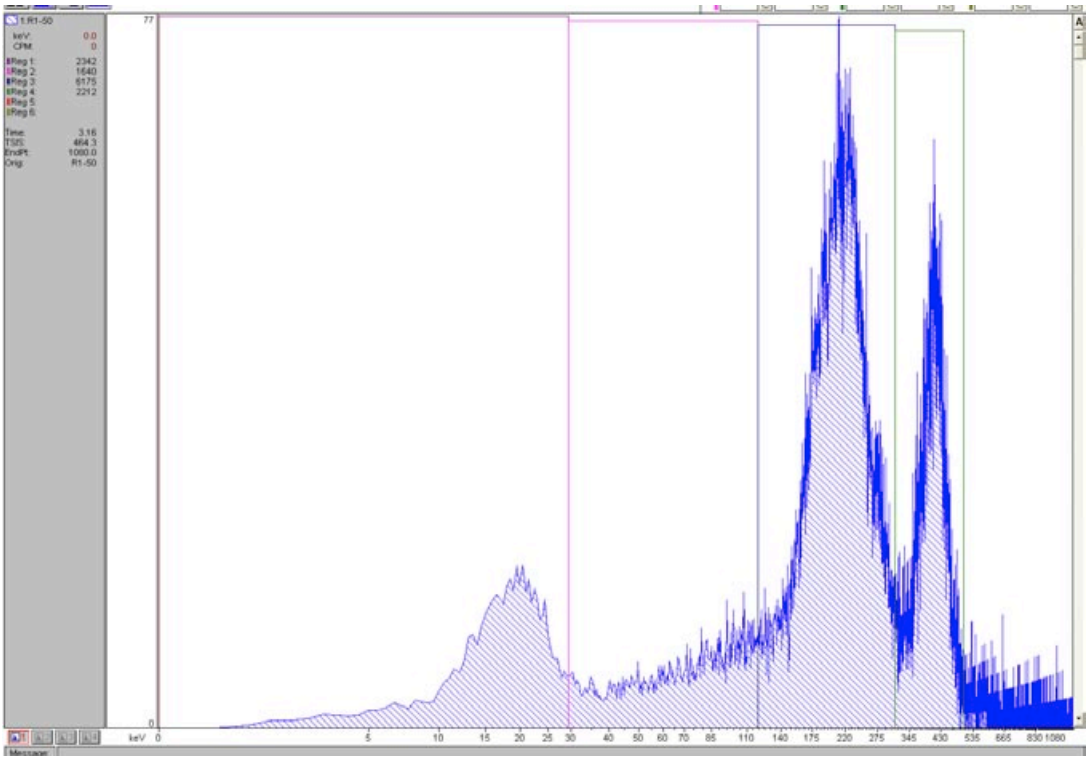

Peak 1: 4,914 [counts]
Peak 2: 1,639 [counts]

R1-51 (47.06 days)

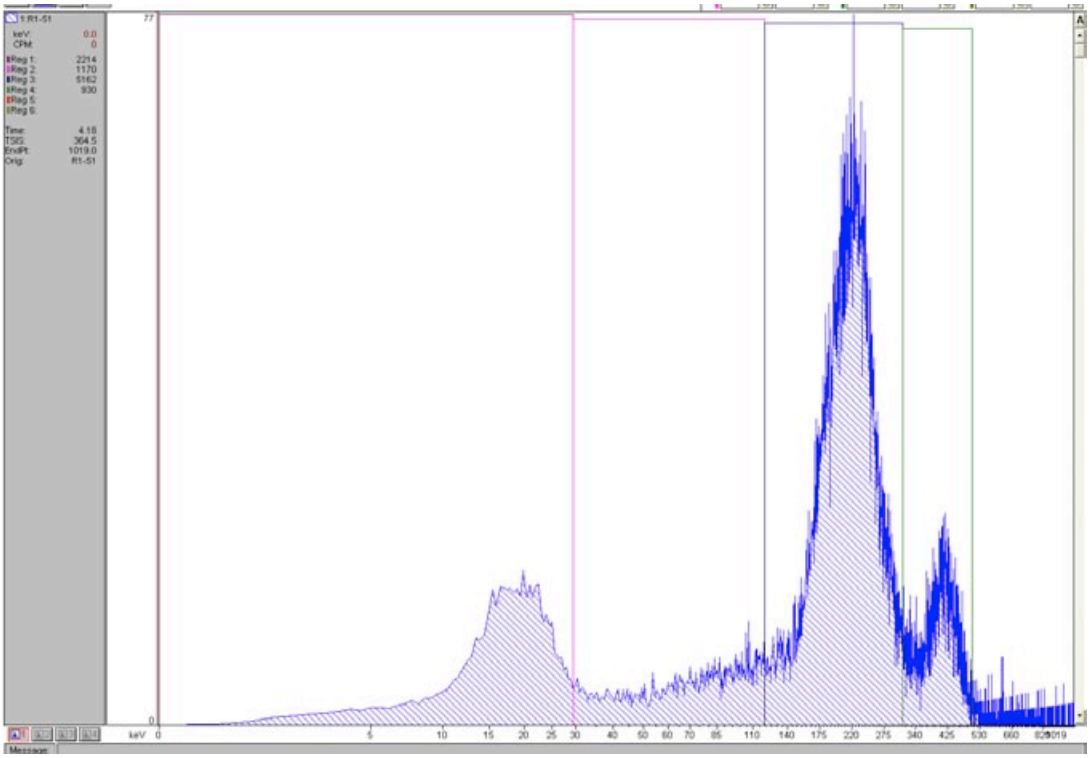

Peak 1: 4,192 [counts]
Peak 2: 357 [counts]

R1-52 (47.81 days)

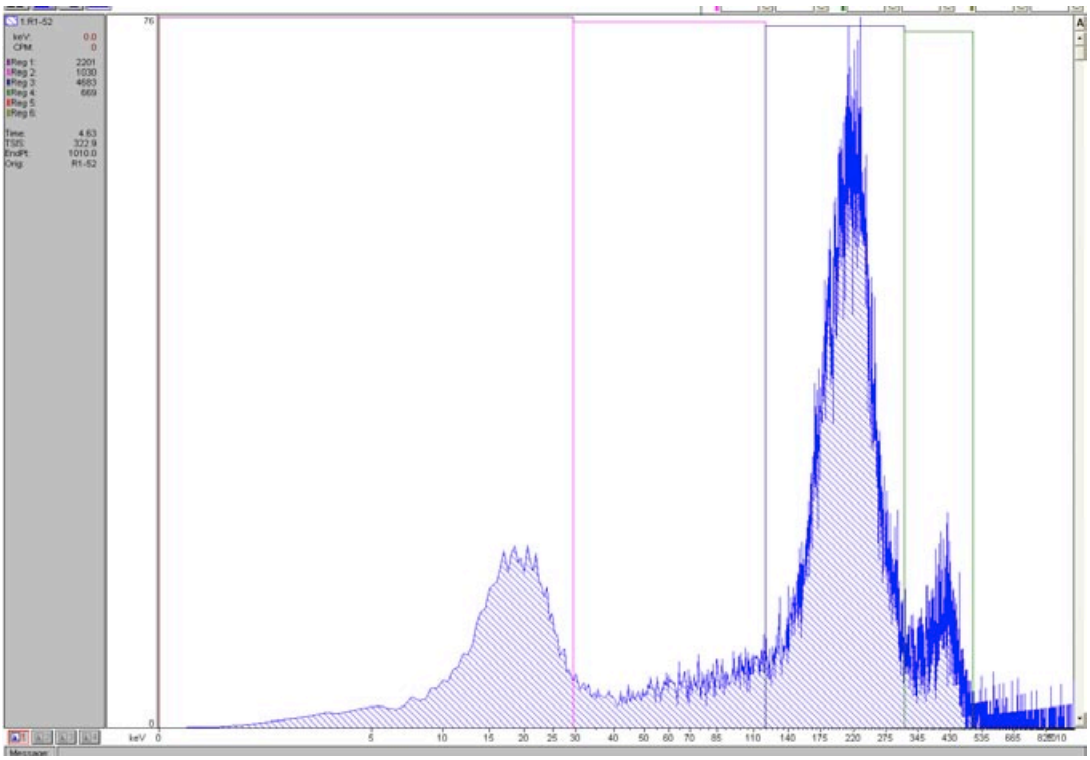

Peak 1: 3,810 [counts]
Peak 2: 382 [counts]

R2-01(0.028 days)

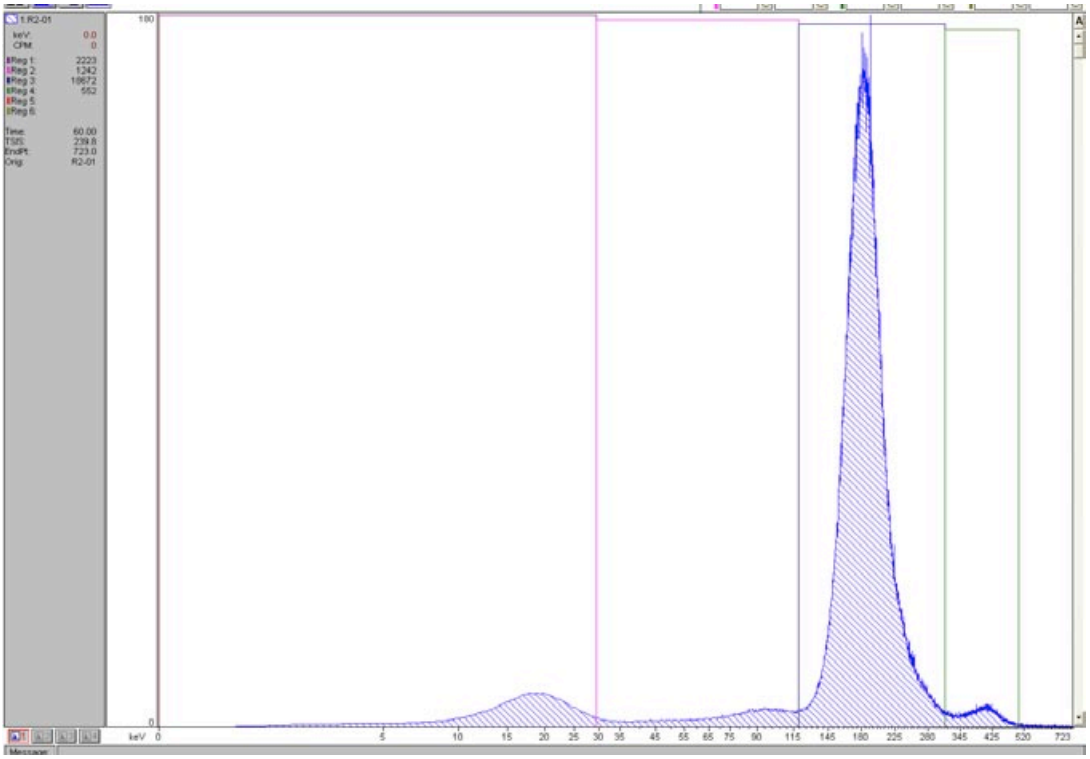

Peak 1: 17,896 [counts]
Peak 2: 361 [counts]

R2-02 (0.108 days)

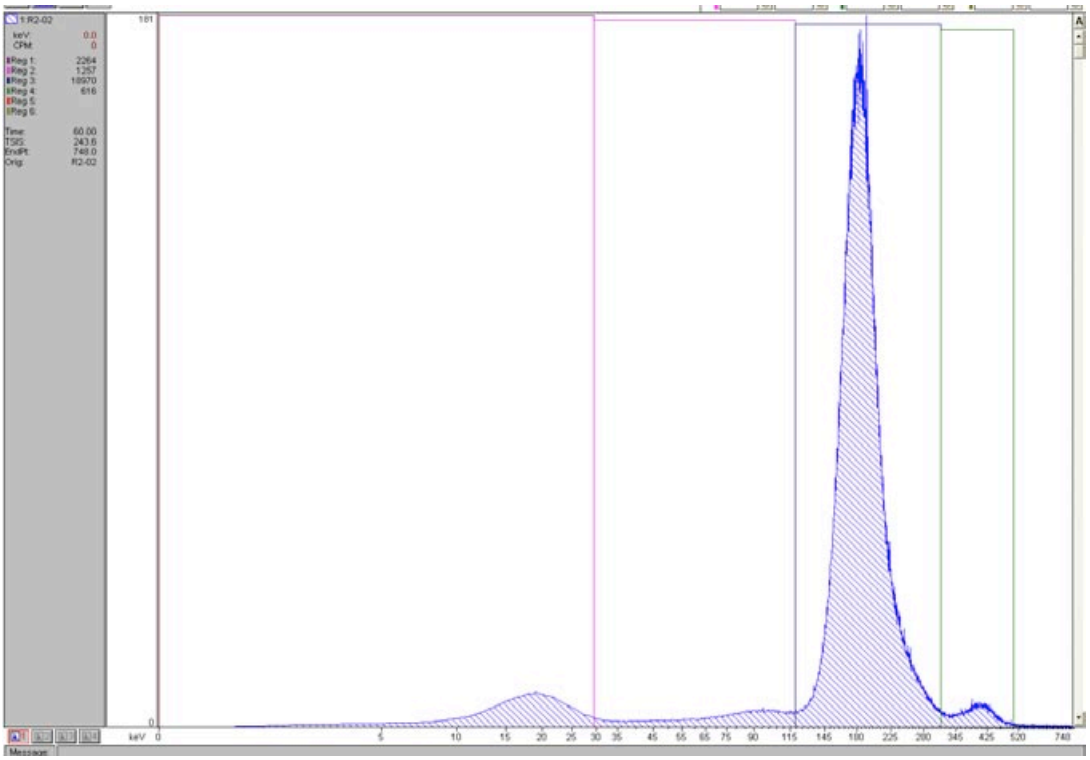

Peak 1: 18,193 [counts]
Peak 2: 425 [counts]

R2-03 (0.903)

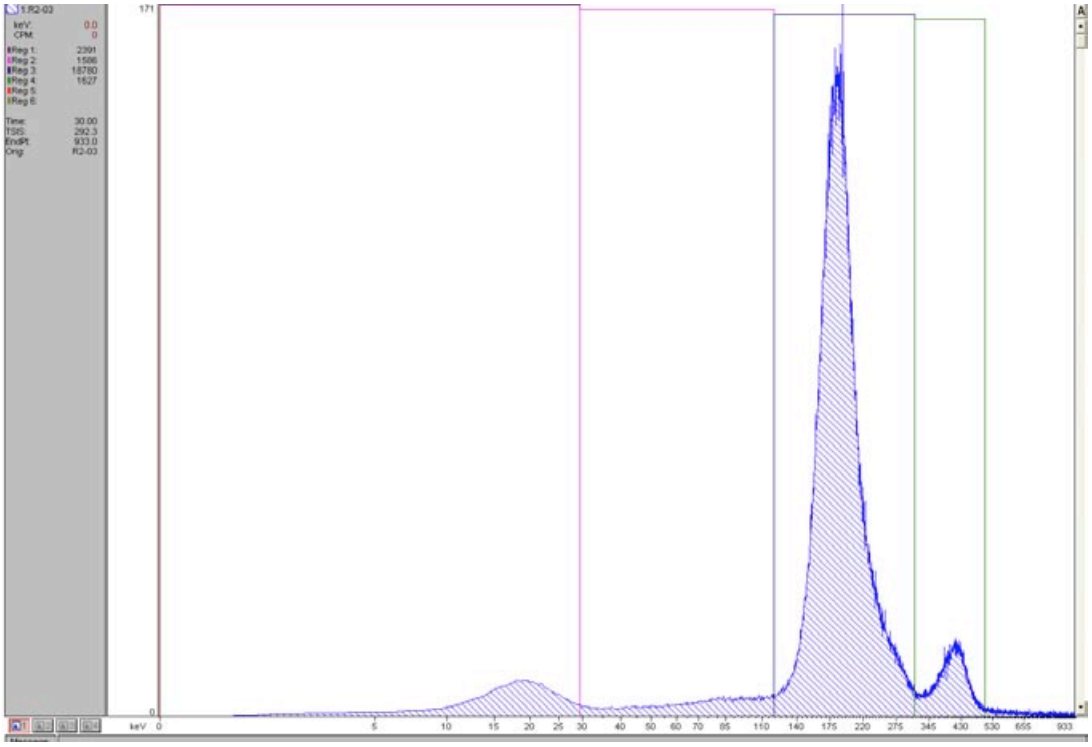

Peak 1: 17,713 [counts]
Peak 2: 1,245 [counts]

R2-04 (1.024 days)

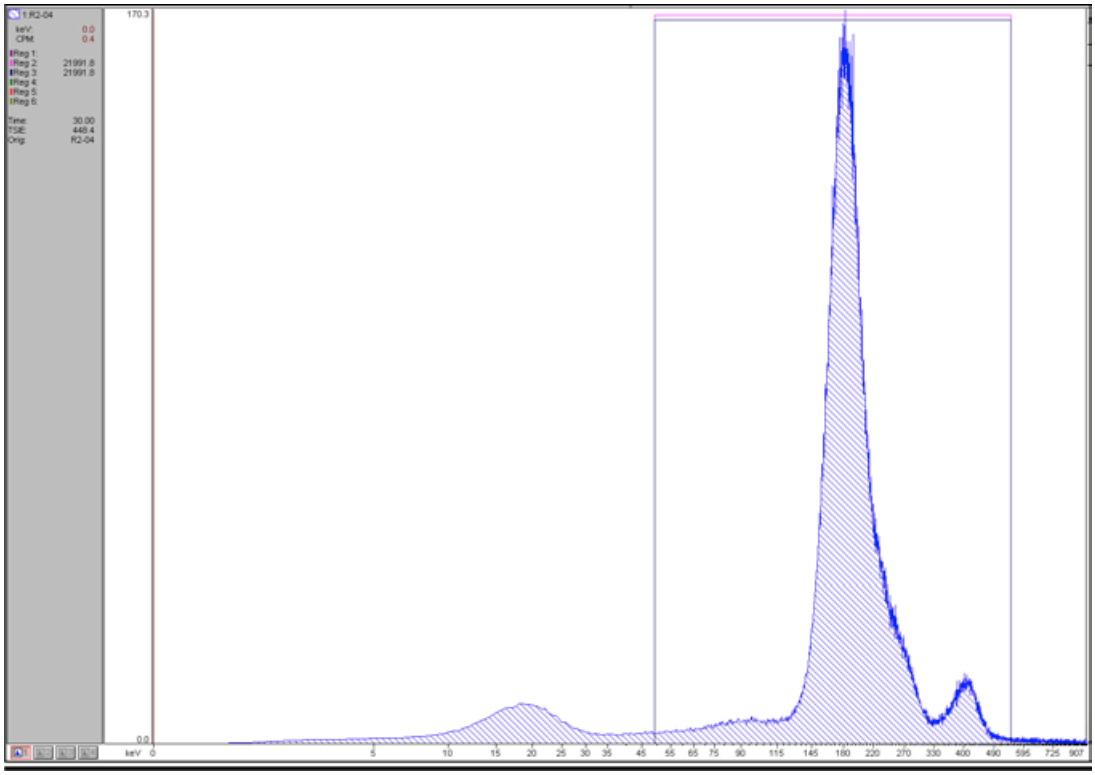

Peak 1: 18,134 [counts]
Peak 2: 864 [counts]

R2-05 (1.802 days)

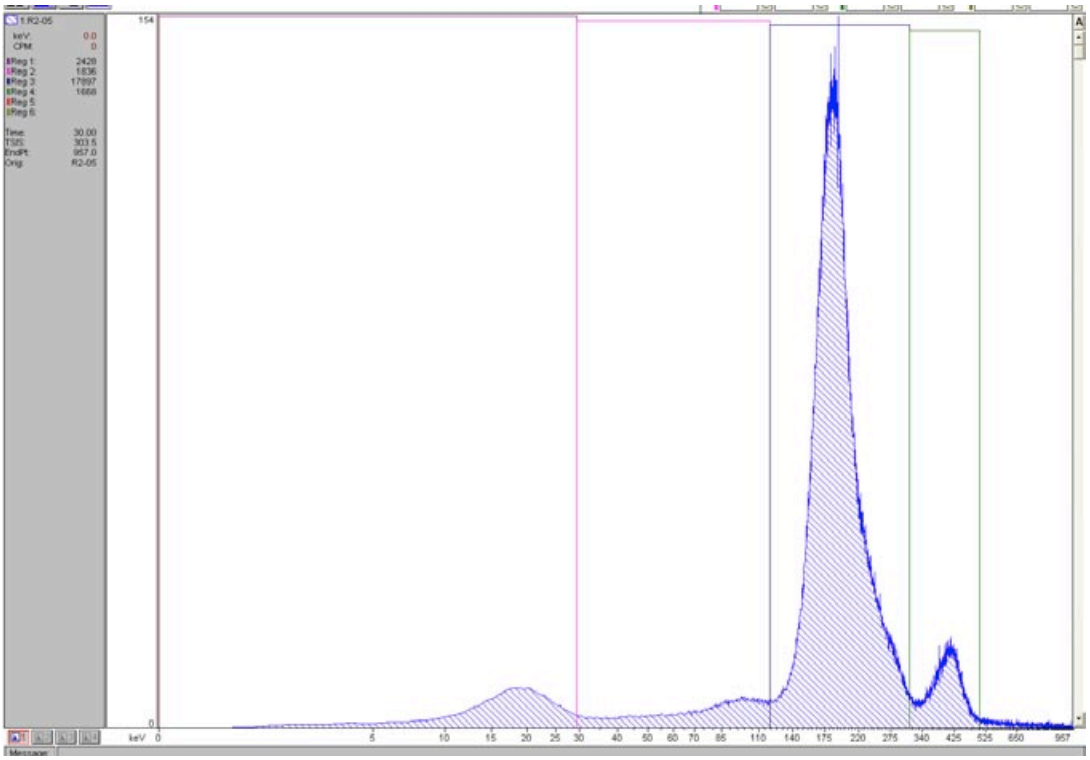

Peak 1: 16,733 [counts]
Peak 2: 1,190 [counts]

R2-06 (2.01 days)

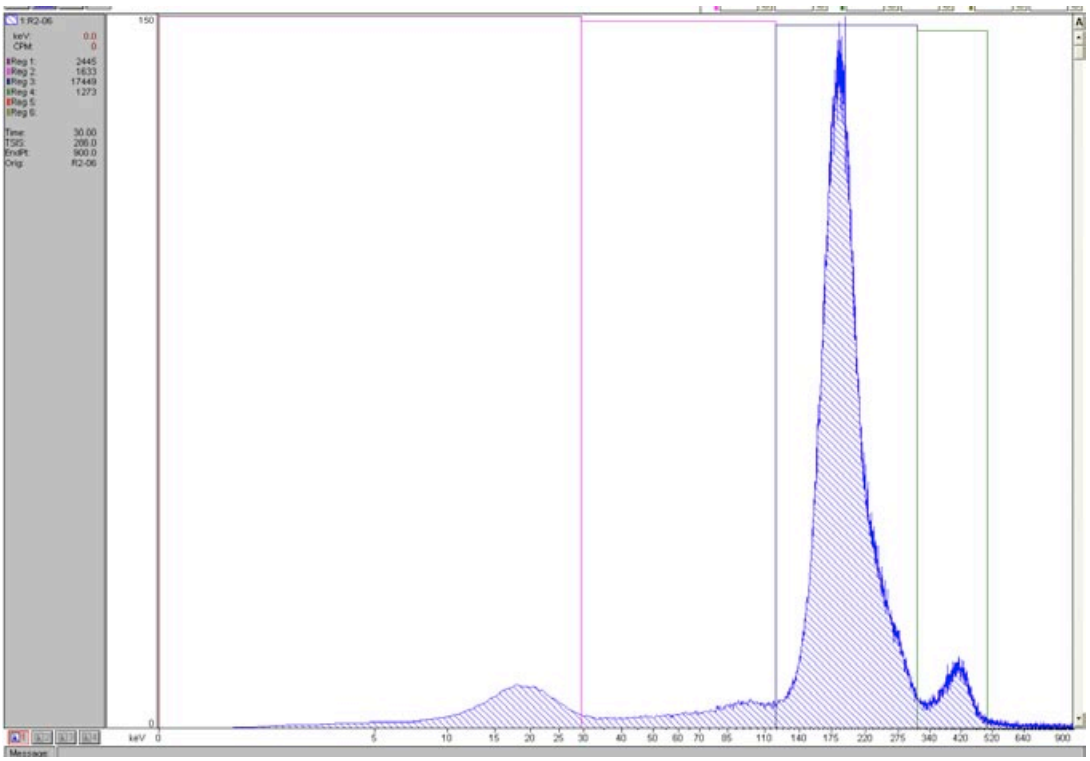

Peak 1: 16,285 [counts]
Peak 2: 795 [counts]

R2-07 (4.858 days)

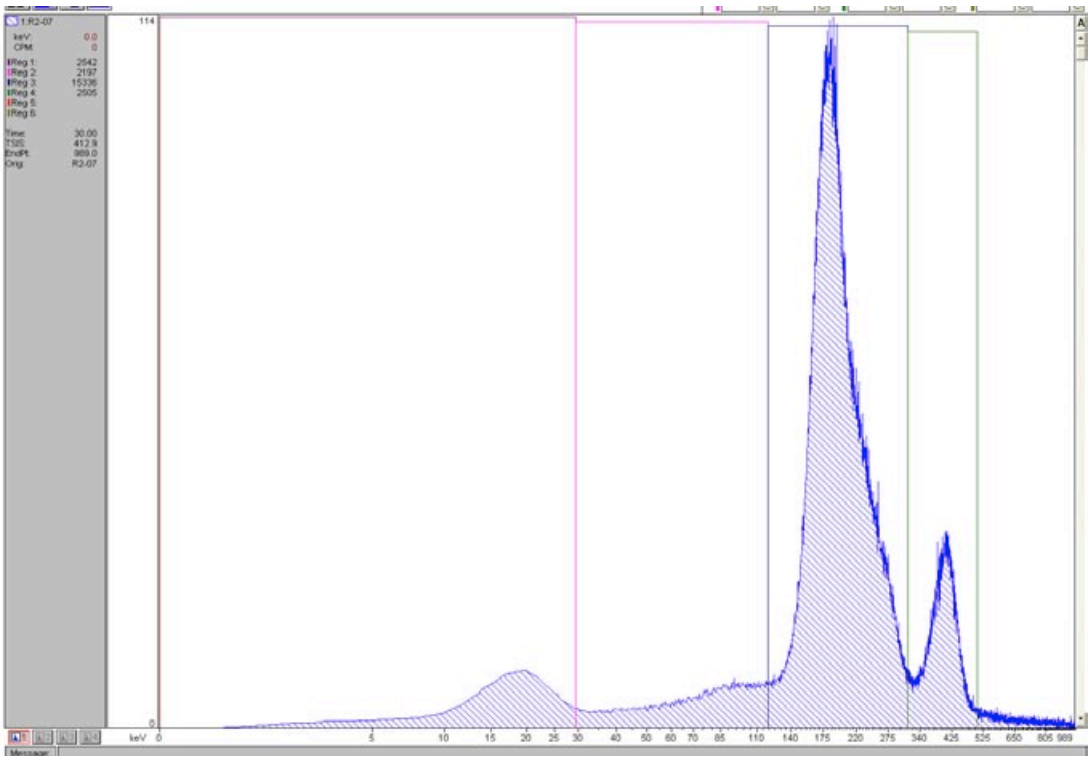

Peak 1: 13,784 [counts]
Peak 2: 1,932 [counts]

R2-08 (5.097 days)

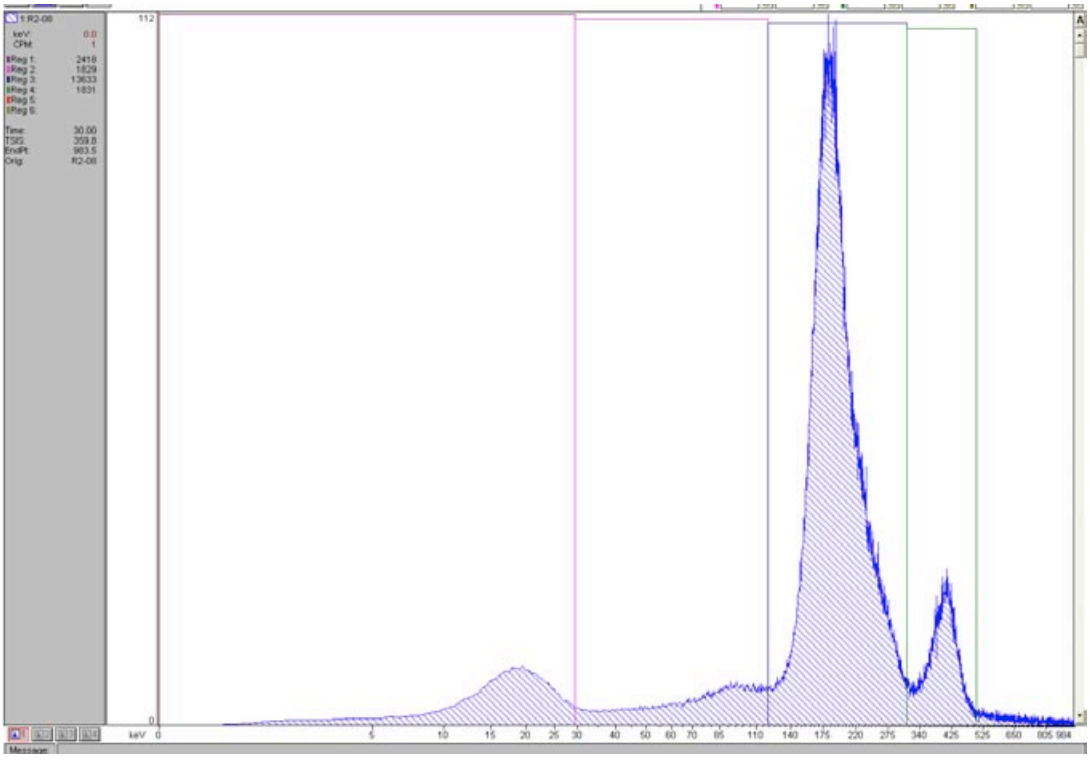

Peak 1: 12,372 [counts]
Peak 2: 1,449 [counts]

R2-09 (5.809 days)

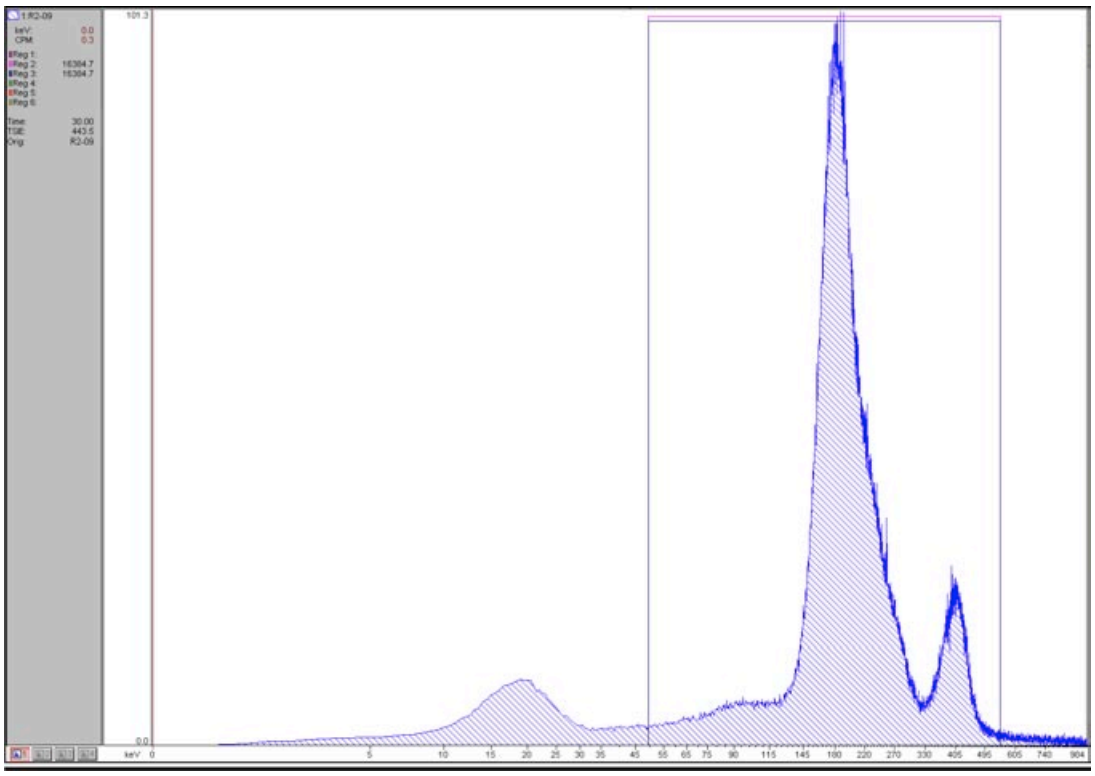

Peak 1: 11,847 [counts]
Peak 2: 1,348 [counts]

R2-10 (6.049 days)

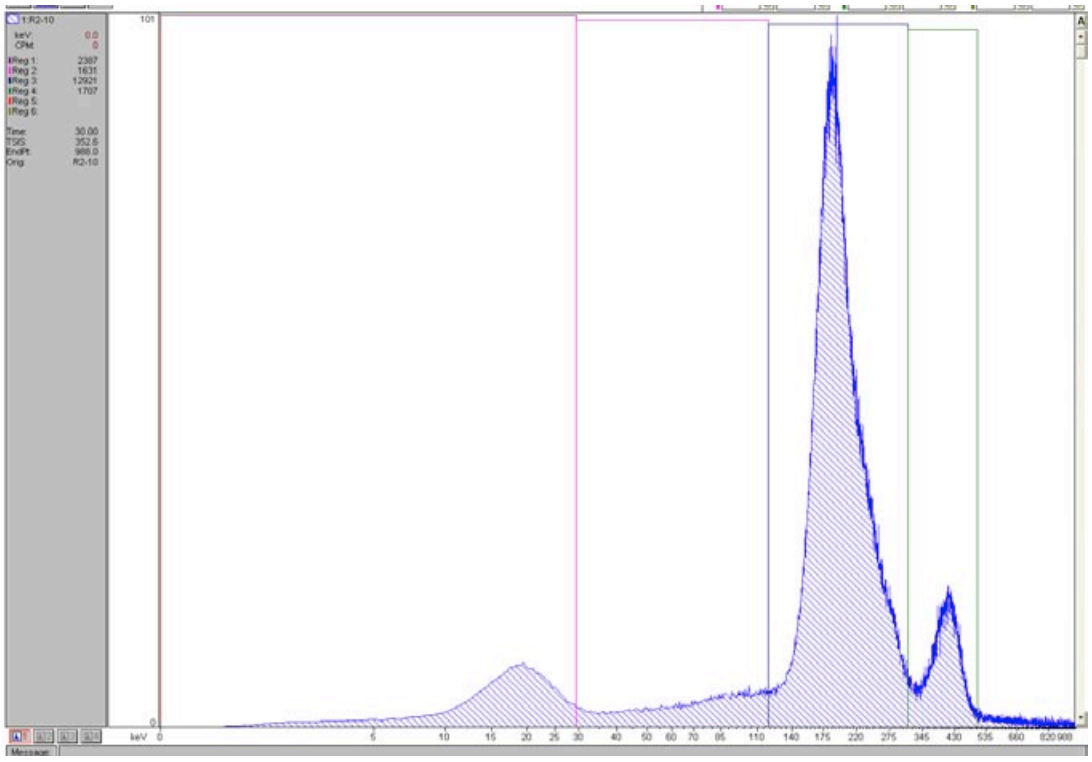

Peak 1: 11,757 [counts]
Peak 2: 1,229 [counts]

R2-11 (6.792 days)

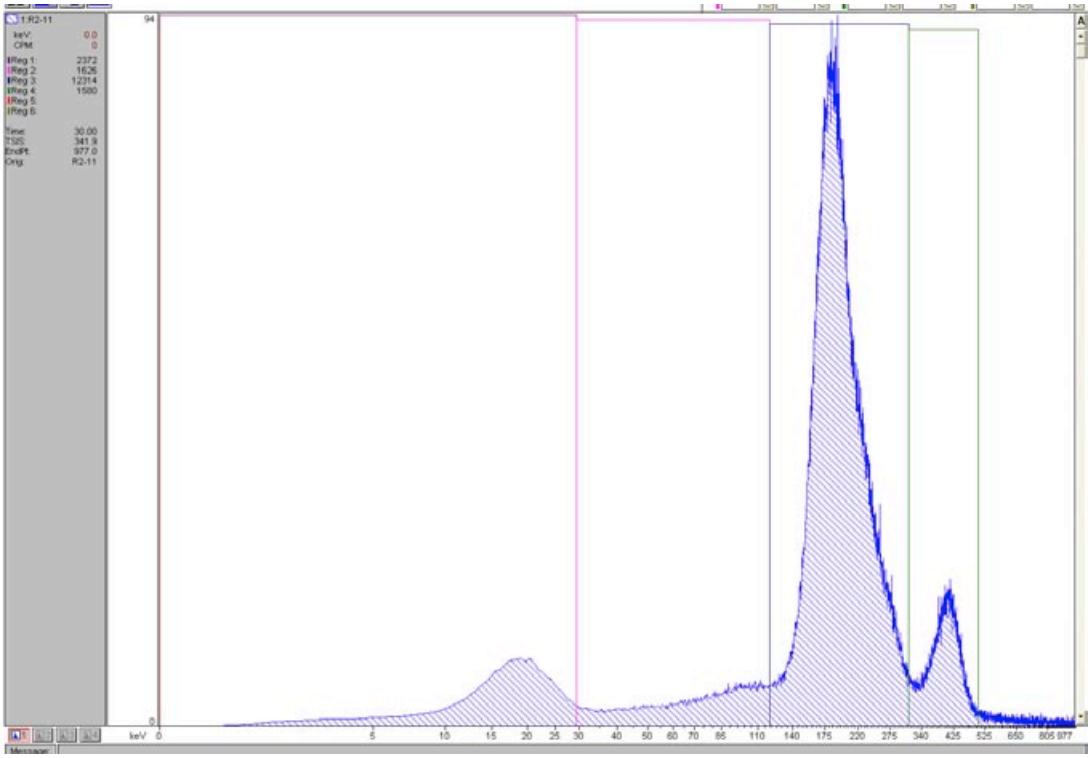

Peak 1: 11,150 [counts]
Peak 2: 1,102 [counts]

R2-12 (7.083 days)

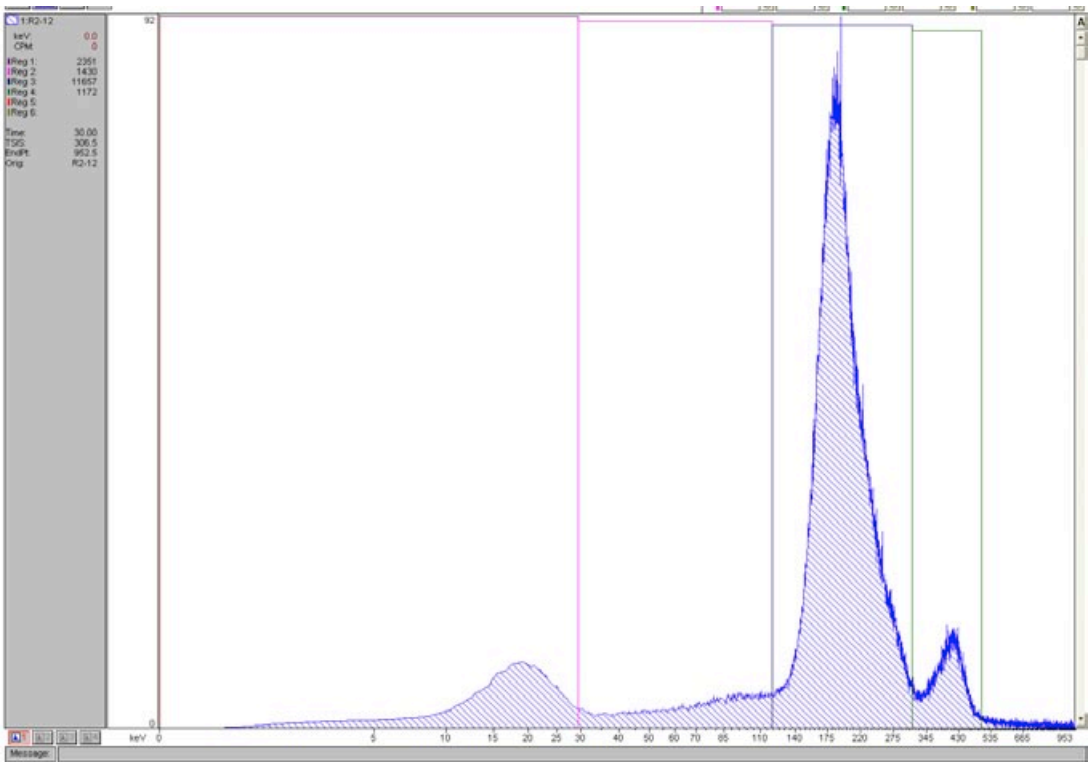

Peak 1: 10,590 [counts]
Peak 2: 694 [counts]

R2-13 (7.795 days)

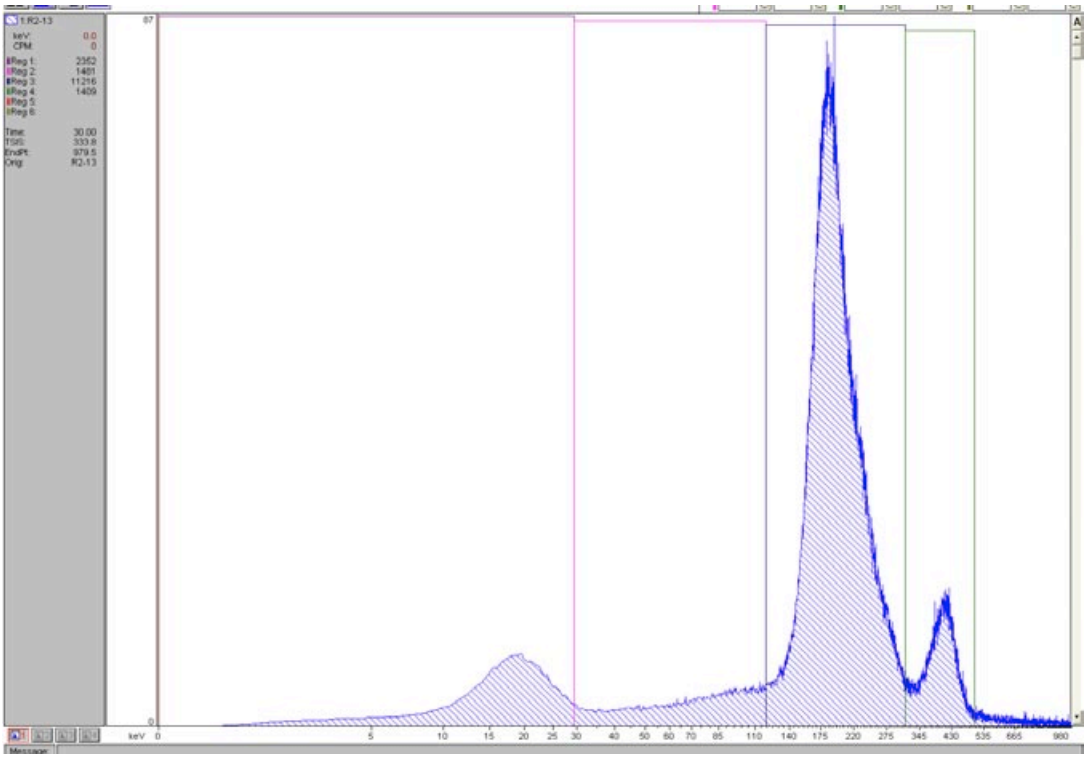

Peak 1: 10,149 [counts]
Peak 2: 1,027 [counts]

R2-14 (8.014 days)

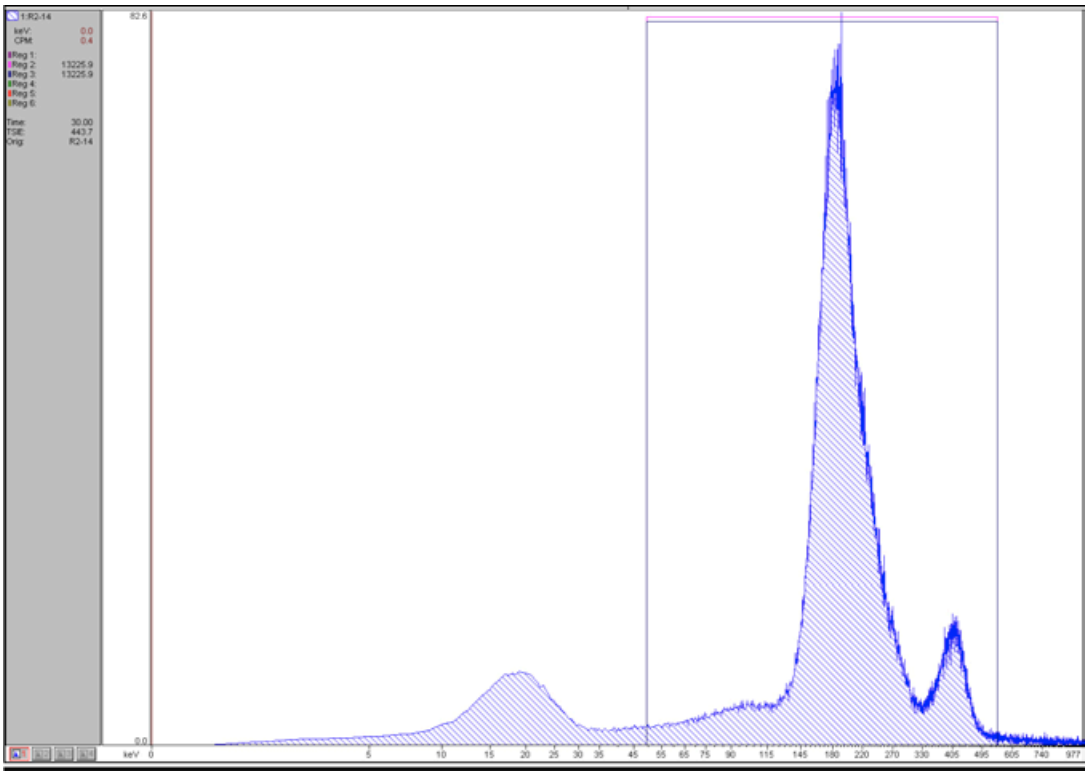

Peak 1: 9,748 [counts]
Peak 2: 893 [counts]

R2-15 (8.799 days)

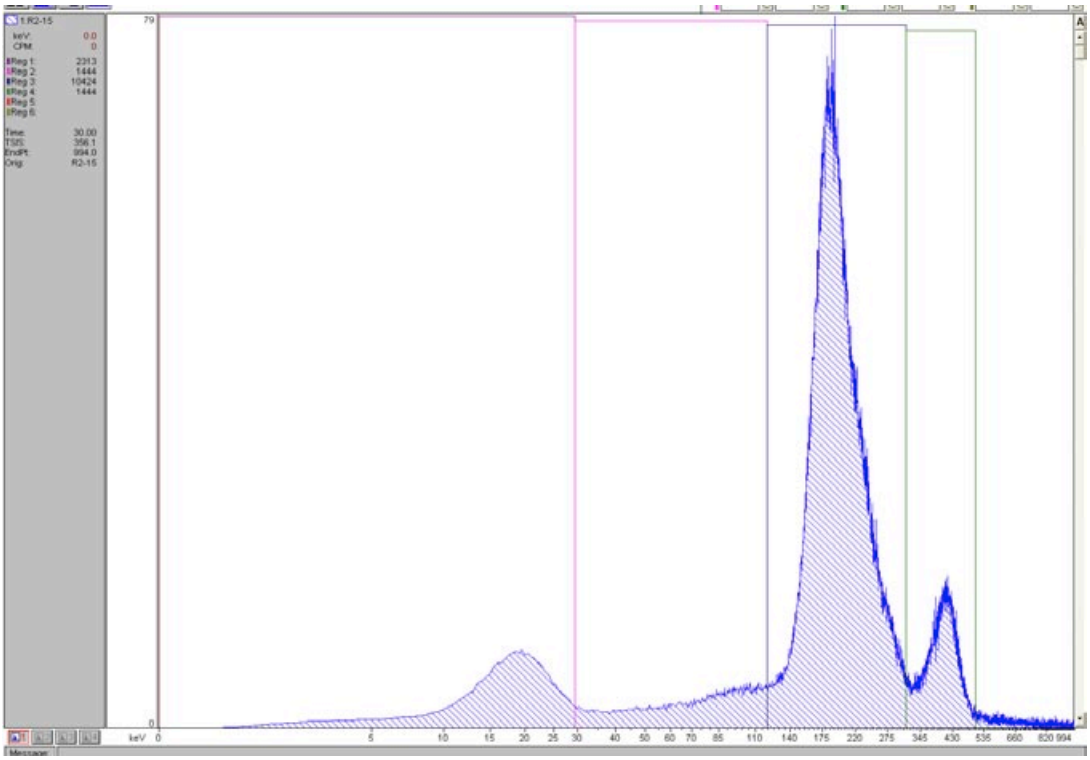

Peak 1: 9,454 [counts]
Peak 2: 1,157 [counts]

R2-16 (9.09 days)

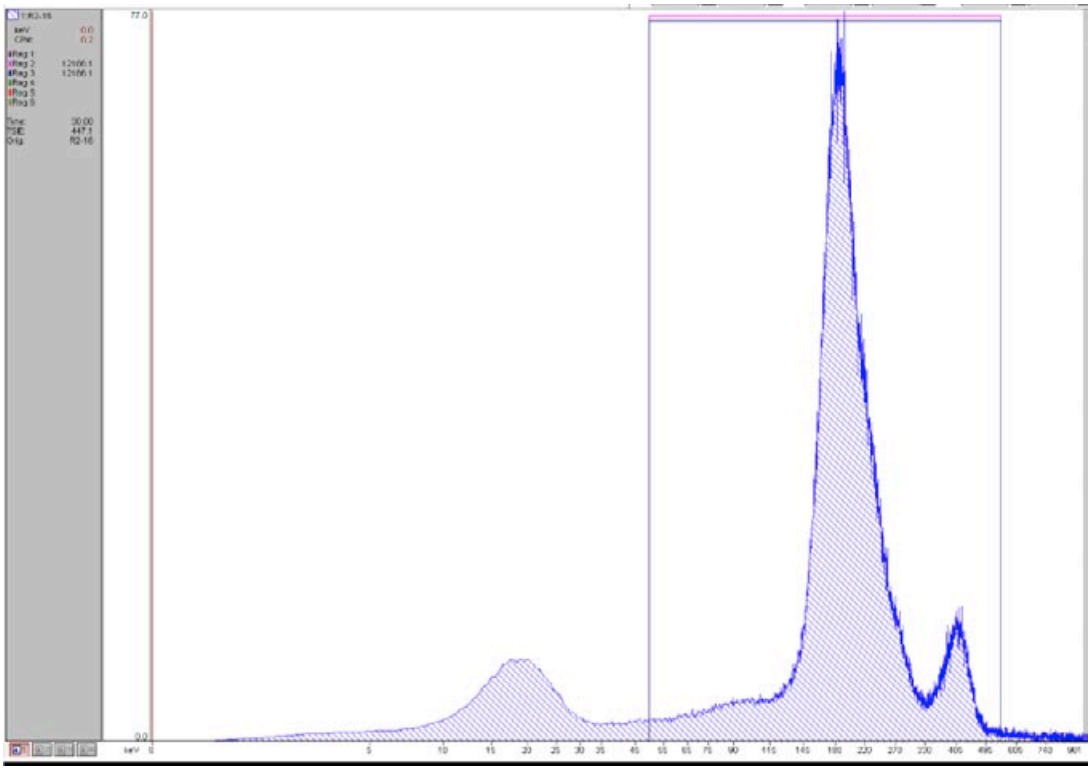

Peak 1: 9,012 [counts]
Peak 2: 837 [counts]

R2-17 (11.795 days)

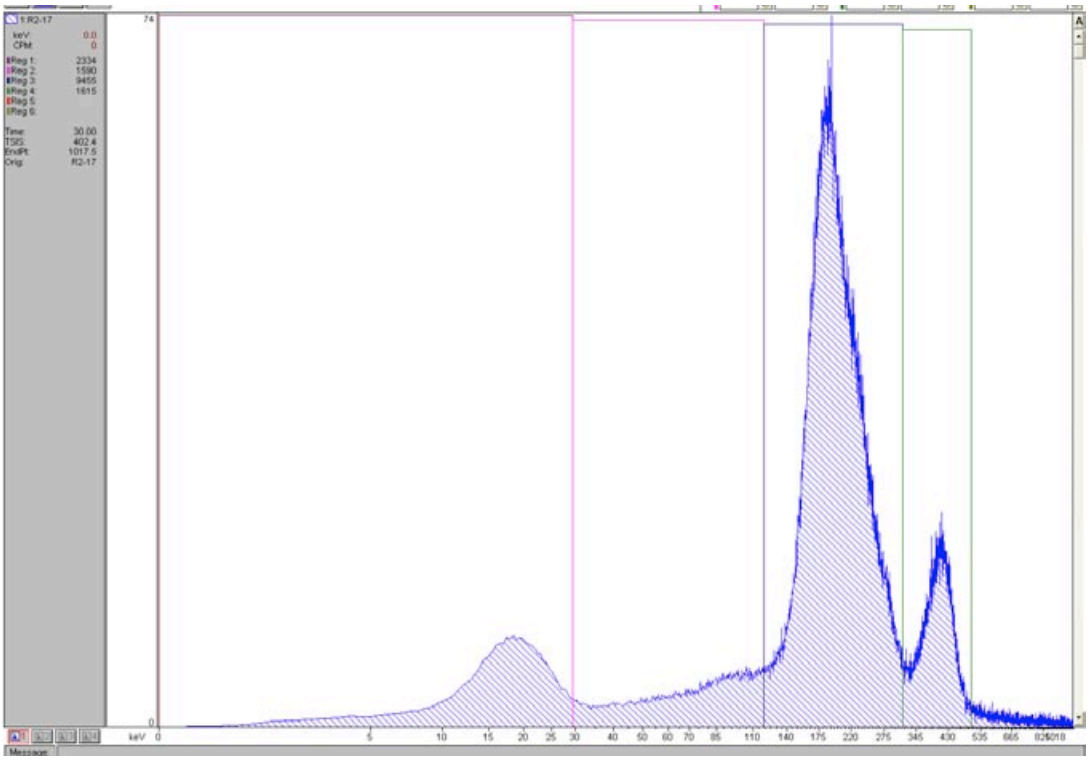

Peak 1: 8,485 [counts]
Peak 2: 1,233 [counts]

R2-18 (12.042 days)

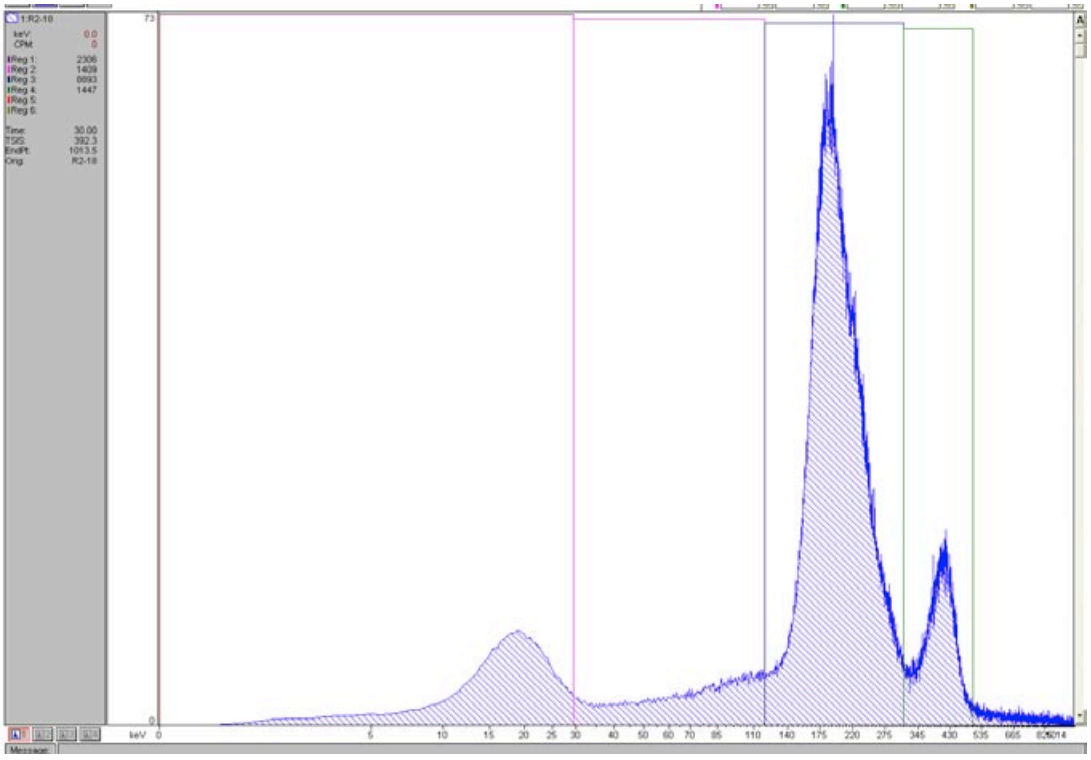

Peak 1: 7,826 [counts]
Peak 2: 969 [counts]

R2-19 (12.809 days)

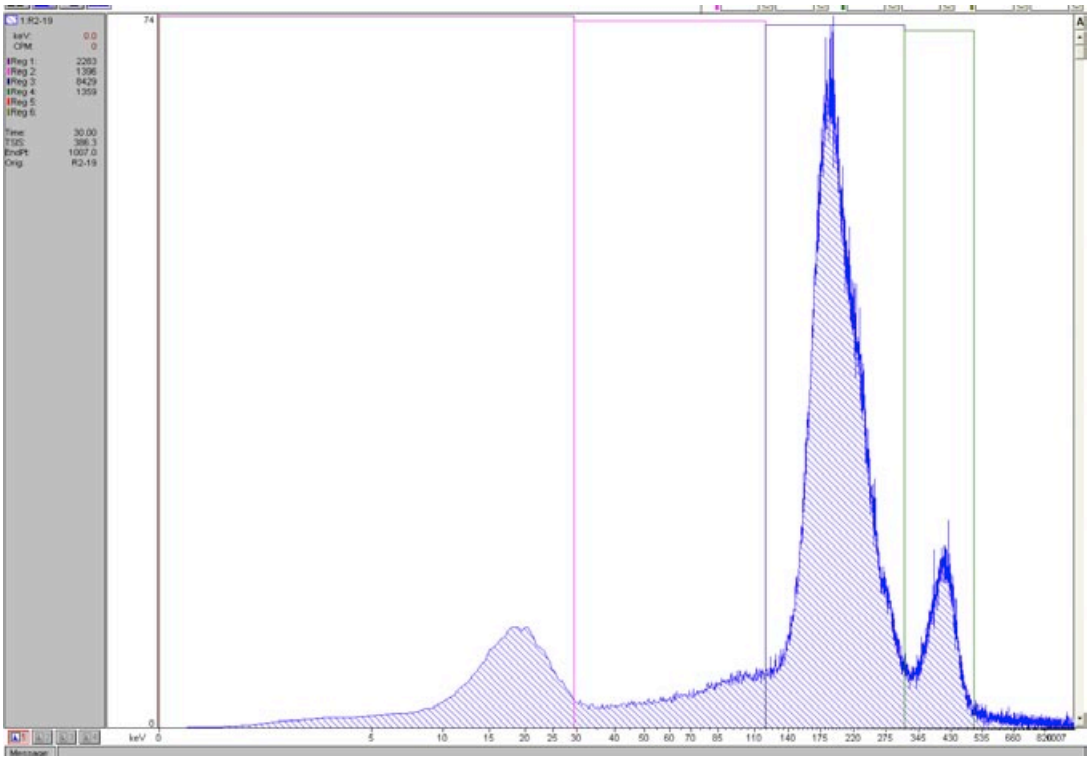

Peak 1: 7,362 [counts]
Peak 2: 1,072 [counts]

R2-20 (13.806 days)

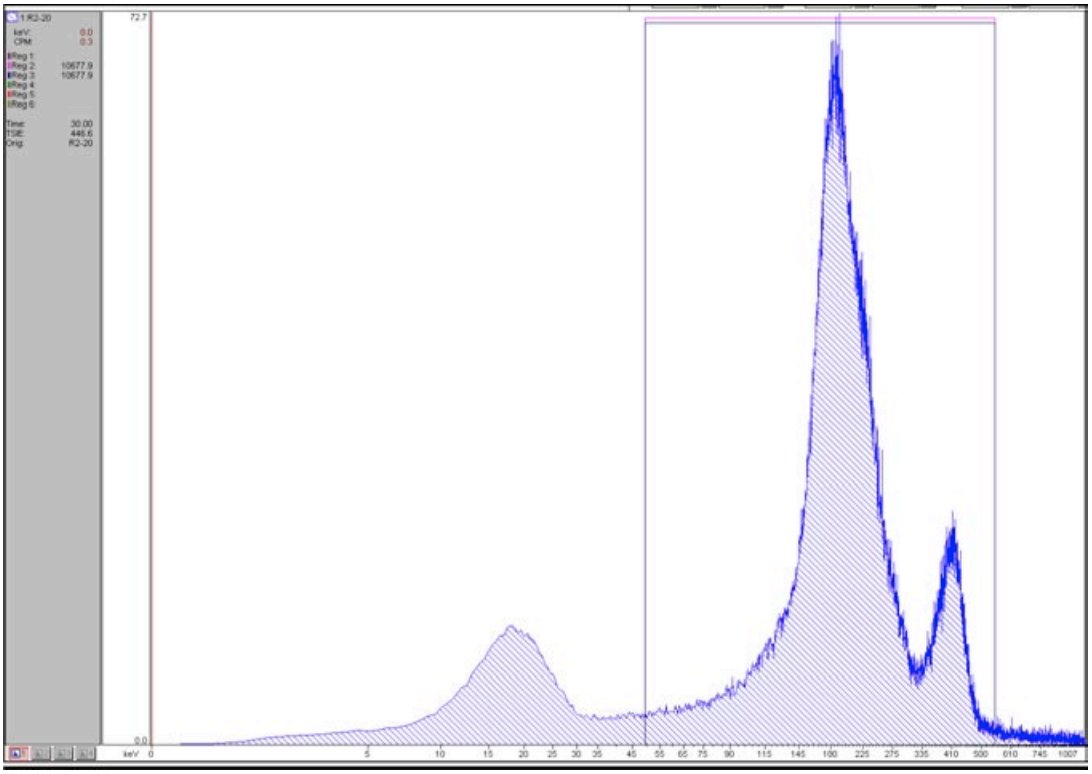

Peak 1: 6,683 [counts]
Peak 2: 998 [counts]

R2-21 (14.785 days)

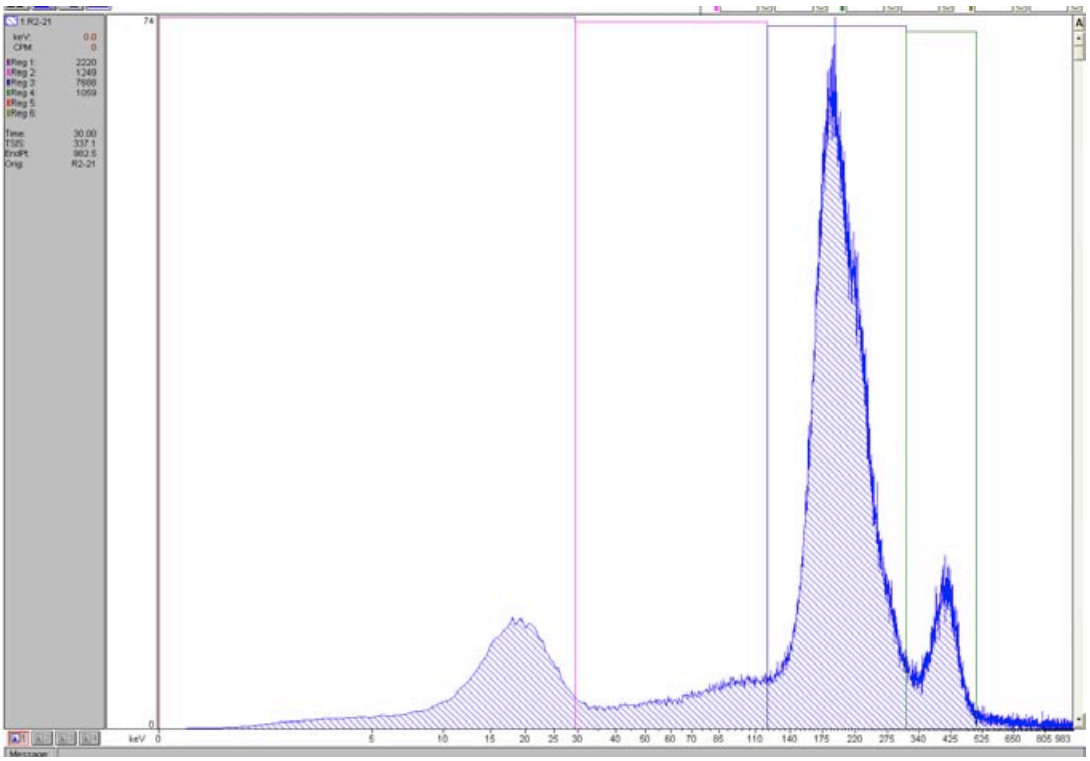

Peak 1: 6,815 [counts]
Peak 2: 677 [counts]

R2-22 (15.035 days)

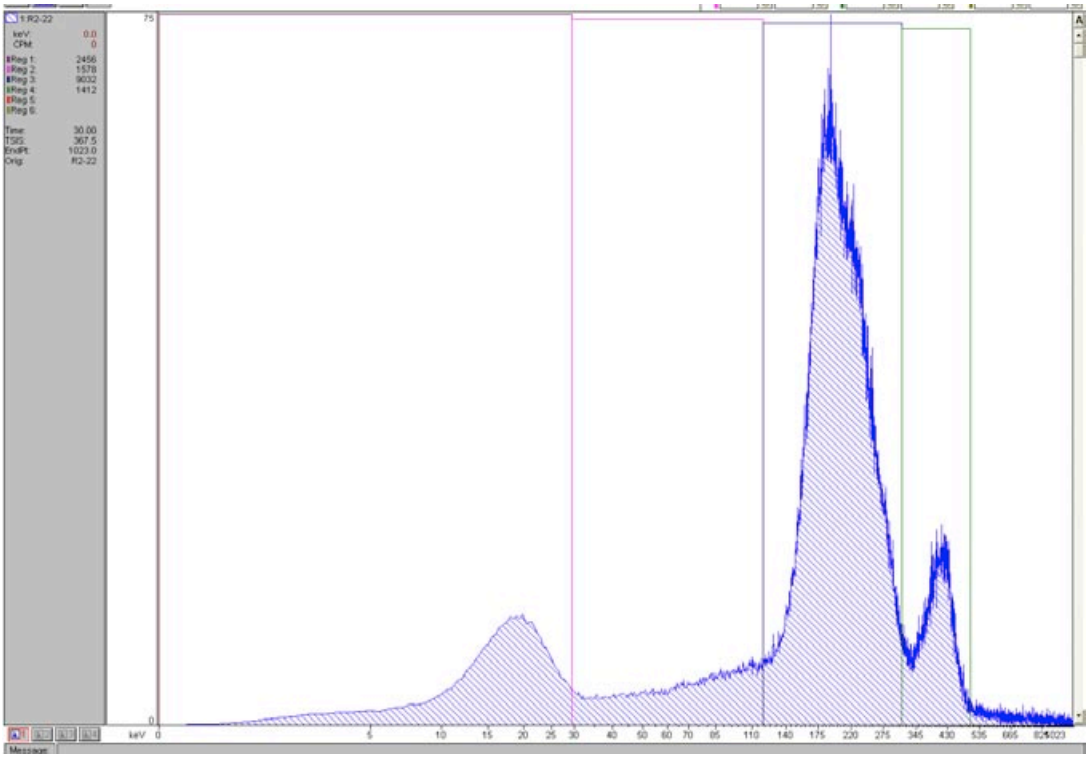

Peak 1: 7,868 [counts]
Peak 2: 1,030 [counts]

R2-23 (15.799 days)

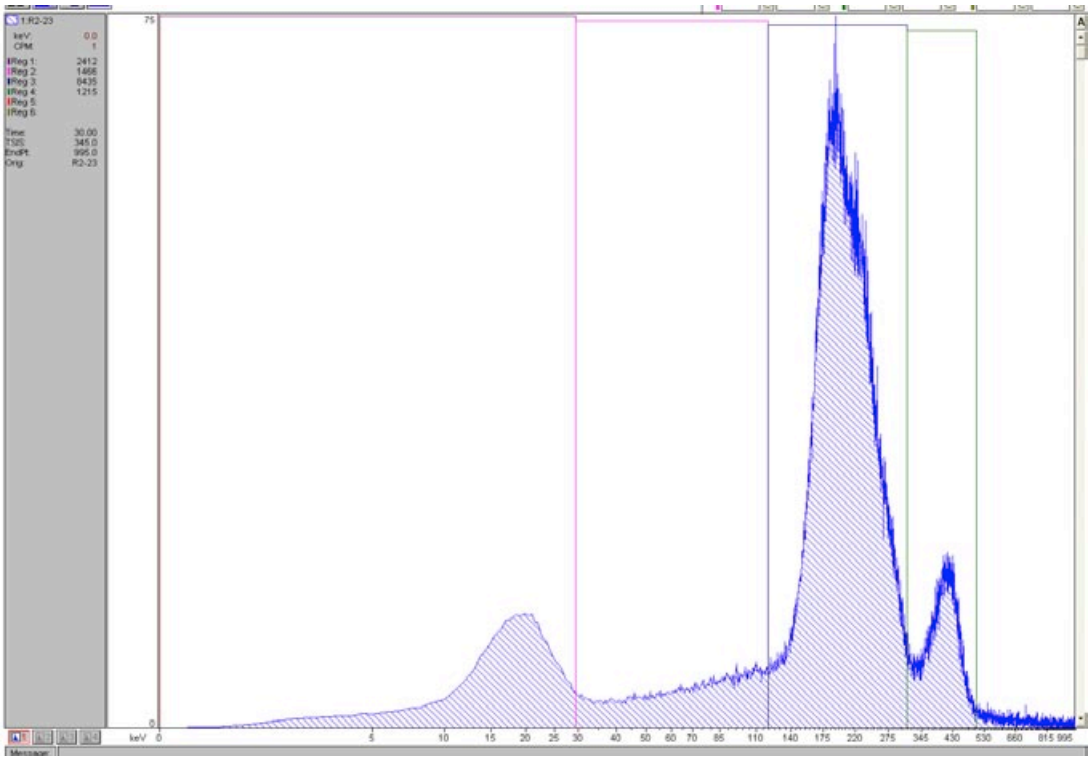

Peak 1: 7,271 [counts]
Peak 2: 737 [counts]

R2-24 (18.802 days)

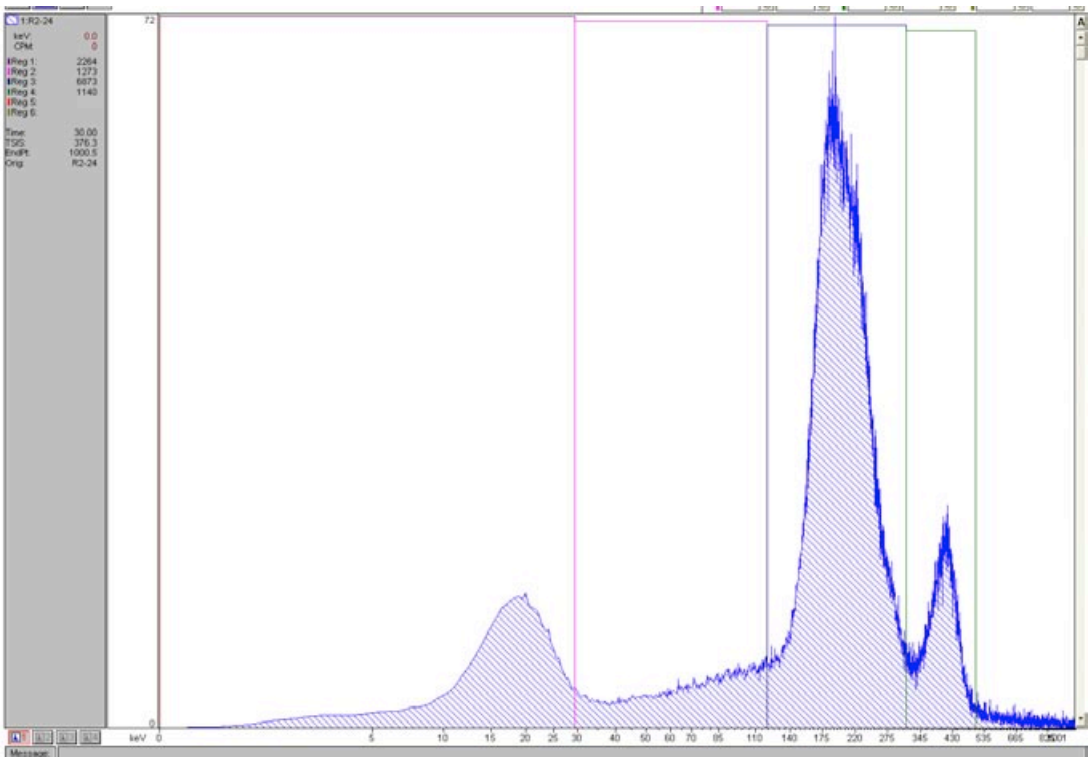

Peak 1: 6,097 [counts]
Peak 2: 949 [counts]

R2-25 (19.0 days)

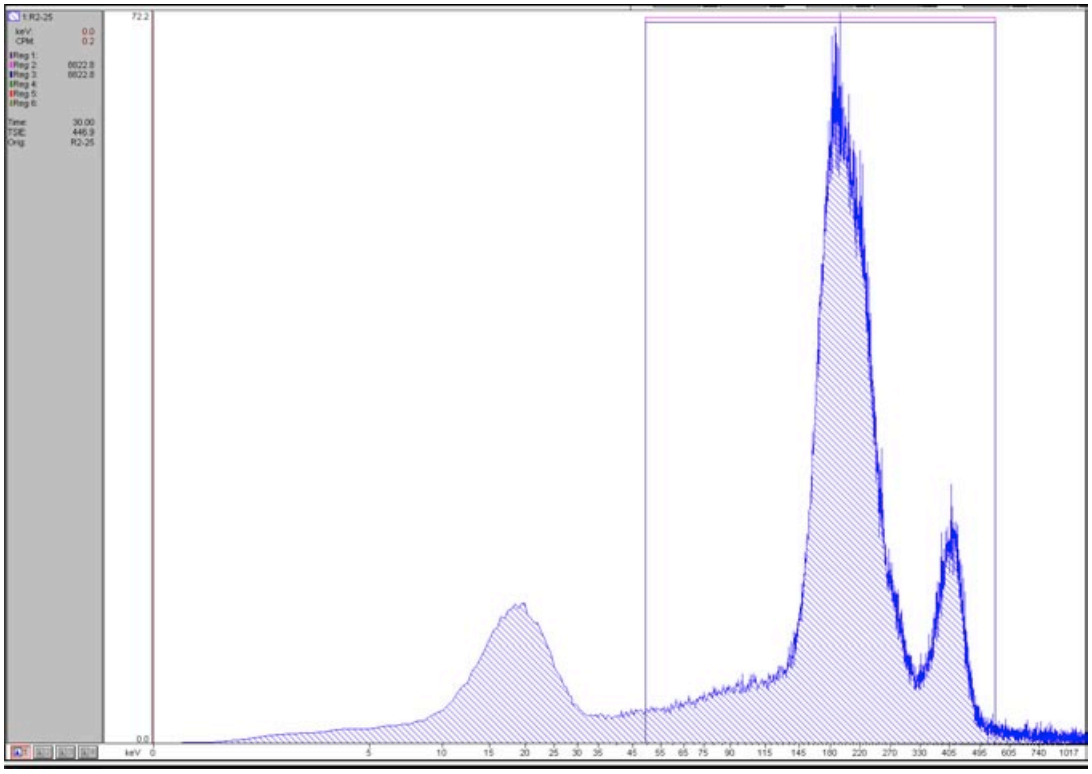

Peak 1: 5,790 [counts]
Peak 2: 919 [counts]

R2-26 (19.792 days)

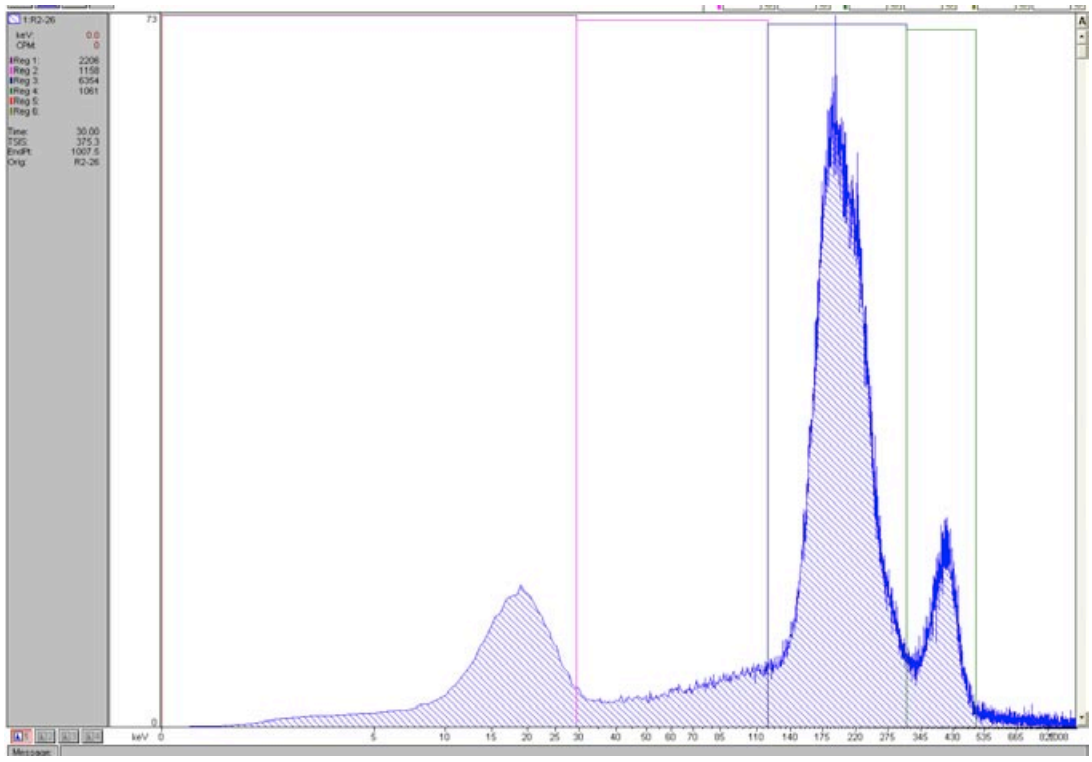

Peak 1: 5,481 [counts]
Peak 2: 679 [counts]

R2-27 (20.792 days)

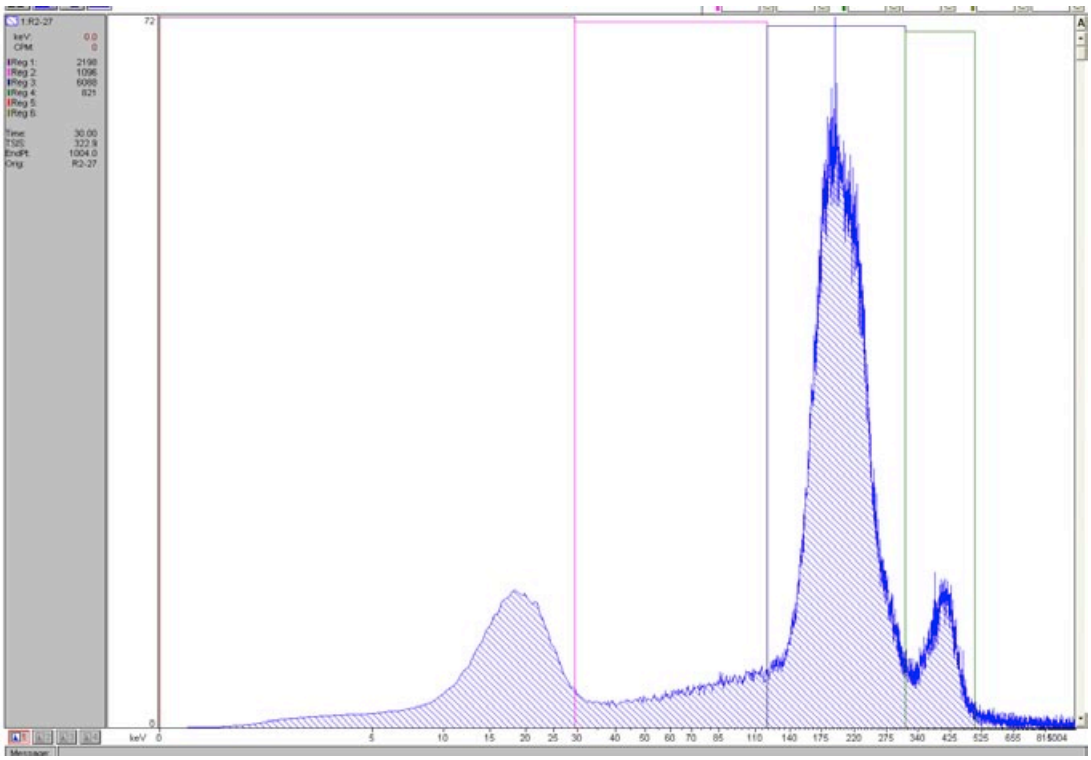

Peak 1: 5,409 [counts]
Peak 2: 630 [counts]

R2-28 (21.063 days)

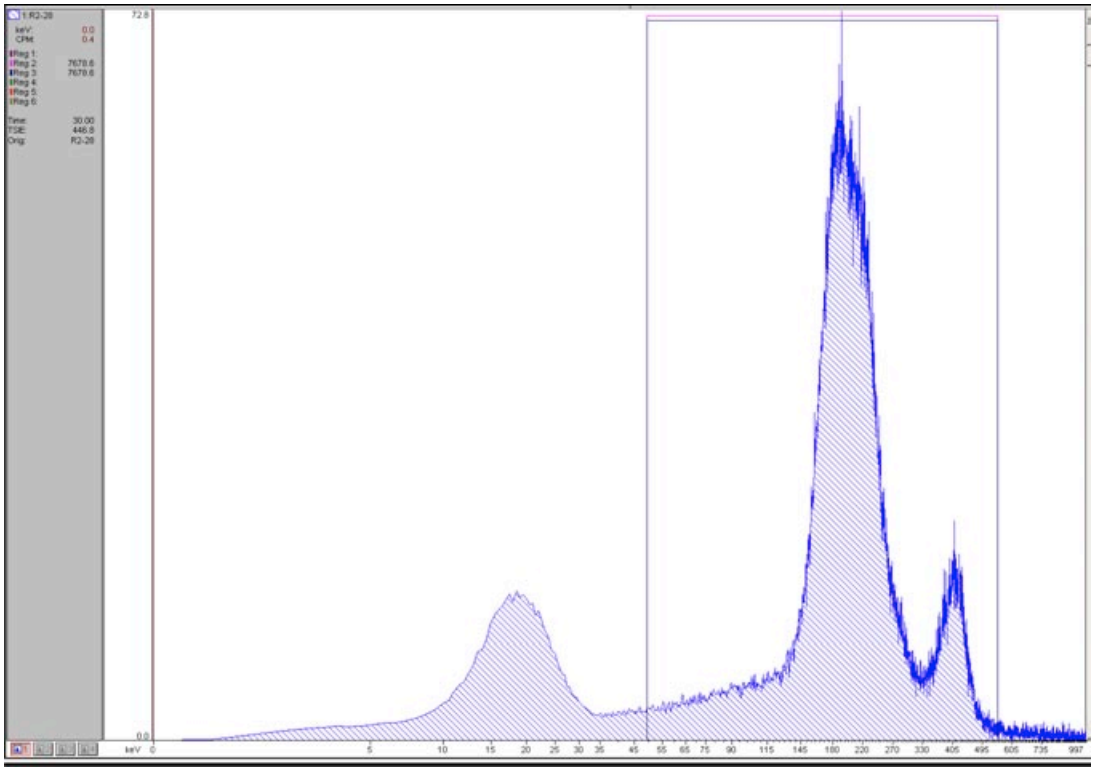

Peak 1: 5,268 [counts]
Peak 2: 707 [counts]

R2-29 (21.823 days)

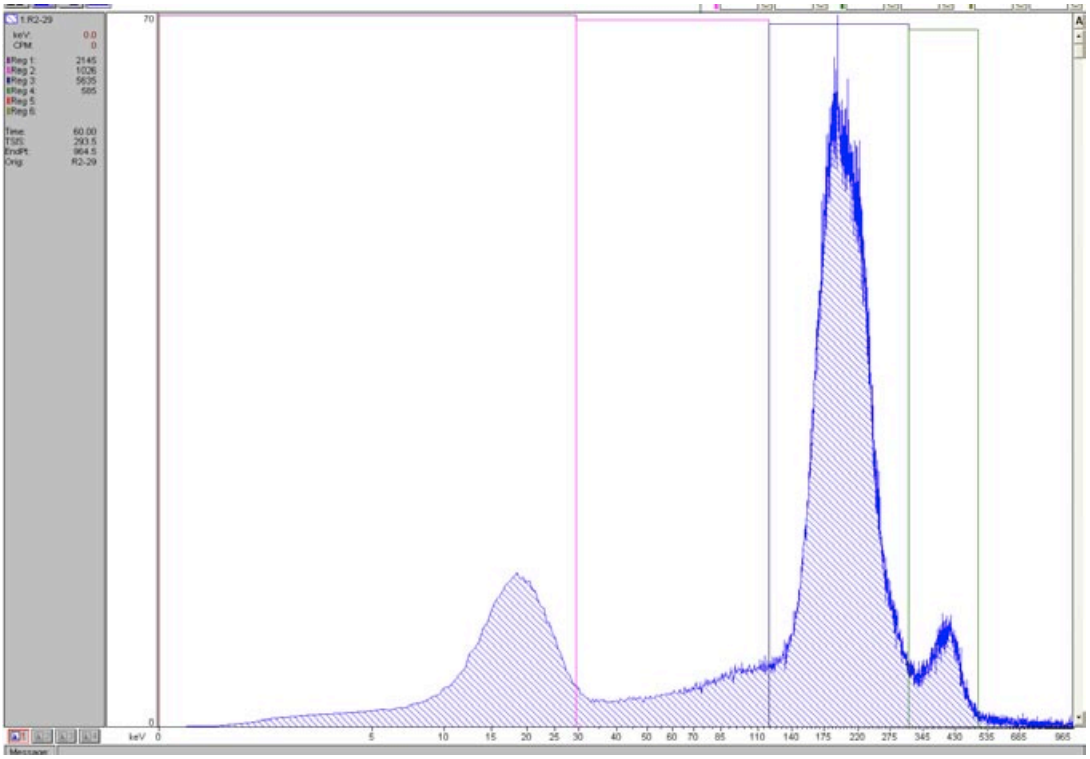

Peak 1: 4,859 [counts]
Peak 2: 394 [counts]

R2-30 (22.04 days)

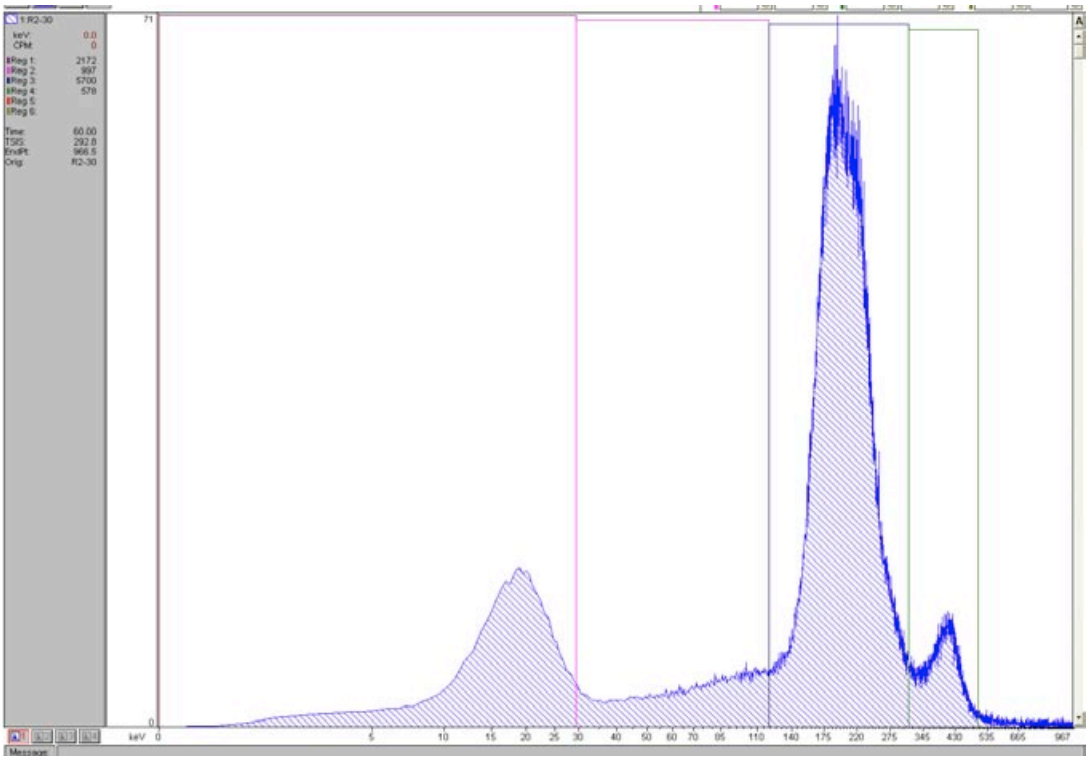

Peak 1: 5,118 [counts]
Peak 2: 387 [counts]

R2-31 (22.83 days)

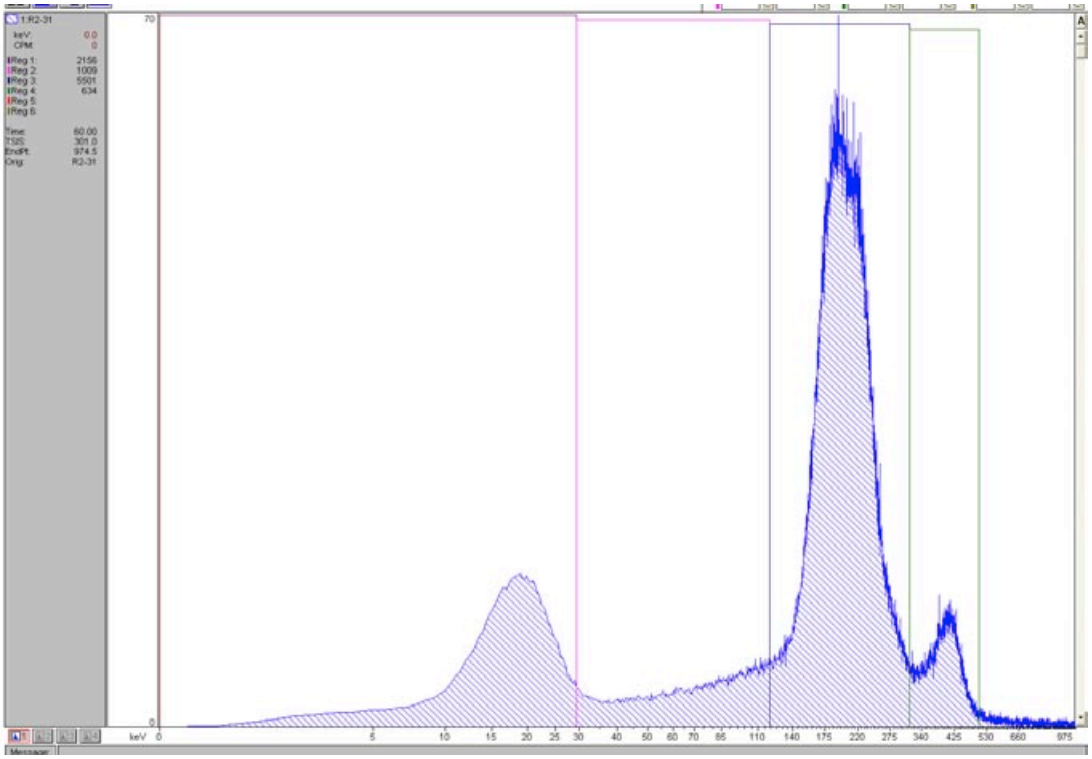

Peak 1: 4,725 [counts]
Peak 2: 443 [counts]

R2-32 (22.99 days)

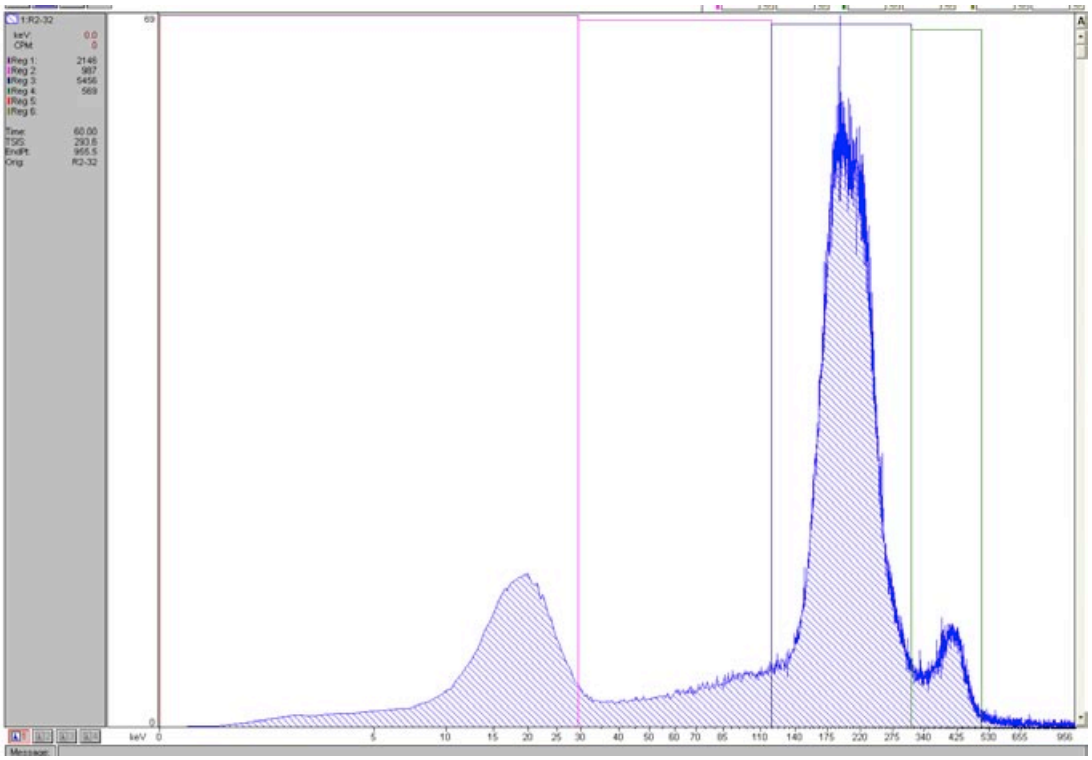

Peak 1: 4,777 [counts]
Peak 2: 378 [counts]

R2-33 (25.88 days)

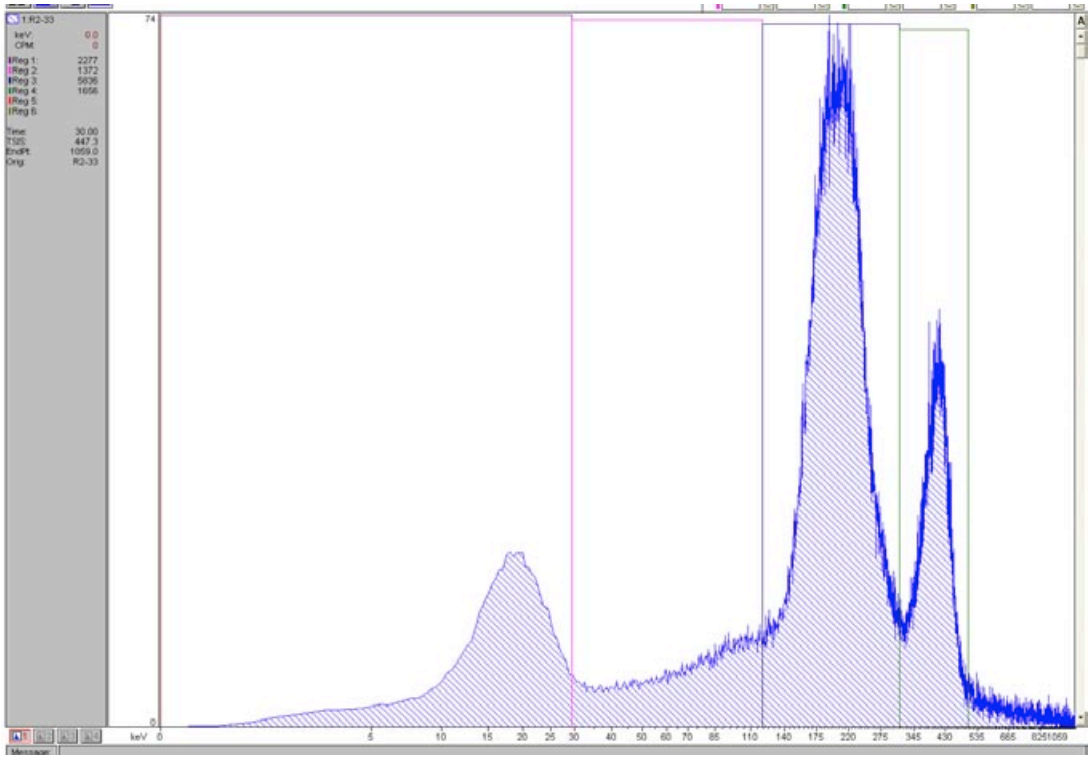

Peak 1: 4,769 [counts]
Peak 2: 1,178 [counts]

R2-34 (25.99 days)

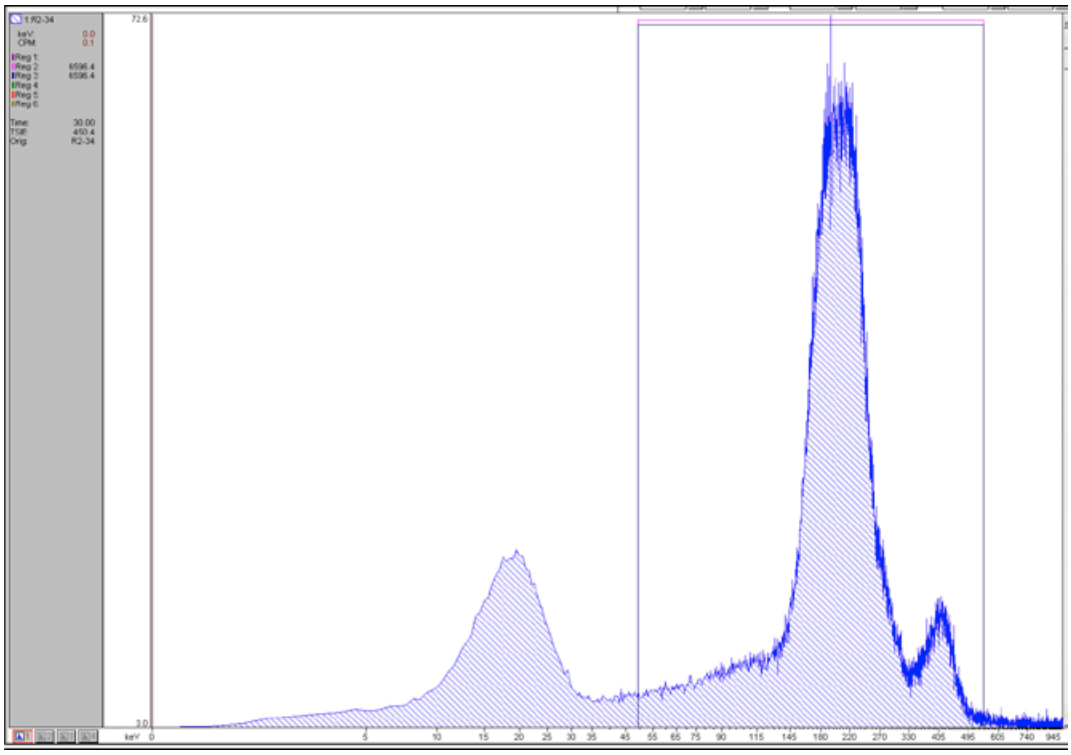

Peak 1: 4,473 [counts]
Peak 2: 391 [counts]

R2-35 (26.84 days)

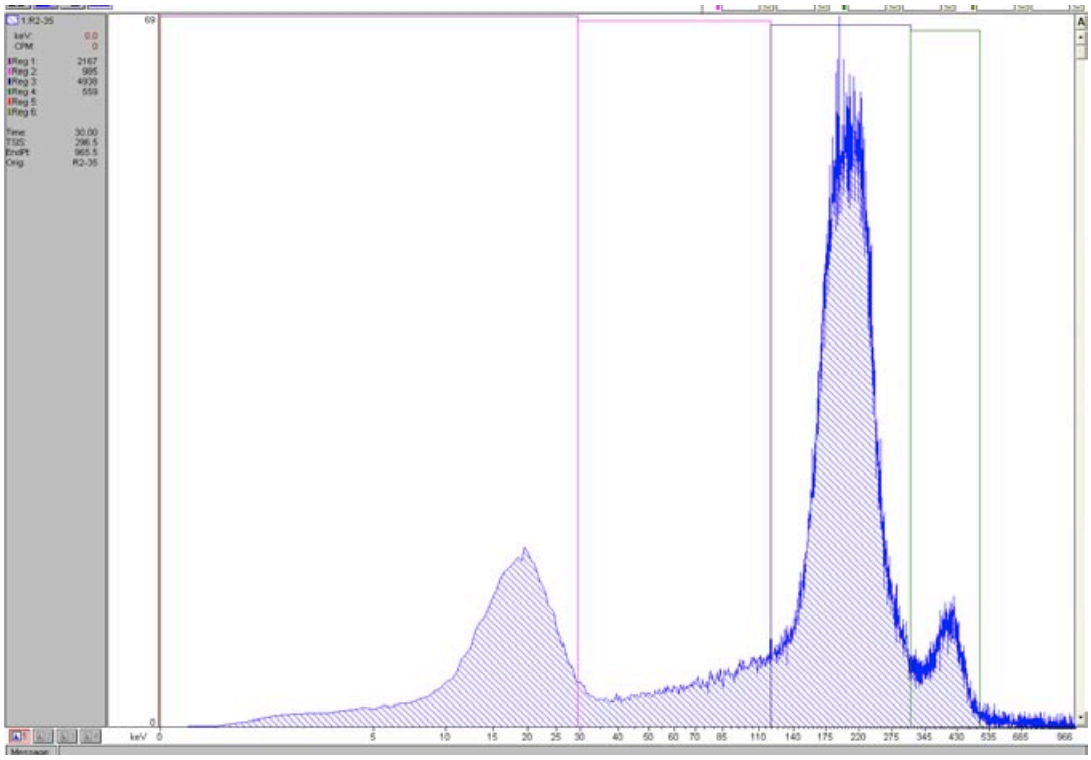

Peak 1: 4,162 [counts]
Peak 2: 368 [counts]

R2-36 (27.02 days)

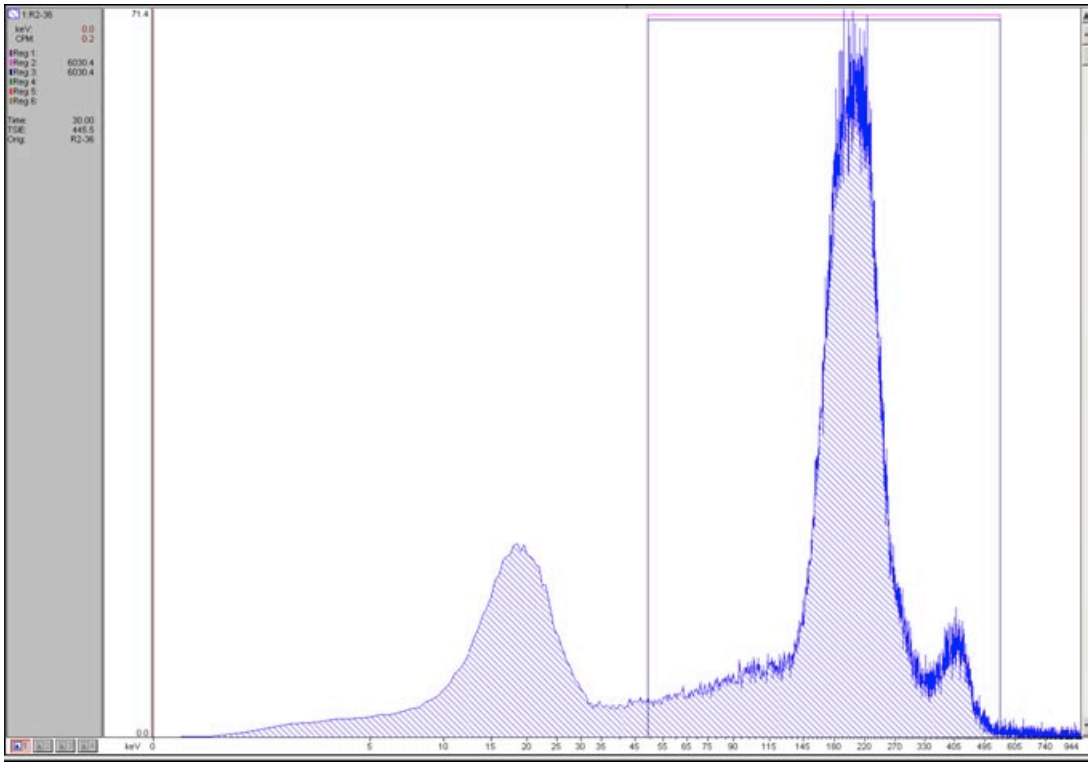

Peak 1: 4,262 [counts]
Peak 2: 371 [counts]

R2-37 (27.81 days)

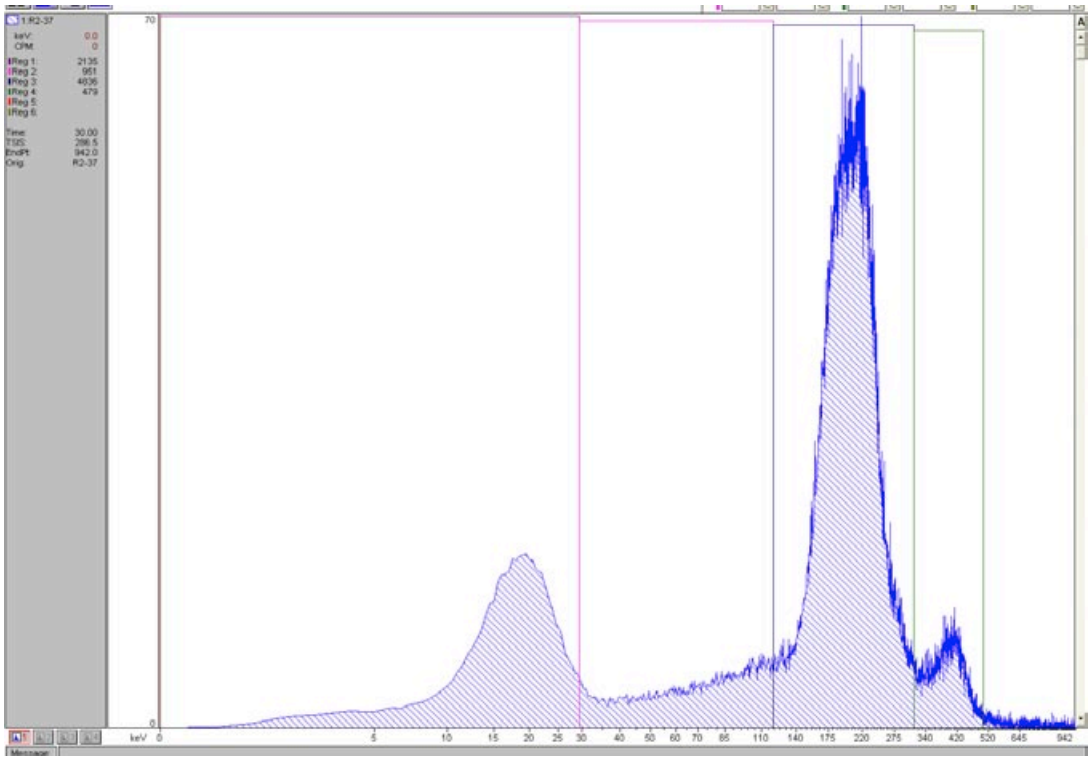

Peak 1: 4,254 [counts]
Peak 2: 288 [counts]

R2-38 (28.0 days)

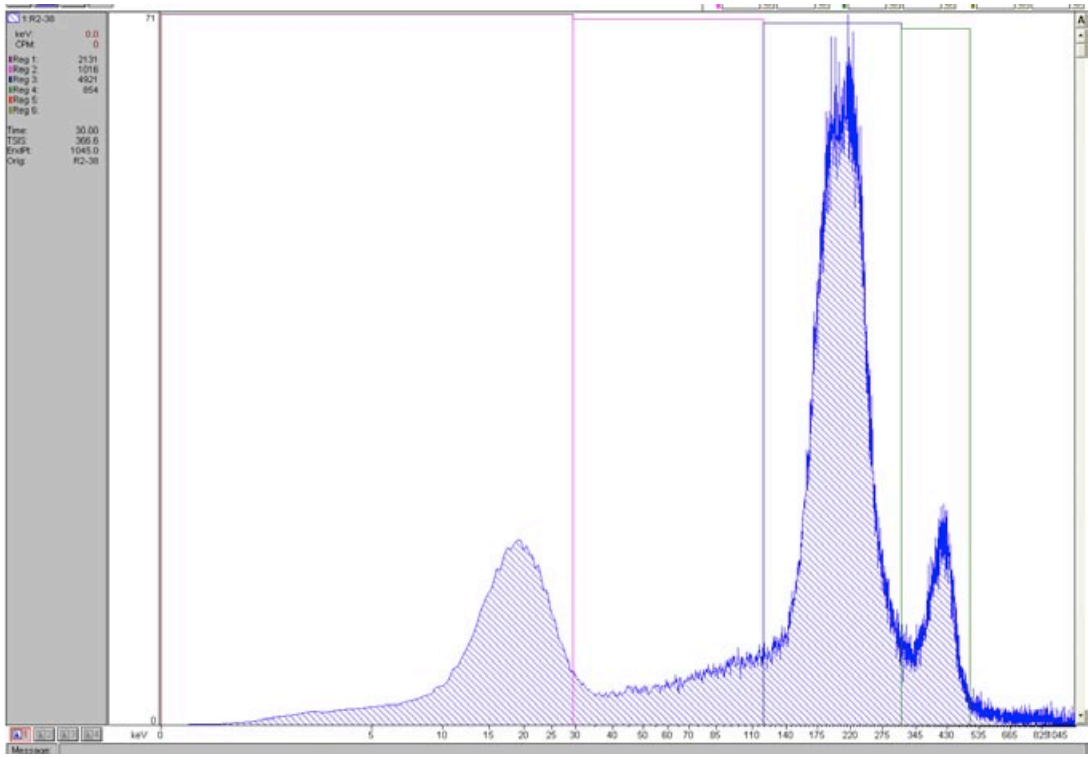

Peak 1: 4,145 [counts]
Peak 2: 567 [counts]

R2-39 (28.79 days)

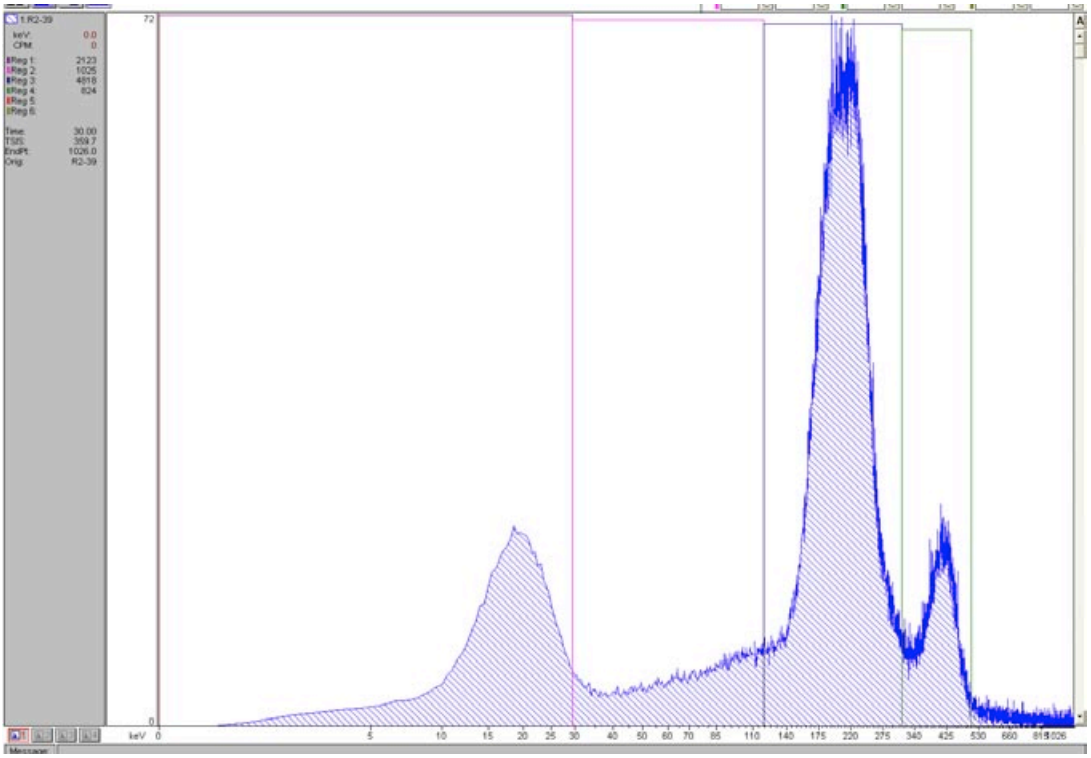

Peak 1: 4,139 [counts]
Peak 2: 633 [counts]

R2-40 (29.04 days)

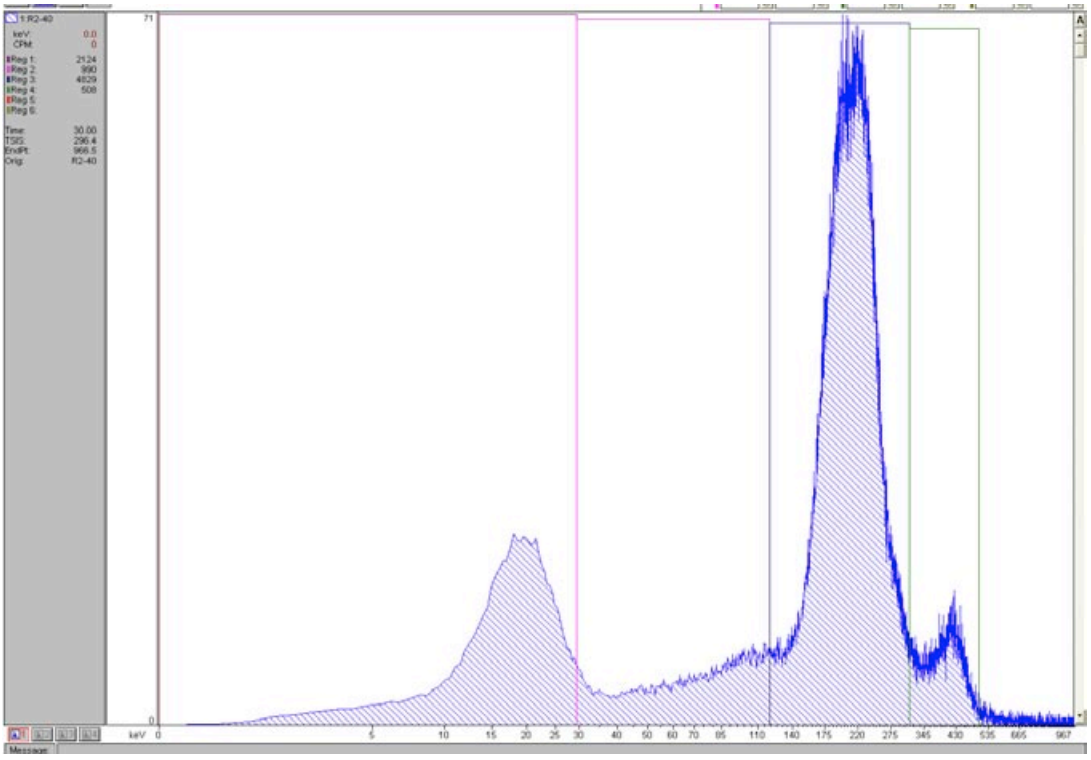

Peak 1: 4,150 [counts]
Peak 2: 317 [counts]

R2-41 (29.79 days)

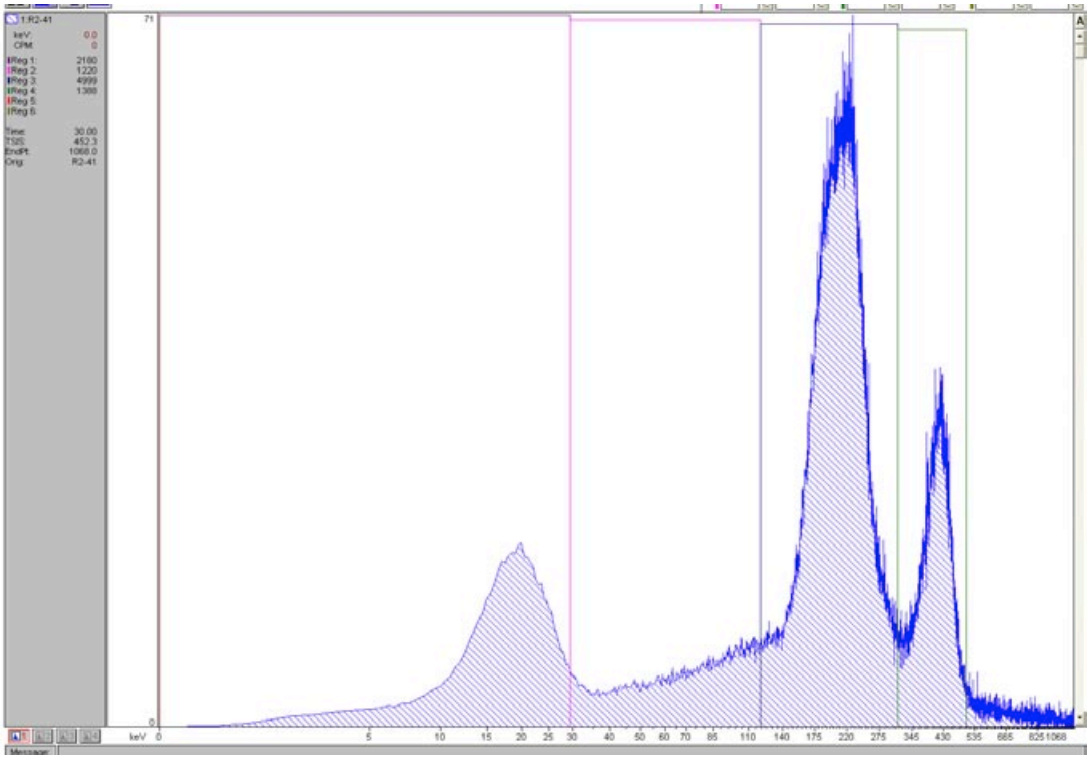

Peak 1: 4,223 [counts]
Peak 2: 1,101 [counts]

R2-42 (32.79 days)

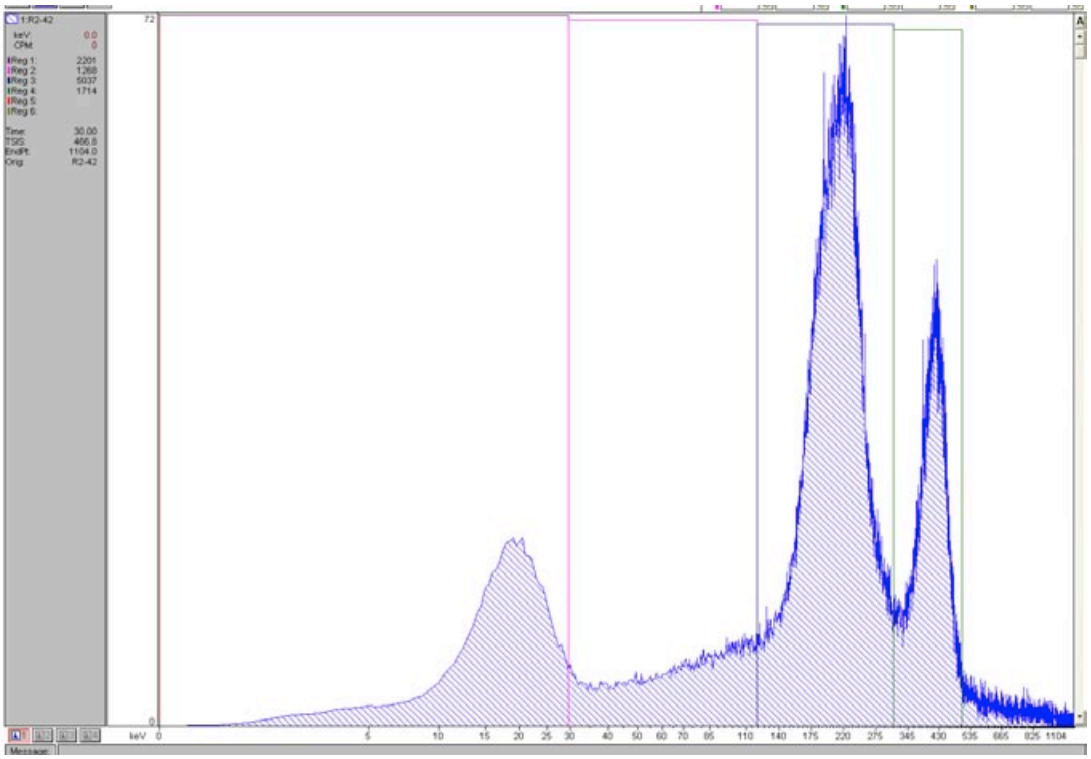

Peak 1: 4,164 [counts]
Peak 2: 1,332 [counts]

R2-43 (33.02 days)

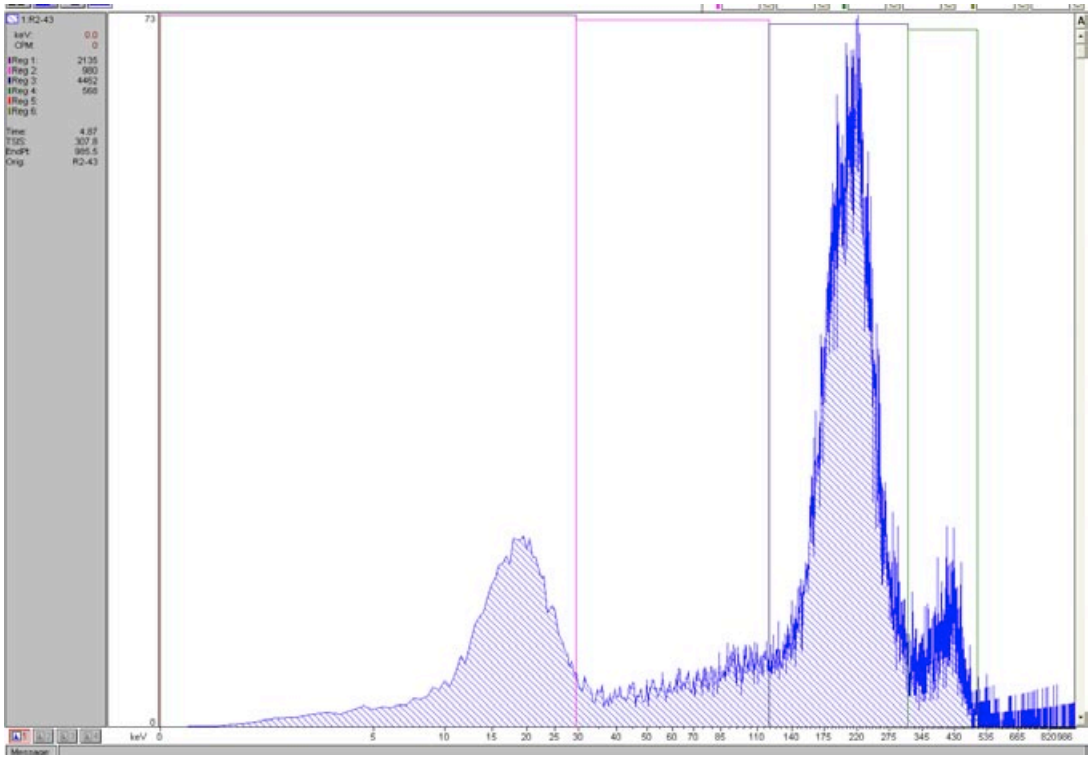

Peak 1: 3,882 [counts]
Peak 2: 377 [counts]

R2-44 (33.79 days)

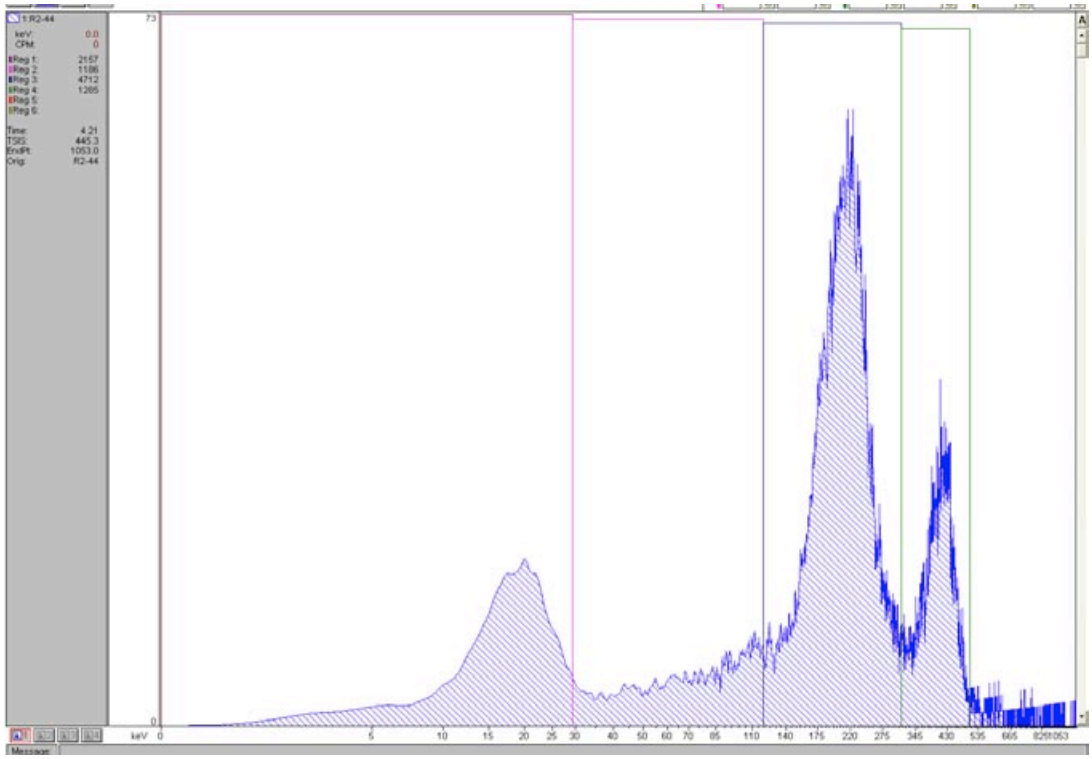

Peak 1: 4,033 [counts]
Peak 2: 1,094 [counts]

R2-45 (34.02 days)

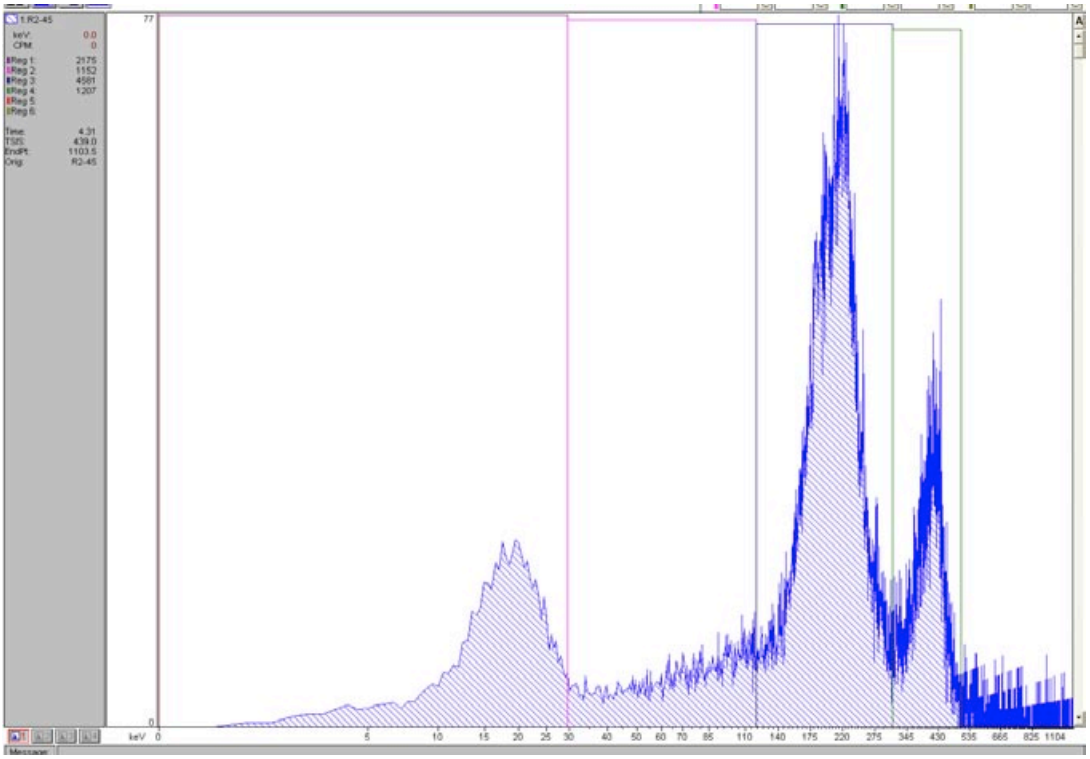

Peak 1: 3,805 [counts]
Peak 2: 920 [counts]

R2-46 (34.79 days)

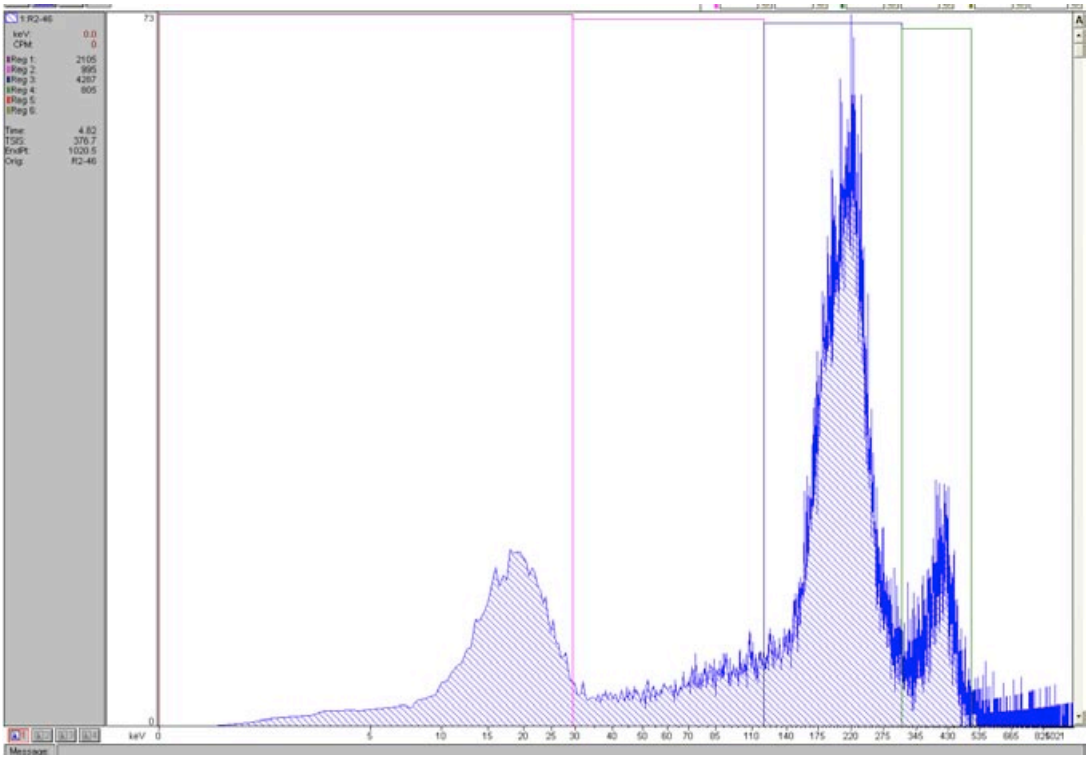

Peak 1: 3,608 [counts]
Peak 2: 518 [counts]

R2-47 (35.02 days)

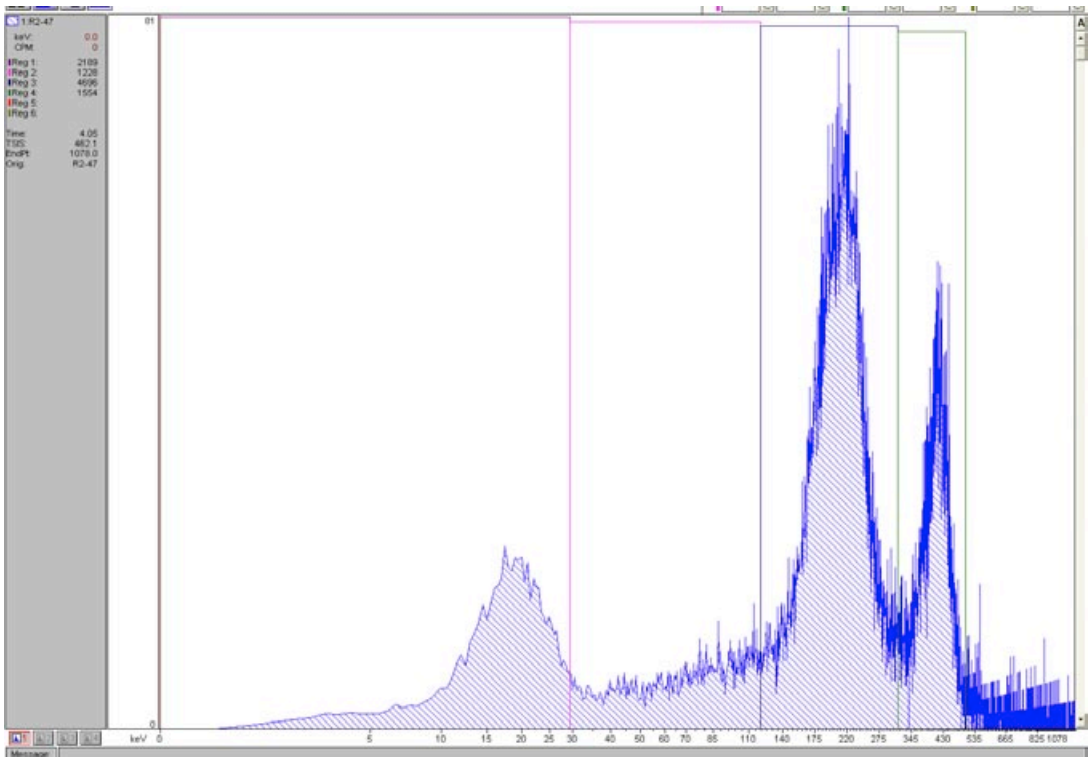

Peak 1: 3,629 [counts]
Peak 2: 1,267 [counts]

R2-48 (35.79 days)

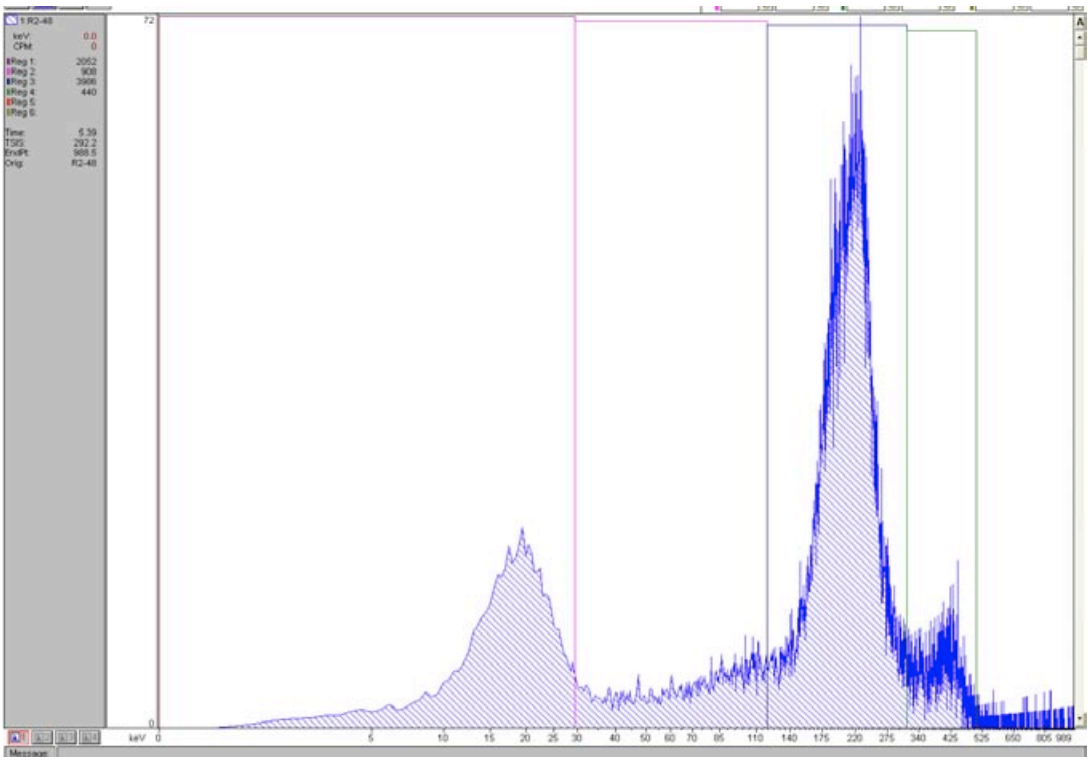

Peak 1: 3,210 [counts]
Peak 2: 153 [counts]

R2-49 (36.02 days)

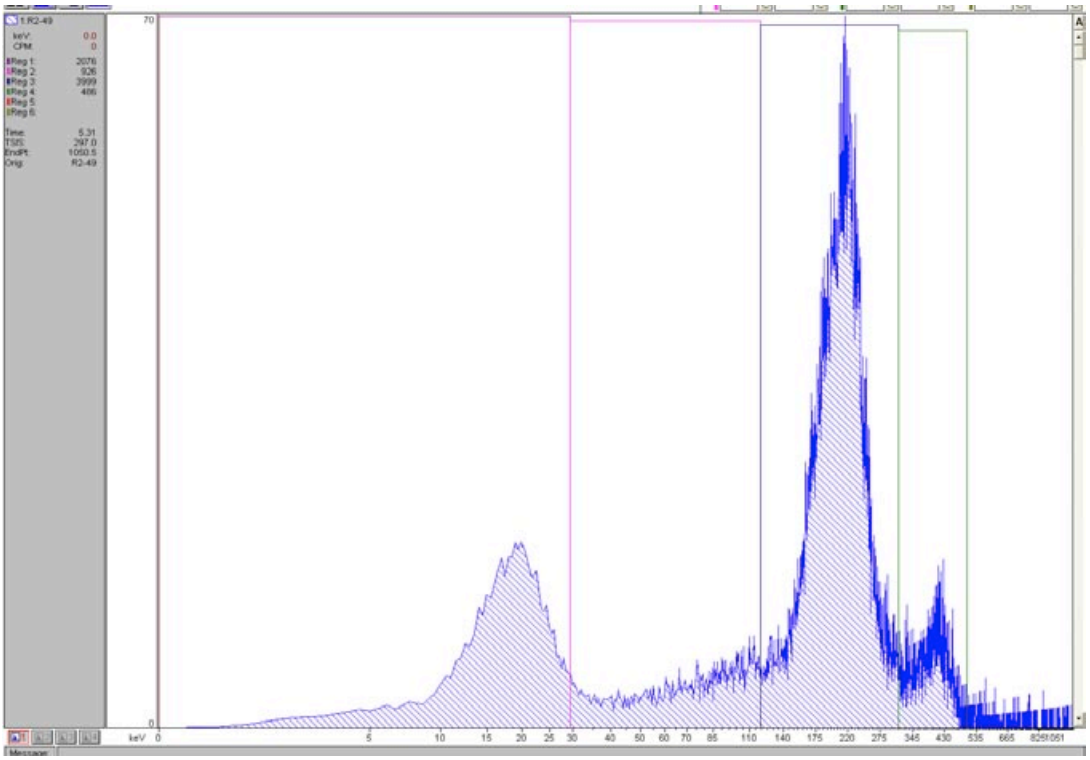

Peak 1: 3,521 [counts]
Peak 2: 486 [counts]

R2-50 (39.79 days)

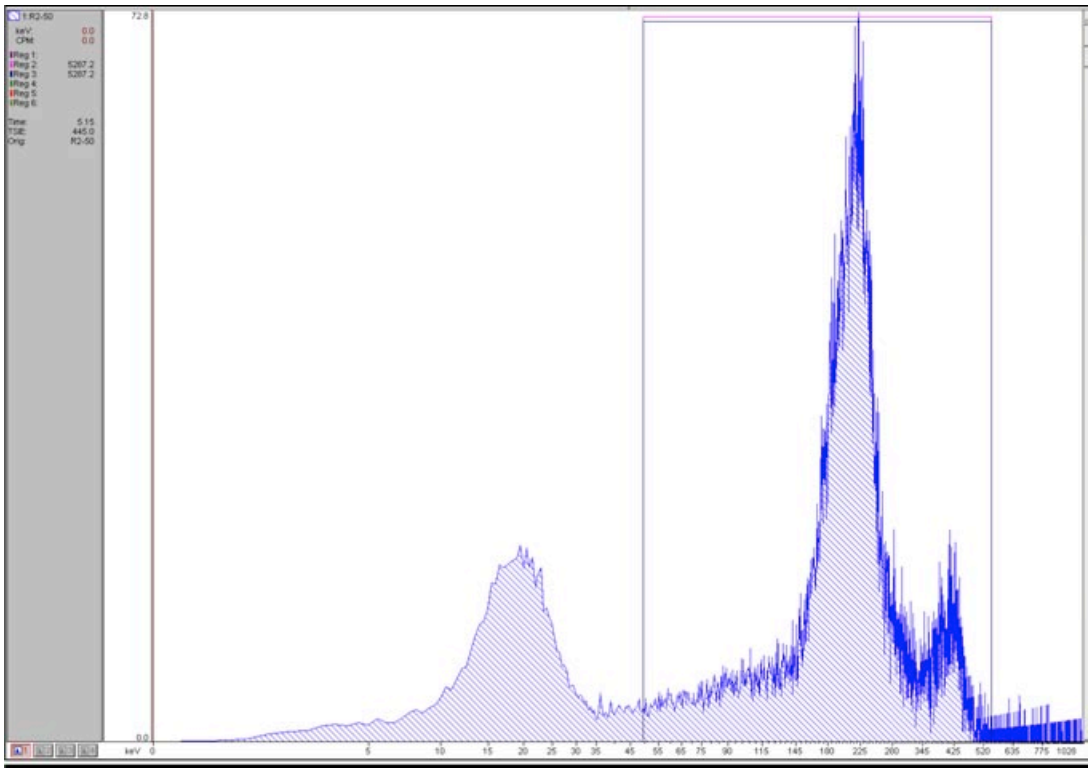

Peak 1: 3,472 [counts]
Peak 2: 304 [counts]

R2-51 (47.06 days)

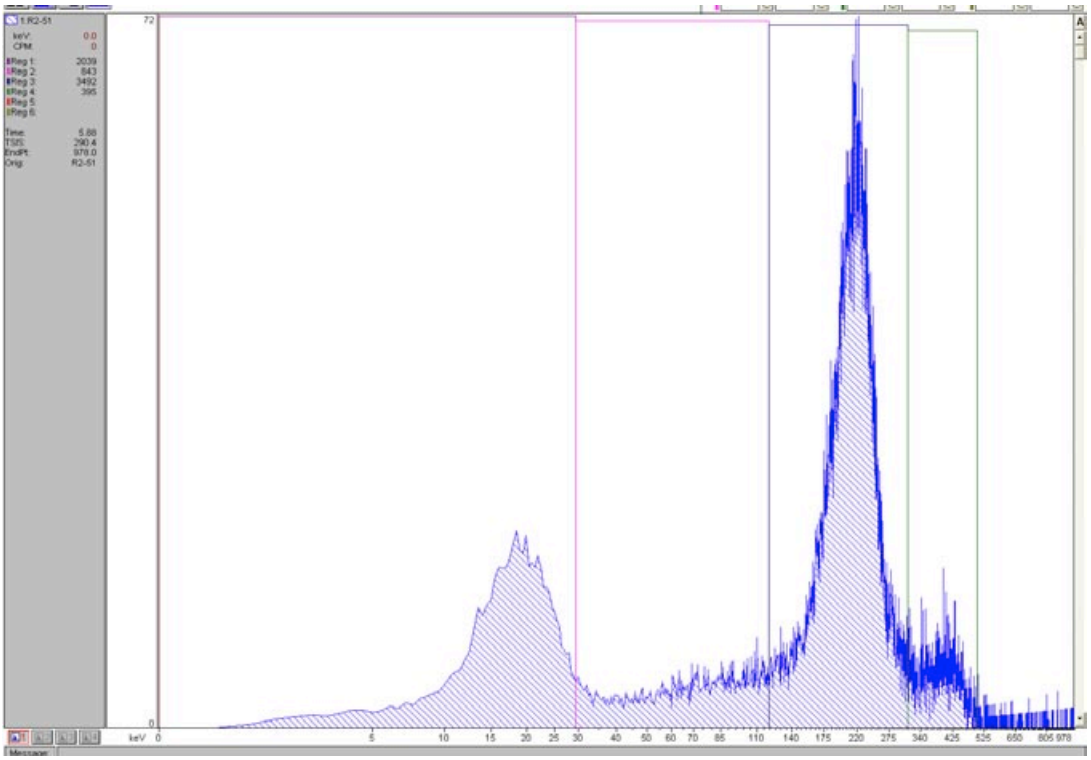

Peak 1: 3,007 [counts]
Peak 2: 299 [counts]

R2-52 (47.81 days)

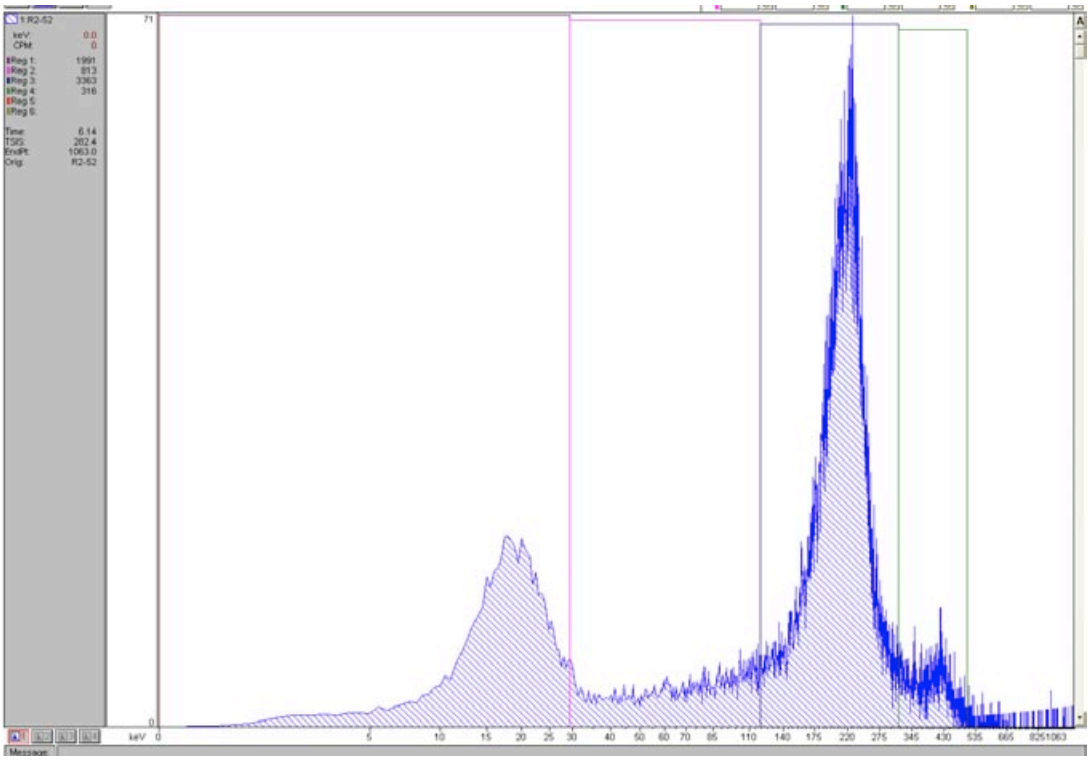

Peak 1: 2,684 [counts]
Peak 2: 29 [counts]

ISSN 1404-0344
CM Gruppen AB, Bromma, 2010